DEVELOPMENT OF KAOLIN CLAY, SILVER OXIDE AND ZINC OXIDE NANOCOMPOSITE FILTER FOR DOMESTIC WASTEWATER TREATMENT

BY

OGUNDIPE Felix Oluwaseun

(PhD/SEET/2017/916)

DEPARTMENT OF CIVIL ENGINEERING

FEDERAL UNIVERSITY OF TECHNOLOGY

MINNA

SEPTEMBER, 2023

DEVELOPMENT OF KAOLIN CLAY, SILVER OXIDE AND ZINC OXIDE NANOCOMPOSITE FILTER FOR DOMESTIC WASTEWATER TREATMENT

BY

OGUNDIPE Felix Oluwaseun

(PhD/SEET/2017/916)

A THESIS SUBMITTED TO THE POSTGRADUATE SCHOOL FEDERAL UNIVERSITY OF TECHNOLOGY, MINNA, NIGERIA IN PARTIAL FULFILMENT OF THE REQUIREMENTS FOR THE AWARD OF THE DEGREE OF DOCTOR OF PHILOSOPHY (PhD) IN CIVIL ENGINEERING (WATER RESOURCES AND ENVIRONMENTAL ENGINEERING)

SEPTEMBER, 2023

DECLARATION

I hereby declare that this thesis titled **"Development of kaolin clay, silver oxide and zinc oxide nanocomposite filter for domestic wastewater treatment"** is a collection of my original research work and it has not been presented for any other qualification anywhere. Information from other sources (published or unpublished) has been duly acknowledged.

OGUNDIPE, Felix Oluwaseun ----------
(PhD/SEET/2017/916) **Signature and Date**
FEDERAL UNIVERSITY OF TECHNOLOGY
MINNA, NIGERIA.

CERTIFICATION

This thesis titled **"Development of kaolin clay, silver oxide and zinc oxide nanocomposite filter for domestic wastewater treatment"** by **Ogundipe Felix Oluwaseun** (PhD/SEET/2017/916) meets the regulations governing the award of the degree of PhD of the Federal University of Technology, Minna and it is approved for its contribution to scientific knowledge and literary presentation.

Engr. Dr. M. Saidu ----------
(Major Supervisor) Signature and Date

Engr. Prof. A.S. Abdulkareem ----------
(Co-Supervisor) Signature and Date

Engr. Dr. A.O. Busari ----------
(Co-Supervisor) Signature and Date

Engr. Dr. M. Alhassan ----------
(H O D) Signature and Date

Engr. Prof. Z.D. Osunde ----------
(DEAN SIPET) Signature and Date

Engr. Prof. O. K. Abubakre ----------
(Dean Postgraduate School) Signature and Date

ACKNOWLEDGMENTS

Glory be to God almighty for making this research work a success. I would like to express my sincere gratitude to my main supervisor, Engr. Dr. M Saidu and the entire supervisory team, Engr. Prof. A.S. Abdulkareem and Engr. Dr. A.O. Busari for their guidance. Special thanks to the Head of the Civil Engineering Department, Engr. Dr. M. Alhassan, my internal supervisor and Postgraduate Coordinator, Engr. Dr. A.R. Adesiji and Engr. Dr. T.E. Adejumo for their commitments. I also appreciate Engr. Prof. O. D. Jimoh, Engr. Prof. T. Y. Tsado, Engr. Prof. A. A. Amadi, Engr. Prof. S. M. Auta, Engr. Dr. S. S. Kolo, Engr. Dr. M. Alhaji, Engr. J. Olayemi, Engr. Dr. A. Yusuf, Engr. Dr. D.N. Kolo, Engr. I. O. Jimoh, Engr. Dr. A. Abdullahi, Engr. H. O. Aminulai, Engr. Mrs. A. O. Gbadebo, Engr. A. O. Ibrahim, Engr. Dr. S.F. Oritola, Engr. S. Adeniyi, Engr. D. Zango, Engr. S. M. Iliayasu, Engr. E. Abese and Mr. Umar for their word of encouragement.

I am indebted to the Nanotechnology Research Group of the Federal University of Technology, Minna, Centre for Genetics Engineering and Biotechnology Laboratory, Federal University of Technology, Minna, and the Industrial Design Department of the Federal University of Technology, Akure, Nigeria for their technical supports. I also thank Origin Lab Corporation, United States of America for the use of their 2021 OriginPro software.

My appreciation goes to the Federal Ministry of Water Resources and Sanitation, Abuja for giving me the approval to embark on this study and for allowing free access to the National Water Quality Reference Laboratory, Minna for analyses.

Finally, I would like to thank my colleagues, friends, my wonderful wife, Mrs. Oluwakemi Ogundipe, and my children, Peace and Elijah Ogundipe for their moral support.

ABSTRACT

Fresh water is a valuable resource that provides drinking water for people. However, domestic wastewater produced by human settlements pollutes this water resource. In an effort to solve the challenges of wastewater pollution, provide safe water for people and protect the ecosystems, this study describes the production of nanocomposite filters from beneficiated kaolin clay (BKC), silver nanoparticles (Ag-NPs) and zinc oxide nanoparticles (ZnO-NPs), to remove contaminants from domestic wastewater collected via sewers. The filter pots were moulded using a jigger and jolly machine and gas-fired in a temperature-controlled kiln at 900 ^{o}C. The produced filter pots were labelled BKC – 1, BKC - 2, BKC/Ag - 1, BKC/Ag – 2, BKC/ZnO – 1, BKC/ZnO – 2, BKC/Ag/ZnO – 1, BKC/Ag/ZnO – 2. The crystal structure, morphology and formations of the nanocomposite adsorbents to produce the filter pots were confirmed using X-Ray Diffractometer (XRD), Dispersive X-Ray Fluorescence (XRF), High-Resolution Transmission Electron Microscope (HRTEM), UV-Spectrophotometer and Brunauer–Emmett–Teller (BET) Nitrogen Absorption analysis. HRTEM results showed that the produced nanocomposite adsorbents were polycrystalline in nature, while the interplanar spacing and average crystalline sizes range from 1.775 – 4.712 nm and 26.834 – 40.258 nm according to XRD analysis. XRF analysis indicated that SiO_2/Al_2O_3 ratios for BKC/Ag, BKC/ZnO and BKC/Ag/ZnO nanocomposite adsorbents were 1.5170, 1.4818 and 1.5231 respectively. BET analysis showed that the desorption average pore sizes of the produced nanocomposite adsorbents fell in the mesopore widths of 13.8994 – 16.9233 nm and surface areas of 1.0545 - 14.5126 m^2/g. The average interplanar spacing for Ag and ZnO nanoparticles were 1.7748 nm and 3.435 nm and the crystallite size was 30.6285 nm and 32.038 nm respectively. The surface area of ZnO-NPs and Ag-NPs were 1.1045 m^2/g and 1.0545 m^2/g. The adsorption-desorption isotherms for the produced nanocomposite adsorbents possessed pore sizes that fell in the mesopore widths which were classified as type IV isotherms. The adsorption studies showed that the total iron, lead, copper, manganese, arsenic, mercury silver, zinc, nitrate, phosphate, ammonium, COD, BOD, oil and grease parameters had a very strong agreement with Langmuir and Freundlich isotherms, while enthalpy ($\Delta H°$) and entropy ($\Delta S°$) for these parameters were found to be positive, which indicated that the adsorption processes were endothermic in nature. The beneficiated kaolin clay of 75 % mixed with silver oxide of 0.5 %, zinc oxide nanoparticles of 1.0 % (BKC/Ag/ZnO) and rice husks of 23.5 % produced the best nanocomposite filter pot by reducing the contaminant concentrations of total iron, lead, copper, manganese, arsenic, mercury silver, zinc, nitrate, phosphate, ammonium, COD, BOD, oil and grease in the domestic wastewater by average of 72 % reduction level with flow rate of 16.5 mL/hr. The BKC/Ag/ZnO filter pot removed 100 % of the total coliforms, faecal coliforms, *Clostridium perfringens*, *E. coli*, turbidity, suspended solids and colour in domestic wastewater between 30 - 60 minutes contact times, 15 – 30 g dosage, and 50 - 80 °C temperature. The physico-chemical analysis of the filtrates from the produced filter pots resulted in contaminants concentrations which were within the maximum permissible limit established for effluent discharge by the National Environmental Standard Regulations and Enforcement Agency. This shows that the filter pots produced are good options that could be deployed for domestic wastewater treatment before discharge to rivers and lakes or being reused for subsistence irrigation farming.

TABLE OF CONTENTS

LIST OF TABLES

LIST OF FIGURES

LIST OF PLATES

ABBREVIATIONS, GLOSSARIES AND SYMBOLS

A	Surface area of the filter pots
AAS	Atomic absorption spectrometer
AC	Activated carbon
AD	Anaerobic Digestion
Ag-NPs	Silver oxide nanoparticles
APHA	American Public Health Association
AS	Activated sludge
ASP	**A**ctivated sludge process
ASTM	America Society for Testing and Materials
BDL	Below detection limit
BET	Brunauer emmett teller
BKC	Beneficiated kaolin clay
BOD	Biochemical oxygen demands
BSE	Back-scattered electrons
Ce	Equilibrium concentration
CEC	Cation exchange capacity
CFU	Colony forming units
cm	Centimetre
CNTs	Carbon nanotubes
COD	Chemical oxygen demand
cP	Viscosity
CST	Conventional septic tank
CSTR	Completely stirred tank reactor
DC	Direct current
DDW	Deionised distilled water
DO	Dissolved oxygen

EC	Electrical conductivity
EDX	Energy dispersive x-ray spectroscopy
EHT	Electron high tension
EP	Emerging pollutants
EPA	Environmental protection agency
f	Co-efficient of friction
FTIR	UV-visible and fourier transform infrared spectroscopy
FWHM	Full width at half maximum
g	gram
HPP	Hydro power plant
HRT	Hydraulic retention time
HRTEM	High resolution transmission electron microscopy
ICDD	International Centre for Diffraction Data
IUPAC	International Union of Pure and Applied Chemistry
JCPDS	Joint committee on powder diffraction standards
KAF	*Kanchan* arsenic filter
K	Kelvin
kg	Kilogram
LOI	Lost on ignition
m	Metre
MARS	Membrane anaerobic reactor system
MB	Methylene Blue
MBR	Membrane bioreactor
meq	Milliequivalent
mg	Milligram
mins	Minutes
N	Newton

NBA	N-butyl amine
NBS	National Bureau of Statistics
NC	Nanocomposite
NESREA	National Environmental Standard Regulations and Enforcement Agency
nm	Nanometre
NORM	National outcome routine mapping
NP	Nanoparticle
NSDWQ	Nigerian standard for drinking water quality
NTU	Nephelometric turbidity units
NWQRL	National Water Quality Reference Laboratory
OMP	Organic-micro pollutants
PDF	Powder diffraction file
PEG	Polyethylene glycol
POU	Point of use
Q	Flow rate
QA	Quality assurance
QC	Quality control
R	particle size radius of clay
RBC	Rotating biological contactor
Re	Reynold number
rpm	Revolution per minutes
s	Second
SAED	Selected area electron diffraction
SBR	Sequencing batch reactor
SDG	Sustainable development goal
SE	Secondary electron
SEM	Scanning electron microscope

SPR	Surface plasmon resonance
TCU	Total colour unit
TEM	Transmission electron microscopy
TKN	Total kjeldahl nitrogen
TSS	Total suspended solid
UASB	Up-flow anaerobic sludge blanket
UN	United Nation
UN	United Nations
UNISA	University of South Africa
UV	Ultraviolet
VIP	Ventilated improved toilets
w	weight
WASH	Water, Sanitation and Hygiene
WRC	Water Research Commission
WWDR	World Water Development Report
XRD	X–ray diffraction
XRF	Dispersive x – ray fluorescence
ZnO -NPs	Zinc oxide nanoparticles
ZSM	Zeolite socony mobile
%	Percent
h_f	Head Loss
C_e	Equilibrium concentration
C_i	Initial concentration of the wastewater
K_f	Freundlich constants
Q_o	Langmuir constants
R_L	Type of isotherm
d_p	Diameter of particle

q_e	Adsorption capacity at equilibrium stage
u_s	particle settling velocity
ρ_p	particle density
ρ_w	density of water
µm	Micrometre
µS	Micro siemens
Å	Ångström
°C	Degree Centigrade
ΔG	Gibb's free energy of adsorption
ΔH	Enthalpy of adsorption
ΔS	Entropy of adsorption
Θ	Theta
λ	wavelength
b	Langmuir constant
μ	liquid viscosity

CHAPTER ONE

1.0 INTRODUCTION

1.1 Background to the Study

Fresh water is a valuable resource that provides food for people through irrigation for agricultural production. However, liquid and solid wastes produced by human settlements and industrial activities pollute this water resource. As the overall water demand grows, the quantity of wastewater produced and its overall pollution load are continuously increasing worldwide. The United Nations (UN) 2017 World Water Development Report (WWDR) on Wastewater showed that the vast majority of wastewater in developing countries is released directly into the environment without adequate treatment, with detrimental impacts on human health, economic productivity, and the quality of ambient freshwater resources and ecosystems (WWDR, 2017).

Unceasing failure to address wastewater as a major social and environmental problem would compromise other efforts towards achieving the 2030 Agenda for Sustainable Development Goal (SDG) 6 explicitly focuses on the treatment and reuse of wastewater and improving ambient water quality (UN-Water, 2018). This suggests the emerging need for technological advancements in water treatment that will benefit people, especially in developing countries.

In efforts to solve the challenges of wastewater pollution, and protect the water quality and the ecosystems, conventional wastewater treatment processes, anaerobic and aerobic wastewater treatment systems, pressure-driven membrane processes, filtration methods, adsorption treatment processes and commercially available activated carbon have been used for wastewater treatment for a while. However, each technology mentioned here has

its peculiar drawbacks. Conventional wastewater treatment methods have a high cost of labour, high chemical consumption, high maintenance cost and sludge handling problems. Anaerobic and aerobic systems are found to have operational limitations in terms of long Hydraulic Retention Time (HRT), space requirement and facilities to capture biogas (Chan *et al.*, 2009). Pressure-driven membrane filtration processes have high energy costs, high maintenance costs, and high cost of chemical consumption for biocides, cleaning and anti-scaling agents. High cost, process complexity, membrane fouling and low permeate flux have been the major drawbacks to the use of filtration methods for wastewater treatment (Fu and Wang, 2011). The price of commercial adsorbents such as commercially available activated carbon is costly and difficult to regenerate. Given the identified drawbacks of each of the above-mentioned technologies, there is a need to develop an alternative treatment process for the removal of contaminants from wastewater using locally available materials. Currently, nanotechnology is becoming a new hope in waste disposal treatment with a promising application in wastewater treatment.

Nanotechnology uses particles that are 1/80,000 the diameter of a human hair (Sulekha, 2016). At such a small scale, new physical, chemical, and biological properties become evident. Research in wastewater treatment by adsorption has resulted in the development of different materials for the removal of metals from solutions and these materials include activated carbon, zeolites, peat kaolin and clay (Vikas *et al.*, 2013). Nanotechnology is defined as the science, engineering, and technology conducted at a scale that ranges between 1 to 100 nanometres. The prefix “nano” is derived from the ancient Greek “nanos”, meaning "dwarf”. Today, “nano” is used as a prefix that means “billionth” or a factor of 10^{-9} (Samanta *et al.*, 2016). Nanotechnology has led to numerous well-organized ways for the treatment of wastewater in a more accurate way on both small as well as

large scale (Sulekha, 2016). Advances in nanoscale science and engineering suggest that many of the current problems involving water quality could be resolved by using nanosorbents, nanocatalysts, bioactive nanoparticles, nanostructured catalytic membranes, nanotubes, magnetic nanoparticles, granules, flake, high surface area metal particle molecular assemblies with characteristic length scales of 9-10 nm including clusters, micro-molecules, nanoparticles and colloids. Nanotechnology relies on the ability to design, manipulate, and manufacture materials at the nanoscale and these materials are called nanomaterials.

Nanomaterials have been under active research and development. Nanomaterials have been successfully applied in many fields such as catalysis, medicine, sensing and biology. Due to their small sizes and thus large specific surface areas, nanomaterials have strong adsorption capacities and reactivity. At present, the most extensively studied nanomaterials for water and wastewater treatment include carbon nanotubes (CNTs), nanocomposites, zero-valent metal nanoparticles and metal oxide nanoparticles (Haijiao *et al.*, 2016).

Among the metal oxide nanoparticles, metallic silver nanoparticles (Ag-NPs) have received considerable attention for their potential application as a biocide in products ranging from facade paints to textiles. The antibacterial activity of silver has been known for centuries and has led to the development of several Ag-based bactericidal products (Ralf *et al.*, 2011). Microbes are unlikely to develop resistance against silver, as they do against conventional and narrow-target antibiotics because the metal attacks a broad range of targets in the organisms, which means that they would have to develop a host of mutations simultaneously to protect themselves. Thus, silver ions have been used as an antibacterial component in dental resin composites, synthetic zeolites, and in coatings of

medical devices (Sukdeb *et al.*, 2007**).** The antimicrobial activity of many nano-sized metal ions (nanoparticles) allows for the design of nanocatalysts (Berekaa, 2016) such as N-doped titanium dioxide, zirconium dioxide and zinc oxide nanoparticles (ZnO-NPs).

As an environmentally friendly material, nano sized ZnO is used in wastewater treatment because of its strong anti-microbial activities. As an adsorbent, ZnO was mostly applied to eliminate hydrogen sulphide and recently, people have found that nanostructured ZnO could efficiently remove heavy metals (Ming *et al.*, 2012), removal of Chromium VI (Rui *et al.*, 2013), enhance adsorption of lead ion (Yang *et al.*, 2008) and use as an antibacterial application (Getie *et al.*, 2017; Haritha *et al.*, 2011; Ying *et al.*, 2017; Stoyanova *et al.*, 2013). As an adsorbent, the impregnation of Ag and ZnO nanoparticles on nano clay will produce a more potent and stronger anti-microbial nanocomposite adsorbent in the treatment of domestic wastewater.

In recent years, the synthesis of various nanocomposites has become the most active subject in the field of nanomaterials and wastewater treatments due to their potency in wastewater treatment. This research work will develop a kaolin clay nanocomposite filter for the treatment of domestic wastewater collected via sewers that connect toilets, baths, showers, kitchens and sinks together. A blend proportion of purified kaolin clay with Ag and ZnO nanoparticles generated by green synthesis for the development of a nanocomposite filter will significantly reduce, by a greater percentage, the contaminants from the wastewater.

1.2 Statement of the Research Problem

One of the major scientific challenges of this century is wastewater management and its potential impacts on freshwater quality (Karishma and Mehali, 2015). Globally, most of the wastewater from homes, cities, industry and agriculture flows back to nature without

being properly treated or reused thereby polluting river water bodies. The wastewater, depending on its source, contains contaminants of high levels of microbes, heavy metals of serious concern, emerging pollutants, and inorganic and organic compounds. The economic and health impact arising from the effect of untreated wastewater effluents discharging into river water bodies is quite enormous.

Wastewater effluents particularly in developing countries like Nigeria are in most cases discharged into the adjoining environment with water bodies being mostly affected. Some of these wastewater effluents are untreated or inadequately treated before being discharged (Okereke *et al.*, 2016; UN-Water, 2018).

A wastewater-polluted river is sometimes consumed and used for irrigation farming by villagers living downstream, who have no other source of potable water. Consumption and the use of this polluted river water always led to disease outbreaks such as cholera, diarrhoea in humans and extreme cases, loss of lives. To overcome these problems and to improve public health, there is a need to effectively remove the contaminants in the wastewater. Therefore, it is essential to treat the domestic wastewater produced from households and within office buildings before it is finally discharged back into the environment to prevent disease outbreaks and protect the freshwater ecosystem.

The treatment will reduce disease-causing organisms, nutrients, organic matter, solids and other impurities in wastewater. According to Water Research Commission (WRC), conventional wastewater treatment processes consist of a combination of preliminary, primary, secondary and tertiary treatments (WRC, 2015) but with the drawback of the high cost of labour, chemicals consumption, maintenance and sludge handling problem (Chan *et al.*, 2009; Al-Rekabi *et al.*, 2007; Syafiqa *et al.*, 2021; Bora and Dutta, 2014; Fu and Wang, 2011). Nanoparticles are gaining strength and popularity in wastewater

treatment due to their efficiency in contaminants removal but with a drawback (Sulekha, 2016). The major problem is the complexity of nanoparticle analysis and the lack of methods of characterizing nanomaterials makes it difficult to detect the nanoparticles in the environment (Karishma and Mehali, 2015; Abdullah *et al.*, 2017; Pradeep, 2009).

To improve the applicability of metal oxide nanoparticles for wastewater treatment, nanocomposite (NC) materials have emerged as suitable alternatives to overcome limitations of growth nanoparticles by employing porous support materials of large areas as matrices or stabilizers to obtain hybrid nanocomposite adsorbents (Bingjun *et al.*, 2009; Odenigbo and Musa, 2018). Among the various matrixes, kaolin clay is considered to be a promising host and stabilizer due to its unique features such as large surface area, high ion exchange capacity cavities with 1.3 nm diameter, hydrophilic, ecofriendly nature and the highly thermal stability. To completely overcome the problems posed by domestic wastewater pollution to the environment and overcome the limitations experienced by the various treatment technologies, this research work will develop a nanocomposite filter that is capable of removing heavy metals, chemicals, physical and microbial contaminants from domestic wastewater through the beneficiation of locally available kaolin clay and mix with silver and zinc oxide nanoparticles.

1.3 Aim and Objectives of the Study

This research aims to develop a beneficiated kaolin clay, silver and zinc oxide nanocomposite filter from locally available materials for the treatment of domestic wastewater collected via sewer. The objectives of this research are:

i. To beneficiate and characterise kaolin clay from Kutigi, Niger State.

ii. To produce and characterise silver nanoparticles, zinc oxide nanoparticles, beneficiated kaolin clay and nanocomposite adsorbents for their surface areas, chemical composition and crystal structure.

iii. To produce nanocomposite filter pots from the optimum materials composition based on batch adsorption studies for the removal of the selected physicochemical and bacteriological contaminants in the domestic wastewater treatment.

iv. To carry out performance evaluation of the produced nanocomposite adsorbents and filter pots for the removal of the selected physicochemical and bacteriological contaminants in the domestic wastewater.

1.4 Justification for the Research

This study will develop a nanocomposite filter that is effective in the removal of contaminants from domestic wastewater using a locally available kaolin clay, silver and zinc oxide nanocomposite filter. Kaolin clay's choice for this research is due to its water treatment ability. Kaolinite is widespread across Niger State, relatively free of charge, non-toxic and environmentally friendly. The choice of Ag and ZnO-NPs using *Mangifera indica* leaf extracts as reducing agents is due to their antibacterial activities. ZnO nanoparticles synthesized using zinc chloride exhibited strong antibacterial prowess on *Staphylococcus aureus* (gram-positive) and *E. coli* (gram-negative) bacteria (Getie *et al.*, 2017). The use of plants for the synthesis of nanoparticles is common because they are available everywhere, safe to handle and possess a wide variety of metabolites that may contribute to the reduction of metal oxides. Silver nanoparticles are very effective and potent against numerous microorganisms which include plant pathogens (Krishan *et al.*, 2013).

Ag and ZnO nanoparticles are potent nanoparticles that are not expensive, not toxic, have high activity, exceptional stability and a long-life span. These nanoparticles are less toxic if properly anchored via green synthesis using extracts from *Mangifera indica leaves* bond to suitable matrices such as kaolin because of their decreased mobility in aqueous media.

Given the foregoing, this research work will develop a nanocomposite filter with locally available materials capable of removing heavy metals, chemicals, physical and microbial contaminants in domestic wastewater. Therefore, beneficiated kaolin clay, silver and zinc nanocomposite adsorbents will be of interest in this research work considering their enormous surface area and enhanced porosity which is expected to ensure the availability of enhanced surface-active sites.

1.5 Scope of the Study

The scope of this research covers the development of kaolin clay, silver oxide and zinc oxide nanocomposite filter using clay from Kutigi in Lavun Local Government Area of Niger State, Nigeria, for domestic wastewater treatment. Biomolecules present in the *Mangifera indica* leaf extracts were used to reduce silver and zinc metal ions to nanoparticles in a single-step green synthesis process. The performance evaluation of the produced nanocomposite filter for the removal of the selected physicochemical and bacteriological contaminants in the domestic wastewater were carried out.

CHAPTER TWO

2.0 LITERATURE REVIEW

2.1 Water Pollution

Water pollution is the contamination of water bodies, usually because of human activities. Water bodies include lakes, rivers, oceans, aquifers, and groundwater. Water pollution results when contaminants are introduced into the natural environment. Releasing inadequately treated wastewater into natural water bodies can lead to degradation of aquatic ecosystems. The people living downstream may use the same polluted river water for drinking, bathing, and irrigation farming which can lead to public health problems. Water pollution is the leading worldwide cause of death and diseases like Cholera, Dysentery, Typhoid, Diarrhoea, Hepatitis, and Jaundice (Thyagaraju, 2016).

Freshwater pollution is prevalent and increasing in many regions worldwide. 844 million people worldwide lack basic water service, and 2.1 billion people lack water accessible on premises, available when needed and free from contamination. The global population using at least a basic drinking water service was 89 % in 2015. Preliminary estimates of household wastewater flows, from 79 mostly high and high-middle-income countries, show that 59 % are safely treated. For these countries, it is further estimated that the safe treatment level of household wastewater flows with sewer connections and on-site facilities are 76 % and 18 % respectively (UN-Water, 2018). However, water and sanitation coverage rates in Nigeria are amongst the lowest in the world.

Water, Sanitation and Hygiene National Outcome Routine Mapping (WASHNORM) showed that only 14 % of the Nigerian population has access to safely managed drinking water supply services. Safely managed drinking water supply services increase from the

North to the South, with the Northeast having the lowest access at 2 % and the Southwest having the highest at 31 %. Two-thirds of the Nigerian population (66 %) use drinking water supplies contaminated by thermo-tolerant coliform at the point of collection and a similar proportion (63 %) ingest contaminated water at the point of consumption within the household (WASHNORM, 2019). This study will develop a kaolin clay nanocomposite filter capable of removing heavy metals, chemicals, physical and microbial contaminants from domestic wastewater to an acceptable level.

2.2 Domestic Wastewater Management in Nigeria

The availability of water resources is intrinsically linked to water quality. Increased discharges of untreated sewage, combined with agricultural runoff, little or nonexistence of wastewater treatment from households, and inadequate treatment of wastewater from industry have resulted in the degradation of water quality around the world. If current trends persist, water quality will continue to degrade over the coming decades, particularly in resource-poor countries, and this will further endanger human health and ecosystems.

On average, high-income countries treat about 70 % of the municipal and industrial wastewater they generate. That ratio drops to 38 % in upper-middle-income countries and to 28 % in lower-middle-income countries. In low-income countries, only 8 % undergo treatment of any kind (WWDR, 2017). These estimates support the often-cited approximation that, globally, over 80 % of all wastewaters is discharged without treatment. In high-income countries, the motivation for advanced wastewater treatment is either to maintain environmental quality or to provide an alternative water source when coping with water scarcity. However, the release of untreated wastewater remains a

common practice, especially in developing countries like Nigeria, due to a lack of infrastructure, technical and institutional capacity, and financing.

Wastewater management in Nigeria remains an environmental problem that is becoming more complex daily. Information about wastewater sources, generation rates, and composition are important as they help in the general planning for an integrated wastewater management system (Adewole, 2006). Every community produces liquid waste in Nigeria. Many industries in Nigeria discharge their wastewater into river water bodies without any form of remediation or treatment. The bulk of the domestic wastewater is discharged into the receiving waters without proper treatment in both rural and urban areas. This has several deleterious consequences such as using polluted water for irrigation farming in Nigeria. National Water Quality Reference Laboratory (NWQRL) water quality monitoring activities report showed that the proportion of rivers, lakes, and dams with good ambient water quality in Nigeria was 46 % in 2020 (NWQRL, 2020). The report revealed that a good number of Nigerian rivers, lakes, and dams are contaminated due to pollution from domestic wastes especially raw sewage and faecal matter. The report further revealed indiscriminate wastewater discharge (Domestic and Industrial), open defecation, and refuse dumping on rivers, gutters, and waterways as the major sources of pollution to Nigeria's freshwater. The report exposed urban cities as the major culprits in polluting Nigeria's freshwater as every river that passes through major cities in Nigeria is heavily polluted because of human activities (NWQRL, 2020) and the non-availability of domestic wastewater treatment plants in most of Nigeria's cities.

Piped sewerage is almost non-existent in Nigeria. The sanitation delivery is therefore poor with no urban centre having a sewerage system except some parts of Abuja which is the Federal Capital Territory and Lagos which is the former Nigerian Headquarters. There is a lack of comprehensive strategy for the disposal of excreta, wastewater, and

solid waste in Nigeria. The wastewater collection and available treatment in many parts of Nigeria are mainly decentralised with onsite facilities such as Ventilated Improved Toilets (VIP), septic tanks, and Imhoff tanks which in most cases are soak-away pits. These wastewater treatment facilities are private and owned by property owners (landlords). The soakaway is designed and constructed together with the houses and the subsequent management of this facility is left in the hands of the landlord. The wastewater treatment in this regard includes dislodging of the sludge when the septic tank is full or overflowing, and repair of breakages and leakage.

Wherever there is a nearby water course or a natural stormwater drain, the nearby households or industries take advantage of the proximity of such a watercourse or stormwater drain and utilize it for the disposal of their wastewater. The crucial event in discharging wastewater into drains is that most of the time when no rainfall events are occurring, wastewater seeps directly into the soil causing serious pollution of both the soil formation as well as the groundwater aquifers. In cases where the hydraulic capacity of the wastewater receiving area cannot accommodate the discharged wastewater, spillage of this wastewater may occur into the surrounding sites.

Domestic wastewater pollution in Nigeria leads to severe economic and social consequences such as the destruction of fish life by poisonous substances; excess organic loads reduce the dissolved oxygen in the water to a critical level and impair the chemical content of the water as seen in most of the Niger Delta communities.

2.2.1 Wastewater health implication

Health hazards caused by exposure to heavy metals, chemicals, physical and microbial contaminants in wastewater have generated public interest in recent times and calls for resolute efforts in research and development programmes in wastewater treatment. Some

constituents in wastewater, especially when untreated, can be a severe risk to human health. The two fundamental reasons why wastewater should be properly managed include the prevention of pollution of water sources and the protection of public health by safeguarding the environment against the spread of diseases. Wastewater that is discharged to the environment is the prime breeding site for mosquitoes, houseflies, rodents, and other vectors of communicable diseases such as dysentery and diarrhoea.

Poorly drained household wastewater could collect at the foot of buildings, commonly along fence lines, building frames, and foundations leading to cracks and eventually collapse of the structure. The most common health hazards associated with domestic wastewater include diseases caused by viruses, bacteria, and protozoa that may get washed into drinking water supplies or receiving water bodies (Idris-Nda *et al.*, 2013).

Microbial pathogens have been identified as critical factors contributing to numerous waterborne disease outbreaks. Many of these pathogens found in domestic wastewater can cause chronic diseases with long-term health effects such as stomach ulcers and degenerative heart disease. Chronic exposure to toxins produced by these organisms can lead to health problems like liver damage, gastro-enteritis, skin irritation, nervous system impairment, and liver cancer in animals (Idris-Nda *et al.*, 2013).

The presence of toxic metals in water sources especially shallow wells, rivers, and streams of small-scale mining areas in the country is a threat to both the environment and human health. Acute lead poisoning in Zamfara State, Nigeria in 2010 led to illness and deaths of more than 400 children mostly under 5 years old in Bukkuyum and Anka Local Government Areas (Roadmap, 2022; Lo *et al.*, 2010; Galadima and Garba, 2012). Also, Mines invariably contaminate surface and groundwater, even when mines have containment systems in place (Muhammad *et al.*, 2014).

Mercury poisoning of fish in water is transferred to humans through fish consumption. This can result in serious human intoxication and deaths following consumption of contaminated fish and polluted water. Currently, there is a very rampant kidney disease in Maiduguri, Borno State, Nigeria which might be associated with the consumption of mercury-polluted water. Consumption of water with intolerable levels of copper ions has also reportedly caused gastrointestinal disturbances, abdominal pains, nausea, and vomiting (Aguilar *et al*., 2009).

Wastewater and its nutrient contents can be used for crop production, thus providing significant benefits to farming communities and society in general. However, wastewater use can also impose negative impacts on communities and ecosystems. Eutrophication due to excessive amounts of nutrients contributes to the depletion of dissolved oxygen (Okereke *et al.*, 2016). Farmers are affected by direct contact with contaminated wastewater, and its use in agriculture causes negative externalities both to public health through the consumption of agricultural produce irrigated with wastewater (Odigie, 2014).

Emerging pollutants (EPs) present a new water quality challenge with potentially serious threats to human and ecosystem health. They include a wide range of chemical pollutants such as pharmaceuticals, personal care products, and pesticides as well as many others that are not routinely monitored. Some of them may cause chronic toxicity, endocrine disruption in humans and aquatic wildlife (Roadmap, 2022), and the development of bacteria pathogen resistance. Aquatic lives are equally affected by the presence of heavy metal ions and organic molecules in wastewater. Refinery wastewater and crude oil spills destroy aquatic life (Edema, 2012). Both micro-plastics pieces (between 2 to 5 millimetres) and macro-plastics (above 20 millimetres) often find their way into the soil

and water bodies where they endanger animals and can enter food chains with health consequences (Roadmap, 2022).

The environment has been seriously polluted by several pollutants such as inorganic ions, organic pollutants, organometallic compounds, radioactive isotopes, gaseous pollutants, and nanoparticles (Briffa *et al.,* 2020). Other health hazards of consumption of polluted water include impairment of the cardiovascular system and reproductive problems caused by Atrazine in runoff from herbicides used on crops (Pathak and Dikshit, 2011).

Having realised the dangers inherent in the indiscriminate discharge of wastewater in Nigeria and in a bid to protect the environment from pollution arising from wastewater discharge, the National Environmental Standard Regulations and Enforcement Agency (NESREA) in Nigeria came up with the effluent discharges, irrigation, and reuse standards. According to NESREA (2011), liquid industrial effluents are to be treated before it is released into the environment. This is contained in the official gazette of the Federal Republic of Nigeria, Government notice No. 136 of 24 May 2011. The effluent maximum limits as contained in the standard are presented in Table 2.1.

Table 2.1: Effluent Limitation Guidelines in Nigeria for all Categories of Industries

Parameters	**Effluent Discharges, Irrigation, and Reuse Standards**	**Quality Criteria Standards for Fisheries and Recreation**
pH	6.5 – 8.5	6.5 – 8.5
Suspended solids	0.75	0.25
Dissolved Oxygen	Minimum 4.0	Minimum 6.0
BOD5	6.0	3.0
COD	30.0	30.0
NH_4^+	2.0	0.05
NO_2^-	0.08	0.02
Phosphates (as PO_4^{3-})	3.5	3.5
Cl^-	350	300
SO_4^{2-}	500	100
Oil and Grease	0.1	0.01
Na+	120	120
K+	50.0	50.0
Ca^{2+}	180	180
Mg^{2+}	40.0	40.0
Total Iron (Fe^{2+}/Fe^{3+})	0.5	0.05
Hg	0.0005	0.001
As	0.05	0.05
Pb	0.1	0.01
Cd	0.01	0.005
Cr^{6+}	0.5	0.001
Cr^{3+}	0.5	0.5
Ni	0.1	0.01
Cu	0.01	0.001
Al	0.2	0.2
Zn	0.2	0.01
CN^-	0.05	0.001
Phenols	0.25	0.001
Coli index/l	100	50
Coli count (lactose positive)/l	5000	20
Coliphages/l	100	100
Pathogens/l	Must be absent	Must be absent

Source: NESREA (2011)

2.2.2 Domestic wastewater

Domestic wastewater is defined as all wastewater produced during different human activities (Kujawa and Zeeman, 2006)**.** It is the liquid component of waste removed from residences, businesses, and institutions. However, it may also include liquid waste from

industrial establishments in many areas. Untreated wastewater impacts water quality and public health through high bacterial loads, nutrient discharge, biological oxygen demand, and salinity. Excessive nutrient from sewage contributes to the growth of algae which is known to cause problems for vessel operators, particularly within marina basins.

Sewage consists of household waste liquid from toilets, baths, showers, kitchens, sinks (Cigdem, 2010), and other liquid that is disposed of via sewers. A lot of sewage also includes some surface water from roofs or hard-standing areas. Municipal wastewater therefore may include stormwater runoff due to the combined sewer system. Black water is a concentrated version of domestic sewage, with a chemical oxygen demand (COD) of around 1000 mg/L and a Total Kjeldahl Nitrogen (TKN) content of around 170–200 mg/L (Hocaoglu *et al*., 2010). It contributes to nutrient build-up in ecosystems that result in changes to habitat and the proliferation of nuisance species. Blackwater is a relatively recent term used to describe wastewater containing faecal matter and urine (Cigdem, 2010). Besides, blackwater contains pathogens requiring decomposition before they can be released safely into the environment, and it is difficult to process blackwater if it contains a large quantity of excess water. Black water contains most of the pathogens, hormones, and pharmaceutical residues (Marthe *et al.*, 2010). The volume of black water depends on the type of toilet and the amount of water needed to flush. Greywater is usually kept separate from blackwater to reduce the amount of water that gets heavily polluted.

Greywater is the wastewater generated from domestic activities such as dishwashing, laundry, and bathing. Greywater comprises 50–80 % of residential wastewater generated from all the house's sanitation equipment except for the toilets (Cigdem, 2010). Grey water is an abundant resource in residential, office, and commercial buildings. Greywater

harvesting is the practice of directing greywater to the primary root zone of perennial plants to help grow beautiful and productive landscapes while achieving wastewater treatment without using energy or chemicals (Brain *et al.*, 2015). Though not suitable as drinking water, greywater can be used for irrigation, particularly for trees and shrubs whose woody stems serve as additional filters for contaminants that may be present (Ludwig, 2012).

Separation of blackwater and greywater is accomplished nowadays within all ecological buildings. In recent years, concerns over dwindling reserves of groundwater and overloaded or costly sewage treatment plants have generated much interest in the reuse or recycling of greywater, both domestically for flushing toilets and use in commercial irrigation (Cigdem, 2010). This research work will develop a nanocomposite filter to treat domestic wastewater collected from toilets, baths, showers, kitchens, sinks, and other liquid that is disposed of via sewers.

2.3 Wastewater Treatment Technique

Wastewater treatment relies on several treatment stages to remove multiple contaminants which are either chemical or microbiological. The wastewater treatment goal is to reduce or remove organic matter, solids, nutrients, disease-causing organisms, and other pollutants from wastewater.

2.3.1 Conventional wastewater treatment processes

Conventional wastewater treatment consists of a combination of physical, chemical, and biological processes and operations to remove solids, organic matter, and sometimes, nutrients from wastewater (Al-Rekabi *et al.*, 2007; WRC, 2015). Conventional wastewater treatment processes rely on chemical coagulants, gravity sedimentation, and

sand or membrane filtration to remove particulate matter from the wastewater stream. The removal of pathogens is augmented by oxidants to inactivate and prevent their replication via the addition of chemicals such as chlorine (Westerhoff *et al.*, 2016). Conventional treatment techniques for removing dissolved heavy metals include chemical precipitation, carbon adsorption, ion exchange, evaporations, and membrane processes (Rajasulochana and Preethy, 2016).

The selection of the treatment method to be used depends on the wastewater characteristics. Each treatment method has its constraints not only in terms of cost but also in terms of feasibility, efficiency, practicability, reliability, environmental impact, sludge production, operation difficulty, pre-treatment requirements, and the formation of potentially toxic by-products (Gregorio and Eric, 2019).

Conventional methods for removing metals are either becoming inadequate to meet current stringent regulatory effluent limits or are increasing in cost. As a result, alternative, cost-effective technologies are in high demand. Gregorio and Eric (2019) listed in Table 2.2 the advantages and disadvantages of different individual techniques in conventional treatment methods.

Table 2.2: Advantages and Disadvantages of the Conventional Methods used for the Treatment of polluted Domestic Wastewater

Process	Advantages	Disadvantages
Chemical precipitation	i. Economically advantageous and efficient ii. Significant reduction in the chemical oxygen demand	i. Chemical consumption (lime, oxidants, H_2S) ii. High sludge production
Coagulation/ flocculation	i. Good sludge settling ii. Reduction in the chemical oxygen demand and biochemical oxygen demand	i. Increased sludge volume generation
Flotation Chemical oxidation	i. Efficient for removal of small particles ii. Effective destruction of pollutants and efficient reduction in colour	i. Energy cost ii. Chemicals required
Biological method	i. Efficiently eliminates biodegradable organic matter, NH_3, NH_4^+, iron	i. Requires management and maintenance of the microorganisms
Adsorption/filtration	i. Technologically simple	i. Elimination of the adsorbent (requires incineration, regeneration, or replacement of the material)
Ion Exchange	i. High regeneration of resin	i. Selective resin maintenance cost
Incineration Electrochemistry	i. Production of energy ii. Efficient technology for the recovery and recycling of valuable metals	i. Initial investment cost ii. High Initial cost of the equipment
Membrane filtration	i. Small space requirement ii. Simple, rapid, and efficient, even at high concentrations	i. High energy requirements ii. High maintenance and operation costs

Source: Gregorio and Eric (2019)

2.3.2 Biological wastewater treatment

Biological wastewater treatment occurs naturally in lakes, streams, and rivers through metabolic purification which enables the degradation of organic contaminants. Wastewater with biodegradable constituents at 0.5 Biochemical Oxygen Demand/Chemical Oxygen Demands (BOD/COD) ratio is easily treated by biological techniques (Anijiofor *et al.*, 2017). Wastewater treatment usually extends from physical treatment to biological treatment systems. Conventional anaerobic and aerobic treatments have received great attention over the past decades due to their numerous advantages (Chan *et al.*, 2009), though with some limitations.

Anaerobic treatment is used to treat high concentrations of biodegradable contaminants in wastewater such as domestic sewage, animal manure slurry, and wastes from bio-solids and food processing. This process is known as the primary method for protecting the environment because it provides a sustainable wastewater treatment when combined with another appropriate system (Anijiofor *et al.*, 2017). Anaerobic treatment yields low amounts of excess sludge. The nutrients are largely conserved in the liquid phase and can be subsequently recovered with physical-chemical processes such as precipitation and ion exchange or removed biologically (Marthe *et al.*, 2010). In particular, the anaerobic reactor with a submerged bacterial bed uses biological processes to remove organic matter and nutrients in a single reactor (Sylla *et al.*, 2018). The conventional septic tank (CST) has been the most used anaerobic system for the onsite treatment of domestic wastewater due to its economic affordability, structural and functional simplicity, and electricity-free operation (Tait *et al*., 2013). Traditional CST is easily adapted to rural areas of developing countries where there is an acute shortage of power supply. Various anaerobic biological treatment techniques to treat wastewater include Anaerobic Digestion (AD), Completely

Stirred Tank Reactor (CSTR), Up-flow Anaerobic Sludge Blanket (UASB), Up-flow Anaerobic Filter, Anaerobic Contact Process, Expanded Bed and/or Fluidized-bed Digesters, Fixed-bed Digesters, and Membrane Anaerobic Reactor System (MARS). The advantages and drawbacks of these methods are laid out in Table 2.3.

Table 2.3: Advantages and Drawbacks of Different Forms of Anaerobic Processes

Reactor Types	Advantages	Disadvantages
Anaerobic Digestion (AD)	i. Methane production, ii. High removal efficiency	i. High capital cost ii. Long start-up periods
Completely Stirred Tank Reactor (CSTR)	i. Continuous operation ii. Ease of operation	i. Very low conversion per unit volume
Upflowed anaerobic sludge blanket (UASB)	i. No support material is required	i. Long start-up period ii. Enough granular seed sludge
Up-flow Anaerobic Filter	i. Stable against organic and hydraulic shock loading ii. No electrical energy is needed	i. Requires expert design and construction. ii. Risk of clogging, depending on pre- and primary treatment
Membrane Anaerobic Reactor System (MARS).	i. Enhances biomass retention. ii. High removal efficiency	i. High retention time
Fixed-bed digester	i. Elimination of bed clogging ii. Low hydraulic head	i. Gas hold-up

Source: Anijiofor *et al.* (2017)

Aerobic biodegradation involves a process that converts oxygen to water by microorganisms to transform organic components into more simple end products (Anijiofor *et al.*, 2017). An aerobic biological treatment technique relies on microorganisms grown in an environment that is rich in oxygen to oxidize organic materials to CO_2, water, and cellular compounds. Many aerobic biological treatment techniques were developed to treat wastewater, such as Activated Sludge (AS), conventional or percolating filters**,** Rotating Biological Contactor (RBC)**,** Sequencing

Batch Reactor **(**SBR), and Membrane Bioreactor (MBR). The pros and cons of these methods are presented in Table 2.4.

Table 2.4: Advantages and Drawbacks of Using Different Types of Aerobic Processes

Reactor Types	Advantages	Disadvantages
Activated sludge process (ASP)	i. Easy to operate and install. ii. Odour-free iii. Light footprint	i. Low effluent quality ii. Higher sludge production iii. Precipitation of iron and carbonates
Conventional or percolating filter	i. High removal efficiency ii. Appropriate for small- to medium-sized communities	i. Can be blocked by precipitated ferric hydroxide and carbonates. ii. Not appropriate for the treatment of high-strength wastewaters
Rotating Biological Contactor (RBC)	i. High removal efficiency ii. Low space requirement iii. Low sludge production	i. Odour problems ii. Contact media not available at a local market
Sequencing Batch Reactor (SBR)	i. Easy to modify cycles. ii. Minor operation and maintenance	i. High energy consumption ii. Frequent sludge disposal
Membrane bioreactor (MBR).	i. High effluent quality ii. Lower sludge production	i. Aeration limitations ii. Membrane pollution

Source: Anijiofor *et al.* (2017)

Biological treatment methods are environmentally friendly for treating wastewater. Various factors, like pH, temperature, and gaseous retention time have significant effects on biological processes and should be in optimum condition for obtaining high efficiency (Anijiofor *et al.*, 2017). Conventional anaerobic and aerobic treatments have received great attention over the past decades due to their numerous advantages such as low energy consumption, low chemical consumption, low sludge production, vast potential for resource recovery, less equipment required, and high operational simplicity. However, conventional anaerobic and aerobic systems are found to have operational limitations in terms of long Hydraulic Retention Time (HRT), space requirement, and facilities to

capture biogas (Chan *et al.*, 2009). The applications of newly developed nanocomposite filter pots will address the limitations identified in the use of conventional anaerobic and aerobic systems concerning space, odours, and minimal sludge production. With simple nanotechnology, it is envisaged that the nanocomposite filter pots will be able to treat a wide range of high organic strength domestic wastewater.

2.3.3 Pressure-driven membrane processes

The ever-rising global demand for high-quality and sustainable water accelerates the concerns about the eco-friendly purification and reuse of wastewater (Guo *et al.*, 2019). The persistence of certain organic-micro pollutants (OMP) in conventional wastewater and reclamation treatments represents a growing concern due to its associated uncertain effects on human health and the environment (Echevarría *et al.*, 2020). Recently, the application of direct pressure-driven membrane filtration for centralized municipal wastewater reclamation has been given more attention. These pressure-driven membrane processes include microfiltration, ultrafiltration, nanofiltration, and reverse osmosis (Echevarría *et al.*, 2020; Al-Rekabi *et al.*, 2007).

The number of pressure-driven membrane processes is finding increased use for advanced water treatment because of their relatively low labour cost (Al-Rekabi *et al.*, 2007). Nanofiltration is a pressure-driven membrane process that lies between ultrafiltration and reverse osmosis in terms of its ability to reject molecular or ionic species. Nanofiltration membranes, organic membranes, or ceramic membranes can be either dense or porous. Nanofiltration membranes may have a larger free space, small pores, or nanovoids (Crespo, 2010; Baker, 2012; Van der, 2009) available for transport. The size of these nanovoids forms a transition between microporous and dense membranes that can be in the range of 0.5 - 1 nm (Baker, 2012).

The major problems of membrane filtration processes are high energy cost, high maintenance cost, and high cost of chemical consumption for biocides, cleaning, and anti-scaling agents. The factors that influence the permeate quality and membrane performance during direct pressure-driven membrane filtration are the types of membrane along with material, pore size, pre-treatment of feed water, and fouling control methods (Hube *et al*., 2020). Fouling is a major challenge experienced in pressure-driven membrane filtration processes due to the relatively higher amounts of organic matter and particulates when treating wastewater. Fouling can lead to an increase in operational costs due to higher feed pressures and a decrease in membrane lifetime due to more frequent physical and chemical cleanings (Anis *et al*., 2019). This research work will reduce the amount of organic matter and particulate through the inclusion of a pre-filtration tank in the design of the nanocomposite filter. Doing this will address the limitation of fouling being experienced through the use of pressure-driving membrane techniques.

2.3.4 Adsorption

Adsorption is a widely used method for the treatment of industrial wastewater containing colour, heavy metals, and inorganic and organic impurities (Bora and Dutta, 2014). Adsorption is found to be one of the effective methods for the removal of toxic heavy metals from industrial waste effluents (Amandeep and Sangeeta, 2017). This method appears to be more suitable for domestic wastewater because of its advantages. Some of these advantages include simplicity in operation, inexpensive, and without sludge formation compared to other separation processes. Adsorption is known to be a promising technique, which produces good quality effluents with low levels of dissolved organic compounds such as dyes, acid dyes, basic dyes, methylene blue, and reactive azo dye (Dhaval and Painter, 2017). Adsorbent treatment processes include activated carbon.

Activated carbon is a low-cost adsorbent and has a high adsorption capacity. Activated carbon is a carbonaceous, highly porous adsorptive medium that has a complex structure composed primarily of carbon atoms. Activated carbon has been used in the fields of purification including water. Activated carbon is effective in removing contaminants and adsorbing pollutants from wastewater (Muharrem and Kaplan, 2017). Because of the large surface area and high number of pores, activated carbons have been used for heavy metals removal. The activated carbon is very expensive (Mohd *et al.*, 2013) and not easy to regenerate due to rapid saturation and clogging of the reactors (Gregorio and Eric, 2019).

Edwin *et al.* (2017) prepared activated carbon (AC) using locally available agricultural wastes like rice husk and sugarcane bagasse. These were used as adsorbents for the removal of chromium from potassium dichromate solution. Batch mode adsorption studies were carried out by varying contact time, adsorbent dosage, and pH. Langmuir and Freundlich adsorption isotherms were applied to model the adsorption data. The adsorption of chromium was pH dependent and maximum removal was observed in the acidic pH range.

Erhan (2017) obtained Talc and chrysotile from Sivas, Turkey, and used as adsorbents for the investigation of the adsorption of the basic dye from aqueous solutions at various dye concentrations (100 – 400 mg/L), initial pH (3 – 7), adsorbent doses (1 – 4 g/L), contact time (2.5 – 1400 min) and temperatures (313 – 333 K). The result showed that the adsorption capacity of the dye increased with increasing initial dye concentration, pH, adsorbent dose, and temperature.

Dina *et al.* (2015) examined the influence of textural and some physicochemical properties of two clays smectite and kaolin in the removal of lead (II) ions in aqueous

solutions. The influence of some environmental parameters such as pH, contact time, and initial concentration was examined. Batch sorption studies showed that the Langmuir model gives a better fit for the smectite and kaolin clays compared to the Freundlich adsorption isotherm. This study also revealed that the properties of the clays strongly influence the sorption of lead (II) ions.

The use of heavy metals in the manufacturing industry over the past few decades has eventually contributed to a rise in the flow of metallic compounds into wastewater and has raised significant ecological and health threats to living things (Syafiqa *et al.*, 2021). Adsorption is an excellent way to treat solid waste effluent, offering significant benefits such as affordability, profitability, ease of operation, and efficiency. However, the price of commercial adsorbents such as activated carbon has soared due to its high demand. This research work will produce a nanocomposite filter pot using locally available kaolin clay. Doing this will address the limitation of the high cost of material being experienced with commercial adsorbents such as activated carbon. Adsorption and filtration treatment techniques have the potential to remove the contaminants in domestic wastewater.

2.3.5 Filtration

Filtration is the process of passing water through the material to remove particulates and other impurities from the water being treated. Filtration processes can generally be classified as being either slow or rapid. Filtration is essentially a physical and chemical process according to the Environmental Protection Agency (EPA) of the United State of America (EPA, 2020). These removal mechanisms include processes such as straining, sedimentation, impaction, interception, adhesion, flocculation, and biological growth (Hussaini *et al.*, 2015). The actual removal mechanisms are interrelated and rather complex, but the removal of colour and turbidity is based on the chemical characteristics

of the water being treated (particularly source water quality), nature of suspension (physical and chemical characteristics of particulates suspended in the water), type and degree of pre-treatment (coagulation, flocculation, and clarification) and filter type and operation.

The relative importance of the filtration will depend largely on the nature of the water being treated, choice of filtration system, degree of pre-treatment, and filter characteristics (EPA, 2020). Biological growth within the filter will reduce the pore volume and may enhance the removal of particles with any of the removal mechanisms. Substances collected on the surface of the filter medium plus available nutrients make the organisms grow on the surface of the filter. A mat is formed containing slimy ‘’zoogleal’’ organisms known as ‘’Schmutzdecke’’. Schmutzdecke helps in the straining action of the filter but must be removed when the head loss through the filter is high and it is undesirable in a rapid sand filter because it encourages the formation of mud balls during backwashing.

Slow sand filters are a relatively simpler construction than rapid sand filters. In the slow sand filter, a bed of sand 0.9 m deep rests on graded gravel in which underdrains of open-jointed tiles are buried (Hussaini *et al.*, 2015). The sand is carried to the full depth of the bed near the outer walls and to avoid carrying it into the underdrains, no pipes should be laid within 0.6 m of the wails. The sand is normally finer than that in a rapid filter and its quality and grading are less exacting.

Pressure filters are like rapid filters but are enclosed in pressure vessels and are normally used where hydraulic conditions in the system make their adoption desirable (Hussaini *et al.*, 2015). They can be installed at any point in a pressure pipeline without unduly

interfering with the hydraulic gradient and often eliminate the need for double pumping. They do not usually follow settling basins and use coagulants to aid their performance.

A mixed media filter is a refinement of the rapid gravity sand type. Instead of a bed of sand supported on gravel with particles of somewhat similar density but greater size, various layers consisting of media of different densities are used. As a result, a very coarse upper layer of lightweight material (anthracites or pumice) can provide increased void space to store the impurities removed from the incoming water (Hussaini *et al.*, 2015). Under normal operating conditions, with the turbidity of the incoming water less than 5 NTU the performance is better, and the filter runs are longer than for the rapid gravity sand filter. Incoming water of 30 – 50 NTU turbidity can be treated in an emergency (Hussaini *et al.*, 2015).

The Iraq-type filter was developed for small-town use in Iraq in 1954. It is a rapid gravity sand filter of very simple construction, in which all controls are eliminated, and automatic operation is attained by the simple expedient of building the pure water tank with its top water level to coincide with that in the filter. It is extremely cheap and effective but does not easily lend itself to scaling up in larger installations (Hussaini *et al.*, 2015).

The green leaf filters are rapid gravity filters that are controlled by an automatic controller, the outlets are controlled by weirs, and the additional head required to maintain uniform flow is supplied by a rise in water level above the sand (Hussaini *et al.*, 2015).

Diatomite filters are not commonly found on waterworks. They are compact, high-efficiency filters that are suitable for meeting short-term emergencies. They are small and portable and depend on the deposition of filter powders of diatomaceous earth on porous filter ‘candles’ for their filtering action (Hussaini *et al.*, 2015). They cannot deal with highly turbid water and because of extremely high head losses in the filter, their running

costs are high. For most practical waterworks applications, they would probably prove to be less satisfactory than other methods.

The filtration method can remove heavy metal ions with high efficiency, but high cost, process complexity, membrane fouling, and low permeate flux have been the major drawbacks in their use in heavy metal ions removal (Fu and Wang, 2011). Pressure-driven membrane filtration processes have high energy costs, high maintenance costs, and high cost of chemical consumption for biocides, cleaning, and anti-scaling agents. Wastewater contaminants are harmful to human health and therefore must be removed before discharging into the environment. The nanocomposite filter pots to be developed in this research work target the removal of contaminants from domestic wastewater to acceptable limits before discharging into the environment.

2.3.5.1 *Design considerations for nanofilter*

Several designs of filters for the treatment of wastewater have been developed. Most of the designs are based on the treatment of potable water from raw water. Little has been done on the development of clay filter pots for continuous treatment of domestic wastewater. Some of the general design questions that need to be addressed in designing a filter for domestic wastewater treatment are as follows:

What are the appropriate flow schemes?

What minimum filter run length is acceptable?

What filter configurations are appropriate for wastewater?

Is pilot scale testing needed, and if so, how should it be conducted?

What filtration rate and terminal head loss should be provided?

What filter media size and depth should be provided?

Should gravity or pressure filters be provided?

What system of flow control should be used?

What backwash provisions are needed for each filter media alternative being considered to ensure effective backwashing in the long term?

What under-drain system is appropriate for the media and backwash regime intended?

Tommy *et al.* (2007) in their paper described a framework for water filter design including the results from a pilot study of three technologies and an extensive technical and social evaluation of the *Kanchan* Arsenic Filter (KAF). The KAF is an innovation that combines two proven water treatment techniques – arsenic adsorption on ferric hydroxide and microbial removal by the slow sand filtration process. The KAF was found to be technically appropriate for the water conditions generally encountered in the Terai region of Nepal. The KAF can treat both groundwater and surface water. The nanocomposite filter to be developed in this research work will remove 100 % of total coliform, faecal coliforms, *E. coli* and *Clostridium perfringes* from domestic wastewater.

2.3.6 Source separation

Source separation offers the possibility of nutrient recovery and reducing the release of micropollutants to the environment. Three waste streams of urine, greywater, and blackwater are identified for source separation. Urine is only 1 % of the domestic wastewater stream but contains 50 – 80 % of the nutrients (nitrogen, phosphorus, and potassium) and the majority of pharmaceuticals and hormones (Kimberly, 2015). Black water has high organic and nutrient content, solids, and pathogens. Gray water is the largest contributor to total wastewater volume but is the least contaminated of the three streams (low in nutrients and pathogens but contains detergents and personal care products). In the absence of kitchen wastewater, greywater is also low in organic content.

When these streams are separated at the source, maximum reuse of water is achieved with minimal treatment.

2.4 Particulate Solids

Total suspended solids (TSS) are particles that are larger than 2 microns found in the water column. Anything smaller than 2 microns (average filter size) is considered a dissolved solid. Most suspended solids are made up of inorganic materials, though bacteria and algae can also contribute to the total solids' concentration (Fondriest, 2014).

Particulate solids include anything drifting or floating in the water, from sediment, silt, and sand to plankton and algae. Organic particles from decomposing materials can also contribute to the TSS concentration. As algae, plants, and animals' decay, the decomposition process allows small organic particles to break away and enter the water column as suspended solids. Even chemical precipitates are considered a form of suspended solids. Total suspended solids are a significant factor in observing water clarity. The more solids present in the water, the less clear the water will be.

The three most important characteristics of an individual particle are its composition, its size, and its shape. Composition determines such properties as density and conductivity, provided that the particle is completely uniform. In many cases, the particle is porous, or it may consist of a continuous matrix in which small particles of a second material are distributed. Particle size is important in that this affects properties such as the surface per unit volume and the rate at which a particle will settle in a fluid. A particle shape may be regular, such as spherical or cubic, or it may be irregular as with a piece of broken glass. Regular shapes are capable of precise definition by mathematical equations. Irregular shapes are not, and the properties of irregular particles are usually expressed in terms of some particular characteristics of a regular-shaped particle. In processes such as the

sedimentation of particles in a liquid, each particle is surrounded by fluid and is free to move relative to other particles. Only very simple cases are capable of a precise theoretical analysis and Stokes' law, which gives the drag on an isolated spherical particle due to its motion relative to the surrounding fluid at very low velocities, is the most important theoretical relation in this area of study. Indeed, many empirical laws are based on the concept of defining correction factors to be applied to Stokes' law.

According to Stokes' law, the particle sedimentation velocity is proportional to the density difference between the solid phase and the liquid phase inversely proportional to the viscosity of the liquid, and proportional to the square of particle diameter (Shuying *et al.*, 2021). Some suspended solids can settle out into sediment at the bottom of a body of water over some time. Heavier particles, such as gravel and sand, often settle out when they enter an area of low or no water flow.

When settleable solids are moved along the bottom of a body of water by a strong flow, it is called bedload transport. Settleable solids are also known as bedded sediments, or bedload (Fondriest, 2014). These settleable solids are removed from the wastewater by sedimentation.

2.4.1 Sedimentation

Sedimentation is the unit operation in which suspended materials are removed from the liquid phase by gravity settling. Historically, sedimentation has been, and continues to be the most common treatment method used in both water and wastewater treatment systems. Common applications of sedimentation in water treatment include pre-treatment of surface water before conventional water treatment, settling of coagulated and flocculated waters before filtration, settling of coagulated flocculated waters in chemical water softening, and settling of waters treated for iron and manganese removal. In

wastewater treatment, the principal uses of sedimentation are for the removal of grit and other coarse solids of suspended solids before biological treatment and of the biological solids produced during biological treatment.

2.4.2 Sedimentary theory

Conceptually, sedimentation operations are quite simple in both water and wastewater treatment. In the idealized system, particles move horizontally with the flow and vertically under gravitational forces. Consideration is given to the forces acting on an isolated particle moving relative to a fluid and it is seen that the frictional drag may be expressed in terms of a friction factor which is, in turn, a function of the particle Reynolds number. If the particle is settling in the gravitational field, it rapidly reaches its terminal falling velocity when the frictional force has become equal to the net gravitational force. In a centrifugal field, the particle may reach a much higher velocity because the centrifugal force may be many thousands of times greater than the gravitational force (Jovanovic and Mujkanovic, 2013).

The collected kaolin clay samples in this study will be pre-treated to remove debris and air-dried at room temperature. The purification of the pulverized oven-dried kaolin clay will be done by sedimentation technique to produce clay fraction of less than 2 μm (< 2 μm) diameter and removal of excess nonclay impurities. The settling velocity of small spherical kaolin clay particles in the fluid medium is calculated using the Stoke's Law Equation. The force balance for a discrete particle that is settling during the production of nano clay through the sedimentation techniques in this research work is represented by Equation 2.1.

$$m_p \frac{dUs}{dt} = F_G - F_B - F_D \qquad (2.1)$$

Where;

m_p = mass of settling particles, kg

dUs = change in particle settling velocity, m/s

F_G = gravitational force, N

F_B = buoyant force, N

F_D = drag force, N

dt = change in Time

The net gravitational force is given in Equation 2.2.

$$F_G - F_B -= (\rho_p - \rho_w) g V_p \quad (2.2)$$

Where;

ρ_p = density of particles, kg/m^3

ρ_w = density of water, kg/m^3

g = acceleration due to gravity, m/s^2

V_p = volume of particles ($\pi \frac{d_p^3}{6}$), m^3

d_p = diameter of particle, m

The drag force is a function of the cross–sectional area of the particle, the settling velocity of the particle, the liquid density, and the coefficient of drag. The drag force $(F_D)$is expressed as given in Equation 2.3.

$$F_D = C_D A_p \rho_w \frac{u_s^2}{2} \quad (2.3)$$

Where;

C_D = coeeficient of drag

A_p = cross – sectional area of particle($\pi \frac{d_p^2}{4}$), m^2

ρ_w = density of water, kg/m^3

u_s = particle settling velocity, m/s

For spherical particles, the coefficient of drag (C_D) is estimated using the relationship in Equation 2.4 and Reynolds number (N_R) expressed in Equation 2.5.

$$C_D = \frac{24}{N_R} + \frac{3}{\sqrt{N_R}} + 0.34 \quad (2.4)$$

Where;

N_R = Reynolds number, dimensionless

$$N_R = \frac{u_s d_p \rho_w}{\mu} \quad (2.5)$$

μ = liquid viscosity, kg/m. s and other terms are as defined previously,

In the ideal system, the terminal settling velocity is attained quickly, and the acceleration term is assumed to be negligible. Thus Equation 2.1 is rewritten as Equation 2.6.

$$F_G - F_B = F_D \quad (2.6)$$

Substituting Equation 2.2 for $F_G - F_B$ and Equation 2.3 for F_D and solving for the settling velocity u_s yields Equation 2.7.

$$the\ u_s = \sqrt{\frac{4}{3}\frac{g(\rho_p - \rho_w)d_p}{C_D\rho_w}} \quad (2.7)$$

Where d_p is the diameter of the particle in meters, and the other terms are as defined previously. When $N_R < 0.3$, the first term of Equation 2.4 predominates, and the discrete particles settling rate becomes Stoke's law as shown in Equation 2.8.

$$u_s = \frac{g(\rho_p - \rho_w)d_p^2}{18\mu} \quad (2.8)$$

2.5 Nanotechnology

Nanotechnology uses particles that are 1/80,000 the diameter of a human hair (Sulekha, 2016). At such a small scale, new physical, chemical, and biological properties become evident (Kovo and Edoga, 2005). The emergence of nanotechnology has given rise to the production and utilization of nanosized materials for use in the removal of wastewater pollutants. The most important characteristics of the nanosized particles that make them ideal as adsorbents are small size, catalytic potential, high reactivity, large surface area per mass, ease of separation and large number of active sites for interaction with different contaminants (Ali, 2012). These properties are responsible for high adsorption capacities by increasing the surface area, free valence, and surface energies of nanoparticles. The most used nanoparticles for the removal of metal ions include oxides of silver oxide (Ralf *et al.*, 2011), zinc oxide (Ming *et al.*, 2012), and titanium (Ali, 2012). Metallic silver nanoparticles (Ag-NPs) have received considerable attention for their potential application as a biocide in products ranging from facade paints to textiles. The antibacterial activity of silver has been known for centuries and has led to the development of several Ag-based bactericidal products (Ralf *et al.*, 2011). As an environmentally friendly material, zinc oxide nanoparticles (ZnO-NPs) are used in wastewater treatment because of their strong anti-microbial activities. As an adsorbent,

ZnO-NPs were mostly applied to eliminate hydrogen sulphide and recently, people have found that nanostructured zinc oxide could efficiently remove heavy metals (Ming *et al.*, 2012), removal of Chromium VI (Rui *et al.*, 2013), enhance adsorption of lead ion (Susan *et al.*, 2017; Yang *et al.*, 2008) and recently used as an antibacterial application (Getie *et al.*, 2017; Haritha *et al.*, 2011; Ying *et al.*, 2017; Stoyanova *et al.*, 2013). The unique material properties that emerge at the nanoscale enable solutions to treat pollutants in water for which existing technologies are inefficient or ineffective (Westerhoff *et al.*, 2016). One of the parameters that are strongly connected to miniaturization and nanotechnology is the surface-to-volume ratio. This parameter is of fundamental importance in applications involving chemical catalysis and nucleation of physical processes (Hossam, 2017).

2.5.1 Silver nanoparticle

Most recently, renewed interest has risen in manufactured silver nanomaterials because of their unusually enhanced physicochemical properties and biological activities compared to the bulk parent materials. Metallic nanoparticles have attracted tremendous interest due to their unique optoelectronic and physicochemical properties (Njagi *et al.*, 2010). Their applications include use in bio-sensing, media recording, optics, catalysis, and environmental remediation. A wide range of applications has emerged in consumer products ranging from disinfecting medical devices and home appliances to water treatment (Thabet *et al.*, 2010). Metallic silver nanoparticles (Ag-NPs) have received considerable attention for their potential application as a biocide in wastewater treatment. The antibacterial activity of silver has been known for centuries and has led to the development of several Ag-based bactericidal products (Ralf *et al.*, 2011). Microbes are unlikely to develop resistance against silver, as they do against conventional and narrow-

target antibiotics because the metal attacks a broad range of targets in the organisms, which means that they would have to develop a host of mutations simultaneously to protect themselves (Sukdeb *et al.*, 2007). Ag-NPs readily transform in the environment and this modifies their properties and alters their transport, fate, and toxicity (Levard *et al*., 2012)

2.5.2 Zinc oxide nanoparticle

As an environmentally friendly material, zinc oxide is used in the catalyst industry, gas sensors, and solar cells. As an adsorbent, zinc oxide is mostly applied to eliminate H_2S. Recently, people have found that zinc oxide nanoparticles (ZnO-NPs) could efficiently remove heavy metals (Ming *et al.*, 2012). ZnO-NPs are synthesized by several different methods such as sol–gel techniques, wet chemical methods, green chemistry, and microwave method (Khushbu *et al.,* 2017). The biosynthesis of ZnO-NPs of different sizes, ranging from 1 – 70 nm, and shapes to include spherical, triangular, and hexagonal has been conducted using bacteria, fungi, and plant extracts. Synthesis of ZnO-NP involves the use of zinc chloride as a precursor. The Reagent-grade ethanol is used for the cleaning of the nanoparticles (Sierra *et al.*, 2018).

2.5.3 Green synthesis of Ag and ZnO nanoparticles

Green synthesis of nanoparticles represents an important part of nanotechnology that offers outstanding eco-friendly and financial benefits when compared to conventional methods that use toxic substances and involve complex processes (Sierra *et al.*, 2018). Metallic nanoparticles of specific sizes and morphologies can be readily synthesized using chemical and physical methods. However, these methods employ toxic chemicals as reducing agents and are therefore potentially dangerous to the environment and biological systems. The biosynthesis of nanoparticles has been proposed as a cost-

effective environmentally friendly alternative to chemical and physical methods and consequently, nanomaterials have been synthesized using microorganisms and plant extracts (Njagi *et al.*, 2010).

Biomolecules present in plant extracts are used to reduce metal ions to nanoparticles in a single-step green synthesis process. A reducing agent is a chemical agent, plant extract, biological agent, or irradiation method that provides the free electrons needed to reduce silver ions and form silver nanoparticles (Thabet *et al.*, 2010). This biogenic reduction of metal ions to base metal is quite rapid, readily conducted at room temperature and pressure, and easily scaled up (Amit *et al.*, 2013). Water-soluble organics present in the leaf are responsible for the reduction of silver ions. The reducing agents involved include various water-soluble plant metabolites such as alkaloids, phenolic compounds, and terpenoids (Daizy, 2010; Amit *et al.*, 2013).

The advantage of using plants for the synthesis of nanoparticles is that they are easily available, safe to handle, and possess a broad variability of metabolites that aid the production of nanoparticles. In recent years plant-mediated biological synthesis of nanoparticles is gaining importance due to its simplicity and eco-friendliness (Krishan *et al.*, 2013). The use of plant extracts for the synthesis of nanoparticles is potentially advantageous over microorganisms due to the ease of scale-up, the biohazards, and the elaborate process of maintaining cell cultures.

Silver nanoparticles have been synthesized using various plant extracts including hibiscus (*Hibiscus rosa sinensis*) leaf extract, neem (*Azadirachta indica*) leaf broth, black tea leaf extracts, Indian gooseberry (*Emblica officinalis*) fruit extract, sundried camphor (*Cinnamomum camphora*) leaves, and Aloe Vera plant extract (Njagi *et al.*, 2010).

Shittu and Ikebana (2017) biologically synthesized silver nanoparticles using *Piliostigma thonningii* aqueous leaf extract and applied it in the purification of laboratory-stimulated wastewater with optimization using the different conditions of silver nanoparticle production such as time, temperature, pH, the concentration of silver nitrate and volume of the aqueous extract. The synthesized silver nanoparticle also showed heavy metal removal activity in laboratory-simulated wastewater. The use of plant material not only makes the process eco-friendly but also the abundance makes it more economical.

Sukdeb *et al.* (2007) investigated the antibacterial properties of differently shaped silver nanoparticles against the gram-negative bacterium *E. coli*, both in liquid systems and on agar plates. Energy-filtering transmission electron microscopy images revealed considerable changes in the cell membranes upon treatment, resulting in cell death.

Njagi *et al.* (2010) synthesized Iron and silver nanoparticles using a rapid, single-step, and completely green biosynthetic method employing aqueous sorghum extracts as both the reducing and capping agent. Silver ions were rapidly reduced by the aqueous sorghum bran extracts, leading to the formation of highly crystalline silver nanoparticles with an average diameter of 10 nm. The absorption spectra of colloidal silver nanoparticles showed a surface plasmon resonance (SPR) peak centred at a wavelength of 390 nm.

Benakashani *et al.* (2016) reported the synthesis of silver nanoparticles by reducing the silver ions present in the solution of silver nitrate by the cell-free aqueous extract of *Capparis spinosa* leaves. Silver nanoparticles were successfully synthesized using *Capparis spinosa* extract and the nature of synthesized nanoparticles was analysed by UV-visible spectroscopy, transmission electron microscopy, X-ray diffraction and Fourier transform infrared spectroscopy. The antimicrobial effect of nanoparticles (NPs) produced by *Capparis spinosa* was studied using different pathogenic bacteria such as *E.*

coli, Salmonella typhimurium, Staphylococcus aureus, and *Bacillus cereus*. From the disc diffusion results, the synthesized silver nanoparticles showed an excellent antibacterial property and a high antimicrobial activity compared to the ionic silver.

Vikas *et al*. (2013) described a cost-effective and environment-friendly approach to explore the synthesis of silver nanoparticles from leaf extract of *Mangifera indica*. The aqueous extract of the leaves of *Mangifera indica* was used as a reducing and stabilizing agent. The rapid reduction of silver ions was monitored using a UV-visible spectrophotometer. The synthesized silver nanoparticles showed antibacterial activity against various human pathogens such as *E. coli, Staphylococcus aureus, Pseudomonas fragi, Bacillus subtilis, Streptococcus agalactiae, and Proteus vulgaris*.

Sierra *et al*. (2018) carried out a synthesis of zinc oxide nanoparticles from leaf extracts of mango (*Mangifera indica*) and soursop (*Annona muricata*) trees, which were used as reducing agents in an aqueous solution of zinc chloride. The extracts were submitted to colorimetry analysis and Fourier-transform infrared (FTIR) spectroscopy for flavonoids, saponins, and tannins confirmation. The material that was obtained with both extracts presented a semi-spherical morphology with average diameters of 23 ± 9 nm (*Mangifera indica*) and 17 ± 4 nm (*Annona muricata*).

Daizy (2010) reported a facile and rapid biosynthesis of well-dispersed silver nanoparticles. The method developed allows the reduction to be accelerated by changing the temperature and pH of the reaction mixture consisting of aqueous silver nitrate and *Mangifera indica* leaf extract. At a pH of 8, the colloid consists of well-dispersed triangular, hexagonal, and nearly spherical nanoparticles having a size of 20 nm. The UV–visible spectrum of silver nanoparticles gave surface plasmon resonance (SPR) at 439 nm.

Maity *et al.* (2018) reported the synthesis of zinc oxide nanoparticles using *Moringa oleifera* leaves as a natural precursor via the precipitation method. The synthesized nanoparticles have a hexagonal wurtzite structure of an average grain size of 52 nm confirmed by X-ray diffraction analysis. Antibacterial activity was also studied and it was found that the synthesized ZnO nanoparticles have potential applications in antibacterial activity.

Thirunavukkarasu *et al.* (2016) prepared zinc oxide nanoparticles using *Moringa oleifera* aqueous extract from leaf, flower, and bark by green synthesis sol-gel method. Zinc Oxide Nanoparticles are analyzed by X-ray diffraction (XRD), Scanning Electron Microscope (SEM), UV-visible, and Fourier Transform Infrared spectroscopy (FTIR). Among this extract prepared from the leaf, flower, and bark of *Moringa oleifera*, ZnO nanoparticles using the bark of the plant showed sharp peaks in XRD, confirming the crystallinity of the particles.

Manokari and Mahipal (2016) investigated the bio-production and characterization of zinc oxide (ZnO) nanoparticles using leaf, stem, flowers, and fruit pods of the medicinal plant *Moringa Oleifera*. The synthesis of zinc oxide nanoparticles from the aqueous extracts was mediated by Zinc Nitrate Hexahydrate as a precursor. The absorption spectral analysis using UV-visible spectroscopy confirms the reduction of zinc ions into zinc oxide nanoparticles from herbal extracts of *Moringa. oleifera*. The formation of zinc oxide nanoparticles from leaves and flowers exhibits an absorption peak at 308 nm. The stem and fruit pods showed an absorption peak at 293 nm.

Parthibana and Sundaramurthy (2015) discussed a low-cost and simple procedure for the biosynthesis of Zinc Oxide nanoparticles (ZnO-NPs) using *Pyrus pyrifolia* leaf extract. The structural, morphological, and optical properties of the synthesized nanoparticles

have been characterized by using UV–visible spectrophotometer, XRD, and FTIR. The synthesized ZnO nanoparticles from zinc nitrate solution using *Pyrus pyrifolia* leaf extract and the biosynthesized ZnO nanoparticles were found to be almost spherical with particle size around 45 nm.

Ramesh and Arumugam (2014) used unreported, inexpensive, nontoxic, eco-friendly, and abundantly available *Citrus aurantifolia* for the rapid synthesis of ZnO-NPs in the range of 9-10 nm. The work portrays a novel method for the biosynthesis of ZnO nanoparticles using *Citrus aurantifolia* for the first time. The morphology structure and stability of the synthesized ZnO nanoparticles were studied using SEM, UV-spectrophotometer, and FTIR spectroscopy. The results depicted that the synthesized nanoparticles are moderately stable, and roughly spherical with maximum particles in size range within 9-10 nm in diameter.

Nadia and Yousef (2015) worked on the synthesis of nano-size zinc oxide for the removal of hexavalent chromium VI. Batch experiments were performed to investigate the effects of chromium (VI) concentration, pH of the solution, adsorbent dose, solution temperature, and contact time variations on the removal efficiency of chromium VI. Zinc oxide nanomaterial was synthesized by a simple heating process using polyethylene glycol (PEG). FTIR analysis and TEM microscopy were applied for the determination of particle size and characterization of produced nanoparticles.

Surya (2012) successfully synthesized ZnO-NPs by a sol-gel method. Zinc acetate dehydrate and triethanolamine were used as the precursor materials. Ethanol and ammonium hydroxide take care of the homogeneity and pH value of the solution and help to make a stoichiometric solution to get zinc oxide nanoparticles. The zinc oxide powder obtained from this method was calcined at 700 °C and 900 °C temperatures.

Robina *et al.* (2013) synthesized ZnO nanoparticles with particle sizes less than 50nm by simple sol-gel method. ZnO nanoparticles powders have been successfully synthesized by the sol–gel technique at different pH values using centrifugation.

Syamala *et al.* (2017) synthesized zinc oxide nanoparticles via a low-temperature solution combustion method using different fuels – glycine, citric acid, urea, and Raphanus sativus (radish) extract. The Direct Current (DC) conductivity studies were performed in the temperature range 320-385 K which showed the semiconducting nature of the zinc oxide nanoparticles.

Getie *et al.* (2017) synthesized various shapes and sizes of the wurtzite structure of ZnO nanoparticles via a wet chemical method for antibacterial applications. The synthesized ZnO-NPs were also modified using a biologically active compound, caffeine. The ZnO nanoparticles were investigated by XRD, SEM, FTIR, UV-visible and fluorescence spectroscopy. The average crystallite size of the ZnO-NPs using XRD was within the ranges of 28.09 – 1.86 nm. The synthesized ZnO-NPs were applied for antibacterial activity against *S. aureus* and *E. coli* bacteria using the agar disc diffusion method.

Zahra *et al.* (2015) synthesized ZnO nanoparticles by a one-step mechano-chemical process using $ZnSO_4$ and NaOH as reactants with NaCl acting as a diluent. The results of the work showed that ZnO nanoparticles can be synthesized in a one-step method using $ZnSO_4$ and NaOH as reactants and NaCl as a diluent. Heat treatment in the presence of a diluent was applied to improve the photocatalytic activity of the resultant materials. The measured particle size in the samples was approximately 50 nm.

Stoyanova *et al.* (2013) synthesized TiO_2/ZnO powders and studied their bactericidal properties. The TiO_2/ZnO nanocomposite was synthesized by a nonhydrolytic reaction between titanium (IV) chloride and zinc (II) salts in a benzyl alcohol medium. The

structure and morphology of the resulting particles were characterized by XRD, FTIR, and SEM analysis. The antibacterial effect of thus obtained composites was examined on *E. coli* bacteria.

Azizi *et al.* (2017) synthesized ZnO nanoparticles (NPs) in zerumbone solution by a green approach and were appraised for their ability to absorb Pb (II) ions from aqueous solution. The biosynthesized nanoparticles exhibited excellent adsorption for the Pb (II) ions that followed the Langmuir adsorption model and pseudo-second-order equation.

Abdullah *et al.* (2017) prepared a Zeolite/Zinc Oxide nanocomposite (Zeolite/ZnO NC) by using a co-precipitation method. The prepared sample was examined for Lead Pb (II) and Arsenic removal from aqua solutions at ambient conditions in batch adsorption systems. The obtained results revealed that the Zeolite/ZnO NC adsorbent was found to have high adsorption capacity and it could be employed as an efficient and low-cost adsorbent for the removal of heavy metals from water.

All the research works reviewed above on the synthesis of silver and zinc oxide nanoparticles were experimented with using only the batch method. The column method of wastewater treatment is not considered by any of the researchers. Furthermore, it is noticed that none of the researchers reported the blending of silver and zinc oxide nanoparticles on kaolin clay support for wastewater treatment. The green synthesis of zinc oxide nanoparticles reported by different researchers as reviewed above, has been very successful. In this research work, *Mangifera indica* leaf will be used as a reducing agent for the synthesis of silver and zinc oxide nanoparticles due to its antimicrobial ability.

2.6 Kaolin Clay Deposit in Niger State

National Bureau of Statistics (NBS) reported that Niger State produced a total of 51,149.80 tons of solid minerals in 2016 (NBS, 2017). The minerals were granite, granite dust, laterite, sand, talc, and gold (NBS, 2017; Ojo *et al.*, 2017). Kaolin is classified as a potential solid mineral in Niger State.

There is a deposit of kaolin clay in 13 local government areas in the state namely, Agaie, Bida, Bosso, Edati, Gbako, Katcha, Lapai, Lavun, Mashegu, Mokwa, Paikoro, Shiroro and Wushishi (NBS, 2017).

2.6.1 Clay minerals

Human society has been using clays and clay minerals since the Stone Age, primarily because clay minerals are common at the earth's surface and are widely utilized for agriculture (soils), ceramics (Auta and Hameed, 2013), and building materials with a very long history. Clay is used by engineering geologists and sedimentologists to describe geological materials of less than 4 μm in size, by soil scientists to denote the soil fraction containing particles of less than 2 μm size, and by colloidal scientists of less than 1 μm (Zhou and Keeling, 2013). Clays and clay minerals are important in geology, agriculture, construction, engineering, process industries, and environmental applications (Murray, 2000). The wide variety of applications include oil refining and absorbents, iron-ore pelletizing, animal feeds, pharmaceuticals, drilling fluids, beverage (Saikia *et al.*, 2003), wastewater treatment, fillers in paint and plastic, and coating paper (Zhou and Keeling, 2013). Another special application for clay is in the production of synthetic zeolites. Kaolinite can be treated with sodium, calcium, magnesium, and potassium hydroxides which when heated to a temperature of 1008 °C will convert the kaolinite to zeolite structures with different pore sizes. These synthetic zeolites are used primarily as

cracking catalysts in petroleum refining and to remove water from gas streams (Saikia *et al.*, 2003).

Clay materials have been increasingly paid attention to because they are cheaper than activated carbons and their sheet-like structures also provide a high specific surface area (Dhaval and Painter, 2017). The clay minerals kaolinite, smectite, palygorskite, and sepiolite are among the world's most important and useful industrial minerals (Murray, 2000). Increased understanding of the mineralogy, structure, and properties of clay minerals has been accompanied by rapid advances in the processing and modification of clay minerals for many new commercial uses. Mineralogists define 'clay' as a naturally occurring material composed of fine-grained minerals, which is generally plastic at appropriate water contents and will harden when dried or fired. Clays may therefore be mixtures of fine-grained clay minerals and clay-sized crystals of other minerals such as quartz, carbonate, and metal oxides.

The term 'clay minerals' however is not restricted by particle size but refers to phyllosilicate minerals and minerals that impart plasticity to clay and which harden upon drying or firing (Zhou and Keeling, 2013). The inherent features of clay minerals that make them attractive for use in a wide variety of applications include a very large surface area that arises from the layered structure, along with its swell ability and the potential for delamination.

Based on their physical properties, clay minerals are often applied as fillers and gallants. The inherent properties of clay minerals also make them chemically active and adsorptive, thereby leading to a variety of uses as absorbent and catalyst products. In clay minerals, the active sites may arise from broken edge sites and exposed surface aluminol and silanol groups, isomorphic substitutions, exchangeable cations, hydrophobic silanol

surfaces, hydration shells of exchangeable cations, and hydrophobic sites on adsorbed organic molecules. These peculiar chemical features combined with the nanometre scale layering and interlayer spacing, allow for a variety of approaches to engineering clay minerals into functional materials with potential applications in advanced technologies, in particular, nanotechnology (Chun and John, 2013).

Pure kaolinite is white in colour and its chemical composition is 46.54 % SiO_2, 39.50 % Al_2O_3, and 13.96 % H_2O. The presence of impurities, particularly iron and titanium-bearing materials, imparts colour to kaolin (Saikia *et al.*, 2003). The mined kaolin is usually associated with various impurities like quartz, anatase, rutile, pyrite, siderite, and feldspar depending on the origin and depositional environment.

Clay materials can be modified using a variety of chemical/physical treatments to achieve the desired surface properties for best immobilization of contaminants (Aroke and Onatola, 2016). The physical and chemical behaviours of clay minerals have been studied by numerous researchers due to their adsorbing and catalytic properties. This behaviour is governed by the extent and nature of their external surface which can be modified by suitable treatment techniques (Sachin *et al.*, 2013). The two different treatments or modification methods of clay minerals are physical modification (thermal or microwave treatment) which involves alteration of chemical composition and crystalline structure by the effect of high temperature and chemical modification (by acids, bases, organic compounds) which is usually by the alteration of structure, surface functional groups and surface area. According to Thair and Olli (2008), all clay minerals have layers of Si tetrahedral and layers of aluminium (Al), Iron (Fe), and magnesium (Mg) octahedral, similar to gibbsite or brucite.

Kaolin is another aluminosilicate mineral that is found among different types of clays (Kuranga *et al*., 2018). It has a high aluminium content compared to other types of clay minerals in its category, which include smectite, illite, and chlorites. Kaolinite is one of the most common clay minerals in sedimentary and residual soils. A unit sheet of kaolinite, which is approximately 0.7 nm thick, is composed of one aluminium octahedral layer and one silicon tetrahedral layer, joined together by shared oxygen (Karl *et al.*, 1996). Kaolin clay is a significant raw material with wide-spread applications in the industrial arena including water treatment plants, porcelain, cement, and ceramics production, and equally used as fillers for polymer, paint, and rubber (Saikia *et al.*, 2003). The kaolin is composed of abundantly 1:1 clay mineral $Al_2Si_2O_5(OH)_4$ structure per alumina-silicate producing bulky congested particles of SiO_4 tetrahedral sheets (Figure 2.1a) and $AlO_2(OH)_4$ octahedral sheets (Figure 2.1b). The AlOHOSi hydrogen bonds are attached to each two unbroken layers since the kaolinite layer is neutral (Yahaya *et al.*, 2017). The major characteristics of kaolin that are crucial for industrial uses include particle size distribution, structural order, particle shape, disorder and crystallinity, specific surface area, and whiteness.

(a) (b)

Figure 2.1: (a) SiO_4 tetrahedral sheets kaolinite Structures; (b). $AlO_2(OH)_4$ octahedral sheets Structure (Thair and Olli, 2008)

Bachiri *et al.* (2014) investigated the potential applicability of Na-bentonite clay to adsorb methylene blue (MB) molecules from aqueous solution at various adsorbent doses. Maximum adsorption of thymol of ≥ 90 % was achieved in aqueous solutions by using 25 mg of clay in 20 mL of thymol solution. The maximum adsorption reached in this case is 309 mg per gram of sodium bentonite. The Freundlich isotherms were found to apply to the adsorption equilibrium data of MB on Na-bentonite.

Kuranga *et al.* (2018) investigated the use of locally sourced kaolinite clay from Okefomo Agbarigidoma, Ilorin South Local Government of Kwara State, to produce aluminium sulphate using sulphuric acid solution. The clay sample was beneficiated and calcined at 700 °C for 7 hrs to obtain meta-kaolin, then later leached using sulphuric acid.

Wilson (2017) studied the growth of Zeolite Socony Mobile (ZSM-5) zeolite crystals from inexpensive natural sources of silica and alumina, as well as N-Butyl Amine as a low-cost structure directing agent. In the case of kaolin, a heat treatment was used to form reactive amorphous meta-kaolinite. Subsequently, dealumination of the raw materials by acid leaching made it possible to reach appropriate Si/Al ratios and to reduce impurities. Finally, leached meta-kaolinite or diatomaceous earth was reacted with sodium hydroxide and N-Butyl Amine.

Cheng *et al.* (2017) used NaCl-modified zeolite to simultaneously remove nitrogen and phosphate from biogas slurry. The effect of pH, contact time, and dosage of absorbents on the removal efficiency of nitrogen and phosphate were studied. The adsorption isotherms of nitrogen and phosphorous removal with NaCl-modified zeolite were well described by Langmuir models, suggesting the homogeneous sorption mechanisms.

Sachin *et al.* (2013) refluxed kaolin with HNO_3, HCl, H_3PO_4, CH_3COOH, and NaOH of 3 molarity concentration at 110 °C for 4 hours followed by calcination at 550 °C for 2

hours. XRF and FTIR studies indicated that acid treatment under reflux conditions led to the removal of the octahedral Al^{3+} cations along with other impurities. XRD of acid-treated clay shows that the peak intensity was found to decrease. The chemical treatment increased the Si/Al ratio, surface area, and pore volume of the clay.

Gushit *et al.* (2010) reviewed the potential of kaolin as an essential naturally occurring mineral raw material employed in the formulation of chemicals, drugs, and other medicinal applications. The quality specifications of kaolin for various industrial applications in Nigeria were outlined.

Clays have been found to have the required physicochemical properties for wastewater treatment. These include high reactive surfaces, large specific surface area, and the ability for physical and organic modification to achieve desired properties. Nano clay is however found to have a larger specific surface area and ability to act as catalyst supports than raw clays.

The researchers used different techniques in the purification of clay as described above. The approach used by Bachiri *et al.* (2014) for the activation of clay using hydrochloric acid and hydrogen peroxide for the removal of carbonate and oxidation of organic matter respectively and the method of Cheng *et al.* (2017) which uses sodium chloride for the nutrient removal will be adopted.

2.7 Production of Clay Filter

Ceramic filtration is the use of porous ceramic (fired clay) to filter microbes or other contaminants from drinking water. Ceramic filtration for drinking water treatment has a long pedigree, having been used in various forms since antiquity; modern historical references to ceramic water "drip" filters with safe storage elements suggest they have

been used widely for over 100 years in Latin America (Joseph, 2007) and ceramic filters have been produced in Britain at least since 1850.

Today, pore sizes can be made small enough to remove virtually all bacteria and protozoa by size exclusion, down to 0.2 μm, in the range referred to as microfiltration. Ceramic filters are also often enhanced with a variety of silver-containing microbiocidal amendments that are either painted onto the surface, impregnated into the ceramic matrix before or after firing, or applied to filter elements in other ways. Silver nitrate solutions or colloidal suspensions of silver are most often used for this purpose, a practice that began in the early 20th century to control the problem of bacterial growth in porcelain (ceramic) Pasteur household-scale water filters (Joseph, 2007).

Ceramic filtration technology may be broadly divided into two categories: the relatively advanced technology of those filters made in more developed countries, which are made to exact specifications with considerable quality control and commensurate cost; and those made in developing countries, where there is some variation in effectiveness but which often employ local materials and expertise, producing a product that is relatively inexpensive and locally available (Lantagne, 2001a; Lantagne, 2001b).

Low-cost ceramic filtration for drinking water treatment in developing countries is diverse, varying by overall design, production method, clay and other materials, Quality Assurance (QA) and Quality Control (QC) procedures, burnout material, firing temperatures and methods, chemical amendments, and other characteristics. Because the design and available materials and methods vary widely from region to region, few generalities can be made about low-cost ceramic filters as a whole. Also, effectiveness data for one ceramic filter design may not be representative of other systems, or even in some cases separate batches of filters made at the same factory.

2.7.1 Local ceramic wastewater filter

Locally produced ceramic filters have the advantages of being lightweight, portable, relatively inexpensive, and low maintenance. Filters provide for the removal of microorganisms from water by gravity filtration through porous ceramic, with typical flow rates of 1-3 litre/hr. Unlike chemical or thermal disinfection, ceramic filters do not significantly change water taste or temperature and do reduce turbidity (Joseph, 2007). Filters have functional stability in the sense that they have only one moving part (the tap) and require no external energy source (such as UV lamps) or consumables (such as chlorine packets, or media that must be regenerated or replaced). They have a potentially long useful life of 5 years (Lantagne, 2001b; Campbell, 2005) with proper care and maintenance, although regular replacement of the filter element may be recommended every 1-2 years.

The ceramic filter surface is regenerated through periodic scrubbing to reduce surface deposits that slow filtration rates. Therefore, the useful life of a ceramic filter may be limited by the frequency of cleaning, and thus the quality of water being treated, and the thickness, since repeated cleaning will eventually degrade the filter element. Filter breakage, however, is more commonly cited as the primary reason for discontinued filter use, although breakage is associated with more frequent handling (including regular cleaning), highlighting the potential links between user behaviours and filter longevity in household use.

2.7.2 Burnouts material for filter production

Ceramic filter membranes have been attractive to researchers in the last decade due to their superior thermal and chemical stability, better mechanical strength, high resistance to acid and base, and good de-fouling properties (Enyew and Tegene, 2019). Fine filters

are easy to make, less expensive, and effective when deployed and used for water filtration. They depend on the micropore of small-sized pores of clay or ceramic materials mixed with sawdust or other combustibles, such as rice husks to separate or filter out debris, dirt, and microbes or bacteria from wastewater (Efeovbokhan *et al.*, 2019).

After mixing, they are then milled and fired to a temperature of up to nearly 860 °C while the particulate biomass materials are burnt out, creating tiny pores within the filters. The clay filters sometimes undergo a filtration rate test and may then be filmcoated with colloidal silver in such a way that it does not leach away. The combined effects of the bactericidal properties of the colloidal Ag and fine pores help to produce very effective clay filters (Efeovbokhan *et al.*, 2019). The silver helps to incapacitate bacteria and prevent the growth of mold and algae in the body of the filter.

The fine pore clay filter system is then set up and made to sit on top of a clean plastic or ceramic container or receiver. Contaminated water is passed through the filter and extraneous matter, dirt, or contaminants bigger than the fine pores of the ceramic filter are left on the top half of the unit. The contaminants are then removed from the filter, or it is cleaned by using a soft brush to remove them and then rinsed off using clean water.

The development of ceramic filter technology in 1981, has been attributed to Fernando Mazariegos of Guatemala (Erhuanga *et al.*, 2014). It was aimed at helping developing nations by providing cheap and sustainable technology for the production of high-quality potable water especially for rural dwellers (Efeovbokhan *et al.*, 2019).

Enyew and Tegene (2019) presented the results of an experimental study on the effects of different ratios of clay, grog, sawdust, and bone char on the efficiency of ceramic composite water filters. Filters of different designs were developed from clay (50, 60, 70, 75, and 80) %, sawdust (15, 25, and 35) %, grog (5 and 15) % bone char, and 5% ratios

by volume and sintered at a temperature of 900 °C for 6 hours. The phase and functional group identification of the sintered filter investigated with x-ray diffraction and infrared spectroscopy revealed the presence of mixed-phase and hydroxyl functional groups on the surface of the sintered filter.

Agbo *et al*. (2019) developed an effective ceramic water filter candle that is inexpensive and affordable by all and sundry. He formulated ceramic bodies from Nsu-clay and combustible materials which act as pore-creating agents. The Casting method of production was used to form a candle shape subjected to atmospheric drying and fired to a temperature of 900 °C. The Nsu-clay filter-treated water samples were compared with that of raw water. The results indicate that the Nsu-clay filter is very effective in removing suspended particles, coloured dissolved substances, unsavoury odours, and tastes.

Odenigbo and Musa (2018) investigated the effectiveness of the rate of flow through ceramic candle filters when locally available raw materials such as hardwood sawdust and rice husk are used as burn-out materials components in the production of water ceramic candle filters. Three different water candle filters were produced using Ekulu coal deposit clay as the major raw material. Sawdust in a ratio of 2:8 with the clay and rice husk in a ratio 2: 8 also as the combustible (burnout) materials. Odenigbo and Musa (2018) observed that the filter that had sawdust as burnt-out materials yielded a filtrate of 100 mL in 2 hours, 900 mL in 6 hours, and 1,500 mL in 12 hours and the candle filter with rice husk yielded a filtrate volume of 90 mL in 2 hours, 120 mL in 6 hours and 220 mL in 12 hours. The low yield of the candle filter with rice husk was due to inability of the husk to be burnt off at temperature 900 °C and below.

Grema *et al.* (2021) developed a ceramic filter pot for rural area water purification. The clay sample was tested for physical properties and the mixtures of the clay and sawdust

were made in seven (7) proportions of 75/25, 70/30, 65/35, 60/40, 55/45, 50/50, and 45/55. The tests conducted on the different portions of the clay and sawdust material revealed that the shrinkage of the sawdust blended clay reduced to the minimum of 6.3 compared to the pure clay with 13.7. A fluid dynamic test experiment on each filter was conducted; similarly, total dissolved solids (TDS), pH, and turbidity tests for both raw water and filtered water were conducted. From fluid dynamic test results, filter 50/50 % tends to have a higher filtration rate compared to the other two filters.

Gadzama *et al.* (2020) developed ceramic water filter candle from locally available materials: grog, clay, and sawdust. The slip-casting method was used to form a candle shape and the results showed that the filter was very effective in removing suspended particles, coloured dissolved substances, unsavoury odours, and tastes. The results showed that the clay/sawdust ratio had the greatest effect on the flow rate response. There was a high percentage removal of total dissolved solids of 75 % and turbidity removal of 92 %. The filters had a hydraulic conductivity of 0.28-0.55 cm/h which showed that the lesser the quantity of sawdust in the filter, the slower the hydraulic conductivity.

Nnaji *et al.* (2016) explored the possibility of improving water quality and eliminating the possibility of recontamination by the use of point-of-use (POU) water filters made from cheap locally available materials. Sawdust was used as a burnout material to enhance the rate of filtration. The clay was first characterized and then various proportions (5 %, 10 %, 20 %, 30 %, and 50 % by weight) of sawdust were mixed with the clay for filter production. The clay was found to have a specific gravity of 2.4, a high liquid limit of 81.6 %, and a medium plastic limit of 48.54 %. The flow rates of the filters ranged between 0.0005 litres/hr for the filter with 5 % sawdust and 0.8 litres/hr for the filter with 50 % sawdust.

CHAPTER THREE

3.0 MATERIALS AND METHODS

3.1 Materials

The major materials and equipment used for this research work are:

- Kaolin clay from its deposit in Kutigi, Niger State, Nigeria.
- Domestic wastewater collected via sewer.
- Dam water samples from the Shiroro hydro-power plant (HPP).
- *Mangifera Indica* leaves collected from River Basin Estate, Tundun Fulani, Minna
- Analytical grade chemicals and reagents used are shown in Table 3.1.
- A detailed list of major equipment used is presented in Appendix A.

Table 3.1: List of Reagents and Chemicals

S/N	Chemical/Reagents	Formula	% Purity	Manufacturer
1	Sodium Hydroxide	NaOH	97	Spark Scientific Limited, Northampton, UK
2	Silver Nitrate	$AgNO_3$	99.5	BDH Chemicals Ltd., Poole, England
3	Deionised Distilled Water (DDW)	DDW	0.5 µS/cm	National Water Quality Reference Laboratory, FMWR, River Basin, Minna
4	Zinc Sulphate, (Heptahydrate),	$ZnSO_4.7H_2O$	99	LOBA Chemie, Mumbai, India
5	Zinc Chloride	ZnCl	99.5	J.T Baker Limited, Philipsburg USA
6	Ethanol	C2H5OH	96	EMD Millipore Corporation, Germany
7	Ammonium Hydroxide	NH_4OH	30-32	Tyuangdang Guanghua Chemical Factory Company Limited, China
8	Hydrogen Peroxide Solution	H_2O_2	30-32	BDH Chemicals Ltd., Poole, England

3.2 Sample Collection and Preservation

The kaolin clay sample used in this study was collected from a clay deposit in Kutigi, Lavun Local Government Area in Niger State, Nigeria. Kutigi Town is located at longitude 9^{o} 12' 0" N and latitude 5^{o} 36' 0" E as shown by Google Maps in Figure 3.1.

Figure 3.1: Kutigi Town, Niger State, Nigeria (Google Map, 2020)

The raw kaolin clay was collected from its deposit in Kutigi Town in a 20 kg capacity leather bag and was transported to the National Water Quality Reference Laboratory Minna for further processing and analysis. The images of the collected raw kaolin clay from clay deposits in Kutigi are presented in Plates I and II.

Plate I: Raw Kaolin Clay

Plate II: Clay Deposit in Kutigi

Domestic wastewater was collected via sewers that connected toilets, baths, showers, kitchens and sinks together. A dam water sample was collected to serve as a control.

Samples collected for physicochemical parameters were transferred into 2 litres of polythene containers after rinsing thrice with the water sample and stored in sample cool boxes at 4 °C before analysis. Samples for metal analysis were preserved with nitric acid in polythene containers (2 mL concentrated HNO_3 per litre). Samples for microbial analysis were transferred aseptically into 200 mL sterilized glass bottles and stored in sample cool boxes at 4 °C before analysis as described in America Public Health Association (APHA) (2017) test methods. Samples for wastewater treatment were collected in a 20-litre keg. Temperature, pH, conductivity, Total Dissolved Solids (TDS) and Dissolved Oxygen (DO) were analysed *in situ*. The images of the sampling location are presented in Plates III and IV.

Plate III: Shiroro Hydropower Office Building

Plate IV: Drainpipe into River Kaduna at Shiroro Dam

3.3 Preparation of Raw Kaolin Clay for Purification

The collected kaolin clay samples were pre-treated to remove debris and air-dried at room temperature for five (5) days. Removal of leaves and dead insects was done on the raw kaolin clay collected and oven-dried at 105 °C for 6 hours. The oven-dried kaolin clay was crushed with a mortar and pestle, ground and crushed to particles then passed through a 250 µm mesh sieve to obtain very fine particles. Purification of the pulverized oven-dried kaolin clay was done by sedimentation technique to produce a clay fraction of less than 2 µm (< 2 µm) diameter, and removal of excess non-clay impurities (Ayalew, 2020).

3.4 Formation of Clay Slurry

Raw kaolin clay was processed by sedimentation technique to produce clay fractions < 2 µm hydrodynamic diameter, and removal of excess non-clay impurities. Raw kaolin clay

lumps of 100 g, 200 g, 300 g and 400 g were dispersed in different containers with 4 litres of Deionized Distilled Water (DDW). These represent 2.5 %, 5 %, 7.5 % and 10 % kaolin clay slurry in DDW.

The raw clays were allowed to swell in distilled water for 24 hours to allow for proper intercalation of the clay structure by water molecules. The resulting clay slurries were stirred for 1 hour using a Heildolph RGL500 High viscosity stirrer at a controlled speed of 40 revolutions per minute for adequate dispersion of the kaolin clay particles in distilled water. Thereafter, the slurries were poured into 4-litre clean beakers. The sedimentation of the slurries was monitored and done according to Stoke's Law in Equation 3.1.

$$u_s = \frac{g(\rho_p - \rho_w)d_p^2}{18\mu} \quad (3.1)$$

Where;

ρ_p = particle density, kg/m^3 (Kaolin clay particle = 1600 kg/m^3)

μ = liquid viscosity, kg/m. s (distilled water = 8.90×10^{-4} Pa·s)

ρ_w = density of water, kg/m^3 (997 kg/m^3)

u_s = particle settling velocity, m/s

d_p = diameter of particle, m

g = acceleration due to gravity, m/s^2 (9.81 m/s^2)

t = Settling Time.

R = particle size (radius) of clay, assumed to be spherical (1µm = 1 X 10^{-6} m)

h = Settling Height of Fluid (12 cm = 0.12 m),

The settling velocity of small spherical kaolin clay particles in the fluid medium was calculated using the Stoke's Law Equation. The kaolin clay particles were allowed to

settle gradually in the slurry to the average height of 8 cm, 12 cm, 11 cm and 10 cm in 2.5 %, 5 %, 7.5 % and 10 % in DDW respectively (Jovanovic and Mujkanovic, 2013).

3.5 Beneficiation of Kaolin Clay

Two hundred grams (200 g) of raw kaolin clay lumps were put in five (5) different 4 Litres of Beakers with 4 Litres of distilled water added. This represents 2.5 % w/w kaolin clay slurry in distilled water. Each Beaker was stirred for 1 hour at 40 revolutions per minute. The raw kaolin clay was allowed to swell in distilled water for 22 hrs 57 mins according to Stoke's Law.

The clay slurries were left to freely settle and the supernatants were collected after the settling time, by decanting them into 1 litre Beaker (Bachiri *et al.*, 2014). The Beaker was covered and allowed to settle and the supernatants were then discarded.

The resultant slurries were thereafter dried in a laboratory oven at a temperature of 105 °C until the water was evaporated and the sample weight became constant. Grinding of the dried samples was done using a laboratory porcelain pestle and mortar. The pulverised kaolin clay samples were stored in a laboratory sterile 100 ml plastic bottle for characterisation and further studies.

3.5.1 Activation of kaolin clay

Activation was done by treating the beneficiated kaolin clay (BKC) with 0.5 M of HCl to remove carbonate and the resulting mixture was washed with 10 % H_2O_2 to oxide organic matter (Bachiri *et al.*, 2014). Filtration of the mixture of acid-activated purified kaolin clay was done using Whatman filter paper. The residue from filtration was washed several times with distilled water and monitored until pH 7 was obtained. This was done to free the suspension of excess acid in the kaolin clay structure. The washed acid-activated

beneficiated kaolin clay was dried at 105 °C until the water was evaporated and the sample weight became constant.

3.5.2 Modification of kaolin clay

The BKC was further modified by treating with 0.01M of NaCl (Cheng *et al.*, 2017) to target the removal of NH_4, NO_3 and PO_4 in the wastewater. The slurry was washed several times with distilled water and monitored until pH 7 was obtained. This was done to free the suspension of excess salt in the clay structure. The obtained activated BKC was stored in 100 mL plastic containers for further use and the yield was calculated.

3.5.3 Kaolin clay yield

The kaolin clay yield was calculated using Equation 3.2. Two hundred grams (200 g) each of raw kaolin clay was processed to obtain BKC. The Mass of the activated BKC obtained was measured and the value was substituted in Equation 3.2 to obtain the percentage yield of the kaolin clay.

$$Y = \frac{Mass\ of\ Purified\ Kaolin\ Clay\ Produced}{Mass\ of\ Raw\ Kaolin\ Clay}\ \text{X}\ 100\% \qquad (3.2)$$

3.6 *Mangifera indica* Leaf Extracts

The *Mangifera indica* leaves were washed severally with deionised water. The leaves were cut with a cutter into small pieces. The beaker was set on a magnetic stirrer with 100 mL of deionised water. Twenty-five grams (25 g) of freshly cut leaves were weighed and put into the 100 mL of deionised water as shown in Plate V. The temperature of the magnetic stirrer was set to 80 °C. After 25 minutes, the solution turned greenish, indicating the formation of leaf extract in water. The extract was filtered and kept for further use. The objective of the screening was to determine the qualitative and

quantitative analysis of the Tannin, Flavonoid and Total Phenols present in the plant part. Tests for the phytochemicals present in the plant materials were conducted.

Plate V: *Mangifera Indica* Leaves.

3.6.1 Determination of tannin

Extract sample of 0.2 g was measured into a 50 mL beaker. 20 mL of 50 % methanol was added and covered with parafilm and placed in a water bath at 77 - 80 °C for 1hr. The mixture was shaken thoroughly to ensure uniformity. The extract was filtered using a double-layered Whatman No.41 filter paper into a 100 mL volumetric flask, 20 mL water, 2.5 mL Folin-denis reagent and 10 ml of Na_2CO_3 were added and the reaction mixture was mixed properly. The mixture was made up to 100 mL mark with distilled water (APHA, 2017). It was mixed well and allowed to stand for 20 minutes for the development of a bluish-green colour. The absorbance of the tannic acid standard solutions as well as samples was read after colour development on the UV-Spectrophotometer at a wavelength of 760 nm.

3.6.2 Determination of total flavonoid

The total flavonoid was determined by colorimetric method. Quercetin was used to establish the calibration curve. 0.5 mL of the diluted sample was added into a test tube containing 1.5 mL of methanol. 0.1 mL of 10 % aluminium chloride solution and 0.1 mL sodium acetate were added, followed by 2.8 mL of distilled water. The reaction mixture was incubated at room temperature for 30 minutes. The absorbance of the reaction mixture was measured on the UV Spectrometer at 415 nm. Distilled water was used as blank (APHA, 2017).

3.6.3 Determination of total phenol

Two grams (2 g) of the sample were defatted with 100 ml of diethyl ether using a Soxhlet apparatus for 2 hrs. The fat-free sample was boiled with 50 ml of petroleum ether for the extraction of the phenolic component for 15 minutes. Five millilitres (5 mL) of the extract were thereafter pipetted into a 50 ml flask after which 10 mL of distilled water was added. Ammonium hydroxide solution of 2 mL and 5mL of concentrated amyl alcohol were also added. The samples were made up to the 50 mL mark and left to react for 30 minutes for colour development. This was measured at 505 nm. Tannic acid was used to establish the calibration curve (APHA, 2017).

3.7 Green Syntheses of Zinc Oxide and Silver Oxide Nanoparticles

3.7.1 Green synthesis of ZnO nanoparticles

Ten grams (10 g) of zinc sulphate heptahydrate powder was measured into a 250 mL beaker and 100 mL of DDW was added. The solution was stirred using a magnetic stirrer for 30 mins at 150 rpm. Prepared concentration of 50 mL was put in a 100 mL conical flask. The conical flask was put on the hot plate and the temperature was set to 80 °C. *Mangifera indica* leaf extract was put in a burette, ready for titration. The solution was

titrated, while continuously stirred at 80 °C through the use of a magnetic stirrer with the *Mangifera indica* leave extract, drop by drop and very slowly until a light-yellow colour was formed. The titration was stopped immediately after the solution had changed to yellow, but the stirring was continued for 10 minutes until a colloid of the solution was obtained. The solution consumed 4.9 mL of the *Mangifera indica* leave extract. The precipitate obtained was filtered with Whatman No. 1 filter paper and washed with DDW until a pH of 7 was obtained. The precipitate was oven-dried at 105 °C for 6 hours and calcined in the furnace at 450 °C for 3 hours to obtain ZnO Nanoparticles (ZnO-NPs). The ZnO-NPs obtained were kept in a glass bottle for further characterisation and use (Sierra *et al.,* 2018).

3.7.2 Green synthesis of Ag nanoparticles

Five grams (5 g) of silver nitrate powder was measured into a 250 mL beaker and 100 mL of DDW was added. The solution was stirred using a magnetic stirrer for 30 minutes at 100 rpm. Prepared concentration of 50 mL was put in a 100 mL conical flask. The conical flask was covered with aluminium foil to avoid the photodegradation of silver. The conical flask was put on the hot plate and the temperature was set to 70 °C. The leaf extract was put in a burette, ready for titration. The solution was titrated with the leaf extract drop by drop and very slowly until a light-yellow colour formed. The titration was stopped immediately after the solution had changed to yellow. The solution consumed 2.8 mL of the *Mangifera indica* leave extract. The precipitate obtained was filtered with Whatman No. 1 filter paper and washed with DDW until a pH of 7 was obtained. The precipitate was oven-dried at 105 °C for 6 hours and calcined in the furnace at 450 °C for 3 hours to obtain Ag Nanoparticles (Ag-NPs). The dried Ag-NPs obtained were kept in a glass bottle for further characterisation and use (Njagi *et al.,* 2010).

3.7.3 Synthesis of BKC/ZnO nanocomposites

One gram (1 g) of $ZnSO_4.7H_2O$ powder was dissolved in 50 mL of DDW and stirred to get a precursor. The solution was stirred using a magnetic stirrer for 30 minutes at 150 rpm. 50 mL of the prepared concentration was put in a 100 mL conical flask. The conical flask was put on the hot plate and the temperature was set to 80 °C. The solution was titrated, while continuously stirred at 80 °C, with the *Mangifera indica* leaf extract until the light-yellow colour was formed. The solution consumed 2.6 mL of the *Mangifera indica* leaf extract. To the suspension formed, 10 g of the BKC was dispersed under vigorous stirring for 1 hour at 40 rpm. A homogeneous gel obtained was filtered with Whatman No. 1 filter paper and washed with DDW until a pH of 7 was obtained. The gel was oven-dried at 105 °C for 6 hours and calcined in the furnace at 450 °C for 3 hours to obtain BKC/ZnO nanocomposite. The BKC/ZnO nanocomposite adsorbent obtained was kept in a glass bottle for further characterisation and use (Jovanovic and Mujkanovic, 2013; Sierra *et al.*, 2018).

3.7.4 Synthesis of BKC/Ag nanocomposite adsorbents

$AgNO_3$ powder of 0.5 g was dissolved in 50 mL of DDW and stirred to get a precursor. The solution was stirred using a magnetic stirrer for 30 mins at 150 rpm. 50 mL of the prepared concentration was put in a 100 mL conical flask. The conical flask was put on the hot plate and the temperature was set to 70 °C. The solution was titrated, while continuously stirred at 70 °C, with the *Mangifera indica* leaf extract until the yellow colour was formed. The solution consumed 0.8 mL of the *Mangifera indica* leave extract. BKC of 10 g was dispersed into the suspension formed and vigorously stirred for 1 hour at 40 rpm. A homogeneous gel obtained was filtered with Whatman No. 1 filter paper and washed with DDW until a pH of 7 was obtained. The gel was oven-dried at 105 °C for 6

hours and calcined in the furnace at 450 °C for 3 hours to obtain BKC/Ag nanocomposite. The BKC/Ag nanocomposite adsorbent obtained was kept in a glass bottle for further characterisation and use (Jovanovic and Mujkanovic, 2013; Njagi *et al.*, 2010).

3.7.5 Synthesis of BKC/Ag/ZnO nanocomposite adsorbents

$AgNO_3$ of 0.5 g and $ZnSO_4.7H_2O$ of 1 g powder were dissolved in two separate 50 mL of DDW and stirred to get precursors. The solutions were stirred using a magnetic stirrer for 30 minutes at 150 rpm. Prepared concentrations of 50 mL for $AgNO_3$ and $ZnSO_4.7H_2O$ were put in separate 100 ml conical flasks. The $AgNO_3$ and $ZnSO_4.7H_2O$ solutions in the conical flasks were titrated with the *Mangifera indica* leaf extract under continuous stirring at 70 °C and 80 °C respectively until the light-yellow colour was formed.

The $AgNO_3$ and $ZnSO_4.7H_2O$ solutions consumed 0.7 mL and 1.5 mL of the *Mangifera indica* leaf extract accordingly. The two formed Ag and ZnO nanoparticles were mixed with 20 g of the BKC and vigorously stirred for 1 hour at 40 rpm. The mixture obtained was filtered with Whatman No. 1 filter paper and washed with DDW until a pH of 7 was obtained. The residue was oven-dried at 105 °C for 6 hours and calcined in the furnace at 450 °C for 3 hours to obtain BKC/Ag/ZnO nanocomposite adsorbents. The BKC/Ag/ZnO nanocomposite obtained was kept in a glass bottle for further characterisation and use (Jovanovic and Mujkanovic, 2013; Njagi *et al.*, 2010; Sierra *et al.*, 2018).

3.8 Characterisation of Raw Kaolin Clay, ZnO Nanoparticles, Ag Nanoparticles, BKC, BKC/Ag. BKC/ZnO and BKC/Ag/ZnO Nanocomposites Adsorbents

3.8.1 UV – visible spectrometer analysis

The formation of Ag and ZnO nanoparticles was confirmed by the UV-visible spectrometer analysis. 5ml samples were taken during the production of Ag and ZnO nanoparticles. for UV-visible spectrum analysis. Spectral analysis was performed with a UV – 1800 series single-beam diode array spectrometer. The machine collects spectra from 200–800 nm using a slit width of 1 nm. Deuterium and tungsten lamps were used to provide illumination across the ultraviolet, visible, and near-infrared electromagnetic spectrum (Shimadzu, 2008). The formation of absorbance peaks corresponded to the formation of zinc and silver oxide nanoparticles.

3.8.2 XRD analysis

The identification of phases and the crystallite sizes of the raw kaolin clay, ZnO-NPs Ag-NPs, BKC, BKC/Ag. BKC/ZnO and BKC/Ag/ZnO nanocomposite adsorbents were determined using the Emma 0141 X-Ray Machine located at the University of South Africa (UNISA) (2022a). Two grams (2 g) of powdered samples of materials to be analysed was used for the studies. This was done to allow the machine to have adequate samples to scan and therefore reduce the noise level in the X-ray diffractogram. The powdered samples were put in sample holders and pressed with a clean glass slide to produce a flat surface. The voltage and the current were set for the X-ray source and the computer software was activated for copper Kα wavelength (Cu K-alpha) = 1.5406 Å. The machine was calibrated using a pure silicon standard sample. After calibration, the sample was loaded into the machine for scanning (Mohan and Renjanadevi, 2016). The X-ray diffraction patterns were recorded on the machine at room temperature within the

range of 5 to 80 °C on the 2θ scale with a scanning speed of 0.05 °/s. At the end of the scan, the d-spacing for each peak was calculated from the values. The interplanar spacing for the diffraction angle of each peak (d-spacing) was calculated using Bragg law in Equation 3.3. The phase identifications were done by comparison with available d-spacing information and peaks from the International Centre for Diffraction Data (ICDD) and Powder Diffraction File (PDF).

$$n\lambda = 2d \sin\theta \tag{3.3}$$

Where;

λ = wavelength of X-Ray = 1.5406 Å.

d = d-spacing in Å

θ = Diffraction angle in radians

The unit cell parameters were calculated and indexed as *h k l*. The average crystallite size of the clay was calculated from the analysis of the peaks in the X-ray diffractogram using Scherer Equation 3.4.

$$D = \frac{K\lambda}{\beta \operatorname{Cos}\theta} \tag{3.4}$$

Where;

λ = Wavelength of X-Ray, CuKa = 1.5406 Angstrom (À)

K = Scherer Constant (0.94 for spherical crystallites with cubic symmetry)

β = Full Width at Half Maximum (FWHM) for the peaks in radians

θ = Bragg's diffraction angle in degrees

Full Width at Half Maximum (FWHM) of the selected peak was determined using the student trial version of 2021 OriginPro data and analysis software from Origin Lab Corporation, Northampton, USA (OriginPro, 2021).

3.8.3 HRTEM and EDX analysis

TECNAI G2 F20 twin model Transmission Electron Microscope was used for the analysis of particle size and distribution pattern of raw kaolin clay, ZnO-NPs, Ag-NPs, BKC, BKC/Ag, BKC/ZnO and BKC/Ag/ZnO Nanocomposite adsorbents. 0.02 g of each sample was suspended in 100 mL of methanol. The mixture was then ultrasonicated for proper dispersion of the sample. A few drops of the slurry were thereafter put onto the carbon grid using a micropipette. This was then dried under photo light. After drying, the carbon grid was loaded onto a slit sample holder and then mounted on the shaft of the Transmission Electron Microscope for analyses.

For the determination of the elemental composition of the samples using energy-dispersive X-ray spectroscopy (EDX) measurements, the secondary electron mode is activated for imaging. A homogenous region of the sample was identified and the microscope operated at electron high tension (EHT) of 20 kV for EDX. SEM and EDX analysis were recorded by using a LEO S430 scanning electron microscope coupled with an energy dispersive X-ray analyser model Oxford Instruments. Samples were prepared by dispersing dry powder on double-sided conductive adhesive tape. Samples were coated with carbon by arc discharge method for HRTEM-EDX (UNISA, 2022b). Samples were scanned in secondary electrons (SE) for morphology and back-scattered electrons (BSE) mode for the compositional image.

3.8.4 BET N_2 technique adsorption

The surface area and pore volume of ZnO-NPs, Ag-NPs, BKC, BKC/Ag. BKC/ZnO and BKC/Ag/ZnO nanocomposite adsorbents were determined using the TriStar II 3020 BET Nitrogen adsorption technique (UNISA, 2022c). Sample mass adapted from the Micrometrics (2009) as specified in Table 3.2 was measured and put in a sample holder for analysis. The sample was degassed at 200 °C for 3 hours to remove moisture and air. Afterwards, the samples were analysed at an equilibration interval of 10 s, bath temperature of 77.350 k and 1.000 g/cm^3 density. BET surface area, pore volume and pore size data were then obtained. The BET surface area and average pore volume distributions were obtained from the plot of the volume adsorbed (cm^3/g STP) against relative pressure. Ambient free space and port volume in which the analyses were performed are presented in Table 3.2.

Table 3.2: Sample Mass for BET N_2 Technique Adsorption

Samples	Sample Mass (g)	Ambient Free Space (cm^3)	Port Volume (cm^3)
BKC	0.8923	14.9830	0.0060
ZnO NP	0.8792	15.3099	0.0148
Ag NP	0.8790	15.3090	0.0140
BKC/Ag	0.5834	15.2931	0.0207
BKC/ZnO	0.8070	15.4163	0.0148
BKC/Ag//ZnO	0.8282	15.20.33	0.0060

Source: Micrometrics (2009)

3.8.5 XRF analysis

The chemical analysis of the raw kaolin clay, ZnO-NPs, Ag-NPs, BKC, BKC/Ag. BKC/ZnO and BKC/Ag/ZnO nanocomposite adsorbents were done using the EDXRF-3600B machine by Oxford instrument (UNISA, 2022d). The EDXRF machine was switched on and the vacuum pump connected to create a vacuum within the machine chamber. Samples for the analyses were prepared in pellet form. The sample holder was

cleaned with ethanol to remove impurities. A pure silver sample was used for the initialisation of the machine. After the initialisation of the machine, the sample was mounted on the sample holder within the machine chamber. The working curve was selected and the machine was set to run. The machine ran for the set time of 100 seconds through the principle of bombardment of generated x-rays on the sample. The result of the analyses was then saved in Excel format.

3.8.6 Determination of loss on ignition

Loss on Ignition (LOI) test was conducted on the raw kaolin clay, ZnO-NPs, Ag-NPs, BKC, BKC/Ag, BKC/ZnO and BKC/Ag/ZnO nanocomposite adsorbents which chemical analyses have been determined by the X-ray fluorescence method. The LOI test was done using International Standard Organisation (ISO) (2015) method. The LOI test determined the mass of the volatile matter present in each sample tested. 2 g of the sample was weighed into a clean ceramic crucible and the weight was recorded. The crucible was then heated to a temperature of 700 °C in a furnace and allowed to stay at this temperature for 60 minutes. The furnace was switched off and the material was allowed to cool down to room temperature inside the furnace. The mass of the sample was then determined after heating. The Loss on ignition of the samples was calculated using Equation 3.5.

$$LOI = \frac{Mi - Mf}{Mi} \quad (3.5)$$

Where;

LOI = Loss on Ignition

Mi = Mass of the sample before heating,

Mf = Mass of sample after heating

3.9 Water and Wastewater Analysis

The treated water and wastewater were subjected to water quality analysis at the National Water Quality Reference Laboratory Minna. Wastewater and treated water samples collected were analysed to determine physicochemical, heavy metals and bacteriological water quality analysis. The heavy metals were analysed using an Atomic Absorption Spectrometer (AAS) and Metalyser HM1000/5000. Metalyser was used because of its ability to measure in micrograms per litre. The water quality analysis was done using APHA (2017) Standard Methods for Examination of Water and Wastewater. Appendix B summarises the method of analysis adopted for the treated and wastewater analysis.

3.9.1 Quality assurance

To ensure the accuracy and precision of data generated in this study, Quality Control (QC) measures were put in place with proper documentation. Field equipment such as conductivity meter and pH meter were calibrated. Before wastewater sampling and analysis, containers were washed with non-foaming detergents, rinsed thrice with tap water and finally with DDW. Containers for microbial sampling and analysis were sterilized in the autoclave. Duplicate analysis was carried out to measure precision at a relative percentage difference of ±10 % for every batch of 10 samples, while quality control standards were used to determine accuracy within recovery of 90 % to 110 % (APHA, 2017).

3.10 Batch Adsorption Processes

The adsorption experiments were carried out to know the adsorption characteristics of the BKC, BKC/Ag, BKC/ZnO and BKC/Ag/ZnO nanocomposite adsorbents. The effects of parameters such as contact time, adsorbent dosage and temperature on physical parameters pH, turbidity, dissolved oxygen, suspended solid, colour, electrical

conductivity (EC), total iron, cadmium, lead, copper, manganese, arsenic, mercury silver, zinc nitrate, phosphate, ammonium, COD, BOD, total coliforms, faecal coliforms, *Clostridium perfringens* and *E. coli were* determined (APHA, 2017).

The percentage removal (% removal) and the adsorption capacity, (mg/g) of pH, turbidity, dissolved oxygen, suspended solids, colour, EC, total iron, cadmium, lead, copper, manganese, arsenic, mercury silver, zinc nitrate, phosphate, ammonium, COD, BOD, total coliforms, faecal coliforms, C*lostridium perfringens* and *E. coli* treated by BKC, BKC/Ag, BKC/ZnO and BKC/Ag/ZnO at different conditions were calculated using Equations 3.6 and 3.7 respectively.

The adsorption capacities of the differently prepared adsorbents - BKC, BKC/Ag, BKC/ZnO and BKC/Ag/ZnO to remove physical parameters pH, turbidity, dissolved oxygen, suspended solid, colour, EC, total iron, cadmium, lead, copper, manganese, arsenic, mercury silver, zinc nitrate, phosphate, ammonium, COD, BOD, total coliforms, faecal coliforms, C*lostridium perfringens* and *E. coli were* determined using Equations 3.6 and 3.7.

$$\text{Percentage (\%) Removal} = \frac{C_i - C_e}{C_e} \; X \; 100\% \tag{3.6}$$

$$q_e = \frac{C_i - C_e}{M} \; X \; V \tag{3.7}$$

Where;

C_i = Initial Liquid Phase Concentration (mg/L)

C_e = Equilibrium liquid phase concentration (mg/L),

V = Volume of the solution (litre)

M = Mass of the adsorbent (g).

q_e = Equilibrium Liquid Phase

3.10.1 Effect of contact time

The effect of contact time on the adsorption capacities of the adsorbents was studied at contact times of 10, 20, 30, 40, 50 and 60 minutes. Twenty five grams (25 g) of the adsorbent was mixed with 100 mL of wastewater in a corked 250 mL conical flask. The flasks were agitated at 40 rpm at room temperature. The flask was removed from the stirrer at 10-minute intervals for the contact time study. The samples were analysed after filtration by Whatman No. 42 filter paper. The final concentrations of pH, turbidity, dissolved oxygen, suspended solids, colour, EC, total iron, cadmium, lead, copper, manganese, arsenic, mercury silver, zinc nitrate, phosphate, ammonium, COD, BOD, total coliforms, faecal coliforms, *Clostridium perfringens* and *E. coli* were analysed using APHA (2017) Methods. The optimum contact time for the adsorbents for metal ions sorption from wastewater was determined. The % removal efficiency for each parameter of interest was calculated using Equation 3.6.

3.10.2 Effect of adsorbent dosage

The effect of the adsorbent dosage on the uptake of pH, turbidity, dissolved oxygen, suspended solid, colour, EC, total iron, cadmium, lead, copper, manganese, arsenic, mercury silver, zinc nitrate, phosphate, ammonium, COD, BOD, total coliforms, faecal coliforms, *Clostridium perfringens* and *E. coli from* wastewater using BKC, BKC/Ag, BKC/ZnO and BKC/Ag/ZnO were investigated with adsorbent doses of 5 g, 10 g, 15 g, 20 g, 25 g and 30 g respectively. The experiments were performed by adding the measured weight of the adsorbent into 250 mL conical flasks containing 100 ml of the wastewater each. The study was done with the flasks stirred at 40rpm at room

temperature. The supernatant was filtered and kept in bottle analyses (APHA, 2017). The % removal efficiency for each parameter of interest was calculated using Equation 3.6.

3.10.3 Effect of temperature

The effect of the temperature on pH, turbidity, dissolved oxygen, suspended solids, colour, EC, total iron, cadmium, lead, copper, manganese, arsenic, mercury silver, zinc nitrate, phosphate, ammonium, COD, BOD, total coliforms, faecal coliforms, *Clostridium perfringens* and *E. coli were* investigated (APHA, 2017). The study was conducted at varying temperatures of 40, 50, 60, 70 and 80 °C. 25 g of the adsorbent was contacted with 100 mL of wastewater in a corked 250 mL conical flask. The corked flasks were agitated in a water bath at the respective temperature for the optimum contact time of 30 minutes, at 40 rpm at room temperature. The supernatant was filtered and kept in a bottle for analysis. The % removal efficiency for each parameter of interest was calculated using Equation 3.6.

3.11 Studies on the Adsorption Isotherms

3.11.1 Adsorption isotherms

Adsorption isotherms of domestic wastewater were measured using the concentration-variation method at constant temperature, time and volume. Langmuir and Freundlich models were employed for the adsorption isotherm study. The adsorption capacity of BKC, BKC/ZnO, BKC/Ag, BKC/Ag/ZnO to remove total iron, cadmium, lead, copper, manganese, arsenic, mercury silver, zinc nitrate, phosphate, ammonium, COD and BOD from the wastewater were tested using both Langmuir isotherms and Freundlich models. Twenty five (25 g) of the BKC, BKC/ZnO, BKC/Ag and BKC/Ag/ZnO nanocomposite adsorbents were mixed with 100 mL of the desired concentrations of the domestic wastewater at 30 °C in a temperature-controlled water bath with constant shaking. The

samples were withdrawn after 30 minutes and treated effluents were separated from the adsorbent using Whatman filter paper. The concentration of the filtrate was measured using the procedure given in APHA (2017).

3.11.2 Langmuir adsorption isotherm

Langmuir isotherm was employed to evaluate the multilayer adsorption at a relatively large distance from the surface of the adsorbents. The model represents one of the first theoretical treatments of non-linear adsorption and suggests that uptake occurs on a homogenous surface by monolayer adsorption without interaction between adsorbed molecules (Bashir *et al.,* 2013). The rate change of concentration due to adsorption equals the rate of concentration due to desorption. As a result, the Langmuir isotherm is expressed in Equation 3.8.

$$\frac{Ce}{q_e} = \frac{1}{Q_o b} + \frac{Ce}{Qo} \tag{3.8}$$

Where;

Ce = Equilibrium concentration (mg/l),

q_e = Amount adsorbed at equilibrium time (mg/g),

Q_o = Langmuir constants derived from the slope

b = Langmuir constants derived from the intercept

The values of the Langmuir constants were calculated from the intercept and slope of the plot of $\frac{Ce}{q_e}$ versus Ce.

The dimensionless separation factor expressed on favourable adsorption nature was calculated from Equation 3.9.

$$R_L = \frac{1}{(1 + bC_i)} \quad (3.9)$$

Where;

C_i = Initial concentration of the wastewater (mg/L)

b = Langmuir constant (l/mg).

R_L = RL values indicate the type of isotherm as shown in Table 3.3

Table 3.3: Isotherm Type

R_L Value	Type of Isotherm
$R_L > 1$	Unfavourable
$R_L = 1$	Linear
$R_L < 1$	Favourable
$R_L = 0$	Irreversible

Source: Bashir *et al.* (2013)

3.11.3 Freundlich adsorption isotherm

The Freundlich isotherm is an empirical relationship which often gives a more satisfactory model of experimental data. The Freundlich model can be applied to heterogeneous surfaces involving multilayer adsorption (Ikhazuangbe *et al.*, 2017).

Freundlich isotherm is expressed in Equation 3.10:

$$K_f C_e^{\frac{1}{n}} \quad (3.10)$$

The linearized Freundlich adsorption isotherm can be expressed as presented in Equation 3.11.

$$Log\ q_e = Log\ (K_f + \frac{1}{n}\ Log\ C_e) \quad (3.11)$$

Where;

C_e = Equilibrium concentration

q_e = Adsorption capacity at equilibrium stage,

K_f and n = Freundlich constants which incorporate all factors affecting the adsorption process (adsorption capacity and intensity).

Values of K_f and n were obtained from the intercept and slope of a plot of adsorption capacity (q_e) against equilibrium concentration (C_e). Both parameters K_f and n affect the adsorption isotherm. The larger the K_f and n values, the higher the adsorption capacity. Furthermore, the magnitude of the exponent n indicates the favourability of the adsorption process (Ikhazuangbe *et al.*, 2017). When the value of n is greater than unity (1< n < 10) that means the adsorption process is favourable (Bashir *et al.*, 2013).

Values of K_f and n can be obtained from the intercept and slope of a plot of adsorption capacity, q_e against equilibrium concentration (C_e). Both parameters K_f and n affect the adsorption isotherm. The larger the $K_f$and n values, the higher the adsorption capacity. Furthermore, the magnitude of the exponent n indicates the favourability of the adsorption process (Ikhazuangbe *et al.*, 2017). The adsorption process is favourable when the value of n is greater than unity (1< n < 10).

3.11.4 Thermodynamic studies

The determination of the basic thermodynamic parameters: enthalpy of adsorption (ΔH), Gibb's free energy of adsorption (ΔG) and entropy of adsorption (ΔS), is important as it

allows to estimate if the process is favourable or not from a thermodynamic point of view, to assess the spontaneity of the system and to ascertain the exothermic or endothermic nature of the process. An adsorption process is generally considered physical if ΔH° < 84 kJ/mol and as chemical when ΔH° lies between 84 and 420 kJ/mol. The thermodynamic parameters of the adsorption process were determined from the experimental data obtained at various temperatures using Equations 3.12 – 3.15 (Bashir *et al.*, 2013; Ikhazuangbe *et al.*, 2017; Al-Kadhi, 2019).

$$\Delta G = -RTlnK_d \tag{3.12}$$

$$K_d = \frac{q_e}{C_e} \tag{3.13}$$

$$lnK_d = \frac{\Delta So}{R} - \frac{\Delta Ho}{RT} \tag{3.14}$$

$$\Delta G° = \Delta H° - T\Delta S° \tag{3.15}$$

Where;

Kd = Distribution coefficient for the adsorption

q_e = Amount of contaminants adsorbed on the adsorbent per litre of wastewater at equilibrium

Ce = Equilibrium concentration (mg/L) of the contaminants in wastewater,

T = Absolute temperature

R = Gas constant

ΔGo = Gibbs free energy change

ΔHo = Enthalpy change

ΔSo = Entropy change

The values of enthalpy change ($\Delta H°$) and entropy change ($\Delta S°$) were obtained from the slope and intercept of ln Kd versus 1/T plots.

3.12 Design of Filter Pots from Nanocomposite Adsorbents

The design for the production of filter pots from BKC, BKC/Ag, BKC/ZnO and BKC/Ag/ZnO nanocomposite adsorbents is presented in this section. The filter pots were designed based on the mixing ratio of beneficiated kaolin clay, rice husk, Ag and ZnO nanoparticles. Rice husk served as burnout material to create pores in the filter pot. The filter pot was designed to contain a pre-filter bucket, filter pot housing and water outlet.

3.12.1 Pre-filter bucket design

The filter bucket was designed to be 2.0 Litre (0.002 m^3) capacities and contained a 5-micron pore size pre-filter screener for the removal of the coarse and large particles that could affect the life span of the nanocomposite filter pot. The filter pot was connected to the pre-filter bucket by a 0.2-metre-long rubber hose.

The wastewater in the pre-filter bucket was controlled by a valve to regulate the flow of domestic wastewater into the filter pot. The opening of the valve introduced wastewater into the filter pots media by gravity. Plastic, round-in shape feed water bucket material purchased in the market was modified to construct the pre-filter bucket. The bucket serves as a wastewater reservoir and aids in the removal of contaminants by gravity through the installed screen. The pre-filter bucket specification parameters are presented in Table 3.4.

Table 3.4: Specification Parameters for the Pre-Filter Bucket

Design Parameters	**Designed Values**
H = Height of the Pre-Filter Bucket, m	0.140 m
D = Top Diameter of the Pre – Filter Bucket, m	0.130 m
R_T = Top Radius of the Pre–Filter Bucket, m	0.065 m
D_B = Bottom Diameter of the Pre-Bucket, m	0.110 m
R_B = Bottom Radius of the Pre-Bucket, m	0.055 m
A = Pre-Filter Bucket Area	0.076 m^2
V = Pre–Filter Bucket Volume	0.0020 m^3
Screener pore size	5-micron

3.12.2 Filter pots design

The filter pots produced from the nanocomposite adsorbents were designed with the following considerations:

i. Removal of bacteriological contaminants.
ii. Removal of physicochemical contaminants.
iii. Affordability, durability, ease of installation, use and maintenance.
iv. Provision of safe water from domestic wastewater.
v. Does not require electrical power or batteries.
vi. Easy operation and requiring minimal maintenance and training.
vii. Flow rate

The filter pot was moulded into shapes via wooden moulds with the capacity to treat 14.6 – 21.5 mL/hr of domestic wastewater. Filter pots were produced based on the Equations 3.16 – 3.22.

$$Q = \frac{V}{t} \quad (3.16)$$

$$Vf = \frac{Q}{A} \quad (3.17)$$

$$A = \pi DL \quad (3.18)$$

$$h_f = \frac{4fLV^2}{D\ X\ 2g} \text{ (Darcy – Weisbach Formula)} \quad (3.19)$$

$$R_e = \frac{V\ X\ D}{K_v} \quad (3.20)$$

$$F = \frac{0.0791}{(Re)^{1/4}} \quad (3.21)$$

$$V = \frac{\text{Filter Pot Diameter}}{\text{Time}} \quad (3.22)$$

Where;

D = Filter Pot Diameter

L = Length of the Filter Pot

f = Co-efficient of friction

A = Surface Area of the Filter Pots

Q = Flow Rate

g = Acceleration due to gravity

t = Unit time

Vf = Velocity of Flow

Kv = Kinetic Viscosity of Water

Re = Reynold Number

π = Ratio of the circumference of the filter pot to its diameter

h_f = Head Loss

3.12.3 Filter pots housing

The nanocomposite adsorbent filter pots produced were housed in a 2-litre capacity filter housing with an outlet tap to collect the filtrate. The clay filter housing design is presented in Figure 3.2.

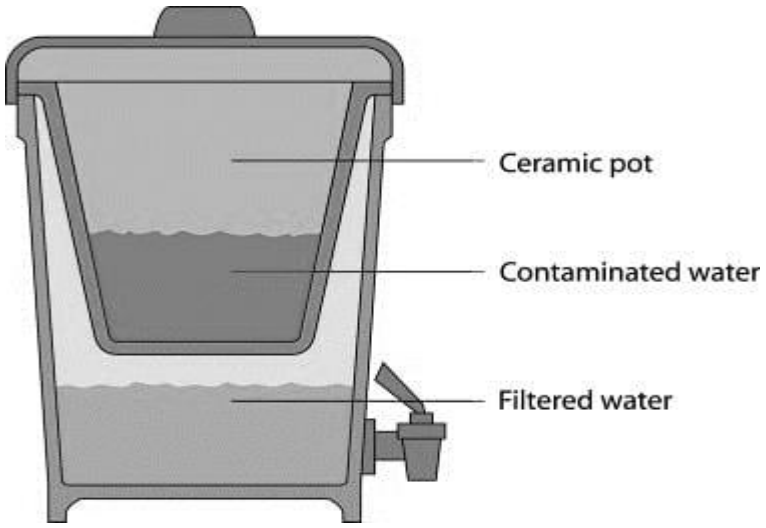

Figure 3.2: Clay Filter Housing Design

3.13 Production of Filter Pots

A laboratory scale was conducted for the production of filter pots from BKC, BKC/Ag, BKC/ZnO and BKC/Ag/ZnO nanocomposite adsorbents. The preparation of the adsorbents for the filter pots and mixing were done at the Centre for Genetics Engineering and Biotechnology Laboratory, Federal University of Technology, Minna. The firing of the filter pots was done at the Industrial Design Department of the Federal University of Technology, Akure, Nigeria.

3.13.1 Preparation for filter pots production

A 70 mesh-screen which is equivalent to 210 μm sieve was used to sieve the rice husk powders. This would give powder particles of diameter less than or equal to 210 μm

(Agbo *et al.*, 2019)**.** The rice husk was dried in the sun and the fine powder was then sieved through the 70-mesh sieve. The produced BKC, BKC/Ag, BKC/ZnO and BKC/Ag/ZnO nanocomposite adsorbents were mixed with the sieved rice husk, Ag-NPs and ZnO-NPs at a proportion in Table 3.5.

Table 3.5: Mixing Ratios for the Production of Filter Pots

Filter	Kaolin Clay (%)	Rice Husk (%)	Ag-NPs (%)	ZnO-NPs (%)
BKC -1	85	15.0	0.0	0.0
BKC – 2	75	25.0	0.0	0.0
BKC/Ag – 1	85	14.5	0.5	0.0
BKC/Ag – 2	75	24.5	0.5	0.0
BKC/ZnO – 1	85	14.0	0.0	1.0
BKC/ZnO – 2	75	24.0	0.0	1.0
BKC/Ag/ZnO – 1	85	13.5	0.5	1.0
BKC/Ag/ZnO – 2	75	23.5	0.5	1.0

The plaster of Paris mould used in the study was produced from the master mould constructed at the Industrial Design Department, Federal University of Technology, Akure. The organic and coarse materials in the rice husks were removed by hand. The produced BKC, BKC/Ag, BKC/ZnO and BKC/Ag/ZnO nanocomposite adsorbents were mixed with water and rice husk until continuous homogeneous colloidal slurry was obtained. Different ratios of beneficiated kaolin clay, rice husk, Ag and ZnO nanoparticles were measured as shown in Table 3.5 and sieved using a 300 μm mesh sieve. The resultant mixture was hydrated with deionized water, homogenously mixed and kneaded with rice husks. The resultant mixture was allowed to age for 7 days. The ageing of the mixture caused plasticity, fermentation and some physical changes in the material. The mixtures were moulded using a gigger and jolly machine and throwing method as shown in Plate VI (a). The lubricant was applied to the surface of the moulds to prevent sticking to their surfaces. The moulded filter pots were dried with a dryer at

150 °C to prevent the produced filter pots from cracking when sintering in a kiln. Afterwards, the dried filter pots were placed inside a gas and electric kiln and then fired at 900 °C in Plate VI (b – c). The firing constitutes different stages namely, dehydration (100-300 °C), oxidation (300-500 °C) and vitrification stage (500-900 °C).

Eight filter pots were produced at different kaolin-to-rice husk ratios using gas and electric-fired controlled temperature kilns. The fired clay pots labelled BKC - 1, BKC/Ag - 1, BKC/Ag – 1, BKC/ZnO – 1, BKC/ZnO – 2, BKC/Ag/ZnO – 1, BKC/Ag/ZnO – 2 were allowed to cool in the kiln as shown in Plate VI (c) for three days and tested for chemical resistance, water absorption, flow rate, porosity, microbial and some physicochemical parameters removal efficiency. Before their use, the filter pots were first soaked in water to ensure the pores were through for the filtration experiments (Efeovbokhan *et al.*, 2019).

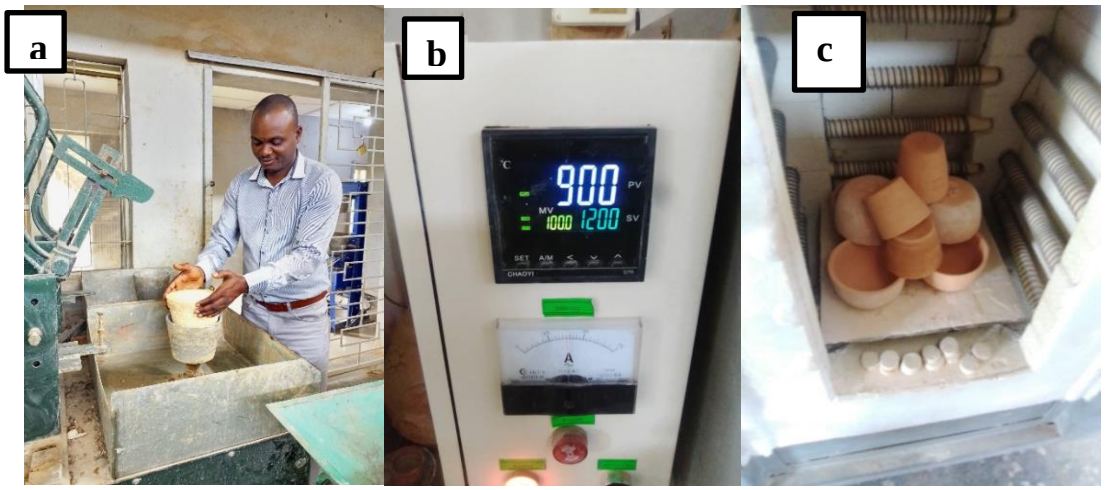

Plate VI: (a). Gigger and Jolly Machine, (b). Electric and Gas Kiln, (c). Dried Filter Pots in a Kiln

3.14 Characterization of Moulded Filter Pots

3.14.1 Chemical resistance analysis

The chemical resistance was performed on the optimum filter fired at 900 °C as described by America Society for Testing and Materials (ASTM) (2001) in method D543. The filter pots were immersed in DDW with the pH varied from 1-12 and adjusted to the desired value using either 0.5 M H_2SO_4 or 0.5 M NaOH. After the adjustment, the filter pot was left in the solution for 48 hours. Thereafter, the filter pot was removed from the solution, weighed and the chemical resistance was computed using Equation 3.23.

$$\% \text{ R} = \frac{M1-M2}{M1} X\ 100 \tag{3.23}$$

where $M1 - M2$ and are the mass of the sample before pH was varied and mass after removing from acidic/basic solution (g), % R is the per cent resistance.

3.14.2 Shrinkage test

The original lengths of the moulded filter pots were recorded immediately after moulding and they were recorded as L1 (cm). The filter pots were air-dried for 3 days and subsequently, oven-dried for 3 days at 105 °C to attain constant weights (Cerato and Lutenegger, 2006). The shrinkage from the marks on the filter pots was determined and recorded as L2 (cm). The filter pots were further calcined at 900 °C. The shrinkage of the filter pots from the marks after firing was recorded as L3 (cm) as shown in Equations 3.24 and 3.25.

$$\text{Linear Shrinkage (\%)} = \frac{L1-L2}{L2} X\ 100 \tag{3.24}$$

$$\text{Total Shrinkage (\%)} = \frac{L1-L2}{L1} X\ 100 \tag{3.25}$$

3.14.3 Determination of water absorption

The filter pots were weighed and the known weights of the dried samples were recorded as M1 (g). Afterwards, the filter pots were soaked in de-ionized water for 24 h, then removed, cleaned and weighed immediately (Timothy *et al.*, 2021). The weights of the samples were recorded as M_2 (g). The percentage of water absorption was calculated using Equation 3.26.

$$\text{Water Absorption (\%)} = \frac{M2-M1}{M1} X\ 100 \qquad (3.26)$$

3.14.4 Determination of porosity

The porosity of the filter pots followed the method described by Alansari *et al*. (2019). The filter pots were weighed and soaked in water for 24 hrs. The apparent porosity was calculated using Equation 3.27.

$$\text{Apparent Porosity (\%)} = \frac{M_w-M_f}{\rho_e V_f} \qquad (3.27)$$

where M_f is the weight of the fired sample (g), M_w is the weight of soaked sample in water for 24 h (g), V_f and ρ_e is the volume of the fired sample (cm^3) and mass volume of water (g/cm^3), respectively.

3.14.5 Flow rates

The flow rate of the produced filter pots was calculated according to the method described by Van *et al.* (2017) using Equation 3.27.

$$Flow\ Rate = \frac{Volume\ of\ Water\ Measured\ at\ Time\ T,mL}{Elapsed\ Time\ From\ the\ Start\ of\ Test,hours} \qquad (3.27)$$

CHAPTER FOUR

4.0 RESULTS AND DISCUSSION

4.1 Brief Introduction

This work focused on the development of nano-based filter pots for domestic wastewater treatment. The kaolin clay samples collected from Kutigi in Niger State, Nigeria were beneficiated to remove impurities and the accrued mud, the results obtained are humbly presented in this section.

4.2 Raw and Beneficiated Kaolin Clay

The yield of kaolin clay fractions of less than 2 µm from the raw kaolin clay is presented in Table 4.1.

Table 4.1: Yield of Beneficiated Kaolin Clay

Kaolin Clay Slurry	Dried Mass of Raw Sample (g)	Dried Mass of Beneficiated Kaolin Clay (g)	Yield (%)	Settling Height (cm)
2.5 %	100	7.60	7.60	8.10
5.0 %	200	18.3	9.15	12.0
7.5 %	300	27.4	9.13	9.20
10 %	400	36.5	9.13	9.20

The yield increased with an increase in the percentage slurry from 2.5 % to 5.0 % and remained constant at 7.5 % and 10 %. The lower yield experienced at 7.5 % and 10 % slurry could be attributed to the repulsive forces between the negatively charged kaolin clay particles which were free in the suspension and hence prevented particles from settling at the experimental calculated time of 22 hrs 57 minutes for particles of less than 2 µm as presented in Table 4.1. Meanwhile, at higher percentage slurry, the particles were not as free as when the percentage slurry was low, hence they tend to aggregate more, causing them to settle faster.

The dried mass of the beneficiated kaolin clay was proportional to the increase in the dried mass of the raw kaolin between 2 %– 5.0 %. However, the yield started decreasing at 7.5 % and remained constant at 10 %. The yield of kaolin clay reached the peak at 5.0 % and was therefore picked for use in further analyses.

Furthermore, when 100 g, 200 g, 300 g and 400 g of raw kaolin clay lumps were dispersed in 4-litre beakers each with Deionised Distilled Water (DDW) representing 2.5 %, 5 %, 7.5 % and 10 % kaolin clay slurry, the particles settled gradually to the average height of 8.10 cm, 12.0 cm, 9.20 cm and 9.2 0 cm respectively.

The optimum settling height of 12.0 cm was obtained at 5.0 % clay slurry. This is an indication that more yield would be obtained from the clay slurry made with 200 g of raw kaolin clay dispersed in 4-litre beakers with DDW. The beneficiated kaolin clay produced after air drying is presented in Plate VII. The beneficiated kaolin clay after grinding was stored in plastic containers.

Plate VII: Beneficiated Kaolin Clay

4.2.1 Kaolin clay sedimentation design parameters

The larger the diameter of the kaolin clay particles, the higher the sedimentation velocity. The higher the density difference between the kaolin clay particle and the liquid, the higher the velocity of the particle and the faster the settling of the kaolin clay particle. This is because soil particles are denser than water, they tend to sink, settling at a velocity that is proportional to their size.

The speed at which the kaolin particles settled during the purification process was calculated to be 1.477 X 10^{-6} m/s as shown in Table 4.2. The particles of different sizes settled at different rates in DDW, with the largest particles settling first. This was because

larger particles have more mass and therefore require more energy to move through a liquid than smaller particles.

Table 4.2: Kaolin Clay Sedimentation Design Parameters

Parameters	Results	Remarks
Liquid Viscosity, kg/m. s	8.90×10^{-4} kg/m. s	Viscosity of Distilled Water
Kaolin Clay Particle Density, kg/m^3	1600 kg/m^3	Particle Density
Density of Water, kg/m^3	997 kg/m^3	Density of Water
Acceleration due to Gravity, m/s^2	9.81 m/s^2	Gravitational Force
particle size (radius) of kaolin clay, m	1µm = 1 X 10^{-6} m	assumed to be spherical
Settling Height, m	0.12 m	Measurement of the Supernatant
Kaolin clay Settling Velocity, m/s	1.477 X 10^{-6} m/s	Calculated using Stoke's Law
Kaolin Clay Settling Time, hrs	22 hrs 57 mins	Calculated using Stoke's Law

The kaolin clay settling time was calculated to determine the exact hours it took for the kaolin particle to settle in DDW by gravity at the settling height of 0.12 m and 5 % yield in a 4-litre volumetric flask. The kaolin clay slurries during the sedimentation technique were allowed to settle according to Stoke's Law.

The settling time was calculated to be 22 hrs 57 minutes as earlier stated at a velocity of 1.477 X 10^{-6} m/s, settling height of 0.12 m, and liquid viscosity of 8.90×10^{-4} kg/m.s, kaolin clay particle density of 1600 kg/m^3, water density of 997 kg/m^3, acceleration due to gravity of 9.81 m/s^2 and kaolin clay particle size (radius) of 1 X 10^{-6} m. The settling time of 22 hrs 57 minutes derived in this work was in line with the 24 hours of settling time obtained by Abdulah (2005).

4.2.2 Selected physicochemical properties of raw and beneficiated kaolin

The physico-chemical properties of the raw and beneficiated kaolin are presented in Table 4.3.

Table 4.3: Selected Physicochemical Properties of Raw and Beneficiated Kaolin

Parameters	**Raw Kaolin Clay**	**Beneficiated Clay**
Colour	Off White	White
Particle Shape	Spherical	Spherical
Texture	Coarse	Fine
pH	5.60	7.02
Organic Carbon, %	0.045	0.00
Cation Exchange Capacity (CEC), meq/100 g	8.65	12.5
Electrical Conductivity, µS/cm	245	297
Density, g/cm^3	2.70	2.60
Viscosity (cP)	6.69	6.89

The pH values of the raw and beneficiated clay were determined to be 5.60 and 7.02 respectively. The pH change was due to the removal of impurities and the accrued mud during the beneficiation of the kaolin clay. The pH value of the beneficiated kaolin clay is slightly neutral and this would promote pollutant precipitation and adsorption. The organic matter in the raw kaolin was removed through the beneficiation technique. The organic matter in the raw kaolin clay could be attributed to the presence of dead animals and insects. The Cation Exchange Capacity (CEC) of the raw kaolin clay and beneficiated clay were 8.65 and 12.5 meq/100 g. The CEC characteristic would make the beneficiated kaolin clay play an important role in the adsorption of metal ions. The Electrical Conductivity (EC) of the beneficiated clay was higher than that of the raw kaolin clay. The higher EC in the beneficiated kaolin showed that it contained dissolved salts that could allow for the removal of phosphate, nitrate and some toxic metal ions in the domestic wastewater. The density of the beneficiated clay was lower than that of the raw kaolin clay. Porosity is directly related to bulk density and particle density. As particle density remains constant, bulk density increases, porosity decreases and vice versa. The porosity of the beneficiated clay was higher than the raw kaolin clay. The high porosity of the beneficiated clay could provide interlayer spacing making it a very good adsorbent for the removal of pollutants in the domestic wastewater.

The beneficiated kaolin was promising in pollutant removal than the raw kaolin considering the physicochemical properties of the raw and beneficiated kaolin clay.

4.3 Characterisation of Raw and Beneficiated Kaolin Clay (BKC)

4.3.1 XRD analysis

The phase purity and crystallinity of raw and beneficiated kaolin clay were examined by X–ray diffraction (XRD) technique and the results are presented and discussed in this section.

4.3.1.1 *XRD analysis of raw kaolin clay*

XRD diffractograms of raw kaolin clay displayed the existence of four crystalline phases of kaolinite – Al (Si_2O_5) $(OH)_4$, kaolinite 1Md – $AlSi_2O_5(OH)_4$, quartz – SiO_2 and muscovite – KAl_2 (Si_3Al) $O_{10}(OH)_2$. The identified phases were chemically identical, but their atoms were arranged differently except for muscovite which contained potassium as shown in Table 4.4. The dominant impurity compound in the raw kaolin clay was quartz with 66.41 % as shown in Table 4.4.

Table 4.4: XRD Phase Identification of Raw Kaolin Clay

Phases	**Formula**	**Percentage (%)**
Kaolinite	Al (Si_2O_5) $(OH)_4$	14.10
Kaolinite 1Md	$AlSi_2O_5(OH)_4$	15.04
Quartz	SiO_2	66.41
Muscovite	$Kal_2(Si_3Al)$ $O_{10}(OH)_2$	4.45

Interplanar spacing between the parallel planes of atoms in raw kaolin clay was gotten to be 3.4994 nm at Scherrer's constant of 0.94 and wavelength (λ) of 1.5406 Å in Table 4.5.

Table 4.5: Interplanar Spacing and Crystallite Size of Raw Kaolin Clay

Diffraction Angle, 2θ	d- spacing, (nm)	FWHM of the Intense Peak, β, (radians)	Crystallite Size, D, (nm)
12.2860	7.2203	0.25190	33.129
24.8213	3.5950	0.32526	26.120
26.5769	3.3613	0.15880	53.688
50.0630	1.8258	0.14218	64.408
62.2406	1.4945	0.40475	23.946
Average	**3.4994**		**40.258**

The average crystallite size for the raw kaolin clay was calculated to be 40.258 nm, while the average crystalline size diameter was calculated to be 40.258 nm. These two calculated parameters clearly showed that the raw kaolin clay is polycrystalline. The best peaks produced were selected and the Full Width at Half Maximum (FWHM) of the intense peak was calculated. The FWHM ranged from 0.1588 – 0.40475 radians. The XRD pattern showing various peaks produced is presented in Figure 4.1 (A). The broad and multiple peaks formation of the XRD pattern in Figure 4.1 (A) and (B) showed that both the raw and beneficiated kaolin clay were polycrystalline.

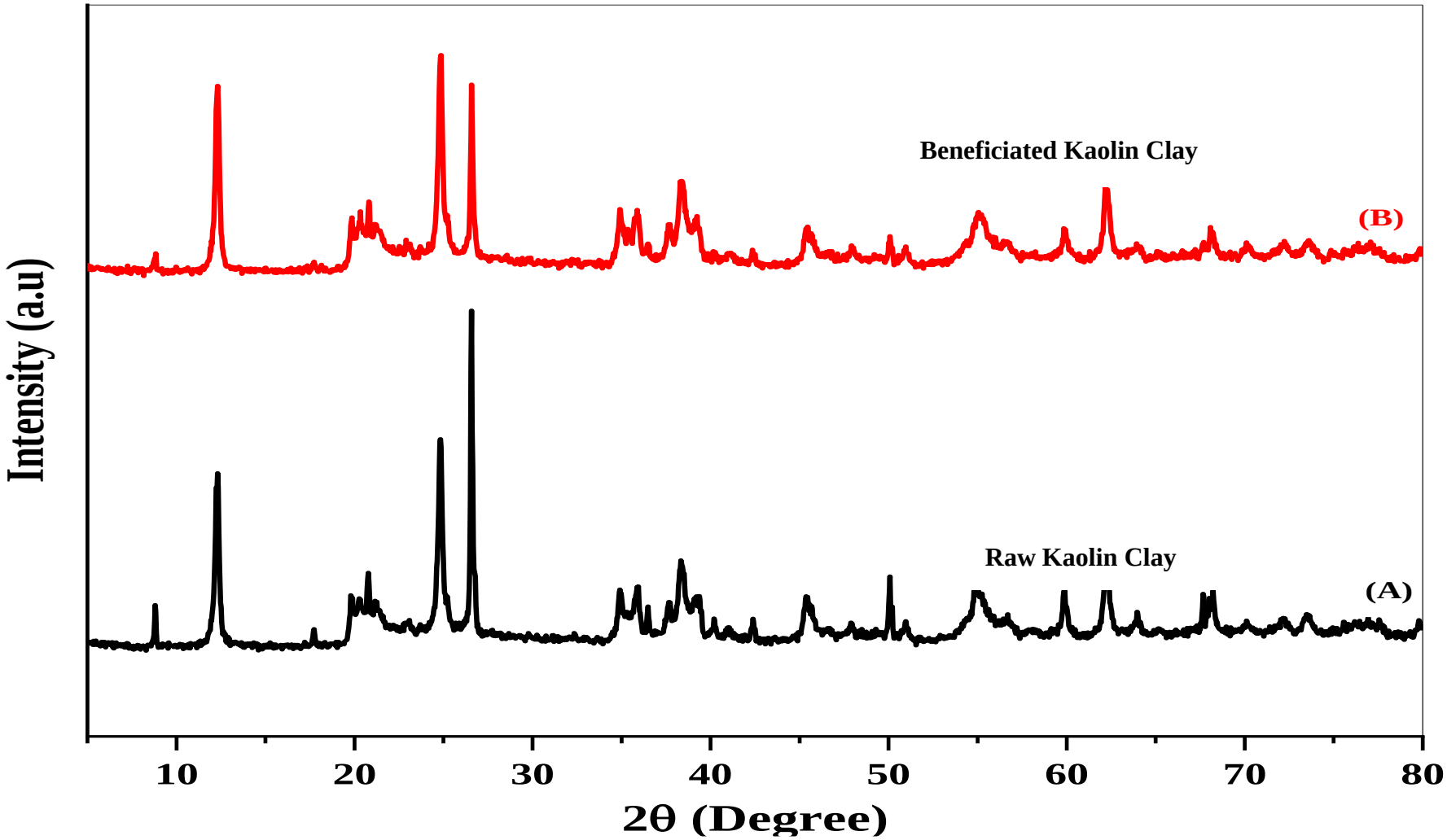

Figure 4.1: XRD Patterns of (A) Raw kaolin and (B) Beneficiated Kaolin

4.3.1.2 *XRD Analysis of beneficiated kaolin clay*

The beneficiated kaolin was analysed and was found to have four (4) different phases of kaolinite – Al (Si_2O_5) $(OH)_4$, kaolinite 1Md – $AlSi_2O_5(OH)_4$, quartz – SiO_2 and muscovite – $KAl_2(Si_3Al)$ $O_{10}(OH)_2$. These four identified phases were chemically identical, but their atoms were arranged differently except that of muscovite which contained potassium (Table 4.6).

Table 4.6: XRD Phase Identification of Beneficiated Kaolin Clay

Phases	**Formula**	**Percentage**
Kaolinite	Al (Si_2O_5) $(OH)_4$	28.52
Kaolinite 1Md	$AlSi_2O_5(OH)_4$	19.01
Quartz	SiO_2	46.85
Muscovite	Kal_2 (Si_3Al) $O_{10}(OH)_2$	5.62

Multiple peaks were detected for each phase between 5.077° to 85.049°. The dominant compound in the beneficiated clay was quartz. Inter-atomic spacing between the parallel planes in the BKC was calculated to be 3.532 nm. The average crystallite size for the BKC was also calculated to be 28.114 nm at Scherrer's constant of 0.94 and wavelength (λ) of 1.5406 Å as presented in Table 4.7. The best peaks produced were selected and the Full Width at Half Maximum (FWHM) of the intense peak was calculated. The FWHM ranged from 0.1825 – 0.5118 radians. The broad peak formation of the XRD pattern showed that the beneficiated clay was polycrystalline.

The XRD pattern showing various peaks produced during the characterisation of beneficiated kaolin clay is presented in Figure 4.1 (B) above.

Table 4.7: Interplanar Spacing and Crystallite Size of Beneficiated Kaolin Clay

Diffraction Angle, 2θ	**d- spacing, (nm)**	**FWHM of the Intense Peak, β, (radians)**	**Crystallite Size, D, (nm)**
12.2966	7.2142	0.3106	26.869
24.8279	3.5940	0.3225	26.348
26.5858	3.3602	0.1825	46.714
45.5049	1.9975	0.5118	17.580
62.2534	1.4942	0.4203	23.060
Average	**3.532**		**28.114**

Generally, crystallite size corresponds to the coherent volume in the beneficiated kaolin clay for the respective diffraction peak. Sometimes, it also corresponds to the size of the grains of a powder sample or the thickness of a polycrystalline thin film or bulk material. The crystallite size is an important parameter as the sizes of the crystals determine whether the material is soft (small crystallites) or brittle (large crystallites), as well as the thermal and diffusion behaviour of semicrystalline polymers (Sanjeeva, 2013).

4.3.2 XRF analysis of raw kaolin clay and beneficiated kaolin clay

XRF analysis was carried out on both raw and beneficiated kaolin clay to know the elemental compositions and the consequent chemical changes that occurred due to treatment.

Table 4.8 shows the results of the chemical analysis of the raw and beneficiated kaolin clay. The raw kaolin clay contained alumina (34.18 %) and silica (52.64 %) in large quantities. The beneficiated kaolin clay contained alumina of 35.95 % and silica of 48.55 % respectively. The data obtained for beneficiated kaolin clay were not much different from the data obtained for raw kaolin because the raw kaolin clay was the parent material.

Table 4.8: Mineralogical Composition of Raw and Beneficiated Kaolin Clay

Compound	Raw Kaolin Clay (%)	Beneficiated Kaolin Clay
Fe_2O_3 %	1.23	1.24
MnO %	0.00	0.00
Cr_2O_3 %	0.02	0.02
V_2O_5 %	0.00	0.00
TiO_2 %	1.69	1.75
CaO %	0.33	0.02
K_2O %	0.61	0.63
P_2O_5 %	0.07	0.05
SiO_2 %	52.64	48.55
Al_2O_3 %	34.18	35.95
MgO %	0.23	0.03
Na_2O %	0.11	0.14
LOI %	8.90	11.62
Total	100	100
SiO_2/Al_2O_3 Ratio	1.54	1.35

The proximity of silicate and alumina compositions obtained in the raw and beneficiated kaolin showed that raw kaolin has silicate more than beneficiated kaolin clay and the beneficiated kaolin clay contained alumina more than the raw kaolin. The loss of silicate and the gain of alumina in the beneficiated kaolin clay could be attributed to the purification and treatment method employed for the beneficiation of the kaolin clay as described in the methodology.

However, there were impurities oxides in trace amounts that were present in both the raw and beneficiated kaolin clay. The impurities and their percentage in trace amounts in raw kaolin clay were magnesium oxide (0.23 %), titanium oxide (1.69 %), phosphate oxide (0.07 %), iron oxide (1.23 %), calcium oxide (0.33 %), potassium oxide (0.07 %), chromium oxide (0.02 %) and sodium oxide (0.11 %). The impurities and their percentage in trace amounts that were present in the beneficiated kaolin clay were magnesium oxide (0.03 %) and phosphate oxide (0.05 %). Calcium oxide (0.02 %) contents decreased in the beneficiated clay, while iron oxide (1.24 %), titanium oxide (1.75 %), sodium oxide (0.14 %) and potassium oxide (0.63 %) increased. The chromium oxide (0.02 %)

remained constant in both the raw and the beneficiated clay. The impurities such as titanium particles with iron influenced the white shade colour in the kaolin clay (Chandrasekhar and Ramaswamy, 2002).

The SiO_2/Al_2O_3 ratio of kaolin clay which is a function of the mineral phase present was found to be 1.54 and 1.35 in raw and beneficiated kaolin clay respectively. Clay minerals are classified by the ratio of their silica and alumina sheets. Alumina and silica in pure kaolin clay according to the literature are ratio 1:1, one layer of silica for every layer of alumina (Abdullahi *et al.*, 2017). The SiO_2/Al_2O_3 ratio of beneficiated clay (1.35) as obtained in this study showed a purer kaolinite than the raw clay (1.54).

Loss on ignition (LOI) for the raw and beneficiated kaolin clay was found to be 11.58 % and 12.28 % respectively. Loss on ignition describes the process of measuring the weight change of the kaolin clay after treatment. LOI for raw and beneficiated kaolin was 8.90 % and 11.62 % respectively. The high LOI for beneficiated clay is attributed to the dihydroxylation reaction in the kaolin mineral. High LOI for beneficiated clay was also an indication of potential normal porosity in the intended kaolin clay filter pots for the treatment of domestic wastewater.

4.3.3 HRTEM and EDX analysis

4.3.3.1 *HRTEM – EDX analysis of raw kaolin clay*

The crystal structure, particle size, distribution patterns and morphology of the raw kaolin clay were studied by HRTEM – EDX.

The crystal patterns of the raw kaolin clay are presented in Plate VIII (a – e). HRTEM of raw kaolin clay showed kaolinite particles of varying sizes arranged in face-to-face patterns.

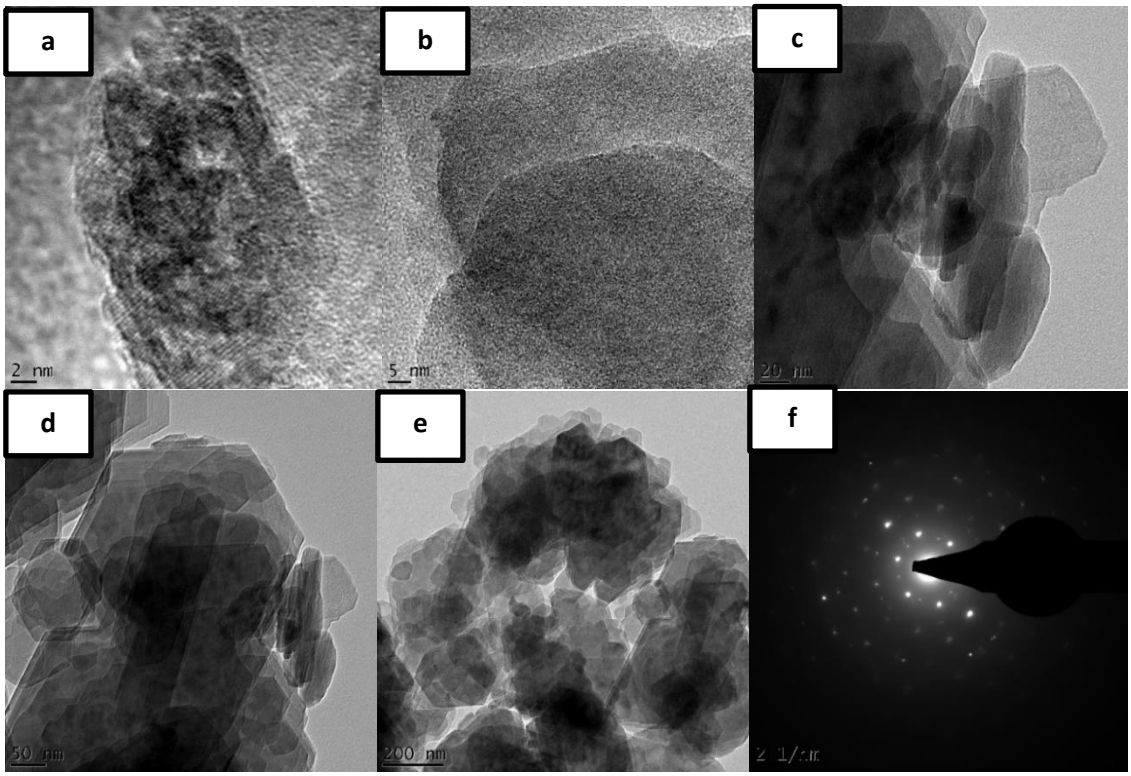

Plate VIII: HRTEM (a – e) and SAED (f) Images of Raw Kaolin Clay

The crystallinity of the raw kaolin clay structure was examined using the Selected Area Electron Diffraction (SAED) pattern in Plate VIII (f). The SAED pattern showed concentric circles of polycrystallinity. The bright spots and rings of the SAED pattern in Plate VIII (a – e) suggested that the raw kaolin clay is polycrystalline and each ring depicted a diffraction pattern of crystals of similar size with each bright spot reflecting individual peaks. SAED resolution patterns obtained were consistent with the results of XRD and XRF characterisation in this study. EDX analysis of the raw kaolin clay showed the presence of oxygen, aluminium and silicon with minor amounts of potassium, titanium and iron. The % atomic weight and % weight sigma of elements identified by the EDX analysis for raw kaolin clay are presented in Table 4.9.

Table 4. 9: EDX Analysis of Raw Kaolin Clay

Element	% weight	% weight Sigma
O	47.6	0.24
Al	22.7	0.15
Si	26.7	0.17
K	0.42	0.05
Ti	1.19	0.07
Fe	1.43	0.09
Total:	**100**	**0.77**

4.3.3.2 *HRTEM – EDX analysis of beneficiated kaolin clay*

HRTEM images in Plate IX (a – e) showed the structure of the beneficiated kaolin clay. HRTEM of beneficiated clay showed kaolinite particles of varying sizes arranged in face-to-face patterns. The crystal structure in Plate IX (f) showed bright rings of the SAED patterns that are polycrystalline. Each ring depicted the diffraction pattern of beneficiated kaolin clay particles.

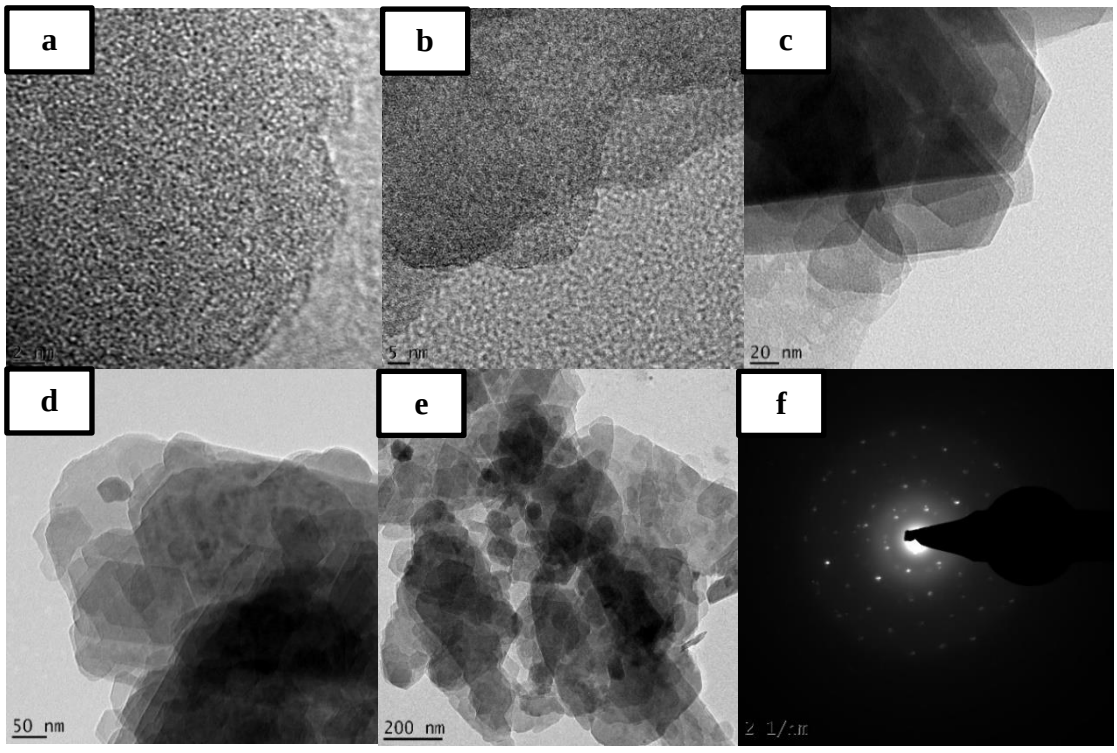

Plate IX: HRTEM (a – e) and SAED (f) Images of Beneficiated Kaolin Clay

The EDX analysis in Table 4.10 displayed silicate flakes of kaolinite for the beneficiated kaolin clay.

Table 4. 10: EDX Analysis of Beneficiated Kaolin Clay

Element	%Weight	%Weight Sigma
O	46.92	0.26
Al	21.42	0.16
Si	28.34	0.19
K	0.53	0.05
Ti	1.48	0.08
Fe	1.30	0.10
Total:	**100**	**0.84**

The EDX analysis indicated the presence of oxygen, aluminium and silicon in high quantities with minor amounts of potassium, titanium and iron. The % atomic weight and % weight sigma of elements identified by the EDX analysis for beneficiated kaolin clay is presented in Table 4.10.

Although the raw and the beneficiated kaolin clay exhibited similar morphologies based on EDX results, their elemental constituent differed. As could be seen, the major difference was attributed to the percentage reduction of iron, oxygen and aluminium and the increase in the presence of potassium, silicon and titanium in the beneficiated clay. These results suggested that there is a possibility of cation exchange between exchangeable cations in the beneficiated kaolin clay and metal ions during treatments. This would enhance high adsorption capacity and improve the removal efficiency of pollutants by the beneficiated kaolin clay. These results were consistent with the XRD and XRF results as earlier discussed**.**

4.4 BET Analysis of Beneficiated Kaolin Clay

The specific surface area, pore size and volume distribution of the beneficiated kaolin clay were studied by BET method in nitrogen adsorption and desorption environment.

The results of the particulate properties of the beneficiated kaolin clay such as surface area, pore size and volume distribution are presented in this section.

Nitrogen (N_2) adsorption-desorption isotherm of the beneficiated kaolin clay is displayed in Figure 4.2. The International Union of Pure and Applied Chemistry (IUPAC) classified N_2 adsorption isotherms into six types, type I - VI (Xu *et al.*, 2020). The beneficiated kaolin clay belongs to type IV isotherm with a hysteresis loop as shown in Figure 4.2.

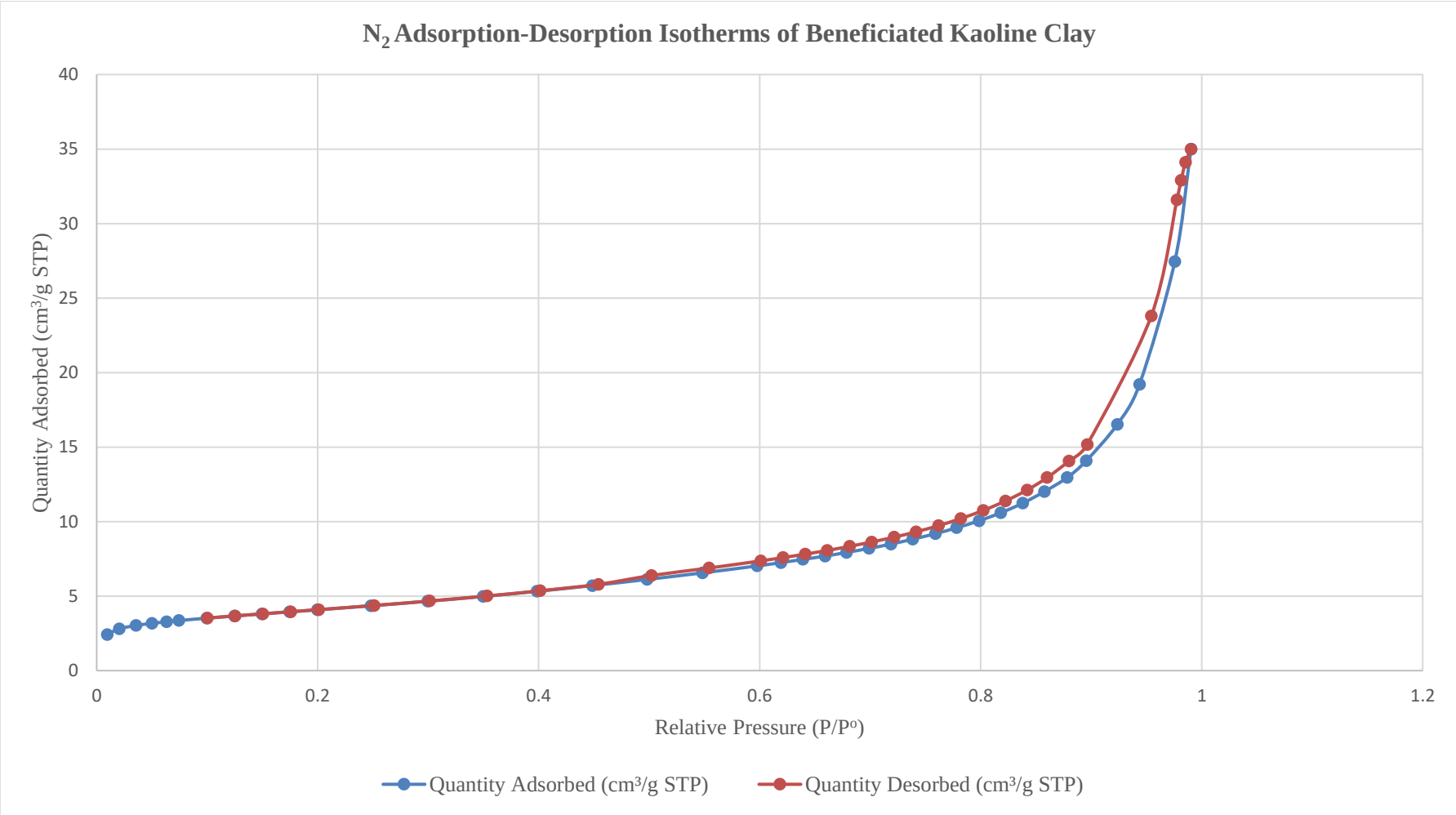

Figure 4.2: N_2 Adsorption-Desorption Isotherms of Beneficiated Kaolin

The quasi-overlapping adsorption-desorption curves in Figure 4.2 above indicated that the nitrogen adsorption-desorption isotherm curve of the beneficiated kaolin clay can be classified as Type IV, indicating a purely mesoporous material with a small pore size. This Type IV adsorption isotherm indicated that the beneficiated kaolin clay could be employed for the treatment of domestic wastewater.

The adsorption isotherms of the beneficiated kaolin clay rose progressively during the relative pressure range of 0 – 0.4 P/Po, which means mono-molecule layer adsorption occurs on the surface. Then, the adsorption curves rose steadily, resulting in the saturation of mono-molecule layer adsorption followed by the multi-molecular layer adsorption. When the relative pressure was 0.4 – 0.9 P/Po, the desorption branch was higher than the adsorption branch, along with the appearance of capillary condensation, which resulted in the hysteresis loop. At the relative pressure of 0.4 – 0.9 P/Po, the adsorption branch and desorption branch suddenly rose and coincided at the end.

Therefore, the occurrences of hysteresis loops indicated that the beneficiated kaolin clay had a lot of mesopores. Similarly, the smaller adsorption amount at P/Po < 0.4 and the large adsorption amount at P/Po > 0.9 showed that the beneficiated kaolin clay had a certain number of macropores (d > 50 nm) and a small number of micropores (d < 2 nm). This particular characteristic is ascribed mainly to mesoporous structures.

Furthermore, the IUPAC classified Hysteresis Loops into four types, each type representing a different pore shape (Xu *et al.*, 2020). Type H1 represents cylindrical pores in which both ends are open and capillary, condensation occurs in the middle of the relative pressure; Type H2 is associated with ink-bottle-shaped pores with poor connectivity and uneven pore structure, Type H3 is attributed to wedge-shaped pores formed by the loose stacking of flaky particles, and Type H4 is a result of slit-shaped

pores resulting from internal parallel pore structure. Hysteresis loops of the beneficiated kaolin clay belong to type H3, demonstrating that wedge-shaped pores took the primary position in the beneficiated kaolin clay.

The surface area of the beneficiated kaolin clay is presented in Table 4.11. The BET surface area was 14.5126 m^2/g. The surface area of the beneficiated kaolin clay is related to its particle shapes and sizes. As the particle sizes of the beneficiated kaolin clay decreases, the surface area increases. The higher the surface area of a particle, the better its capacity to adsorb pollutants in domestic wastewater treatment. The higher the surface area, the larger the adsorptive capacity.

Table 4.11: Surface Areas of BKC

Sample	Surface Area at p/p° (m^2/g)	BET Surface Area (m^2/g)	Adsorption Cumulative Surface Area of Pores (m^2/g)	Desorption Cumulative Surface Area of Pores (m^2/g)
BKC	14.2360	14.5126	16.0403	16.8099

The pore volume of the BKC is presented in Table 4.12. The adsorption total pore volume was 0.003740 cm^3/g. The pore volume is the total volume of very small openings in BKC particles.

Table 4.12: Pore Volume of BKC

Sample	Adsorption Total Volume of Pores (cm^3/g)	Desorption Total Volume (cm^3/g)	Adsorption Cumulative Volume of Pores (cm^3/g)	Desorption Cumulative Volume of Pore (cm^3/g)
BKC	0.003740	0.054122	0.055738	0.054830

The adsorption average diameter was 1.0309 nm and the adsorption average pore width was 13.8994 nm as shown in Table 4.13. The results showed that the adsorption-

desorption isotherms for the beneficiated kaolin clay possessed pore sizes that fell in the desorption average pore width of 13.0470 nm.

Table 4.13: Pore Size of BKC

Sample	Adsorption Average Pore Diameter (nm)	Desorption Average Pore Diameter (nm)	Adsorption Average Pore Width	Desorption Average Pore Width (nm)
BKC	1.0309	14.9174	13.8994	13.0470

These pore widths are classified as type IV isotherms when compared with the IUPAC classification of pore sizes. Type IV isotherms are given by mesoporous adsorbents. The adsorption behaviour in the mesopore is determined by the adsorbent-adsorptive interactions and by the interactions between the molecules in the condensed state. The BET analysis showed the BKC as a promising material to be used as adsorbent and filter pot production. It has also been reported that strong adsorbents used for water treatment have large surface areas (Worch, 2012).

4.5 Phytochemical Screening of *Mangifera indica*

The results of the phytochemical composition and antibacterial activity of leaf extracts of *Mangifera indica* were presented and discussed in this section. The process of its extraction is depicted on Plate X (a) and the extract is on Plate X (b).

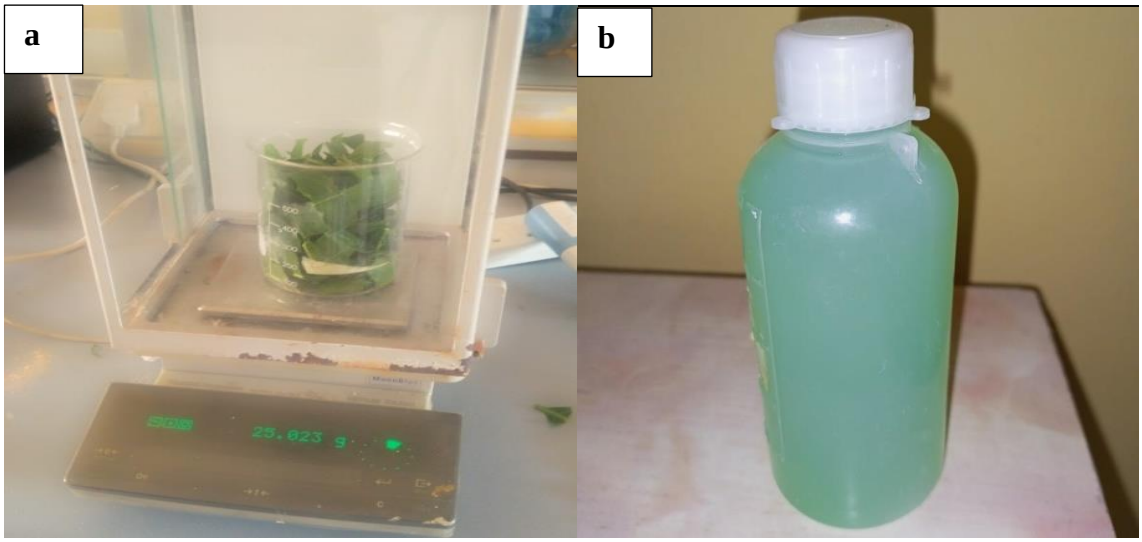

Plate X (a – b): (a). *Mangifera Indica* Leaf Phytochemical Screening (b). *Mangifera indica* Leaf Extracts

The result of the phytochemical screening of *Mangifera Indica* is presented in Table 4.14. The results indicated a reasonably high phenol, flavonoids and tannin contents with biologically active compounds that possess some disease-preventive properties and were, therefore, a suitable phytochemical screening agent to produce Ag/ZnO nanoparticles.

Table 4.14: Phytochemical Screening of *Mangifera indica*

Plant Part	Tannin (mg/g)	Flavonoid (mg/g)	Total Phenol (mg/g)
Mango Leaves	0.90	0.0183	5.348

The phenol composition of the *Mangifera indica* was found to be 5.348 mg/g. Phenolic is the largest category of phytochemicals and is most widely distributed in *Mangifera indica*. Phenol is an antiseptic and disinfectant. It is active against a wide range of micro-organisms including some fungi and viruses, but slowly effective against spores. The mechanisms of action of phenolic compounds on bacterial cells have been partially attributed to the damage of the bacterial membrane, inhibition of virulence factors such as enzymes and toxins, and suppression of bacterial biofilm formation. Some natural

polyphenols, aside from direct antibacterial activity, exert a synergistic effect when combined with common chemotherapeutics (Miklasińska *et al.*, 2018).

The flavonoid composition of the *Mangifera indica* was 0.0183 mg/g. Flavonoids possess many useful properties such as anti-inflammatory activity, oestrogenic activity, enzyme inhibition, antimicrobial activity, antiallergic activity, antioxidant activity, vascular activity and cytotoxic antitumour activity (Cushnie and Lamb, 2005).

The antimicrobial properties of *Mangifera indica* are attributed to its high flavonoid content. The flavonoid mode of antibacterial activity is due to cell lysis and disruption of the cytoplasmic membrane upon membrane permeability. Flavonoids show antimicrobial effects by inhibiting virulence factors, biofilm formation, membrane disruption, cell envelop synthesis, nucleic acid synthesis, and bacterial motility inhibition.

The tannin composition of the *Mangifera indica* was 0.90 mg/g. The antibacterial effectiveness of tannins is explained by their ability to pass through the bacterial cell wall up to the internal membrane, interfering with the metabolism of the cell that results in their destruction. In gram-positive bacteria, the activity of tannins is rapid. Tannic acid inhibits the bacteria attachment to the surfaces and a lack of bacteria adhesion to the surface results in bacteria cell death. Moreover, the sugar and amino acid uptake are inhibited by tannic acid and therefore limits the bacteria growth (Kaczmarek, 2020) in the wastewater.

4.6 Synthesis of Nanoparticles

Biomolecules present in plant extracts were used to reduce silver and zinc metal ions to nanoparticles in a single-step green synthesis process using *Mangifera indica* plant extract, a biological agent which includes the various water-soluble plant metabolites

such as alkaloids, phenolic compounds and tannin as a reducing agent and the results are presented and discussed under the section.

4.6.1 Syntheses of silver oxide and zinc oxide nanoparticles

The synthesised Ag and ZnO nanoparticles are shown in Plate XI (a - b). The synthesised Ag and ZnO nanoparticles oven-dried at 105 °C for 6 hours, calcined in the furnace at 450 °C for 3 hours were kept in a plastic bottle for further characterisation.

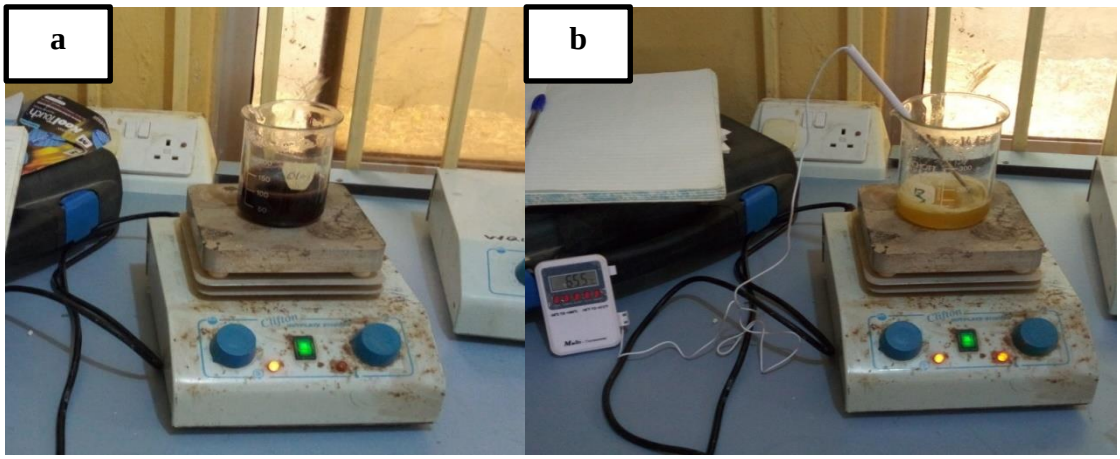

Plate XI (a – b): (a) Green Syntheses of Silver Oxide Nanoparticles, (b). Zinc Oxide Nanoparticles

4.6.2 XRD analysis of Ag nanoparticles

An XRD profile of Ag nanoparticles was found to contain one distinctive phase of silver – 3C with formula Syn-Ag between 15.000° and 80.019°. XRD pattern for Ag nanoparticles showed four distinct diffraction peaks at 38.117°, 44.278°, 64.427° and 77.475° and indexed the planes at 1 1 1, 2 0 0, 2 2 0 and 311 of the face-centred cubic silver respectively. The data obtained was matched with the database of the Joint Committee on Powder Diffraction Standards (JCPDS) File No. 00-004-0783.

The average interplanar spacing of Ag nanoparticles was calculated to be 1.7748 nm. The average crystallite size of the Ag nanoparticles was calculated to be 30.6285 nm at Scherrer's constant of 0.94 and wavelength (λ) of 1.5406 Å as presented in Table 4.15.

Table 4.15: Interplanar Spacing and Crystallite Size of Ag Nanoparticles

Diffraction Angle, 2θ	**d- spacing, (nm)**	**FWHM of the Intense Peak, β, (radians)**	**Crystallite Size, D, (nm)**
38.117	2.3660	0.2176	40.344
44.278	2.0500	0.2875	31.158
64.427	1.4490	0.3581	27.385
77.475	1.2342	0.4502	23.626
Average	**1.7748**		**30.6285**

The XRD pattern showing various peaks produced in the characterisation of Ag nanoparticles is presented in Figure 4.3 (A).

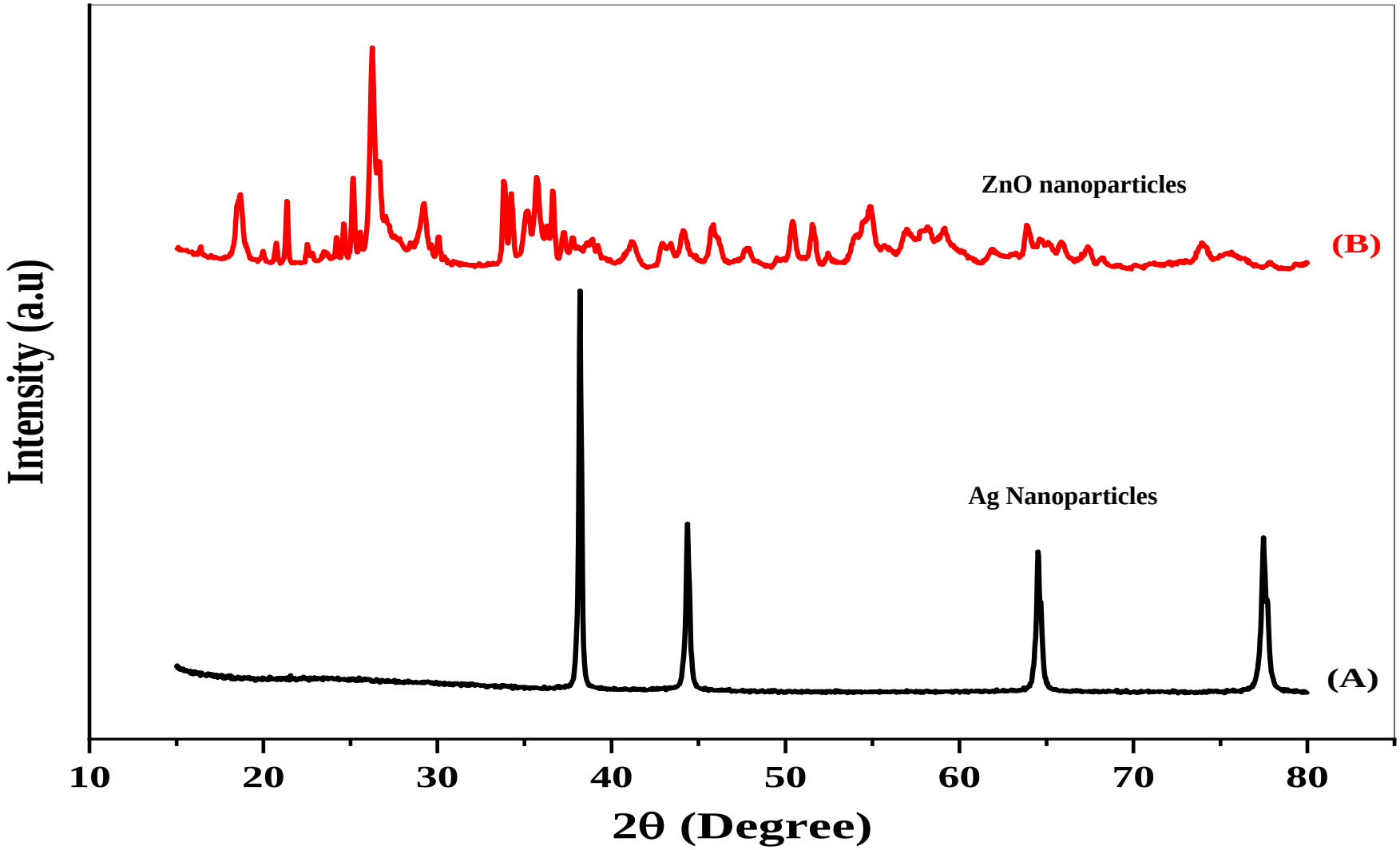

Figure 4.3: XRD patterns of (A) Ag and (B) ZnO Nanoparticles

As presented in Figure 4.3 (A), no trace of any impurities was detected, signifying the high purity of the synthesised Ag nanoparticle. XRD results confirmed that Ag nanoparticles were successfully synthesized with high crystallinity. Similar XRD patterns for silver nanoparticles have been reported elsewhere (Ng *et al.*, 2015).

4.6.3 XRD analysis of ZnO nanoparticles

XRD profiles of the ZnO nanoparticles showed seven (7) different phases which are Zinkosite Syn (NR) – $ZnSO_4$, zinkosite – Zinkosite, Gunnigile, Syn - $ZnSO4\ H_2O$, Zinc Oxide Sulphate - $Zn_3O(SO4)_2$, Zinc Hydroxide - $Zn\ (OH)_2$ and Zinc Hydrogen Sulphate - $Zn\ (HSO_4)_2$. The identified phases were arranged differently except zinkosite, Syn (NR) and zinkosite as shown in Table 4.16. The dominant compound was Gunnigile, Syn at 26.77 % followed by zinkosite, Syn (NR) and zinkosite at 24.74 % each as shown in Tables 4.16.

Table 4.16: XRD Phase Identification of ZnO Nanoparticles

Phases	**Formula**	**Percentage**
Zinkosite, Syn (NR)	$ZnSO_4$	24.74
Zinkosite	$ZnSO_4$	24.74
Gunnigile, Syn	$ZNSO_4\ H_20$	36.08
Zinc Oxide Sulphate	$Zn_3O(SO_4)_2$	8.25
Zinc Hydroxide	$Zn\ (OH)_2$	4.12
Zinc Hydrogen Sulphate	$Zn\ (HSO_4)_2$	2.06

Multiple peaks were detected for each phase presented in Table 4.17 between 5.000^o to 80.003^o. The XRD spectra confirmed that the ZnO nanoparticles have polycrystalline hexagonal structure and crystallite size in the range of 32.038 nm. XRD results confirmed that ZnO nanoparticles were successfully synthesized.

Table 4.17: Interplanar Spacing and Crystallite Size of ZnO Nanoparticles

Diffraction Angle, 2θ	d- spacing, (nm)	FWHM of the Intense Peak, β, (radians)	Crystallite Size, D, (nm)
12.3308	7.1942	0.3843	21.718
24.8750	3.5873	0.2997	28.351
26.6338	3.3543	0.1529	55.773
59.9510	1.5460	0.3192	30.009
62.2992	1.4933	0.3984	24.337
Average	**3.435**		**32.038**

Interplanar spacing for ZnO nanoparticles produced was calculated to be 3.435 nm and the average crystallite size was 32.038 nm at Scherrer's constant of 0.94 and wavelength (λ) of 1.5406 Å as shown in table 4.17. The XRD pattern showing various peaks produced for the identified phases of ZnO nanoparticles is presented in Figure 4.3 (B) above.

4.6.4 XRF analysis of ZnO/Ag nanoparticles

The XRF analysis to know the chemical composition of ZnO/Ag nanoparticles is presented in Table 4.18. The SiO_2/Al_2O_3 ratio did not exist for the synthesised Ag and ZnO nanoparticles and loss on ignition was 52.13 % and 51.1 % respectively.

Table 4.18: Mineralogical composition (XRF) of ZnO/Ag Nanoparticles

Compound	ZnO Nanoparticles	Ag Nanoparticles
Fe_2O_3 %	0.01	0.00
MnO %	0.00	0.00
Cr_2O_3 %	0.01	0.00
V_2O_5 %	0.00	0.00
TiO_2 %	0.05	0.01
CaO %	0.18	0.02
K_2O %	0.42	0.01
P_2O_5 %	0.04	0.00
SiO_2 %	0.00	0.00
Al_2O_3 %	0.02	0.00
MgO %	0.06	0.00
Na_2O %	9.21	0.02
LOI %	52.13	51.10
Total	62.15	53.56
SiO_2/Al_2O_3 Ratio	0.000	0.000

4.6.5 UV–visible spectrometer analysis of ZnO and Ag nanoparticles

4.6.5.1 *Ag nanoparticle spectrum peak formation*

The spectrum peak formation of Ag nanoparticles was confirmed by the UV-visible spectrometer analysis. The UV-visible spectrometry results of the synthesized Ag nanoparticles are presented in Figure 4.4. The formation of absorbance peaks corresponded to the formation of silver nanoparticles. Ag nanoparticles spectrum was observed at the characteristic absorption peak of 298.5 nm wavelength and absorbance of 0.444. The UV–visible spectrometer confirmed the formation of Ag nanoparticles.

4.6.5.2 *ZnO nanoparticle spectrum peak formation*

The synthesized ZnO nanoparticle is presented in Figure 4.5. The formation of absorbance peaks corresponded to the formation of ZnO nanoparticles with the spectrum observed at the characteristic absorption peak of 264.5 nm and absorbance of 0.977. The UV–visible spectra confirmed the formation of ZnO nanoparticles.

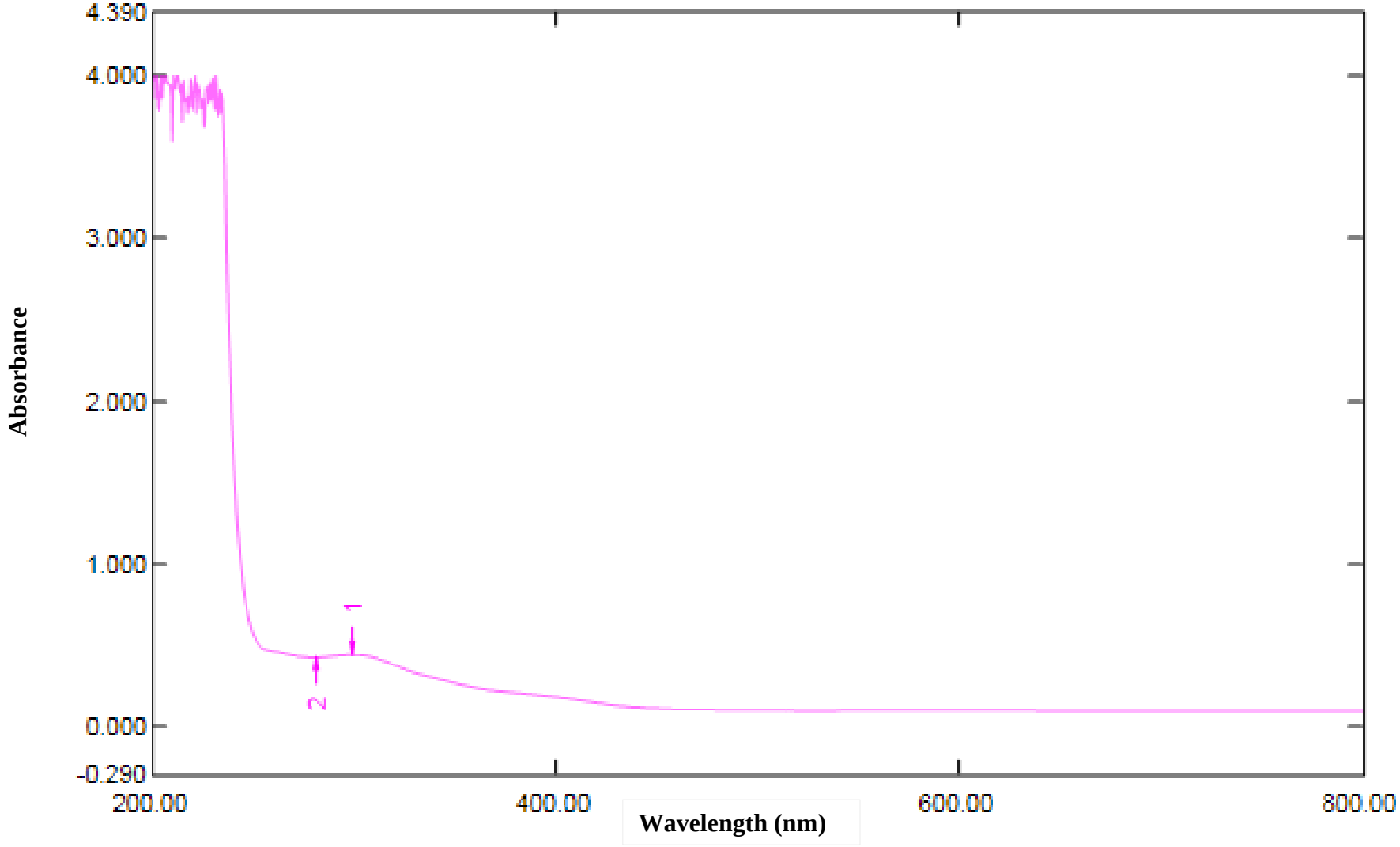

Figure 4.4: Ag Nanoparticle Spectrum Peak Formation

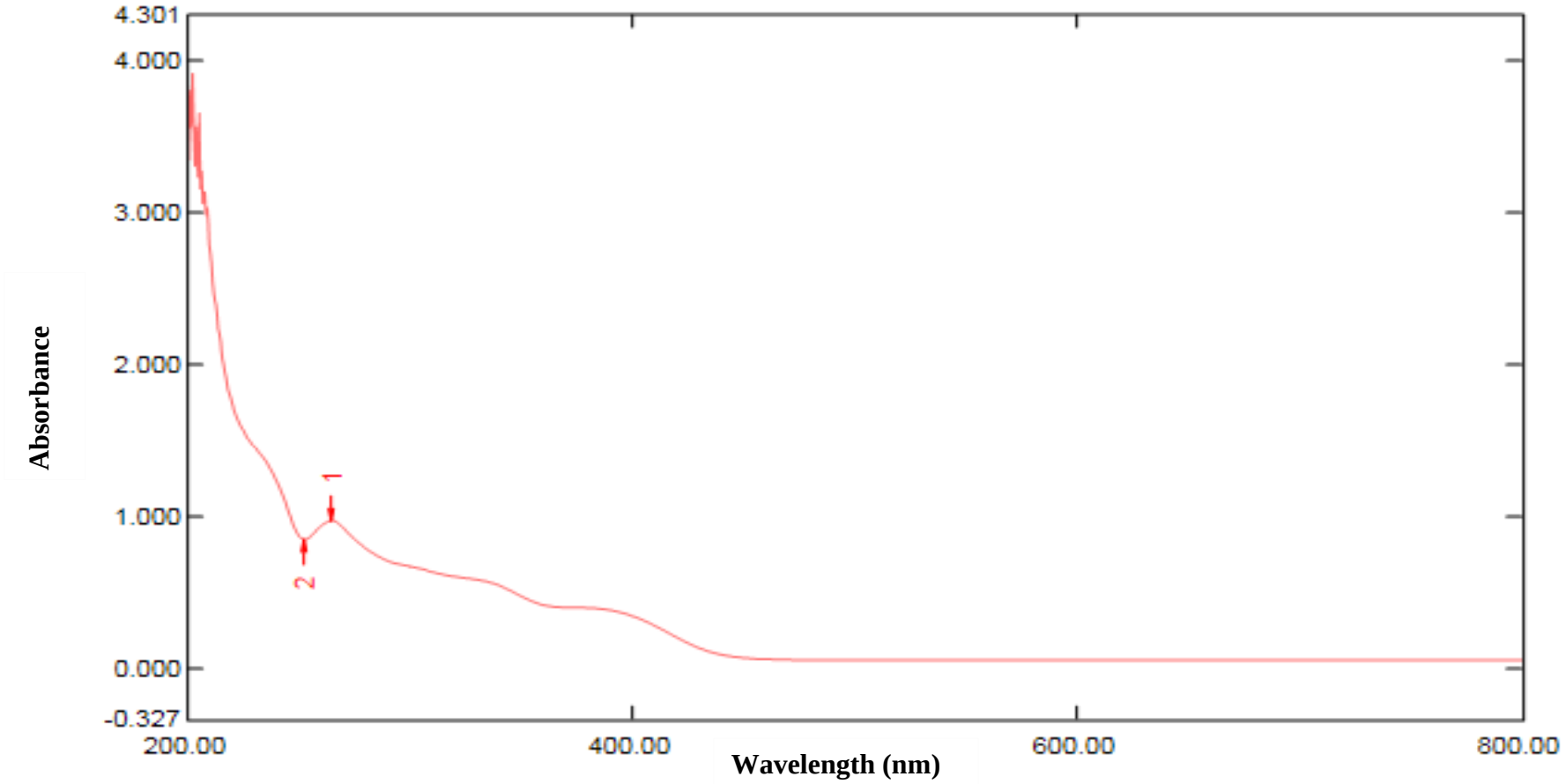

Figure 4.5: ZnO Nanoparticle Spectrum Peak Formation

4.7 HRTEM – SAED Analysis of Nanoparticles

4.7.1 HRTEM – SAED analysis of Ag nanoparticles

The crystal structure of the Ag nanoparticle was further studied by HRTEM and the image patterns are presented in Plate XII (a – e).

The crystallinity of the Ag nanoparticle was examined using the SAED pattern and the results are presented in Plate XII (f). The SAED pattern in Plate XII (f) showed concentric circles which are monocrystalline. The bright spots and rings of the SAED patterns suggested the Ag nanoparticle is monocrystalline. SAED resolution patterns are consistent with the XRD and XRF results of Ag nanoparticles as earlier stated in this study.

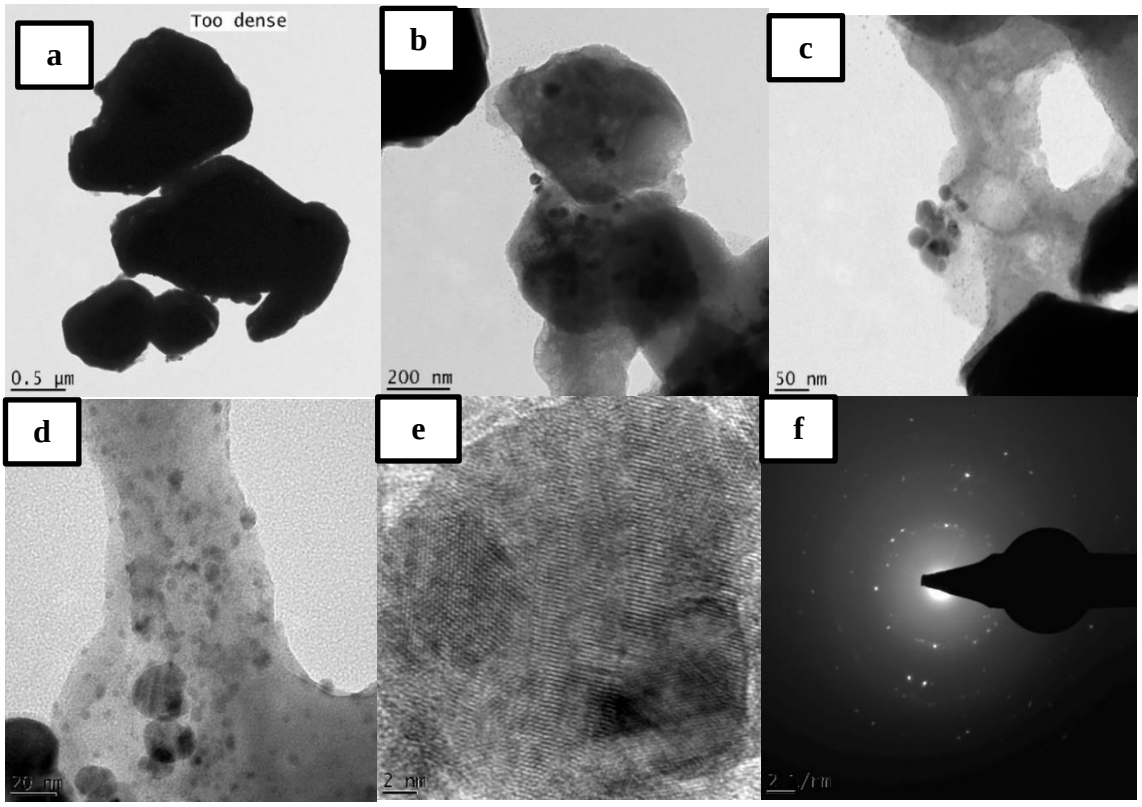

Plate XII: HRTEM (a – e) and SAED (f) Images of Ag Nanoparticles

4.7.2 HRTEM – SAED analysis of ZnO nanoparticles

The crystal structure of the ZnO nanoparticle was analysed by HRTEM to know the crystal pattern at the scales approaching a single atom. The HRTEM patterns are presented in Plate XIII (a – e). The crystallinity of the ZnO nanoparticle was examined using the SAED pattern and the results are presented in Plate XIII (f). The SAED pattern in Plate XIII (f) showed faded circles which are polycrystalline.

The bright spots and rings of the SAED patterns suggest that the ZnO nanoparticle is polycrystalline and each ring depicted a diffraction pattern of crystals of similar size with each bright spot reflecting individual peaks.

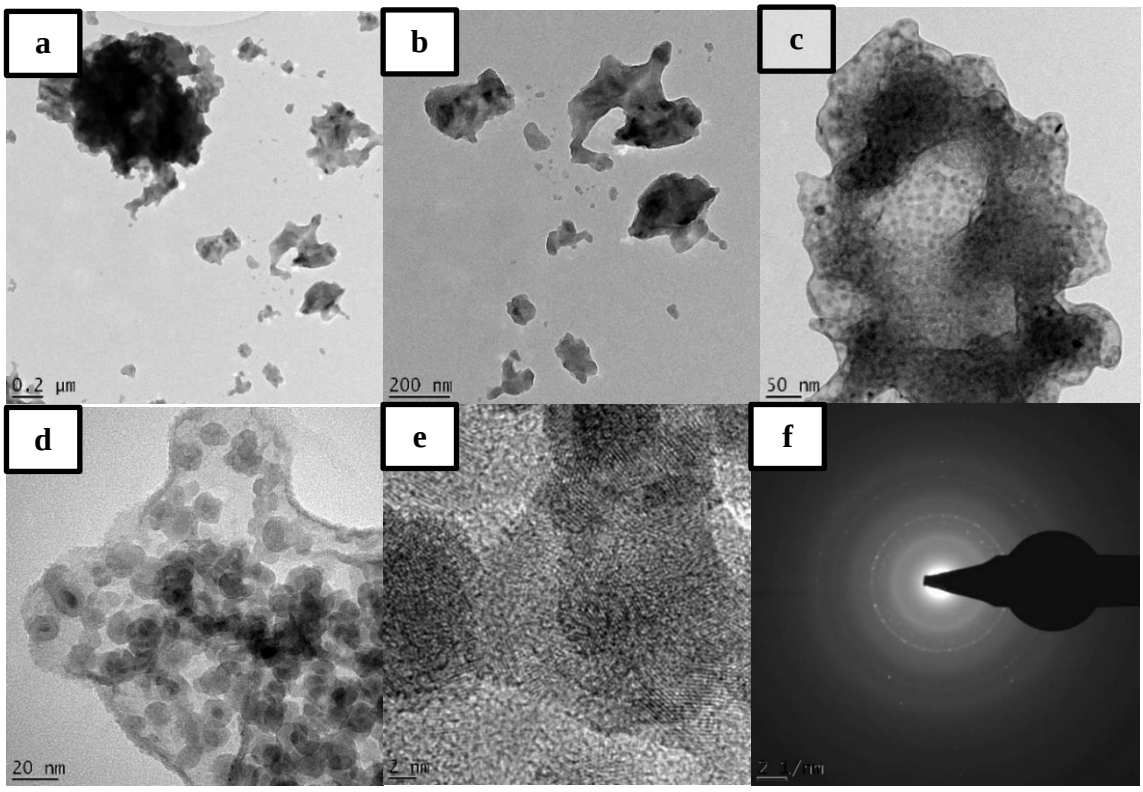

Plate XIII: HRTEM (a – e) and SAED (f) Images of ZnO Nanoparticles

4.7.3 BET analysis of ZnO and Ag nanoparticles

The surface area, pore volume and pore size of the ZnO and Ag nanoparticles were presented in Tables 4.19 – 4.21 respectively. The BET surface areas of the ZnO and Ag nanoparticles are 1.1045 m^2/g and 1.0545 m^2/g respectively (Table 4.19).

Table 4.19: Surface Areas of ZnO nanoparticles and Ag nanoparticles

Sample	Single Point Surface Area at p/p° (m^2/g)	Surface Area (m^2/g [1])	Adsorption Cumulative Surface Area of Pores (m^2/g)	Desorption Cumulative Surface Area of Pores (m^2/g)
ZnO -NPs	1.0819	1.1045	0.9246	1.8467
Ag – NPs	1.0319	1.0545	0.8646	1.7860

The single point adsorption total pore volume of ZnO and Ag nanoparticles were 0.000319 cm^3/g and 0.000269 cm^3/g respectively (Table 4.20).

Table 4.20: Pore Volume of ZnO and Ag Nanoparticles

Sample	Adsorption Total Volume of Pores (cm^3/g)	Desorption Total Volume of Pores (cm^3/g)	Adsorption Cumulative Volume of Pores (cm^3/g)	Desorption Cumulative Volume of Pore (cm^3/g)
ZnO - NPs	0.000319	0.003908	0.003904	0.003910
Ag – NPs	0.000269	0.003408	0.003307	0.003310

Adsorption average pore size of the ZnO and Ag nanoparticles were 1.1555 nm and 1.1057 nm and the BJH adsorption average pore width was 16.8893 nm and 15.9899 nm respectively as presented in Table 4.21.

Table 4.21: Pore Size of ZnO and Ag Nanoparticles

Sample	Adsorption Average Pore Diameter (nm)	Desorption Average Pore Diameter (nm)	BJH Adsorption Average Pore Width	BJH Desorption Average Pore Width (nm)
ZnO -NPs	1.1555	14.1536	16.8893	8.4686
Ag – NPs	1.1057	14.1035	15.9899	8.3788

These results showed that the adsorption-desorption isotherms for the ZnO and Ag nanoparticles possessed pore sizes that fell in the mesopore widths. Mesopore widths are classified as type IV isotherms when compared with the IUPAC classification of pore sizes. Type IV isotherms are given by mesoporous adsorbents. The adsorption behaviour in the mesopore is determined by the adsorbent-adsorptive interactions and by the interactions between the molecules in the condensed state.

Also, the occurrences of hysteresis loops indicated that the ZnO nanoparticle had a lot of mesopores (Figure 4.6). Similarly, the smaller adsorption amount at P/Po < 0.4 and the large adsorption amount at P/Po > 0.9 showed that the ZnO nanoparticle had a certain number of macropores (d > 50 nm) and a small number of micropores (d < 2 nm). This particular characteristic is ascribed mainly to mesoporous structures.

The quasi-overlapping adsorption-desorption curves in Figure 4.6 above indicated that the nitrogen adsorption-desorption isotherm curve of the ZnO nanoparticle can be classified as Type IV, demonstrating a purely mesoporous material with a small pore size.

Figure 4.7 above shows the typical nitrogen sorption isotherms of Ag nanoparticles as a type IV adsorption in the low-pressure region (P/P0 < 0.7). At the relative high-pressure region (P/P0 > 0.7), due to the capillary agglomeration phenomenon, the isotherms increase rapidly and form a lag loop.

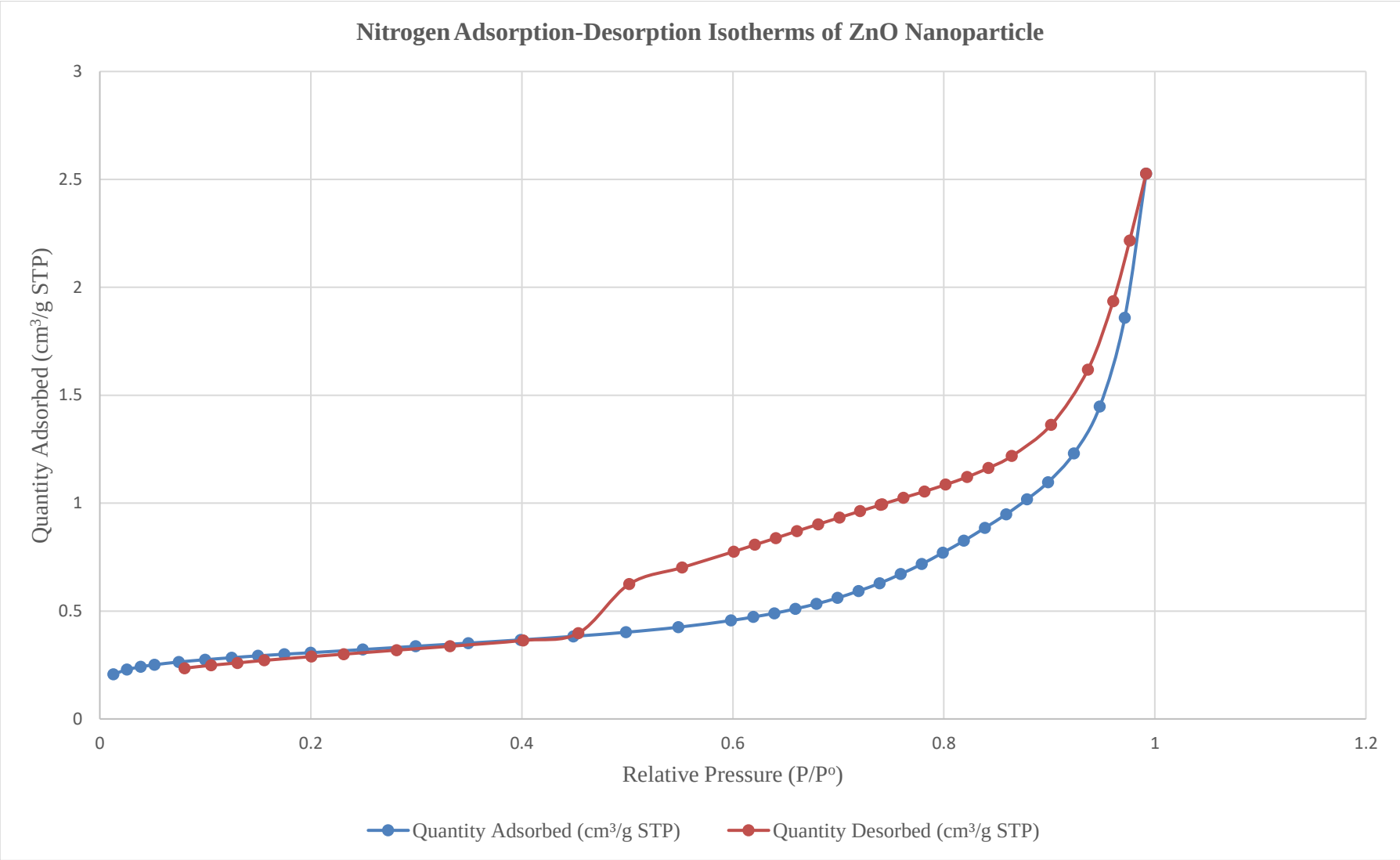

Figure 4.6: N_2 Adsorption-Desorption Isotherms of ZnO Nanoparticle

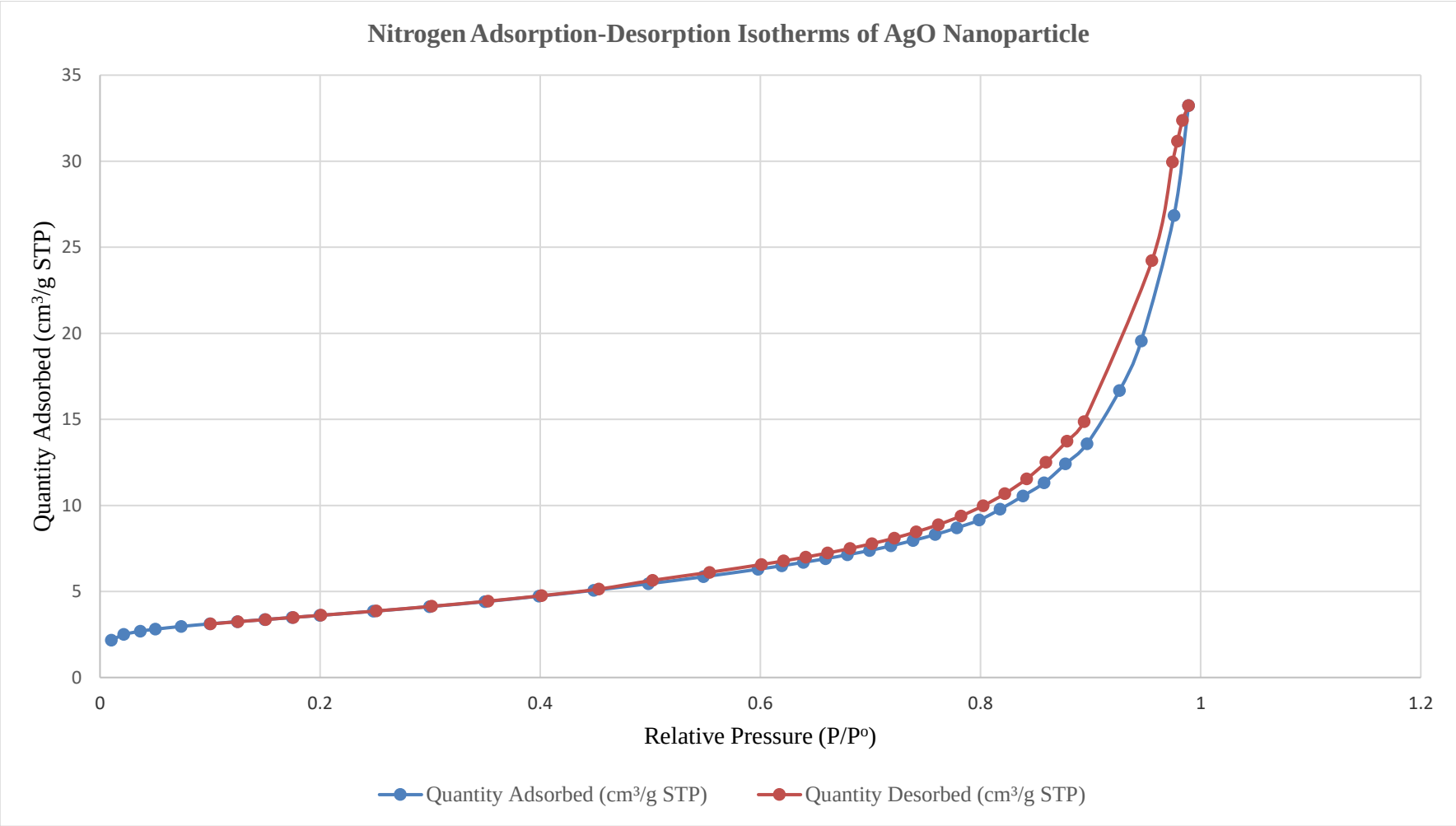

Figure 4.7: N_2 Adsorption-Desorption Isotherms of Ag Nanoparticles

It can be seen from Figure 4.7 that the adsorption-desorption isotherms of Ag nanoparticles were completely superimposed because the adsorption of the Ag nanoparticles mostly occurs in the micropores.

4.8 Syntheses of Nanocomposite Adsorbents

The characterisation results of Ag/ZnO nanoparticles produced by green syntheses and blended with BKC to produce nanocomposite adsorbent through wet impregnation methods for the treatment of domestic wastewater were presented and discussed in this section.

4.8.1 XRD analysis of BKC/Ag nanocomposite adsorbent

XRD profiles of the BKC impregnated with Ag nanoparticles were found to contain four (4) different phases of kaolinite – Al (Si_2O_5) $(OH)_4$, quartz – SiO_2, muscovite – KAl_2 (Si_3Al) $O_{10}(OH)_2$ and Silver – 3C-Syn-Ag. The analysis clearly showed the impregnation of Syn-Ag at 13.93 % on the BKC. These four identified phases were arranged differently (Table 4.22).

Table 4.22: XRD Phase Identification of BKC/Ag Nanocomposite Adsorbent

Phases	Formula	Percentage
Kaolinite	Al (Si_2O_5) $(OH)_4$	47.01
Quartz	SiO_2	38.23
Muscovite	KAl_2 (Si_3Al) $O_{10}(OH)_2$	0.82
Silver – 3C	Syn – Ag	13.93

Quartz and a little trace of muscovite were the impurities present in the purified kaolin clay impregnated with Ag nanoparticles. The dominant compound in the BKC/Ag nanocomposite was kaolinite. The average Interplanar spacing (d-spacing) was 3.818 nm and the average crystallite size was 25.574 nm (Table 4.23) at Scherrer's constant of 0.94 and wavelength (λ) of 1.5406 Å.

Table 4.23: Interplanar Spacing and Crystallite Size of BKC/Ag Nanocomposite Adsorbent

Diffraction Angle, 2θ	d- spacing, (nm)	FWHM of the Intense Peak, β, (radians)	Crystallite Size, D, (nm)
12.2865	7.2200	0.51288	16.271
24.8586	3.5897	0.32121	26.452
26.6117	3.3570	0.17624	48.379
34.9694	2.5714	0.30723	28.315
38.3830	2.3502	1.03927	8.454
Average	**3.818**		**25.574**

The XRD pattern for BKC impregnated with Ag nanoparticles is presented in Figure 4.8 (A). The XRD pattern showed that the BKC/Ag nanocomposite was polycrystalline.

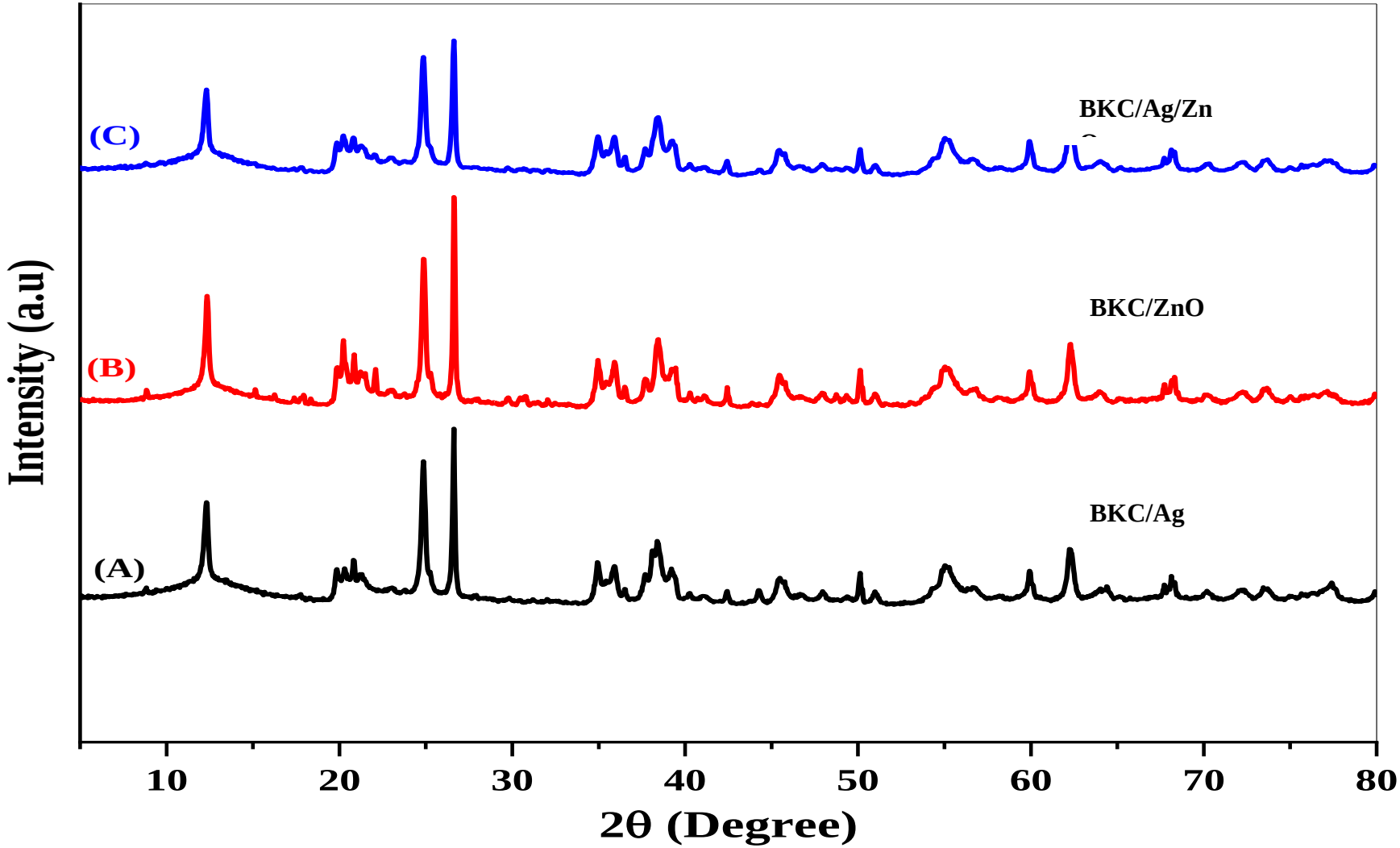

Figure 4.8: XRD patterns of (A). BKC/Ag, (B). BKC/ZnO and (C). BKC/Ag/ZnO

4.8.2 XRD analysis of BKC/ZnO nanocomposite adsorbent

The XRD pattern showing various peaks produced is presented in Figure 4.8 (B) above. The broad peak formation of the XRD pattern showed that the BKC/ZnO nanocomposite adsorbent was polycrystalline.

XRD profiles of the purified kaolin clay mixed with ZnO nanoparticles were found to contain four (4) different phases of kaolinite – Al (Si_2O_5) $(OH)_4$, quartz – SiO_2, muscovite – KAl_2 (Si_3Al) $O_{10}(OH)_2$ and Zinc Sulphate Hydrate - $ZnSO_4$ $6H_2O$. The four phases were arranged differently as shown in Table 4.24.

Table 4.24: XRD Phase Identification of BKC/ZnO Nanocomposite Adsorbent

Phases	Formula	Percentage
Kaolinite	Al (Si_2O_5) $(OH)_4$	35.56
Quartz	SiO_2	53.38
Muscovite	KAl_2 (Si_3Al) O10$(OH)_2$	3.16
Zinc Sulphate Hydrate	$ZnSO_4$ $6H_2O$	7.90

Multiple peaks were detected for each phase between 5.000^o and 80.003^o. The analysis showed the impregnation of zinc sulphate hydrate at 7.90 % on the purified kaolin clay as shown in Table 4.24.

The lattice spacing of the BKC/ZnO nanocomposite adsorbent produced was calculated to be 4.712 nm, while the average crystallite size was calculated to be 35.692 nm at Scherrer's constant of 0.94 and wavelength (λ) of 1.5406 Å as shown in Table 4.25.

Table 4.25: Interplanar Spacing and Crystallite Size of BKC/ZnO Nanocomposite Adsorbent

Diffraction Angle, 2θ	d- spacing, (nm)	FWHM of the Intense Peak, β, (radians)	Crystallite Size, D, (nm)
12.3311	7.1940	0.3754	22.234
24.8750	3.5873	0.2962	28.686
26.6338	3.3543	0.1518	56.155
Average	**4.712**	**0.30723**	**35.692**

4.8.3 XRD analysis of BKC/Ag/ZnO nanocomposite adsorbent

XRD profiles of the BKC impregnated with Ag/ZnO nanoparticles were found to have five (5) different phases of kaolinite – Al (Si_2O_5) $(OH)_4$, quartz – SiO_2, muscovite – KAl_2 (Si_3Al) $O_{10}(OH)_2$ Zinc Sulphate Hydrate - $ZnSO_4$ $6H_2O$ and silver – 3C. These five phases were arranged differently as presented in Table 4.26.

Table 4.26: XRD Phase Identification of BKC/Ag/ZnO Nanocomposite Adsorbent

Phases	Formula	Percentage
Kaolinite	Al (Si_2O_5) $(OH)_4$	51.27
Quartz	SiO_2	41.69
Muscovite	KAl_2 (Si_3Al) $O_{10}(OH)_2$	0.90
Zinc Sulphate Hydrate	$ZnSO_4$ $6H_2O$	3.80
Silver – 3C	Syn-Ag	2.34

Multiple peaks were detected for each phase between 5.049^o to 80.041^o. The dominant compound in nanocomposites was kaolinite with 51.27 %. The XRD analyses showed the impregnation of silver – 3C and zinc sulphate hydrate on the beneficiated kaolin clay at 2.34 % and 3.80 % respectively (Table 4.26). The XRD various peaks pattern for BKC/Ag/ZnO nanocomposite adsorbent is presented in Figure 4.8 (C) above. The broad peak formation of the XRD pattern showed that the BKC/Ag/ZnO nanocomposite was polycrystalline.

The average Inter-atomic spacing of beneficiated kaolin clay impregnated with Ag/ZnO nanoparticles was 3.887 nm while the average crystallite size was calculated to be 26.934 nm at Scherrer's constant of 0.94 and wavelength (λ) of 1.5406 Å as shown in Table 4.27.

Table 4.27: Interplanar Spacing and Crystallite Size of BKC/Ag/ZnO Nanocomposite Adsorbent

Diffraction Angle, 2θ	d- spacing, (nm)	FWHM of the Intense Peak, β, (radians)	Crystallite Size, D, (nm)
12.2779	7.225	0.505	16.525
24.8520	3.591	0.352	24.155
26.6085	3.357	0.205	41.551
68.2487	1.377	0.393	25.507
Average	**3.887**		**26.934**

4.8.4 XRF analysis of BKC/ZnO, BKC/Ag and BKC/Ag/ZnO nanocomposite adsorbents

The XRF analysis was carried out on BKC/ZnO, BKC/Ag and BKC/Ag/ZnO nanocomposites adsorbents to know the chemical compositions and the consequent chemical changes that occurred during the impregnation of Ag/ZnO nanoparticles on BKC. Table 4.28 shows the results of chemical analysis of the BKC/ZnO, BKC/Ag and BKC/Ag/ZnO nanocomposite adsorbents.

Table 4.28: XRF Analysis of BKC/ZnO, BKC/Ag and BKC/Ag/ZnO Nanocomposite**s** Adsorbents

Compound	BKC/Ag	BKC/ZnO	BKC/Ag/ZnO
Fe_2O_3 %	1.00	1.04	0.97
MnO %	0.00	0.01	0.00
Cr_2O_3 %	0.03	0.03	0.02
V_2O_5 %	0.03	0.03	0.02
TiO_2 %	1.61	1.69	1.58
CaO %	0.00	0.09	0.05
K_2O %	0.56	0.53	0.54
P_2O_5 %	0.05	0.04	0.03
SiO_2 %	45.80	44.13	46.21
Al_2O_3 %	30.19	29.78	30.34
MgO %	0.00	0.00	0.00
Na_2O %	0.18	1.16	0.40
LOI %	9.61	16.31	12.37
Total	89.10	94.82	92.55
SiO_2/Al_2O_3 Ratio	1.517	1.4818	1.5231

The BKC/Ag/ZnO nanocomposite contains alumina (30.34 %) and silica (46.21 %) with other oxides such as iron oxide (0.97 %), calcium oxide (0.05 %) and phosphorous oxide (0.03 %). The SiO_2/Al_2O_3 ratio which is a function of the mineral phase present was found to be 1.5231 in BKC/Ag/ZnO, 1.517 in BKC/Ag and 1.4818 in BKC/ZnO nanocomposites adsorbents respectively. Loss on ignition for BKC/Ag/ZnO, BKC/ZnO and BKC/Ag nanocomposite adsorbents was found to be 12.37 %, 16.31 % and 9.61 % respectively.

The SiO_2/Al_2O_3 ratio of BKC/Ag, BKC/ZnO and BKC/Ag/ZnO nanocomposites adsorbents was found to be 1.517, 1.4818 and 1.5231 respectively. The SiO_2/Al_2O_3 ratio of BKC/Ag, BKC/ZnO and BKC/Ag/ZnO nanocomposites showed a purer kaolinite than the raw clay.

Loss on ignition (LOI) for BKC/Ag, BKC/ZnO and BKC/Ag/ZnO nanocomposites was found to be 9.61%, 16.31% and 12.37 % respectively. Loss on ignition describes the process of measuring the weight change of the nanocomposite adsorbents after

production. The high LOI for BKC/Ag/ZnO nanocomposite adsorbents may be attributed to the dihydroxylation reaction in the kaolin mineral. High LOI for BKC/Ag/ZnO was also an indication of potential normal porosity in the intended kaolin clay filter adsorbent for the treatment of domestic wastewater.

4.8.5 HRTEM – SAED analysis of BKC/Ag nanocomposite adsorbents

HRTEM images in Plate XIV (a – e) clearly showed the impregnation of Ag nanoparticles on the purified kaolin clay. The BKC/Ag nanocomposite crystal structure in Plate XIV (f) showed bright rings of the SAED patterns. The SAED pattern showed concentric circles of polycrystallinity.

The bright spots and rings of the SAED pattern suggested that the BKC/Ag nanocomposite adsorbent is polycrystalline and each ring depicted a diffraction pattern of crystals of similar size with each bright spot reflecting individual peaks. SAED resolution patterns obtained were consistent with the results of XRD and XRF characterisation in this study.

The heavy dark colour images in Plate XIV (a-e) indicated the presence of silver atoms, while the light or grey colour indicated crystals of different sizes.

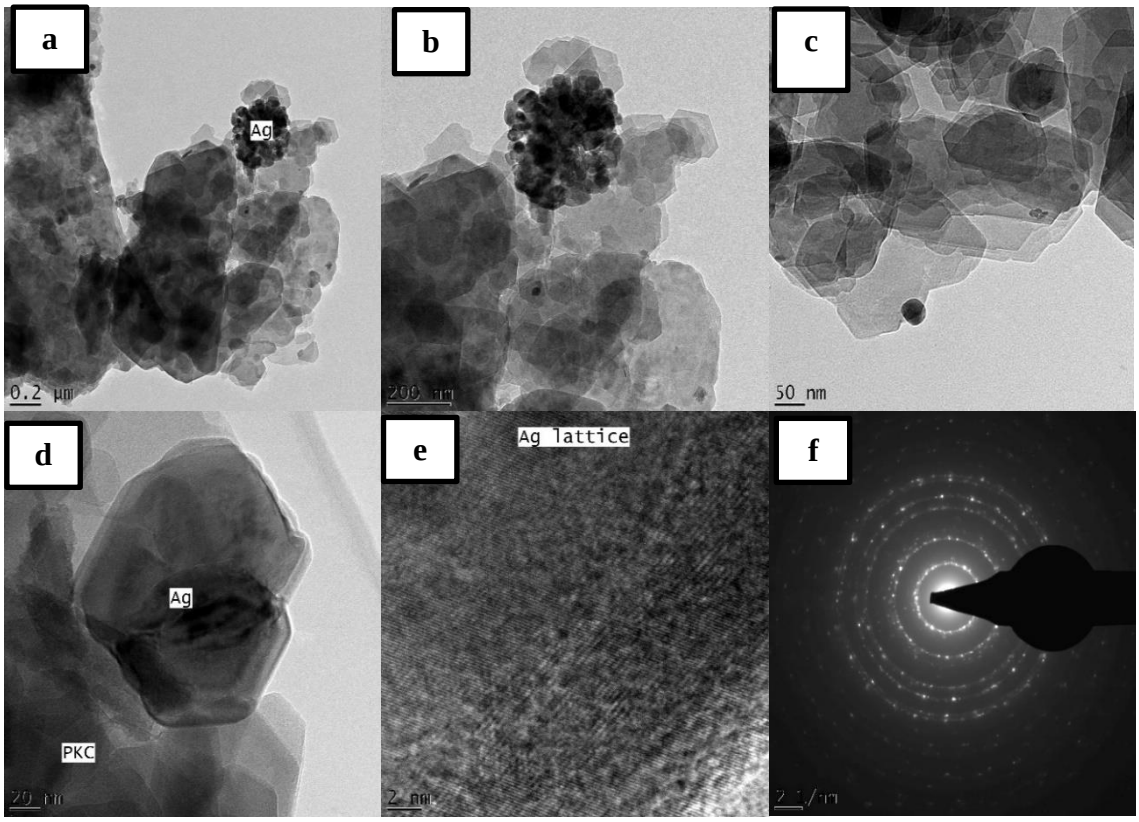

Plate XIV: HRTEM (a – e) and SAED (f) Images of BKC/Ag Nanocomposite Adsorbent

4.8.6 HRTEM – SAED analysis of BKC/ZnO nanocomposite adsorbents

HRTEM images in Plate XV (a – e) visibly displayed the impregnation of ZnO nanoparticles on BKC. The heavy dark colour in Plate XV (b and d) indicated the presence of zinc atoms, while the light or grey colour indicated the presence of purified kaolin clay.

The bright spots and rings of the SAED pattern suggested that the BKC/ZnO nanocomposite adsorbent is polycrystalline and each ring depicted a diffraction pattern of crystals of similar size with each bright spot reflecting individual peaks. SAED resolution patterns obtained were consistent with the results of XRD and XRF characterisation in this study. The heavy dark colour images in Plate XV (a-e) indicated the presence of zinc atoms, while the light or grey colour indicated crystals of different sizes.

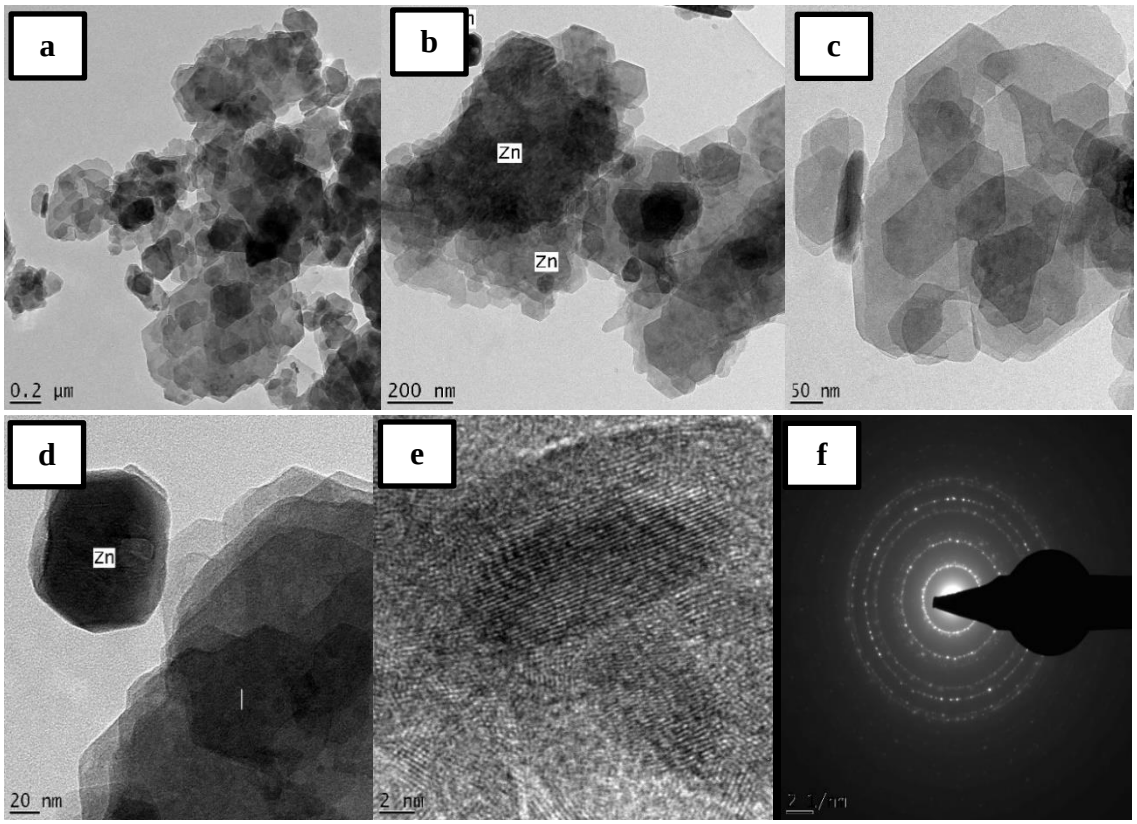

Plate XV: HRTEM (a – e) and SAED (f) Images of BKC/ZnO Nanocomposite Adsorbents

4.8.7 HRTEM – SAED analysis of BKC/Ag/ZnO nanocomposite adsorbents

HRTEM images in Plate XVI (a – e) clearly showed the impregnation of Ag/ZnO nanoparticles on BKC. The BKC/Ag/ZnO nanocomposite crystal structure in Plate XVI (f) showed bright rings of the SAED patterns that are polycrystalline. Each ring depicted the diffraction pattern of purified kaolin clay mixed with Ag/ZnO nanoparticles.

The bright spots and rings of the SAED pattern suggested that the BKC/Ag/ZnO nanocomposite adsorbent is polycrystalline and each ring depicted a diffraction pattern of crystals of similar size with each bright spot reflecting individual peaks. SAED resolution patterns obtained were consistent with the results of XRD and XRF characterisation in this study. The heavy dark colour images in Plate XVI (a-e) indicated

the presence of zinc and silver atoms, while the light or grey colour indicated crystals of different sizes.

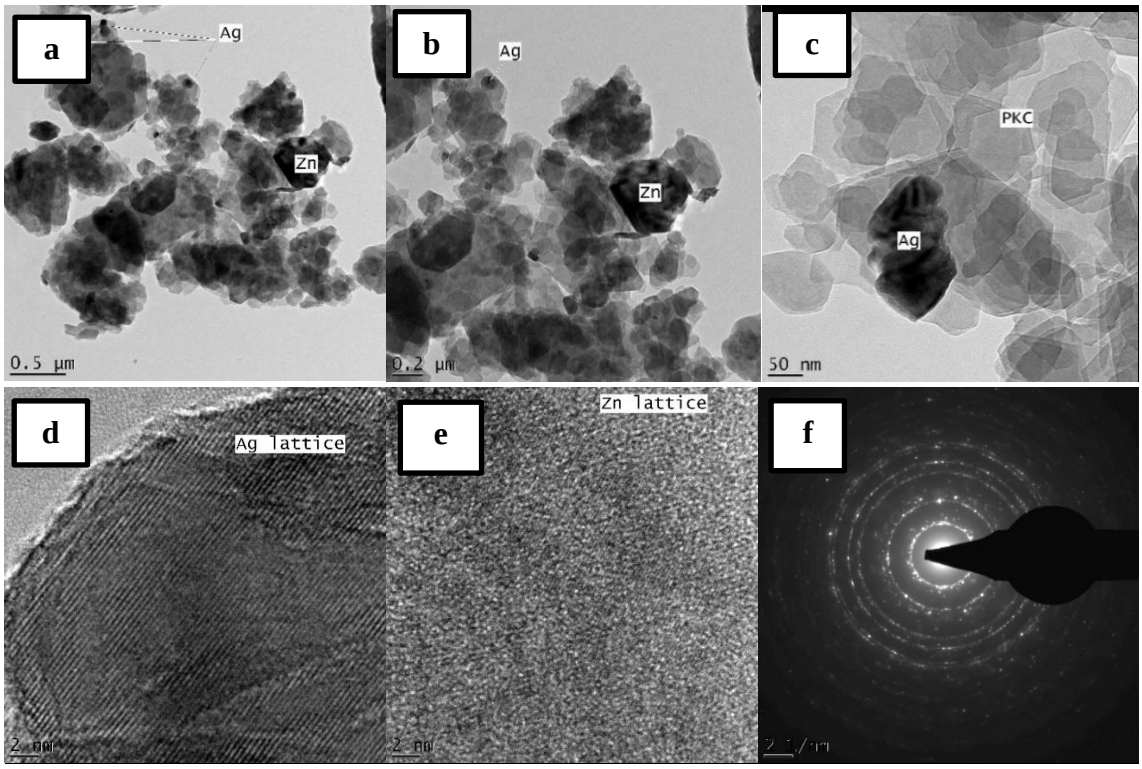

Plate XVI: HRTEM (a – e) and SAED (f) Images of BKC/Ag/ZnO Nanocomposite Adsorbent

4.8.8 BET analysis of BKC/ZnO, BKC/Ag and BKC/Ag/ZnO nanocomposite adsorbents

The BET surface areas for BKC/ZnO, BKC/Ag and BKC/Ag/ZnO nanocomposites adsorbents are between 11.9222 – 12.8278 m^2/g (Table 4.29), It was also noticed that the surface area of the BKC/Ag/ZnO nanocomposite was appreciably higher than that of BKC/Ag and BKC/ZnO nanocomposites, the higher the surface area, the larger its adsorptive capacity. The synthesised BKC/Ag/O/ZnO nanocomposite adsorbent had the highest surface area and was expected to perform better for filter pot production.

Table 4.29: Surface Areas of BKC/ZnO, BKC/Ag and BKC/Ag/ZnO nanocomposites Adsorbents

Sample	Surface Area at p/p^o (m^2/g)	BET Surface Area (m^2/g)	Adsorption Cumulative Surface Area of Pores (m^2/g)	Desorption Cumulative Surface Area of Pores (m^2/g)
BKC/Ag	11.7720	11.9222	13.4986	14.2661
BKC/ZnO	12.5890	12.8245	14.4462	15.3424
BKC/Ag//ZnO	12.6217	12.8278	15.0494	16.0650

The results of the pore volume of BKC, ZnO/Ag nanoparticles, BKC/ZnO, BKC/Ag and BKC/Ag/ZnO nanocomposite adsorbents are presented in Table 4.30. The results range from 0.046930 – 0.063671 cm^3/g.

The BKC/Ag/ZnO nanocomposite adsorbent has the largest pore volume of 0.063671 cm^3/g. The higher the pore volume of the nanocomposite adsorbents, the higher the porosity of the kaolin clay.

Table 4.30: Pore Volume of BKC/ZnO, BKC/Ag and BKC/Ag/ZnO nanocomposites Adsorbents

Sample	Adsorption Total Volume of Pores (cm^3/g)	Desorption Total Volume of Pores (cm^3/g)	Adsorption Cumulative Volume of Pores (cm^3/g)	Desorption Cumulative Volume of Pore (cm^3/g)
BKC/Ag	0.003374	0.045479	0.046930	0.045730
BKC/ZnO	0.003342	0.051400	0.053012	0.052223
BKC/Ag//ZnO	0.003375	0.061678	0.063671	0.062816

Adsorption average diameter ranges from 1.0422 – 1.1319 nm and BJH adsorption average pore width ranges from 13.8994 – 16.9233 nm as shown in Table 4.31.

Table 4.31: Pore Size of BKC/ZnO, BKC/Ag and BKC/Ag/ZnO nanocomposites Adsorbents

Sample	Adsorption Average Pore Diameter (nm)	Desorption Average Pore Diameter (nm)	Adsorption Average Pore Width	Desorption Average Pore Width (nm)
BKC/Ag	1.1319	15.2588	13.9066	12.8221
BKC/ZnO	1.0422	16.0317	14.6784	13.6154
BKC/Ag//ZnO	1.0524	19.2325	16.9233	15.6404

The N_2 adsorption-desorption isotherms of BKC/Ag, BKC/ZnO and BKC/Ag/ZnO are presented in Figures 4.9 – 4.11.

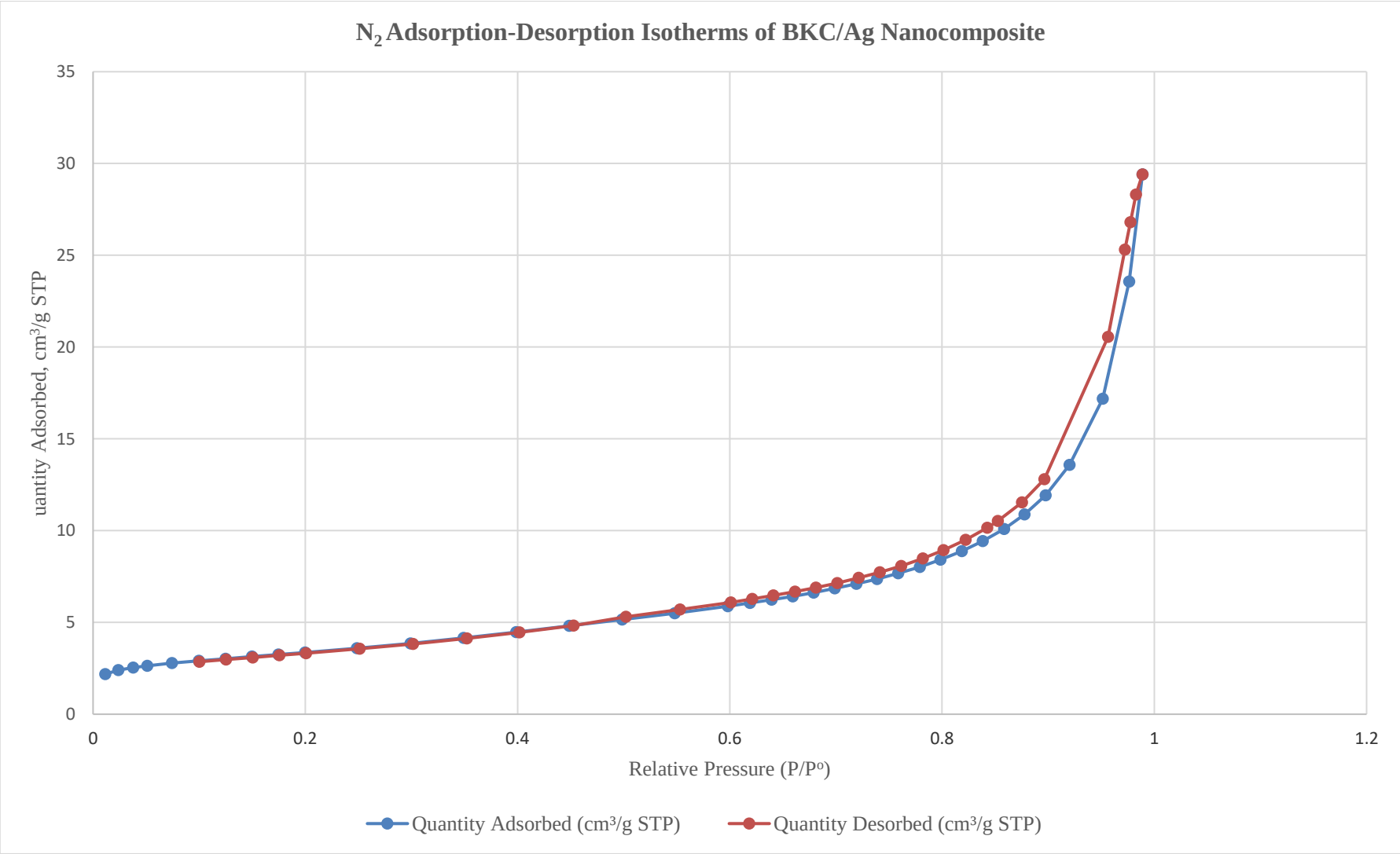

Figure 4.9: N_2 Adsorption-Desorption Isotherms of BKC/Ag Nanocomposite

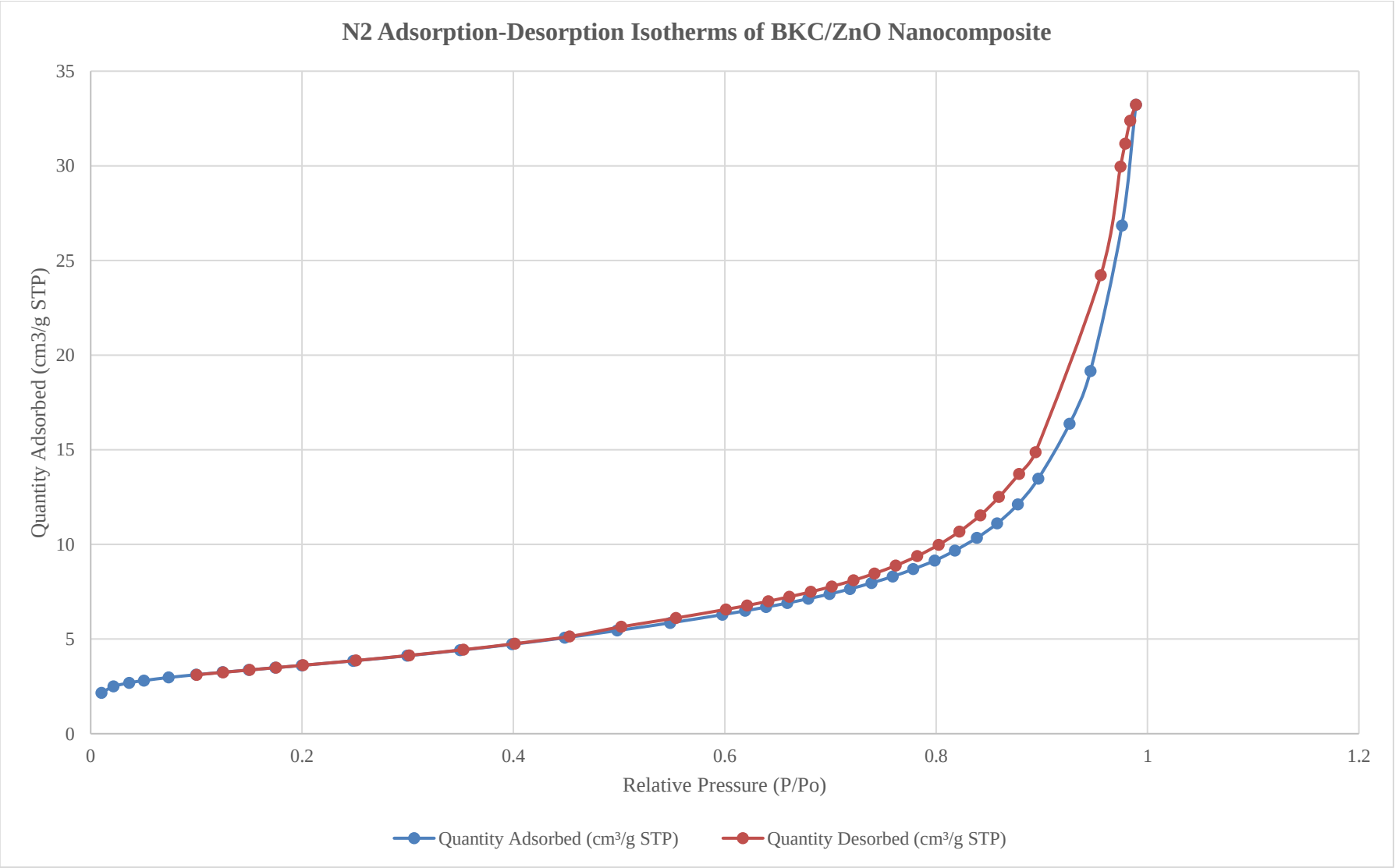

Figure 4.10: N_2 Adsorption-Desorption Isotherms of BKC/ZnO Nanocomposite

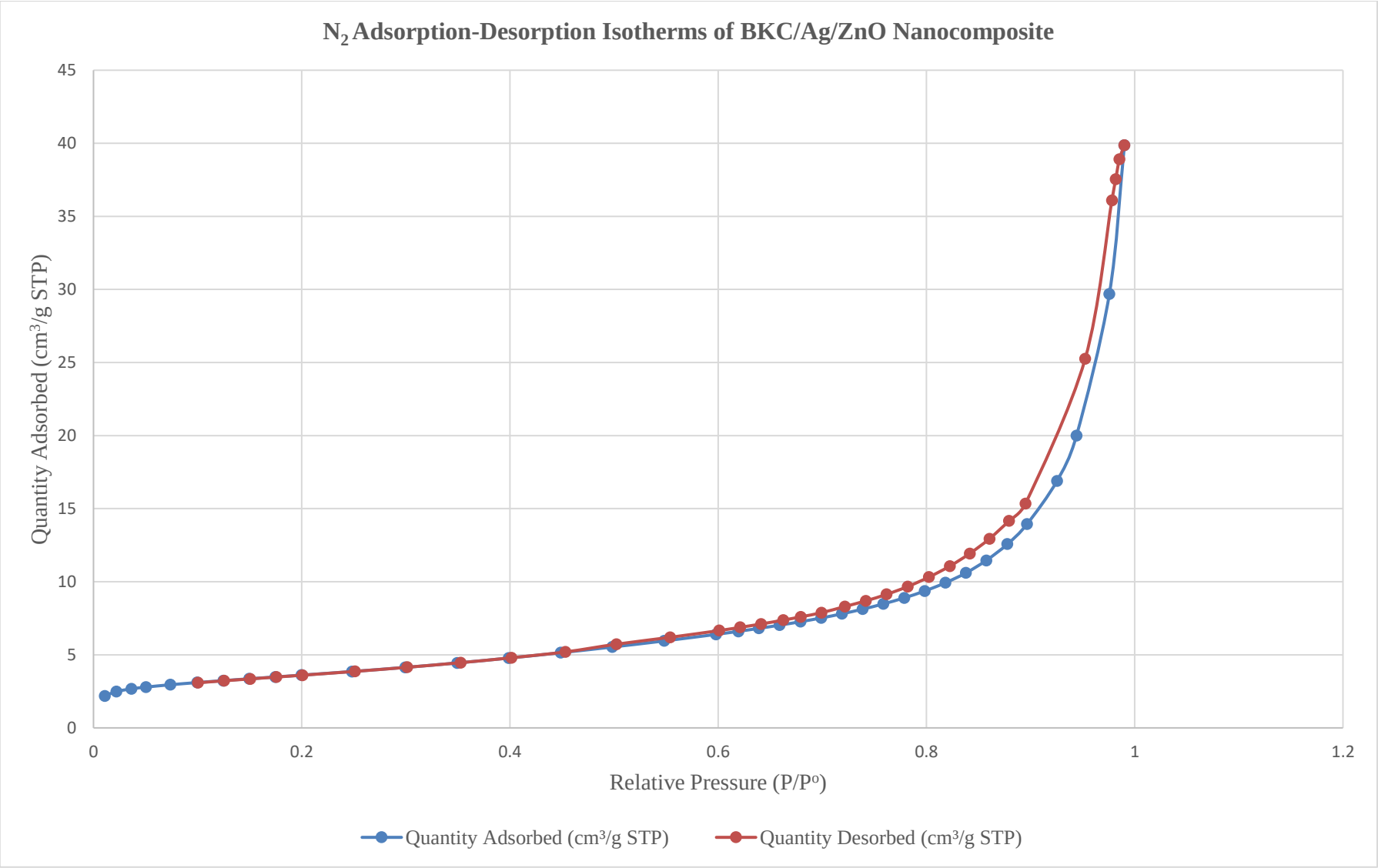

Figure 4.11: N_2 Adsorption-Desorption Isotherms of BKC/Ag/ZnO Nanocomposite Adsorbents

The results as plotted in Figures 4.9 – 4.11 above, showed that the adsorption-desorption isotherms for the BKC/ZnO, BKC/Ag and BKC/Ag/ZnO nanocomposites adsorbents possessed pore sizes that fell in the mesopore widths of between 13.9066 – 16.9233 nm. These mesopore widths are classified as Type IV isotherms when compared with the IUPAC classification of pore sizes. The adsorption behaviour in the mesopore is determined by the adsorbent-adsorptive interactions and by the interactions between the molecules in the condensed state.

The three nanocomposite adsorbents produced belong to type IV isotherm with a hysteresis loop, which resulted from capillary condensation in the mesopores (diameter, $2 < d < 50$ nm) at the relative pressure range of 0.45 –0.9, P/Po. The quasi-overlapping adsorption-desorption curves of the three produced nanocomposite adsorbents indicated that the N_2 adsorption-desorption isotherm curve of the adsorbents is classified as Type IV, indicating a purely mesoporous material with small pore size.

The adsorption isotherms of BKC/Ag, BKC/ZnO and BKC/Ag/ZnO rose progressively during the relative pressure range of 0 – 0.4 P/Po, which means mono-molecule layer adsorption occurring on the surface. The adsorption curves rose steadily, resulting in the saturation of mono-molecule layer adsorption, followed by multi-molecular layer adsorption. When the relative pressure was 0.4 – 0.9 P/Po, the desorption branch was higher than the adsorption branch, along with the appearance of capillary condensation, which resulted in the hysteresis loop. At the relative pressure of 0.4 – 0.9 P/Po, the adsorption and desorption branches suddenly rose and coincided at the end.

Also, the occurrences of hysteresis loops indicated that the BKC/Ag, BKC/ZnO and BKC/Ag/ZnO had a lot of mesopores. Similarly, the smaller adsorption amount at P/Po < 0.4 and the large adsorption amount at P/Po > 0.9 showed that the BKC/Ag, BKC/ZnO

and BKC/Ag/ZnO had a certain number of macropores (d > 50 nm) and a small number of micropores (d < 2 nm). This particular characteristic is ascribed mainly to mesoporous structures.

Furthermore, hysteresis loops of the BKC/Ag, BKC/ZnO and BKC/Ag/ZnO belong to type H3, demonstrating that wedge-shaped pores took the primary position in the beneficiated kaolin clay.

The BET analysis results showed the BKC/Ag, BKC/ZnO and BKC/Ag/ZnO as promising materials to be used as adsorbents for filter production.

4.9 Domestic Wastewater Analyses

Domestic wastewater collected via sewer was analysed to determine the level of contamination and to know precisely the initial physico–chemical and bacteriological characteristics of the domestic wastewater before treatment.

4.9.1. pH

The pH of the domestic wastewater was found to be 8.96 which is basic as shown in Table 4.32. The pH value of the domestic wastewater was above the specified permissible value of effluent discharges, irrigation and reuse standards set by the National Environmental Standard and Regulation Enforcement Agency (NESREA) (2011). The pH of the wastewater was basic and the discharge of this domestic wastewater into waterbodies would be detrimental to zooplankton and fishes, thus affecting their physiology.

Table 4.32: Domestic Wastewater Quality Analysis

Parameters	Units	Wastewater	NESREA (2011)
Odour	-	Smelling	
pH	-	8.96	6.5 -8.5
Turbidity	NTU	248	
EC	µS/cm	1382	
Dissolved Oxygen	mg/L	1.00	4 (Min)
TSS	mg/L	233	0.75
TDS	mg/L	926	
Colour	TCU	1620	
Nitrate	mg/L	230	40
Phosphates	mg/L	11.8	3.5
Ammonium	mg/L	37.2	2.0
Chloride	mg/L	133	350
COD	mg/L	312	30
BOD5	mg/L	30.6	6
Oil and Grease	mg/L	10.1	0.1
Sodium	mg/L	29.0	120
Potassium	mg/L	23.0	50
Cadmium	mg/L	0.01	0.01
Total Iron	mg/L	0.83	0.5
Lead	mg/L	0.14	0.1
Copper	mg/L	0.05	0.01
Manganese	mg/L	0.25	
Arsenic	mg/L	0.22	0.05
Chromium (Cr^{+6})	mg/L	0.04	0.5
Mercury	mg/L	0.11	0.0005
Silver	mg/L	0.02	
Zinc	mg/L	2.46	0.2
Total Coliforms	cfu/100ml	6.45×10^3	5×10^3
E. coli	cfu/100ml	400	Absent
Faecal Coliforms	cfu/100ml	640	Absent
Clostridium perfringens	cfu/100ml	48	Absent

4.9.2 Turbidity

The turbidity of the domestic wastewater as analysed was found to be 248 NTU as shown in Table 4.32. Though, no maximum recommended value for turbidity of wastewater in NESREA, 2011, the turbidity of water for human consumption should not exceed 5 NTU and ideally below 1 NTU when compared with Nigerian Standard for Drinking Water Quality (NSDWQ) (2015). High turbidity will impact aquatic ecosystems by dispersing

sunlight and reducing the oxygen concentration. It also affects photosynthesis as well as the respiration and reproduction of fish. It also harbours microorganisms, and therefore the wastewater requires treatment to get rid of turbidity.

4.9.3 Colour

The colour of the domestic wastewater analysed was found to be 1620 TCU as shown in Table 4.32. The most common cause of watercolour is the minerals present in the wastewater. Red and brown colours in the wastewater are due to iron. Black colour is to manganese or organic matter and yellow colour is to dissolved organic matter such as tannins. Highly coloured water has significant effects on aquatic plants and algal growth. Light is very critical for the growth of aquatic plants and coloured water will limit the penetration of light. Thus, a highly coloured body of water will not sustain aquatic life and if not treated, could lead to the long-term impairment of the ecosystem.

4.9.4 EC

The EC value in the wastewater was obtained as 1382 µS/cm as shown in Table 4.32. The EC analysis measures the number of dissolved ions in wastewater. The obtained EC value is on the high side. Conductivity is a measure of water's capability to pass electrical flow. This ability is directly related to the concentration of ions in the water. These conductive ions come from dissolved salts and inorganic materials such as alkalis, chlorides, sulphides and carbonate compounds and during the domestic generation of wastewater. The higher the conductivity of the wastewater the more pollution it will introduce to the receiving waterbodies.

4.9.5 Dissolved Oxygen (DO)

The DO of the domestic wastewater analysed was found to be 1.0 mg/L as shown in Table 4.32. Adequate DO is necessary for good water quality. As DO levels in water drop below 4.0 mg/L, aquatic life is put under stress, the lower the concentration of DO, the greater the stress to aquatic life. Oxygen levels that remain below 2 mg/L for a few hours can result in large fish kills.

4.9.6 Total Suspended Solids (TSS)

The obtained TSS value in the wastewater sample was 233 mg/L and this is higher than the permissible TSS level of 0.75 mg/L set by NESREA (2011). The result for TSS showed that the domestic wastewater for this study could be categorized as strong wastewater. If TSS is not removed properly through treatment, high concentrations can lower the water quality in the receiving environment. The suspended solids absorb light, causing increased water temperature and decreased oxygen thereby creating an unfavourable environment for aquatic life. Suspended solids will clog fish gills and this can either kill them or reduce their growth rate. High TSS could also reduce light penetration and reduce the ability of algae to produce food and oxygen.

4.9.7 Nutrients

The obtained results for nitrate, phosphate and ammonium according to Table 4.32 were 230 mg/L, 11.8 mg/L and 72 mg/L respectively. These nitrate, phosphate and ammonium results were far above the specified maximum permissible standard of 40 mg/L, 3.5 mg/L and 2.0 mg/L set by NESREA (2011). Waterbodies require some nutrients to be healthy, but too much can be harmful. Eutrophication of a water body occurs when these nutrients, specifically nitrogen and phosphorus, accumulate in the water column and bottom

sediments. This process naturally occurs in lakes and ponds at a very slow pace as organic matter builds up during ecological succession. When rivers receive an overabundance of nutrients, they become polluted by excessive amounts of algae. The decomposition of algae blooms reduces dissolved oxygen and suffocates fish and other aquatic life. Some forms of algae (blue green) may produce toxins that can be harmful if ingested by humans and animals (Ballah *et al.*, 2019; Rathore *et al.*, 2016). Some major sources of nutrient loading into ponds include runoff from fertilizers, open defecation into rivers and leakage from septic systems. Control of these excessive nutrients depends heavily on stopping the external flow into water systems.

4.9.8 Oxygen demands

The obtained analytical results for Biochemical Oxygen Demand (BOD) and Chemical Oxygen Demand (COD) were 30.6 mg/L and 312 mg/L respectively as presented in Table 4.32. These results were found to be far above the maximum permissible limit set by NESREA (2011). COD is a measure of the oxygen equivalent of the organic matter in wastewater that is susceptible to oxidation by a strong chemical oxidant, such as dichromate. The COD is widely used as a measure of the susceptibility to oxidation of the organic and inorganic materials present in water bodies and a general indication of pollution. BOD is an approximate measure of the amount of biochemically degradable organic matter present in a water sample (Dar, 1999). It is necessary to reduce the BOD and COD of the wastewater before it is discharged to receiving water to avoid pollution.

4.9.9 Oil and grease

The obtained analytical result for oil and grease was 10.1mg/L which was far above the 0.1 mg/L maximum permissible limit specified by NESREA (2011). Oil and grease include fats, oils, waxes, and other related constituents found in wastewater. Fats and oils

are regularly used in the preparation of food, with residual cooking oil, margarine and butter. These fats and oils collect inside the sewers and over time, harden to a concrete-like material and restrict the flow of wastewater in the pipes.

4.9.10 Heavy metals

The obtained analytical results for the iron, cadmium, lead, copper, manganese, arsenic, mercury silver and zinc were found to be 0.83 mg/L, 0.05 mg/L, 0.14 mg/L, 0.05 mg/L, 0.25 mg/L, 0.22 mg/L, 0.11 mg/L, 0.02 mg/L and 2.46 mg/L These listed values were far above the maximum permissible limit set by NESREA (2011). The ability of a waterbody to support aquatic life, as well as its suitability for other uses depends on many trace elements. Some metals, such as manganese, zinc and copper, when present in trace concentrations are important for the physiological functions of living tissue and regulate many biochemical processes. The same metals, however, discharged into natural waters at increased concentrations in sewage, can have severe toxicological effects on humans and the aquatic ecosystem (NWQRL, 2021).

4.9.11 Indicator organisms

The obtained analytical results for total coliforms, faecal coliforms, *Clostridium perfringens* and *E. coli* were found to be 6450 cfu/100 mL, 640 cfu/100 mL, 48 cfu/100 mL and 400 cfu/100 mL respectively. The water pollution caused by faecal contamination is a serious problem due to the potential for contracting diseases from pathogens. Coliforms such as *E. coli* come from the same sources as pathogenic organisms. These indicator organisms are required to be removed from the wastewater before it is discharged to the rivers.

4.10 Batch Adsorption Treatment Studies

In this section, the pollutants in the wastewater were reduced to an acceptable level by the synthesised BKC/Ag, BKC/ZnO and BKC/Ag/ZnO nanocomposite adsorbents before discharging into the receiving water bodies. The effect of contact time, temperature and dosage on the produced nanocomposite adsorbents to remove the pollutants from domestic wastewater collected via sewer were tested and the results are presented in this section.

4.10.1 Effect of contact time on heavy metals removal

The effect of contact time on the adsorption of iron, lead, copper, manganese, arsenic, mercury silver and zinc onto BKC, BKC/ZnO, BKC/Ag and BKC/Ag/ZnO nanocomposite adsorbents was studied at a contact time of 10, 20, 30, 40, 50 and 60 minutes using an adsorbent dosage of 25 g/100 mL of wastewater at a temperature of 29.5 °C and pH of 6.9.

It was observed that an increase in the fraction of the heavy metals adsorbed occurred with a corresponding increase in the contact time. The effects of contact time on the adsorption of these selected heavy metals onto the adsorbents are important to achieve equilibrium adsorption.

The percentage removal of iron, lead, copper, manganese, arsenic, mercury silver and zinc after treatments with BKC, BKC/ZnO, BKC/Ag and BKC/Ag/ZnO nanocomposite adsorbents at various contact times are presented in Figures 4.12 (a – d). As presented in Figures 4.12 (a – d), the rates of adsorption were faster initially but became slow on reaching the equilibrium. Different equilibrium times were observed for all the parameters on the adsorbents. Rapid adsorption rates were obtained between the contact time of 10 – 40 minutes. The increase in contact time from 10 minutes gradually reduced

the heavy metal contaminants to 50 minutes contact time. On reaching the equilibrium adsorption, the rate of adsorption equals the rate of desorption; therefore, slow uptake of pollutants was observed from 40 minutes upward. The slow uptake and the slight or no decrease in percentage removal with a further increase in contact time might be due to saturation of the surface area of the adsorbent with heavy metal pollutants.

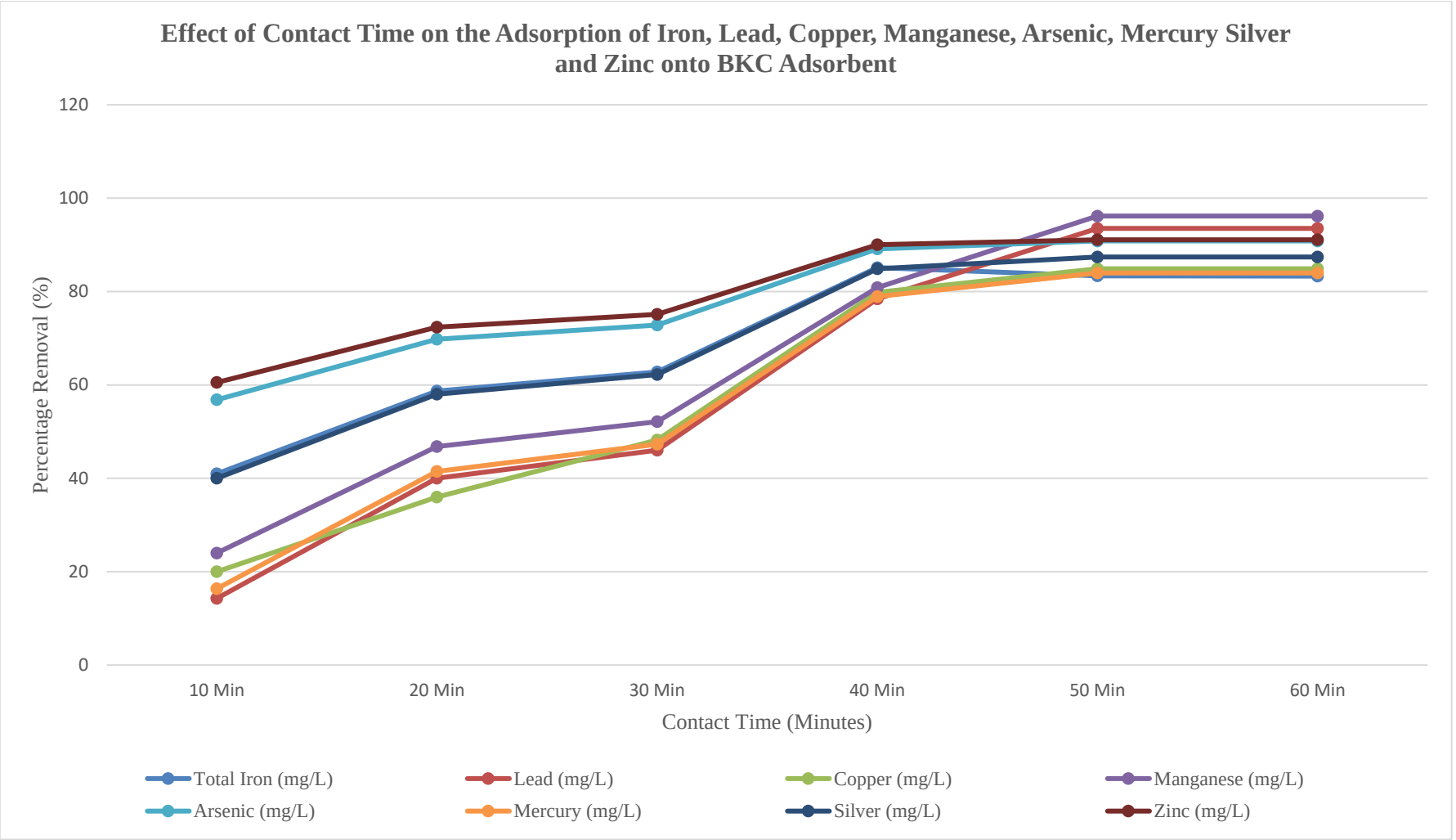

Figure 4.12 (a): Effect of Contact Time on the Removal of Iron, Lead, Copper, Manganese, Arsenic, Mercury Silver and Zinc by BKC Adsorbent

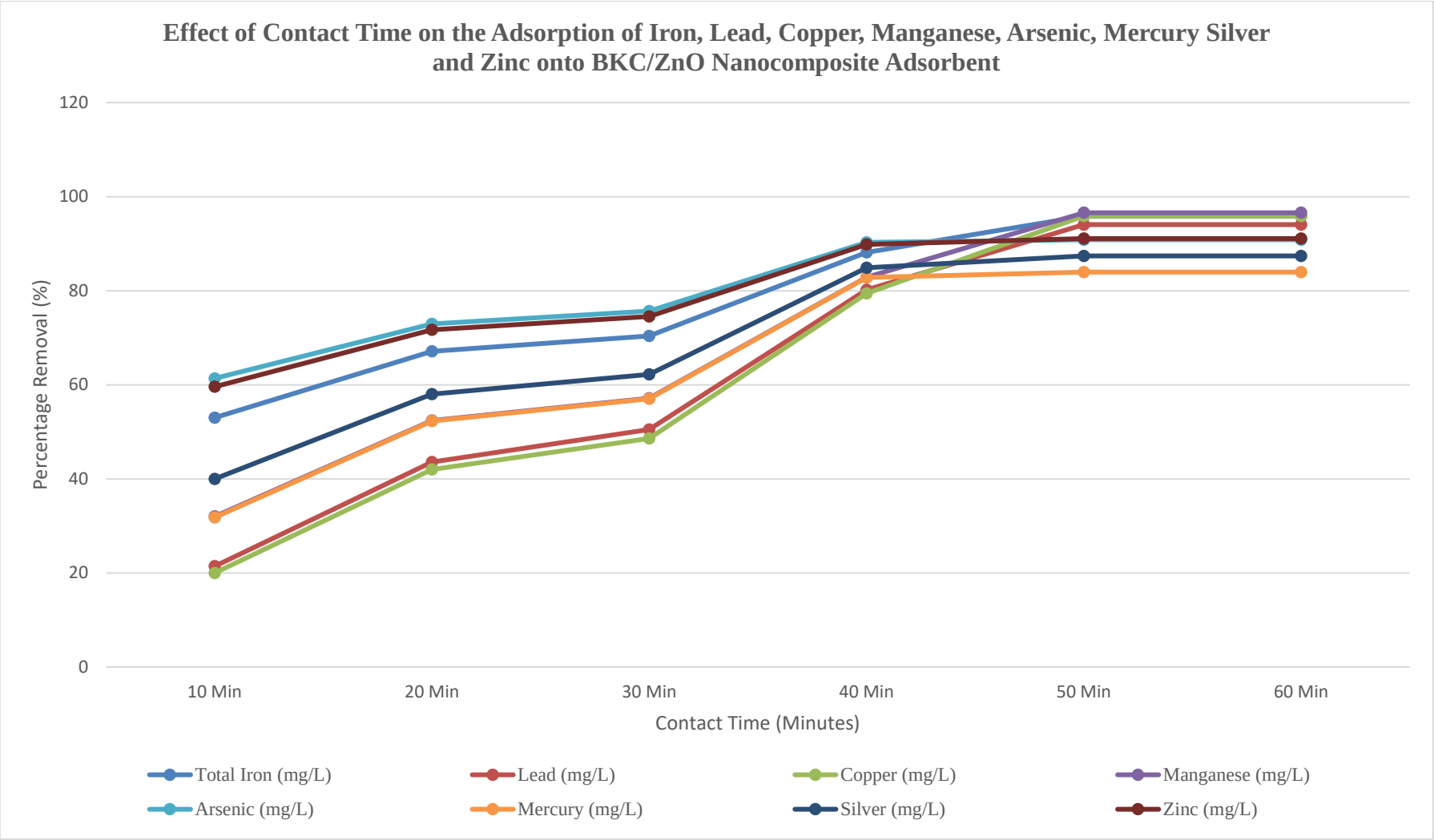

Figure 4.12 (b): Effect of Contact Time on the Removal of Iron, Lead, Copper, Manganese, Arsenic, Mercury Silver and Zinc by BKC/ZnO Nanocomposite Adsorbent

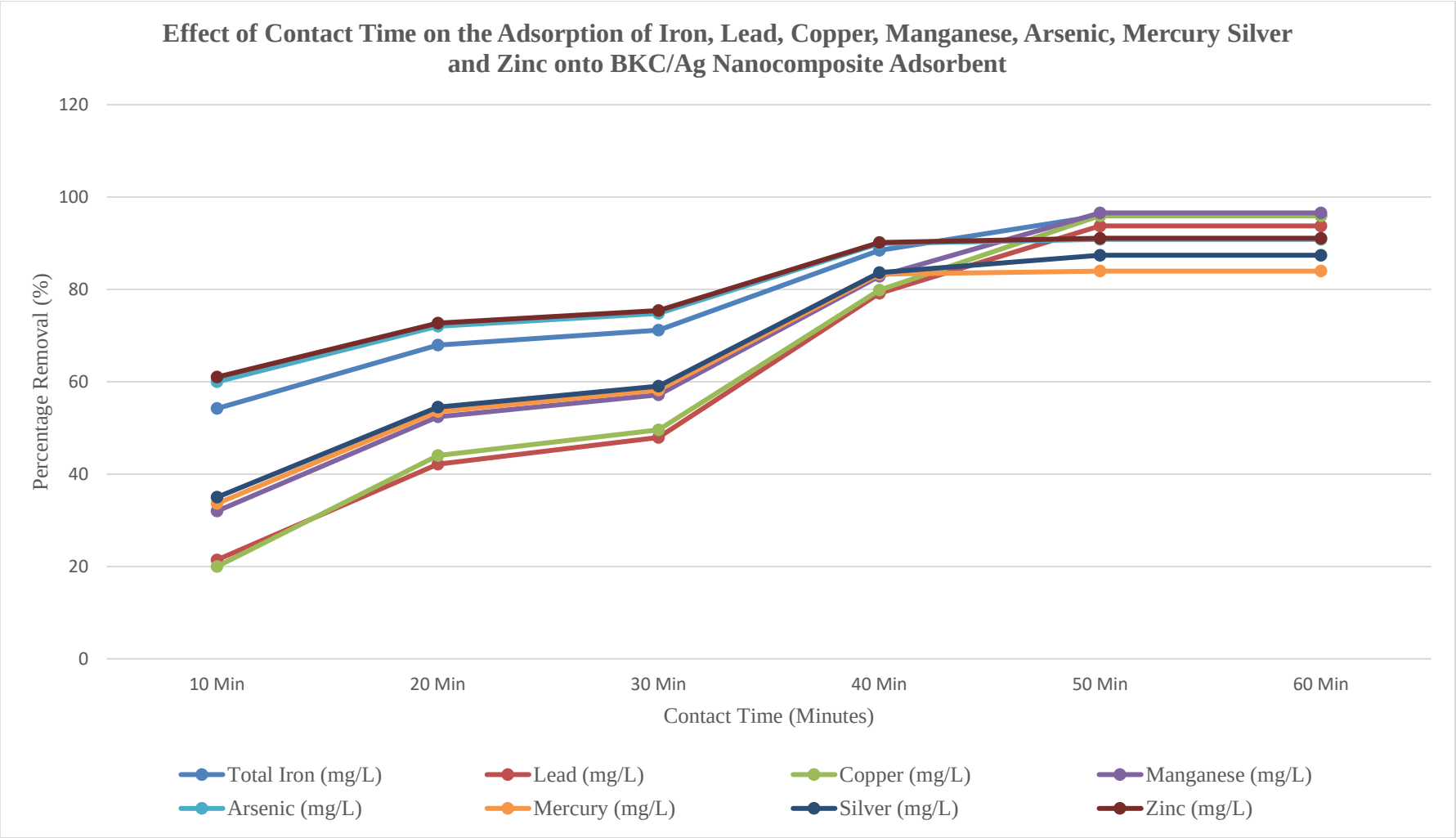

Figure 4.12 (c): Effect of Contact Time on the Removal of Iron, Lead, Copper, Manganese, Arsenic, Mercury Silver and Zinc by BKC/Ag Nanocomposite Adsorbent

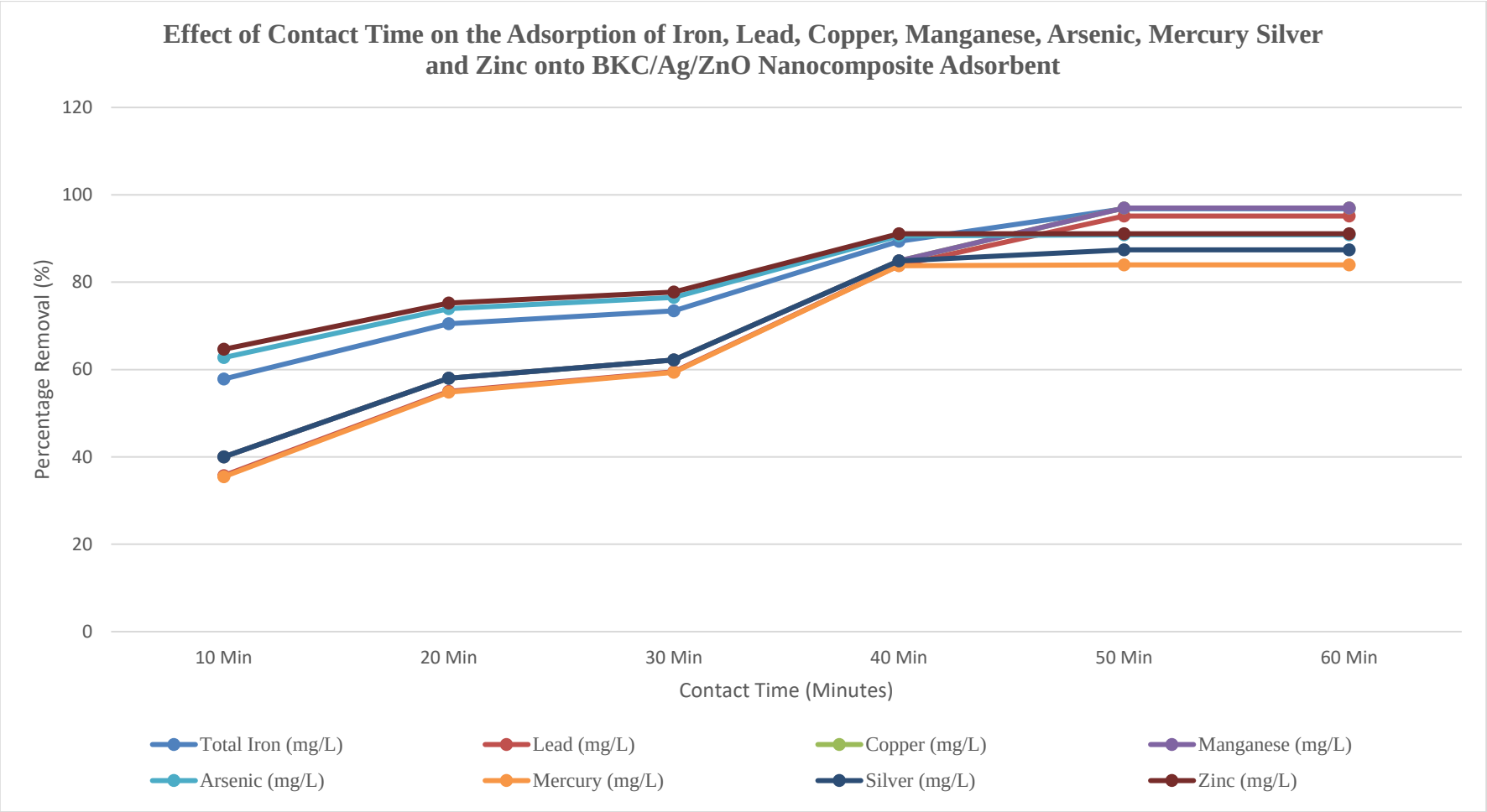

Figure 4.12 (d): Effect of Contact Time on the Removal of Iron, Lead, Copper, Manganese, Arsenic, Mercury Silver and Zinc by BKC/Ag/ZnO Nanocomposite Adsorbent

4.10.2 Effect of contact time on nutrients, COD, BOD and oil and grease removal

The effect of contact time on the adsorption of nitrate, phosphate, ammonium, COD, BOD and oil and grease onto BKC, BKC/ZnO, BKC/Ag and BKC/Ag/ZnO nanocomposites adsorbents was studied at contact time of 10, 20, 30, 40, 50 and 60 minutes using an adsorbent dosage of 25 g/100 ml of wastewater at a temperature of 29.5 °C and pH of 6.9.

The rate of adsorption equals the rate of desorption on reaching the equilibrium, therefore slow or no uptake of nitrate, phosphate, ammonium, COD, BOD, oil and grease was observed. The slow uptake and the no increase in percentage removal with a further increase in contact time were due to saturation of the surface of the adsorbent with pollutants.

The percentage removal of nitrate, phosphate, ammonium, COD, BOD and oil and grease after treatment with BKC, BKC/ZnO, BKC/Ag and BKC/Ag/ZnO nanocomposites adsorbents at various contact times were presented in Figure 4.13 (a – d).

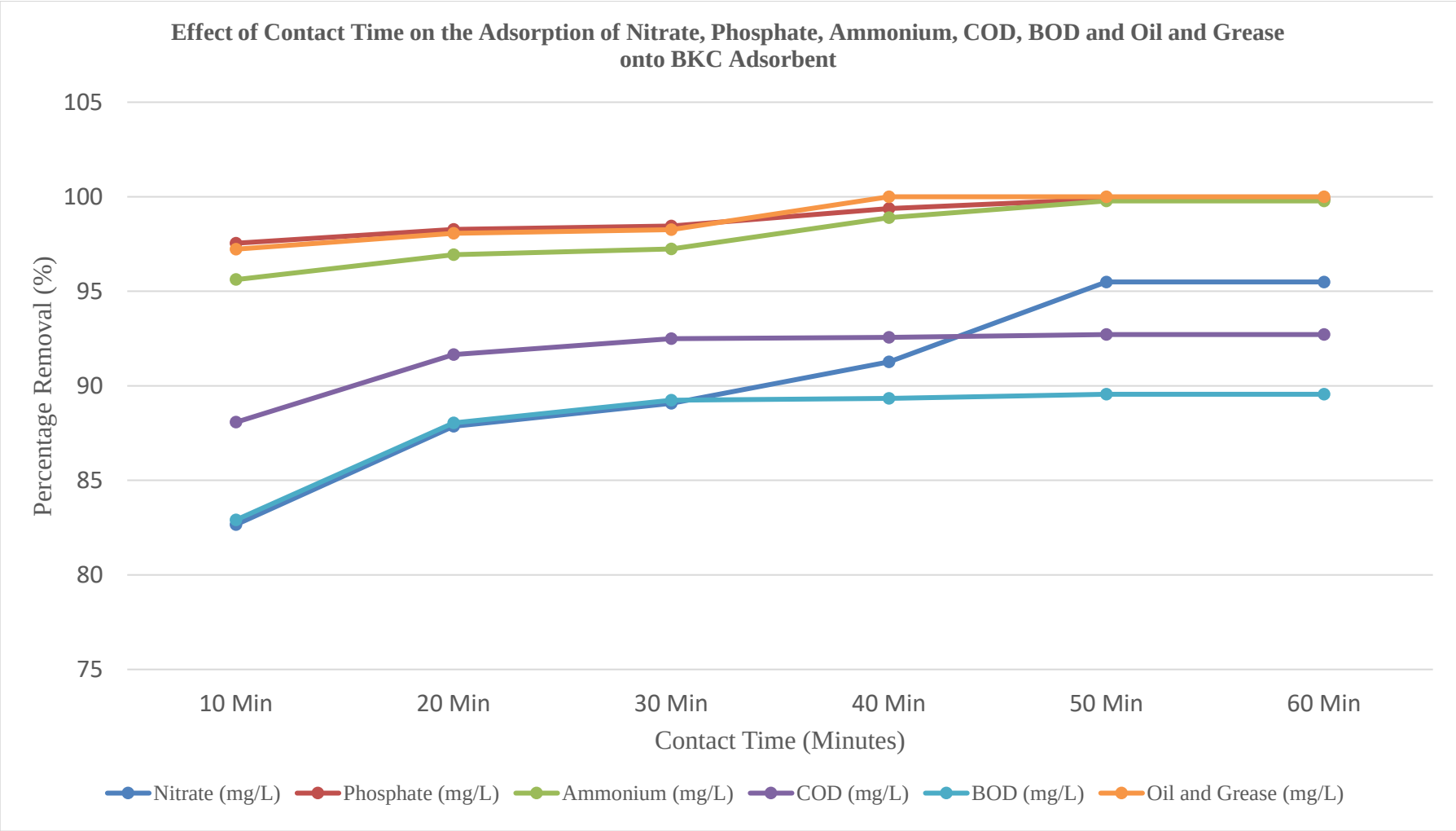

Figure 4.13 (a): Effect of Contact Time on the Removal of Nitrate, Phosphate, Ammonium, COD, BOD and Oil and Grease by BKC Adsorbent

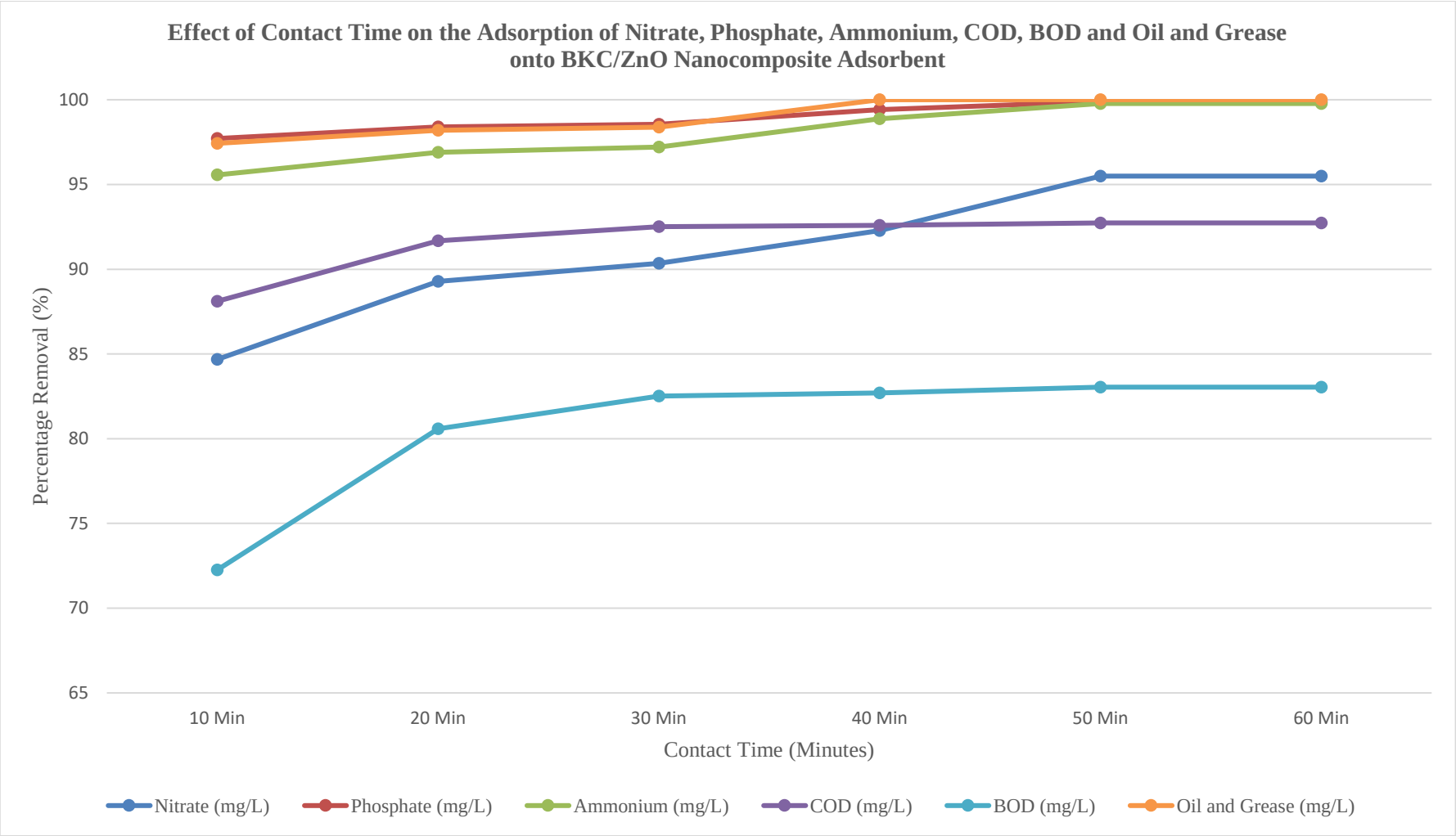

Figure 4.13 (b): Effect of Contact Time on the Removal of Nitrate, Phosphate, Ammonium, COD, BOD and Oil and Grease by BKC/ZnO Nanocomposite Adsorbent

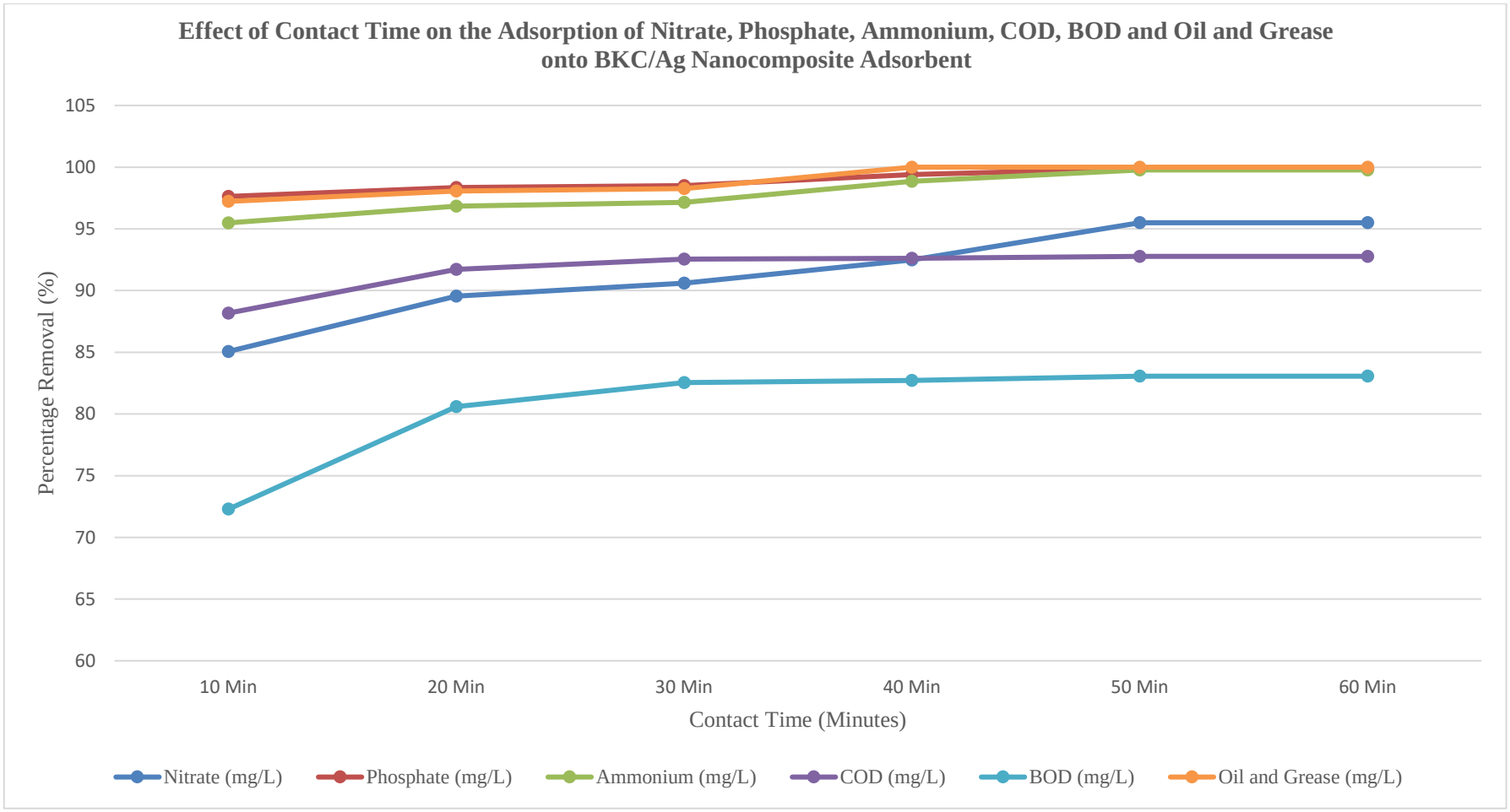

Figure 4.13 (c): Effect of Contact Time on the Removal of Nitrate, Phosphate, Ammonium, COD, BOD and Oil and Grease by BKC/Ag Nanocomposite Adsorbent

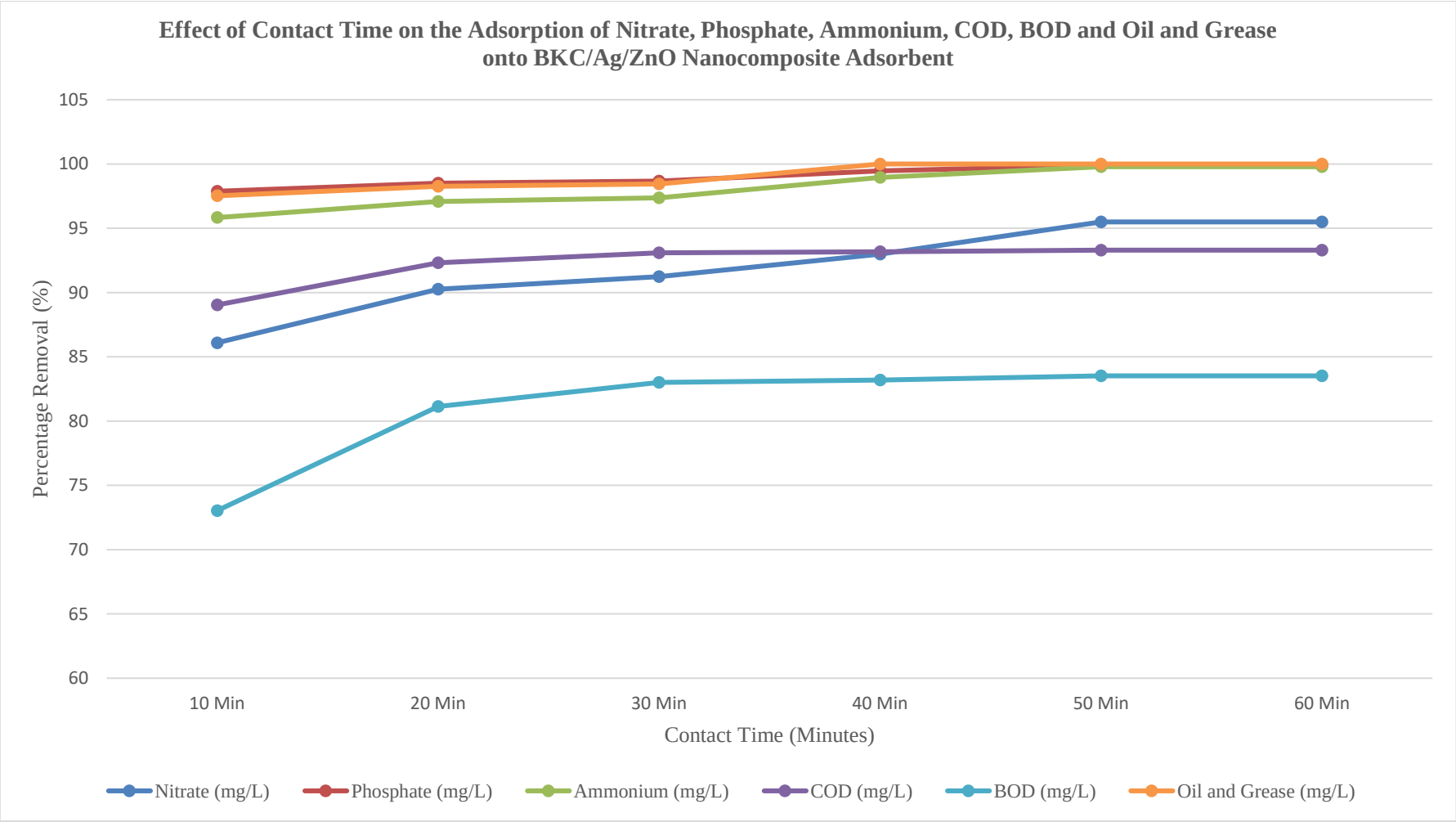

Figure 4.13 (d): Effect of Contact Time on the Removal of Nitrate, Phosphate, Ammonium, COD, BOD and Oil and Grease by BKC/Ag/ZnO Nanocomposite Adsorbent

4.10.3 Effect of contact time on physical parameters

Figure 4.14 (a – e) describes the effect of contact time on the removal of turbidity, suspended solids, colour, EC, improvement of pH and dissolved oxygen using BKC Adsorbent, BKC/Ag, BKC/ZnO and BKC/Ag/ZnO nanocomposite adsorbents.

The effect of contact time on the removal of turbidity, suspended solids, colour, EC and improvement of pH and dissolved oxygen of the wastewater during treatment with BKC, BKC/ZnO, BKC/Ag and BKC/Ag/ZnO nanocomposites adsorbents was studied at a contact time of 10, 20, 30, 40, 50 and 60 minutes using an adsorbent dosage of 25 g/100 mL of wastewater at a temperature of 29.5 °C and pH of 6.9.

It was revealed that an increase in the reduction of turbidity, suspended solids, colour, EC and improvement in pH and dissolved oxygen occurred with a corresponding increase in the contact time until equilibrium adsorption was achieved. The percentage removal of turbidity, suspended solids, colour, EC and improvement in pH and dissolved oxygen values at various contact times were attached as presented in Figures 4.14 (a – e).

It was also observed that rapid percentage removal was obtained between the contact times of 10 – 20 minutes for the physical parameters. However, the contact time has no significant effect on turbidity, suspended solid, colour, or EC removal from 30 minutes upward as presented in Figure 4.14 (a –e). The slight increase in the removal of turbidity, suspended solids, colour, and EC with a further increase in contact time was due to saturation of the surface area of the adsorbent with pollutants.

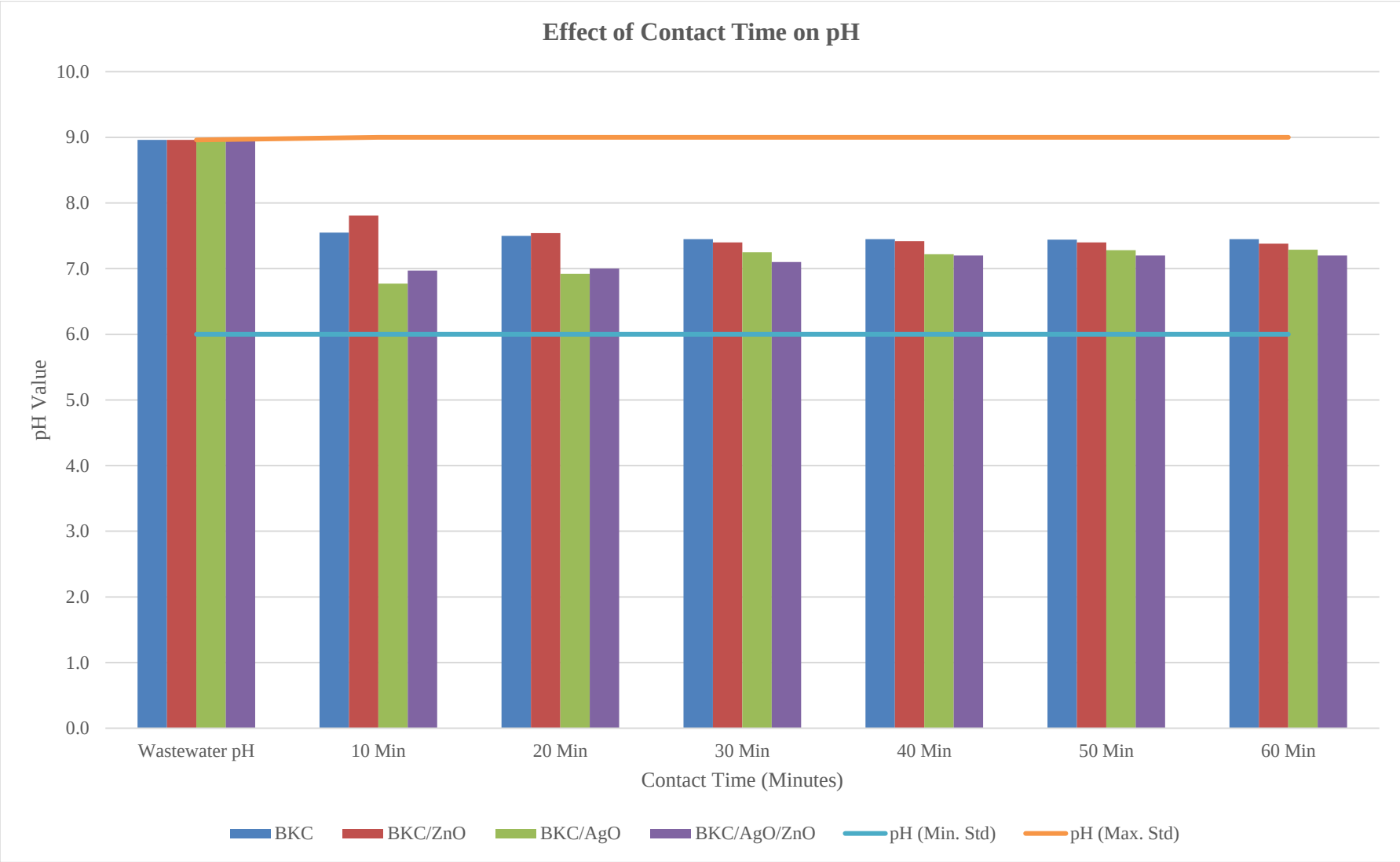

Figure 4.14 (a): Effect of Contact Time on the pH by BKC, BKC/Ag, BKC/Ag and BKC/Ag/ZnO Nanocomposite Adsorbent

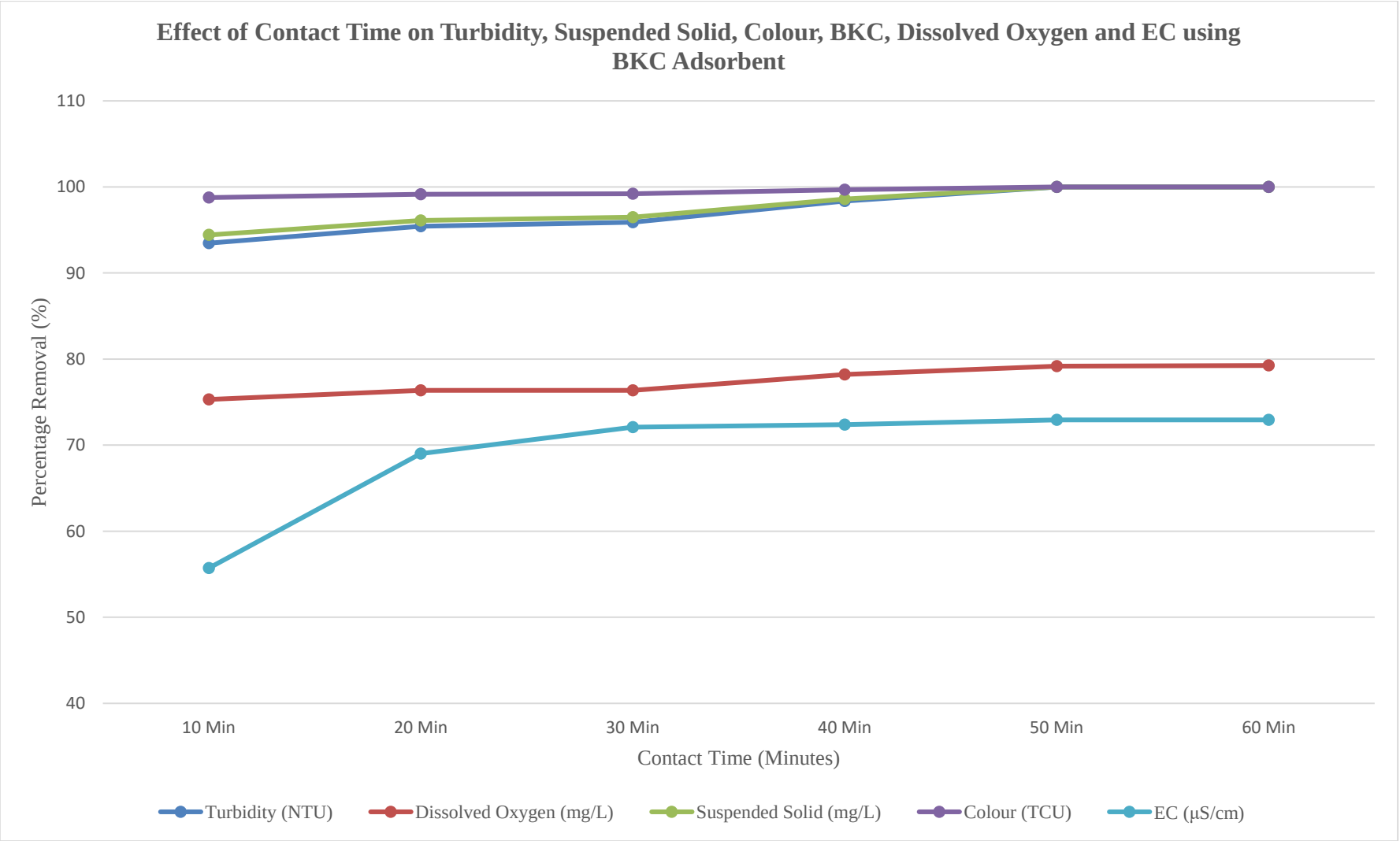

Figure 4.14 (b): Effect of Contact Time on Turbidity, Suspended Solid, Colour, BKC, Dissolved Oxygen and EC using BKC Adsorbent

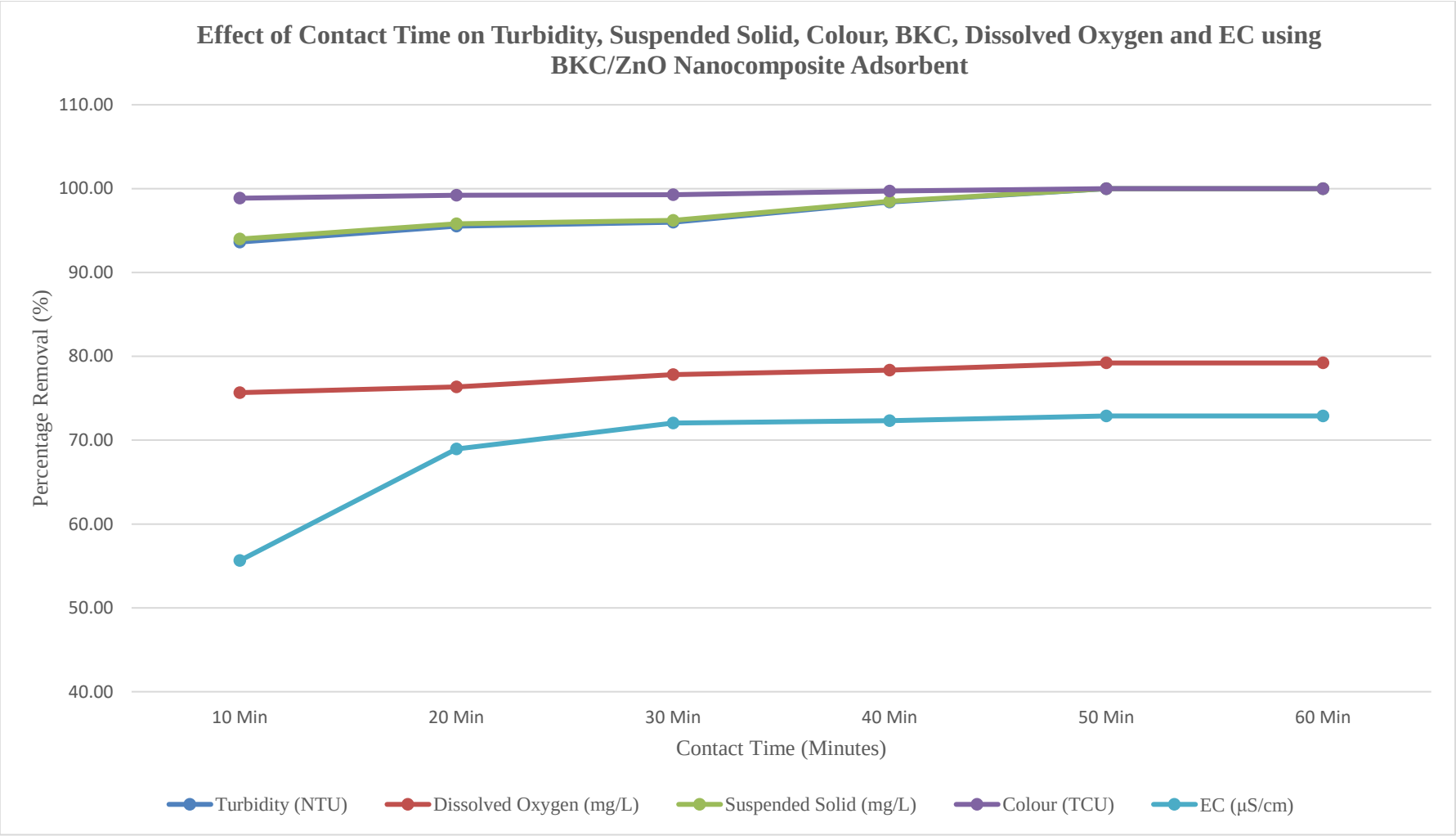

Figure 4.14 (c): Effect of Contact Time on Turbidity, Suspended Solid, Colour, BKC, Dissolved Oxygen and EC using BKC/ZnO Nanocomposite Adsorbent

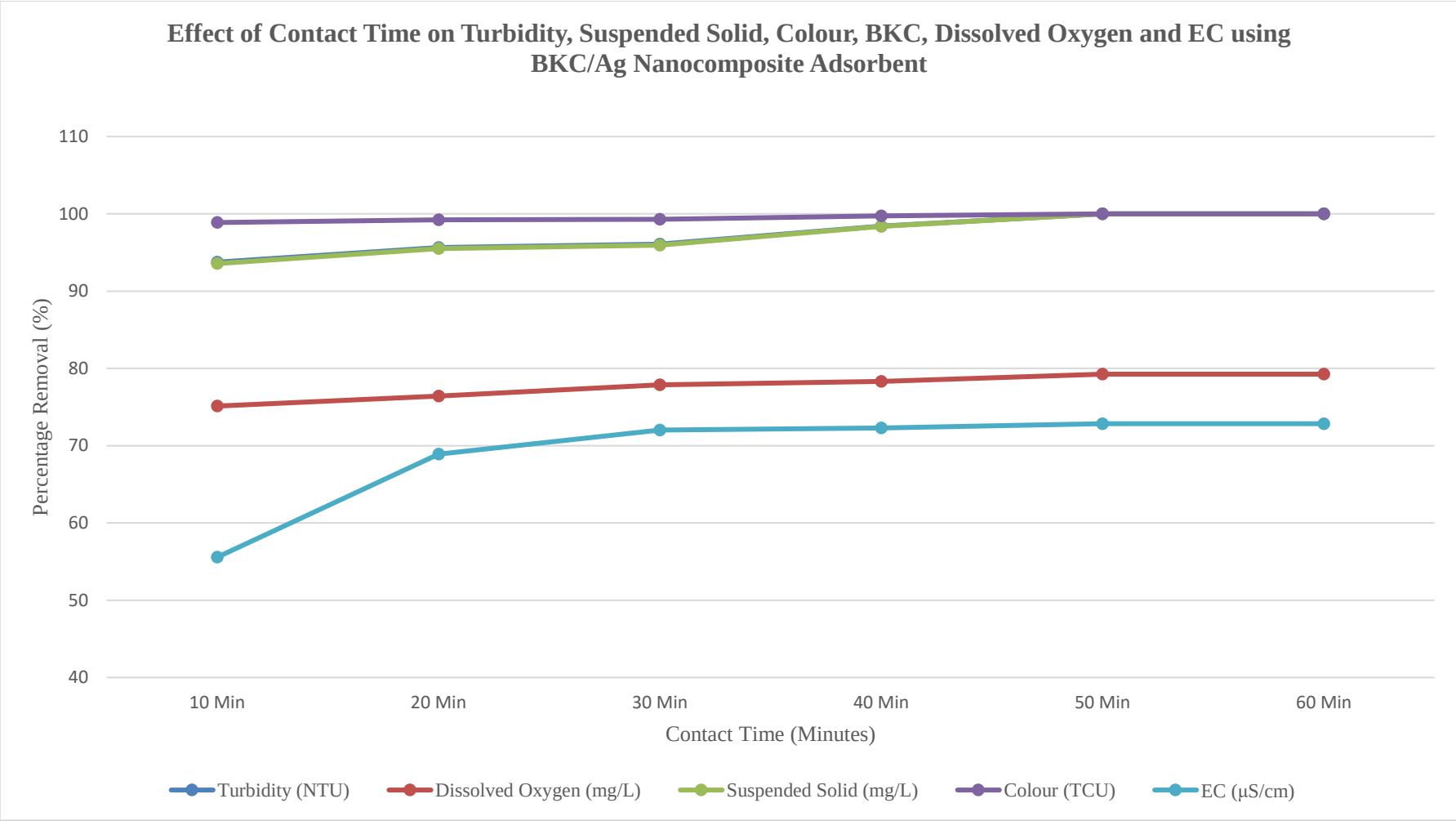

Figure 4.14 (d): Effect of Contact Time on Turbidity, Suspended Solid, Colour, BKC, Dissolved Oxygen and EC using BKC/Ag Nanocomposite Adsorbent

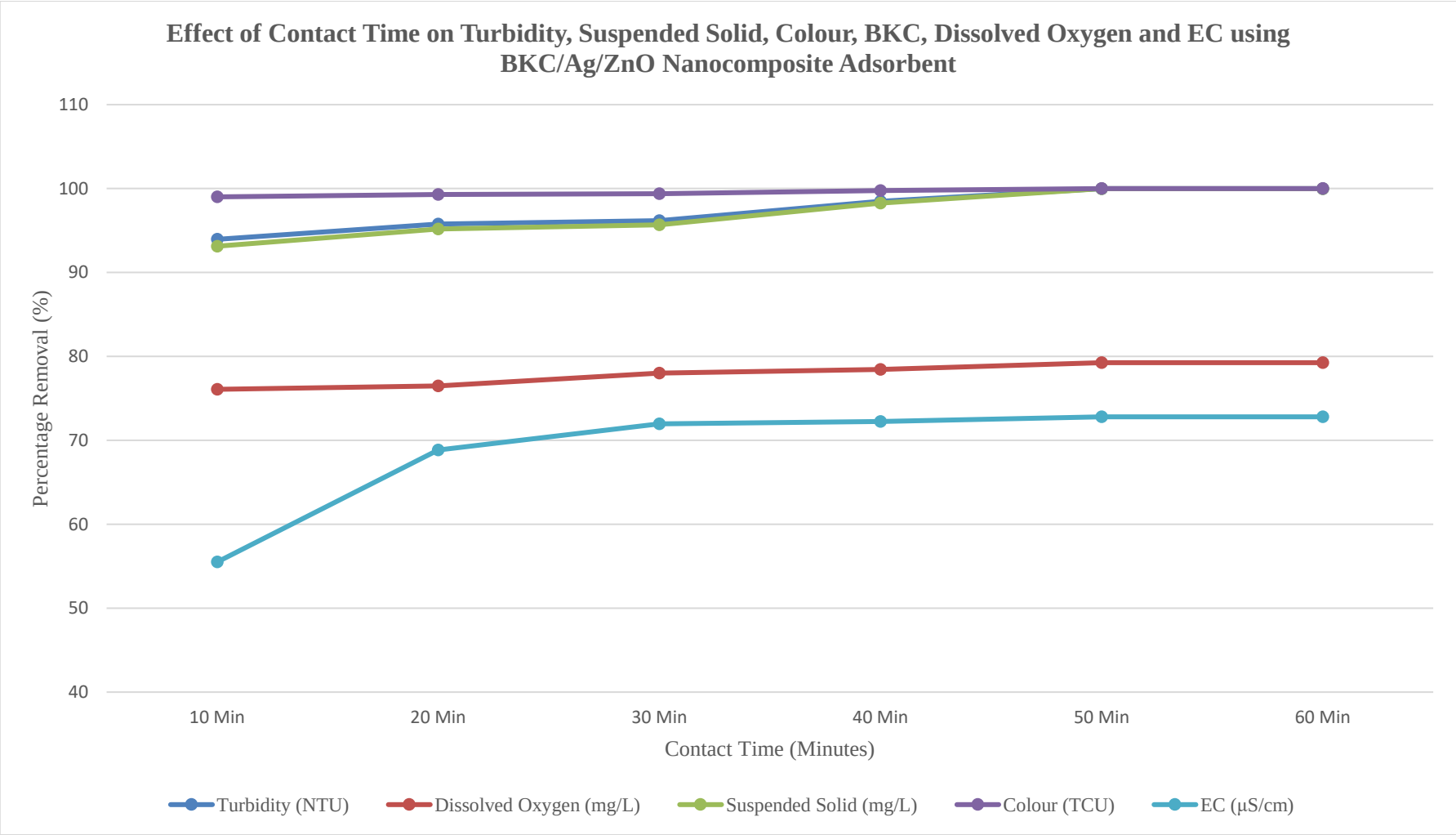

Figure 4.14 (e): Effect of Contact Time on Turbidity, Suspended Solid, Colour, BKC, Dissolved Oxygen and EC using BKC/Ag/ZnO Nanocomposite Adsorbent

4.10.4 Effect of contact time on microbial parameters

Figure 4.15 (a – d) describes the effect of contact time on the removal of total coliforms, faecal coliforms, C*lostridium perfringens* and *E. coli* onto BKC Adsorbent, BKC/Ag, BKC/ZnO and BKC/Ag/ZnO nanocomposite adsorbents. The effect of contact time on the removal of total coliforms, faecal coliforms, C*lostridium perfringens* and *E. coli* by BKC, BKC/ZnO, BKC/Ag and BKC/Ag/ZnO nanocomposites adsorbents was studied at a contact time of 10, 20, 30, 40, 50 and 60 minutes using an adsorbent dosage of 25 g/100 mL of wastewater at a temperature of 29.5 °C and pH of 6.9.

Rapid percentage removal was obtained between the contact times of 10 – 20 minutes for BKC adsorbent and BKC/ZnO nanocomposite adsorbent. The slight decrease in percentage removal of C*lostridium perfringens* and *E. coli* when treated with BKC adsorbent and BKC/ZnO nanocomposite adsorbents with further increase in contact time was due to non-impregnation of nanoparticles on BKC and weak strength of zinc nanoparticles against microorganisms respectively. BKC/ZnO nanocomposite adsorbent also showed potential as an antimicrobial material but was very weak in the removal of *Clostridium perfringens* as shown in Figure 4.15 (b). The complete removal of total coliforms, faecal coliforms, *Clostridium perfringens* and *E. coli* at 30 minutes contact time for BKC/Ag and BKC/Ag/ZnO nanocomposite adsorbents was due to the antibacterial activity of Ag/ZnO-NPs. The detailed results of the contact time effect on the removal of contaminants by BKC, BKC/ZnO, BKC/Ag and BKC/Ag/ZnO nanocomposite adsorbent are presented In Appendix C.

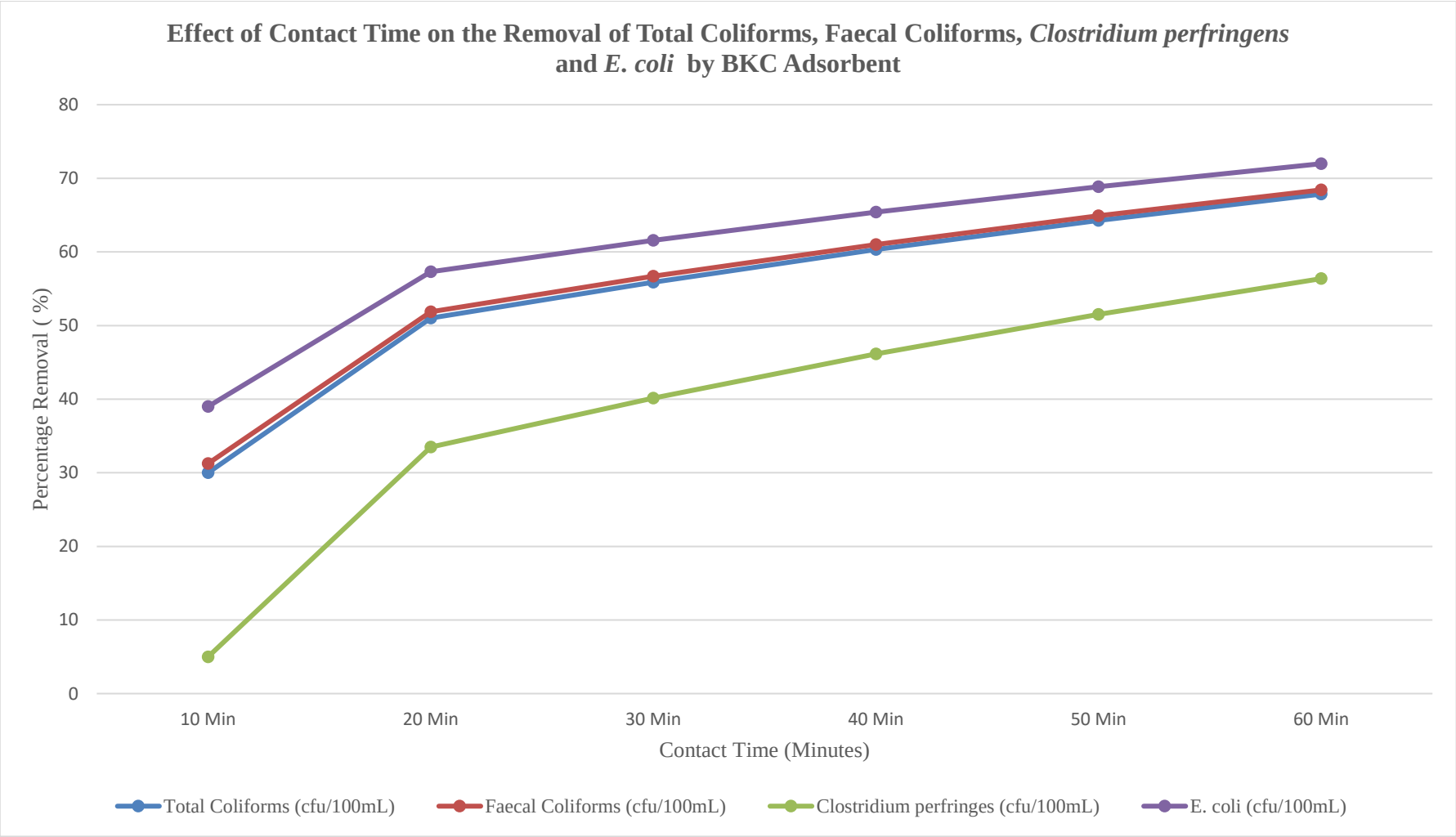

Figure 4.15 (a): Effect of Contact Time on the Removal of Total Coliforms, Faecal Coliforms, *Clostridium perfringens* and *E. coli* by BKC Adsorbent

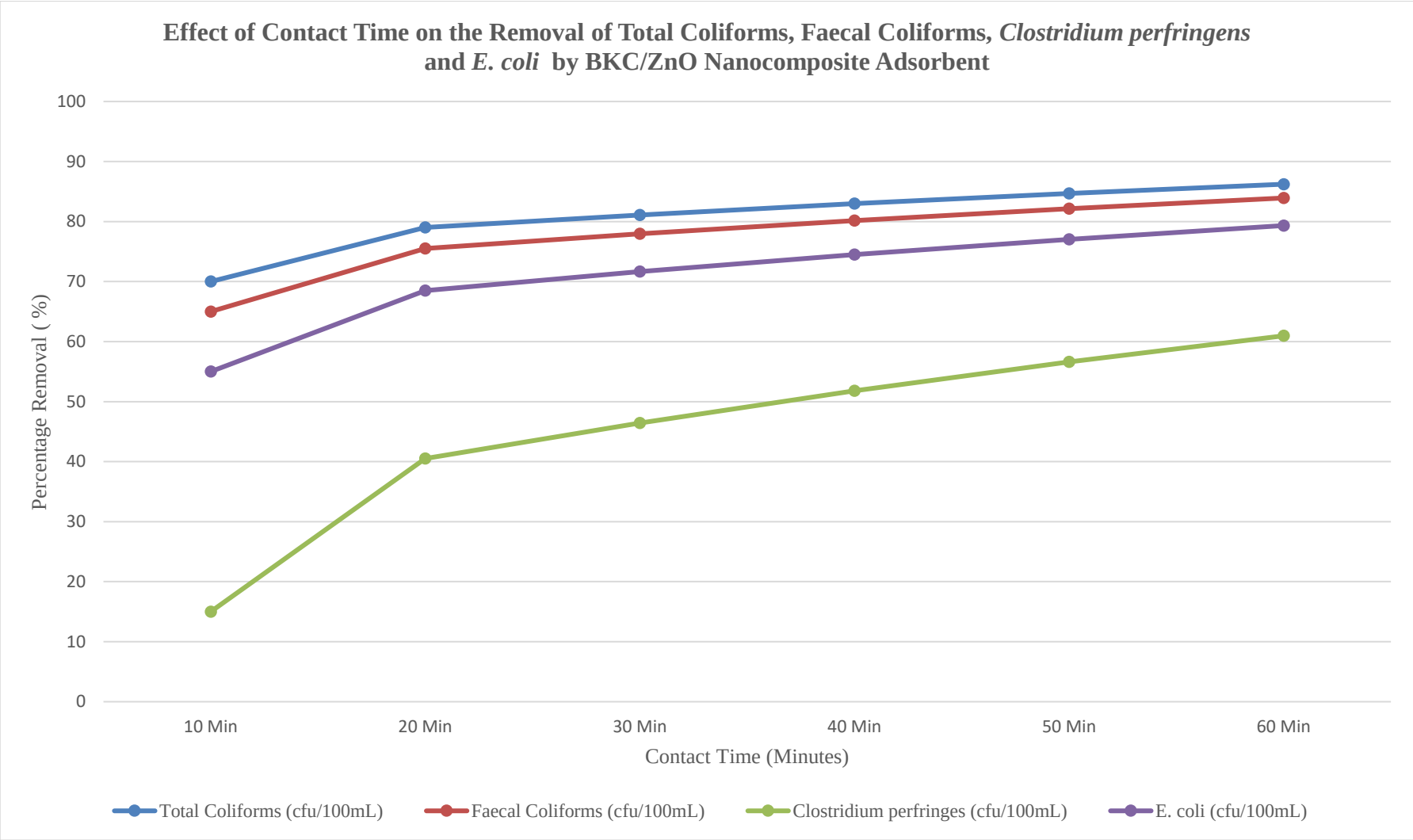

Figure 4.15 (b): Effect of Contact Time on the Removal of Total Coliforms, Faecal Coliforms, *Clostridium perfringens* and *E. coli* by BKC/ZnO Adsorbent

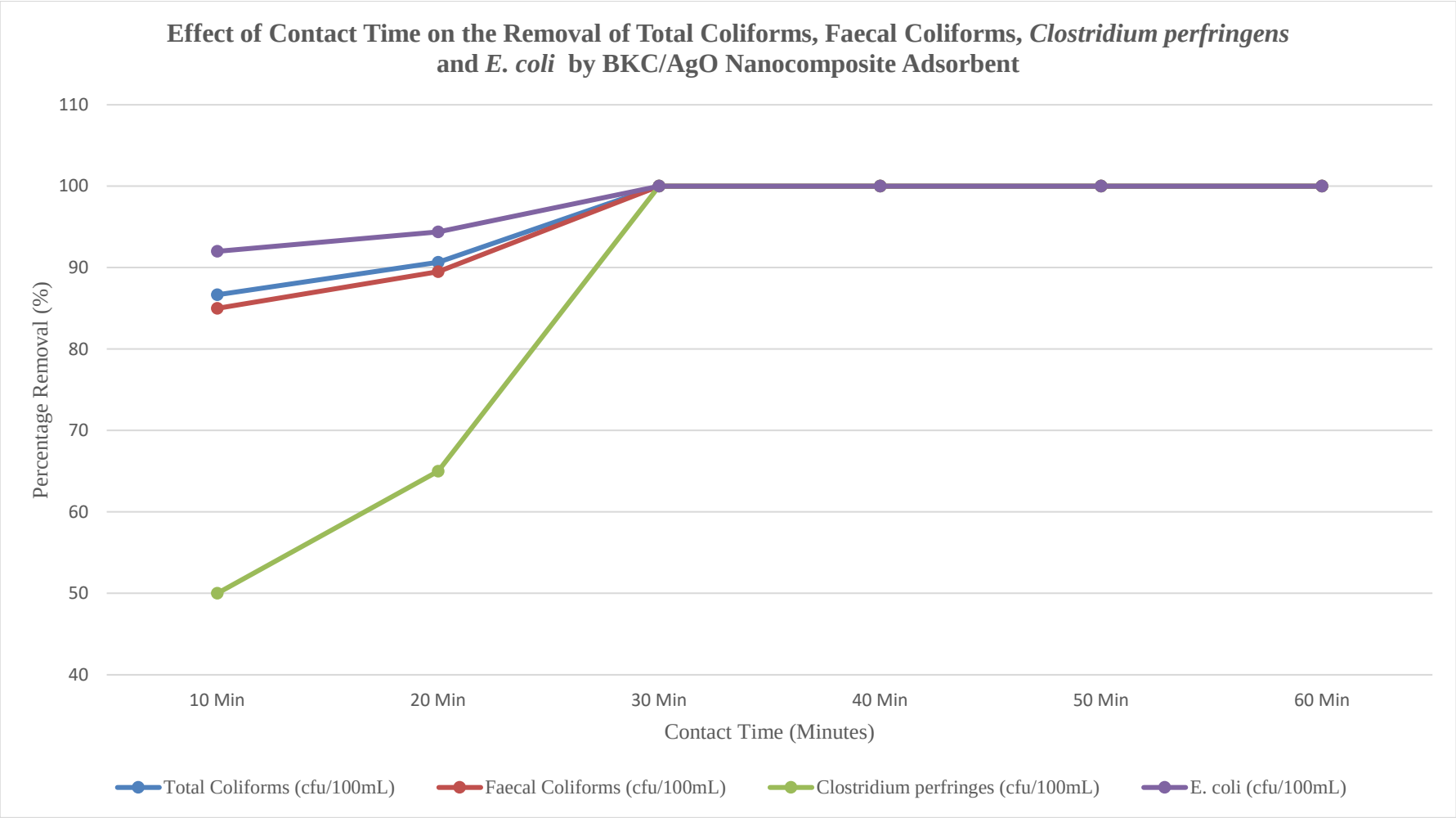

Figure 4.15 (c): Effect of Contact Time on the Removal of Total Coliforms, Faecal Coliforms, *Clostridium perfringens* and *E. coli* by BKC/Ag Adsorbent

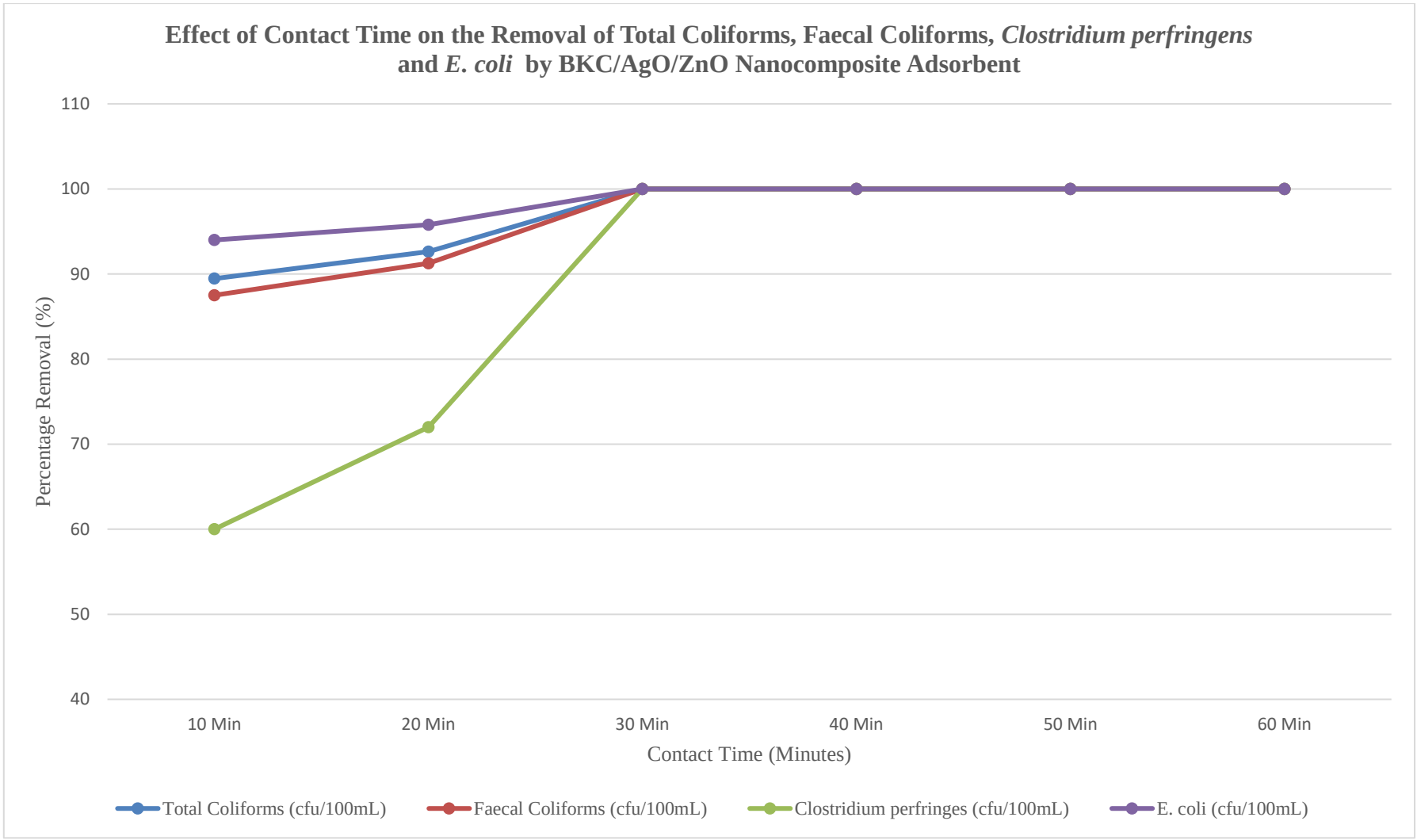

Figure 4.15 (d): Effect of Contact Time on the Removal of Total Coliforms, Faecal Coliforms, *Clostridium perfringens* and *E. coli* by BKC/Ag/ZnO Adsorbent

4.11 Effect of Dosage

4.11.1 Effect of dosage on heavy metal removal

Figure 4.16 (a – d) describes the effect of dosage on the removal of iron, lead, copper, manganese, arsenic, mercury silver and zinc onto BKC Adsorbent, BKC/Ag, BKC/ZnO and BKC/Ag/ZnO nanocomposite adsorbents.

The effects of adsorbent dosage when the wastewater was treated with BKC adsorbent, BKC/ZnO, BKC/Ag and BKC/Ag/ZnO nanocomposites adsorbents to remove iron, lead, copper, manganese, arsenic, mercury silver and zinc from wastewater was studied at adsorbent dosages of 5 – 30 g, constant pH of 6.9, temperature of 29.4 °C and contact time fixed at 30 minutes.

It was observed that the removal of iron, lead, copper, manganese, arsenic, mercury silver and zinc followed similar trends. At higher dosages, the adsorption increased due to the availability of more active binding exchangeable sites for the adsorption of the target pollutants (Abukhadra and Mohamed, 2019). This is because of an increase in the availability of the active binding sites and large surface areas of the adsorbents. This could also be inferred to be due to the availability of vast exchangeable sites for adsorption. The higher the adsorbent dosages used in the treatment, the higher the removal efficiencies of the pollutants from the wastewater by the adsorbents. The observed trend in terms of heavy metals removal was BKC/Ag/ZnO > BKC/Ag > BKC/ZnO > BKC. This behavioural pattern could be linked to the differences in the atomic weights and ionic radii of the concerned metal ions. It was found that BKC/Ag/ZnO performed best due to its crystallise size, high surface area and functional groups. Thus, the pollutant removal efficiency in domestic wastewater strongly depends on the dosage of the nano-adsorbents.

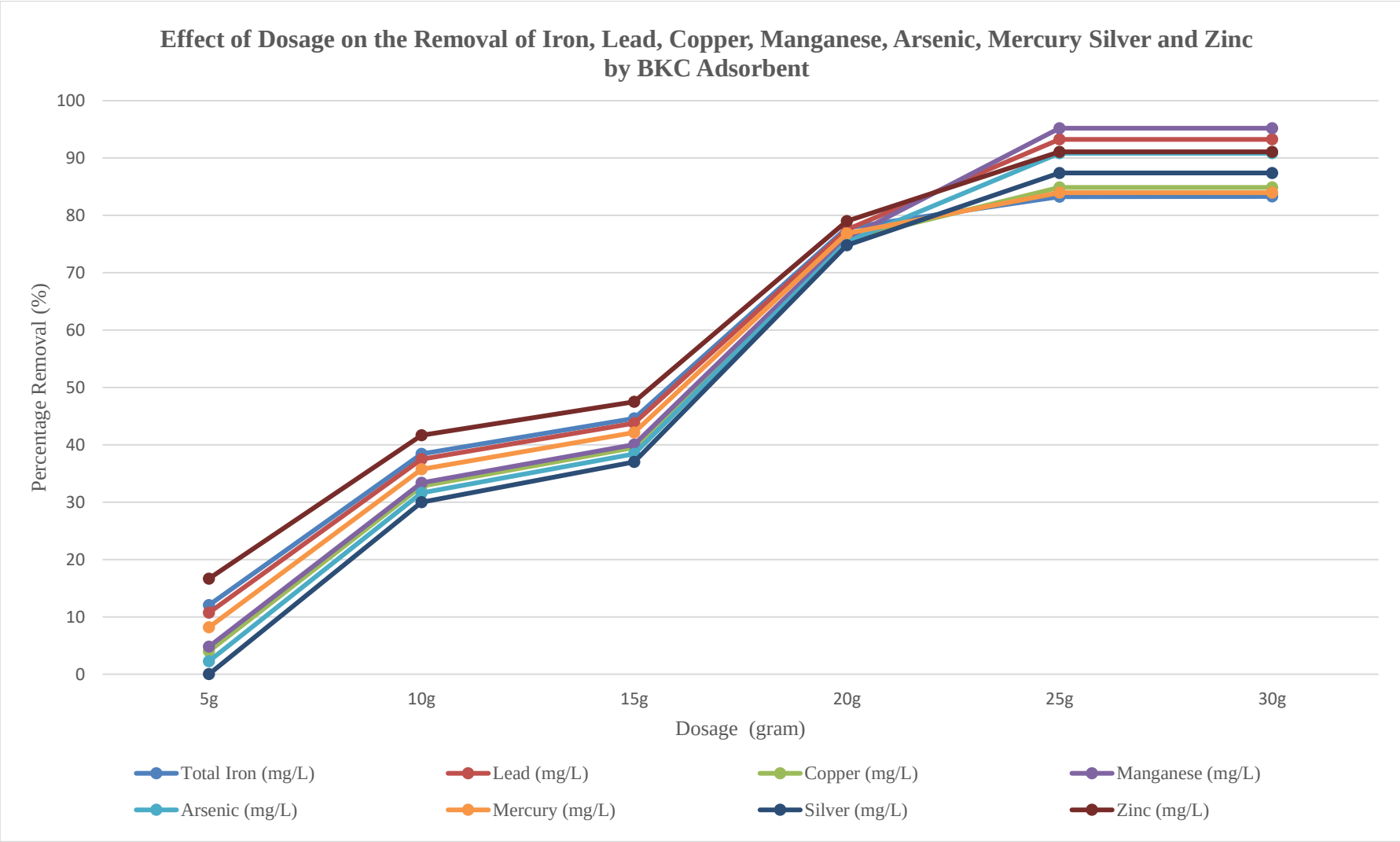

Figure 4.16 (a): Effect of Dosage on the Removal of Iron, Lead, Copper, Manganese, Arsenic, Mercury Silver and Zinc by BKC Adsorbent

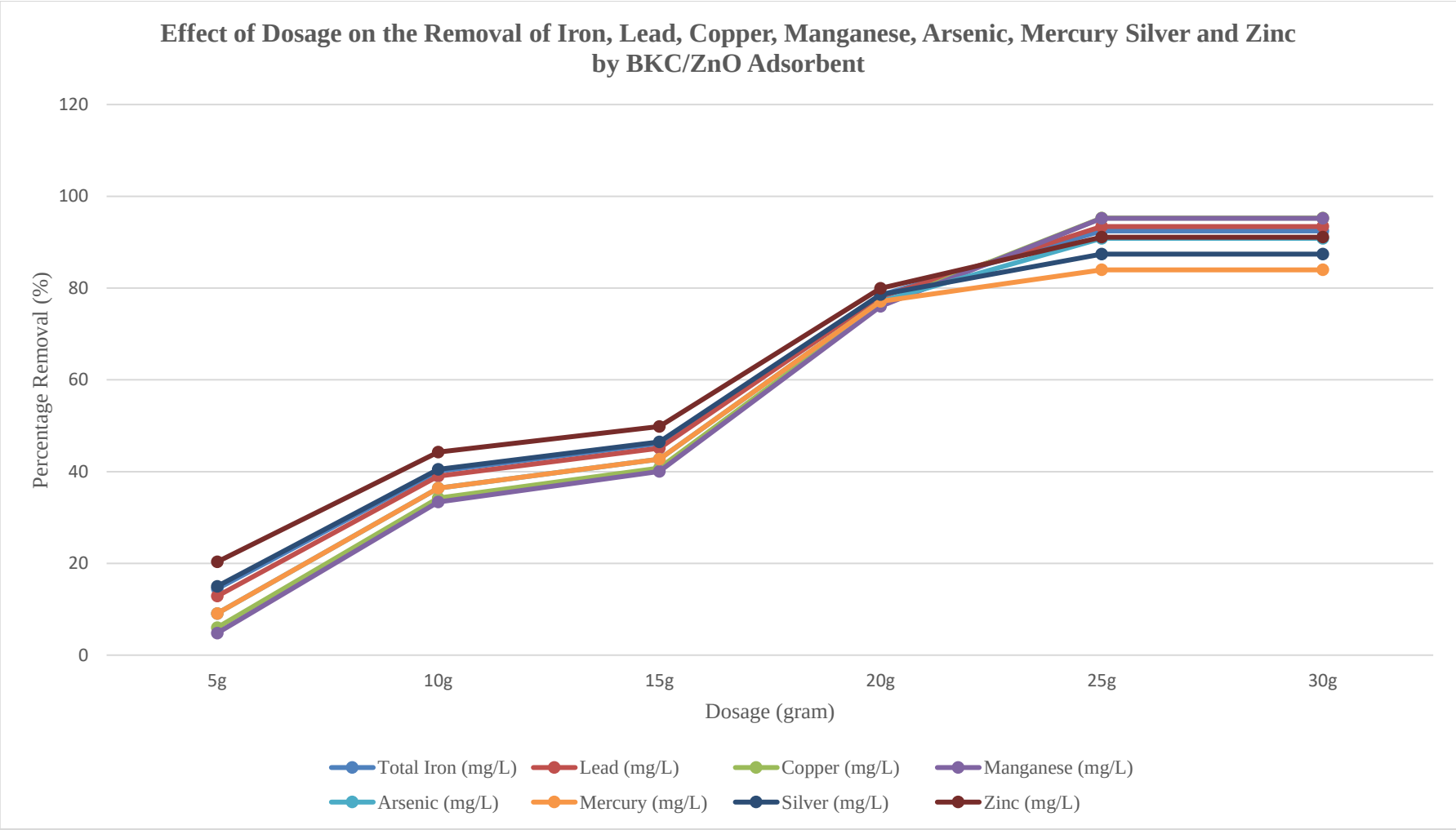

Figure 4.16 (b): Effect of Dosage on the Removal of Iron, Lead, Copper, Manganese, Arsenic, Mercury Silver and Zinc by BKC/ZnO Adsorbent

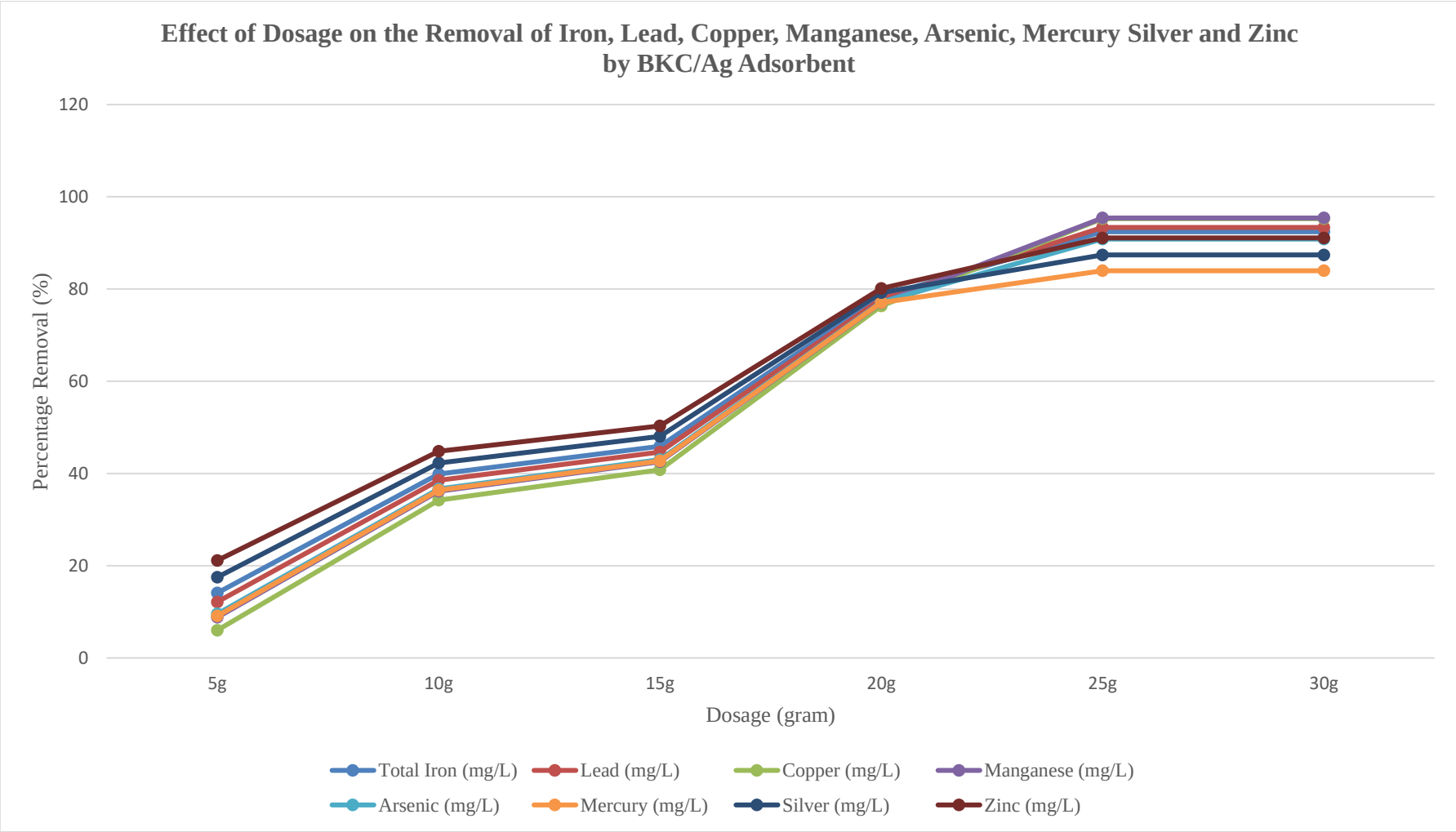

Figure 4.16 (c): Effect of Dosage on the Removal of Iron, Lead, Copper, Manganese, Arsenic, Mercury Silver and Zinc by BKC/Ag Adsorbent

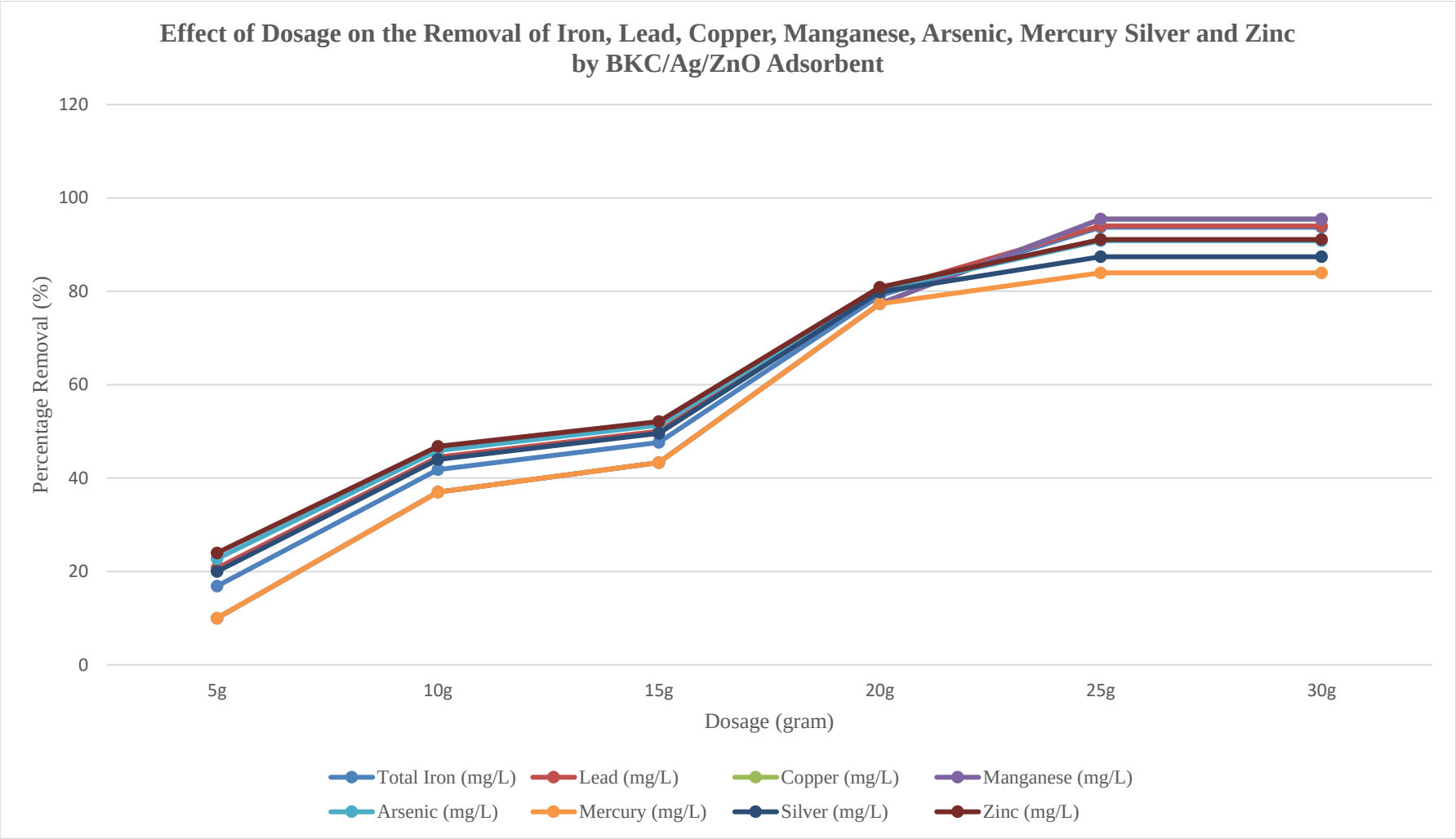

Figure 4.16 (d): Effect of Dosage on the Removal of Iron, Lead, Copper, Manganese, Arsenic, Mercury Silver and Zinc by BKC/Ag/ZnO Adsorbent

4.11.2 Effect of dosage on nutrients, COD, BOD, Oil and grease removal

Figure 4.17 (a – d) describes the effect of dosage on the removal of nitrate, phosphate, ammonium, COD, BOD and oil and grease onto BKC Adsorbent, BKC/Ag, BKC/ZnO and BKC/Ag/ZnO nanocomposite adsorbents.

The effects of BKC adsorbent, BKC/ZnO, BKC/Ag and BKC/Ag/ZnO nanocomposite adsorbent dosages on the removal of nitrate, phosphate, ammonium, COD, BOD and oil and grease were studied at adsorbent dosages of 5 – 30 g, constant pH of 6.9, temperature of 29.4 °C and contact time of 30 minutes.

It was observed that the removal of the nitrate, phosphate, ammonium, COD, BOD and oil and grease pollutants followed similar trends. At a lower dosage, the rate of adsorption was influenced by inter-ionic competition and at a higher dosage, the adsorption process was observed to increase. This is because of an increase in the availability of the active binding sites and large surface areas of the adsorbents. This could also be inferred to be due to the availability of vast exchangeable sites for adsorption. The higher the adsorbent dosages used in the treatment, the higher the removal efficiencies of the pollutants from the wastewater by the adsorbents.

The observed trend in terms of nitrate, phosphate, ammonium, COD, BOD and oil and grease pollutants removal was BKC/Ag/ZnO > BKC/Ag > BKC/ZnO > BKC. This behavioural pattern can be linked to the differences in the atomic weights and ionic radii of the concerned ions. it was found that BKC/Ag/ZnO performed best due to its crystalise size, high surface area and functional groups. Therefore, the adsorbent dosage is a paramount parameter responsible for the adsorption of pollutants in domestic wastewater treatment.

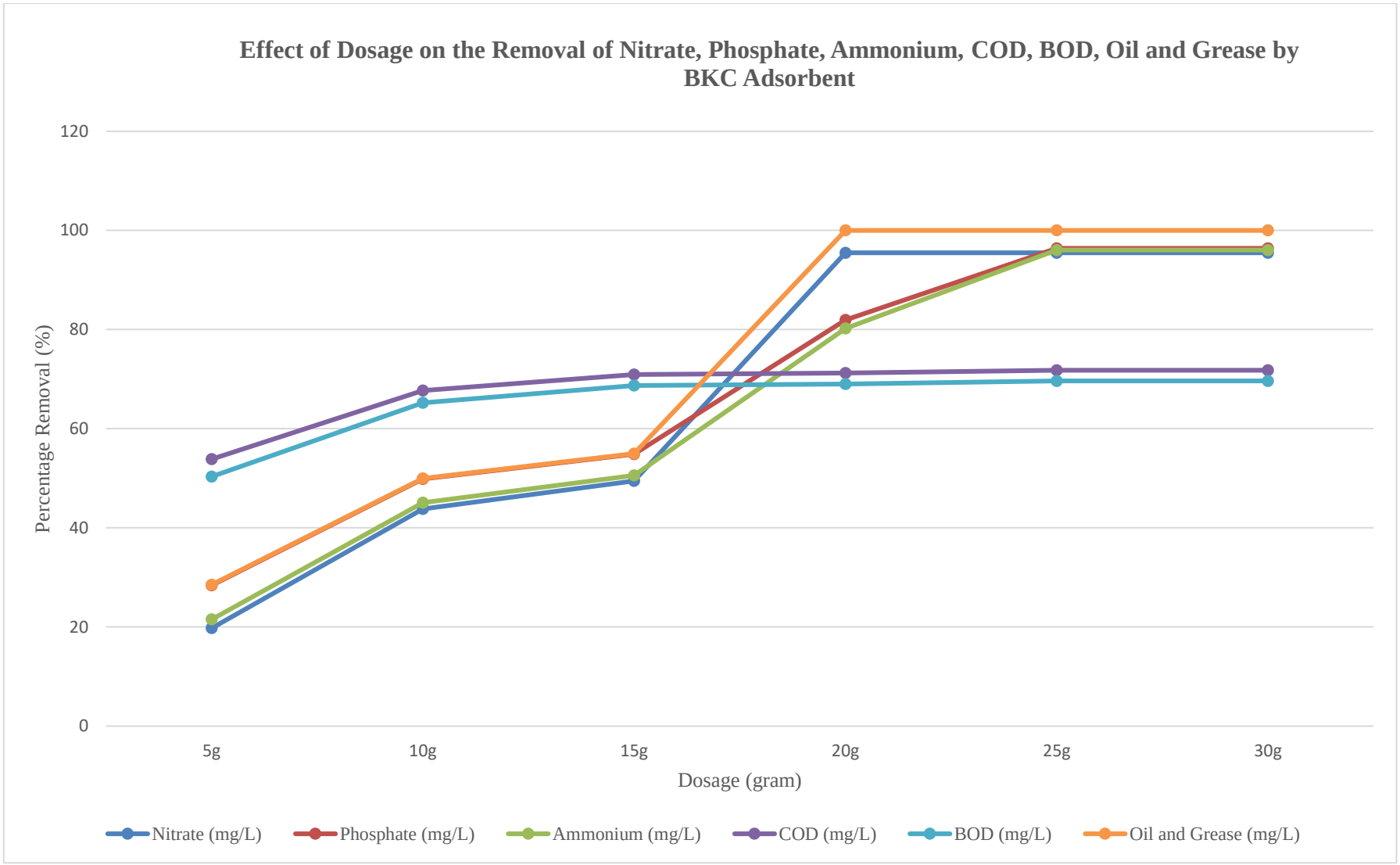

Figure 4.17 (a): Effect of Dosage on the Removal of Nitrate, Phosphate, Ammonium, COD, BOD, Oil and Grease by BKC Adsorbent

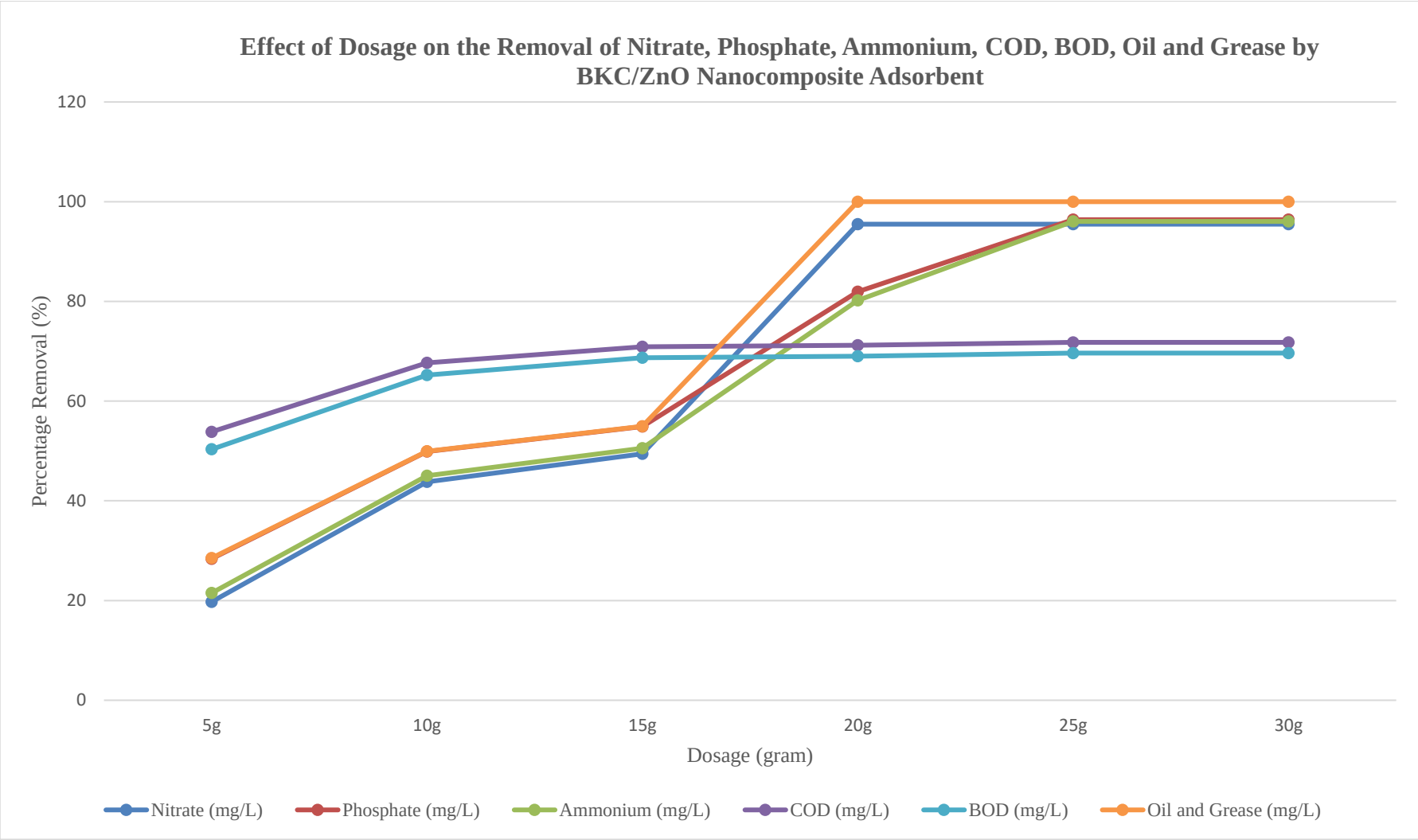

Figure 4.17 (b): Effect of Dosage on the Removal of Nitrate, Phosphate, Ammonium, COD, BOD, Oil and Grease by BKC/ZnO Nanocomposite Adsorbent

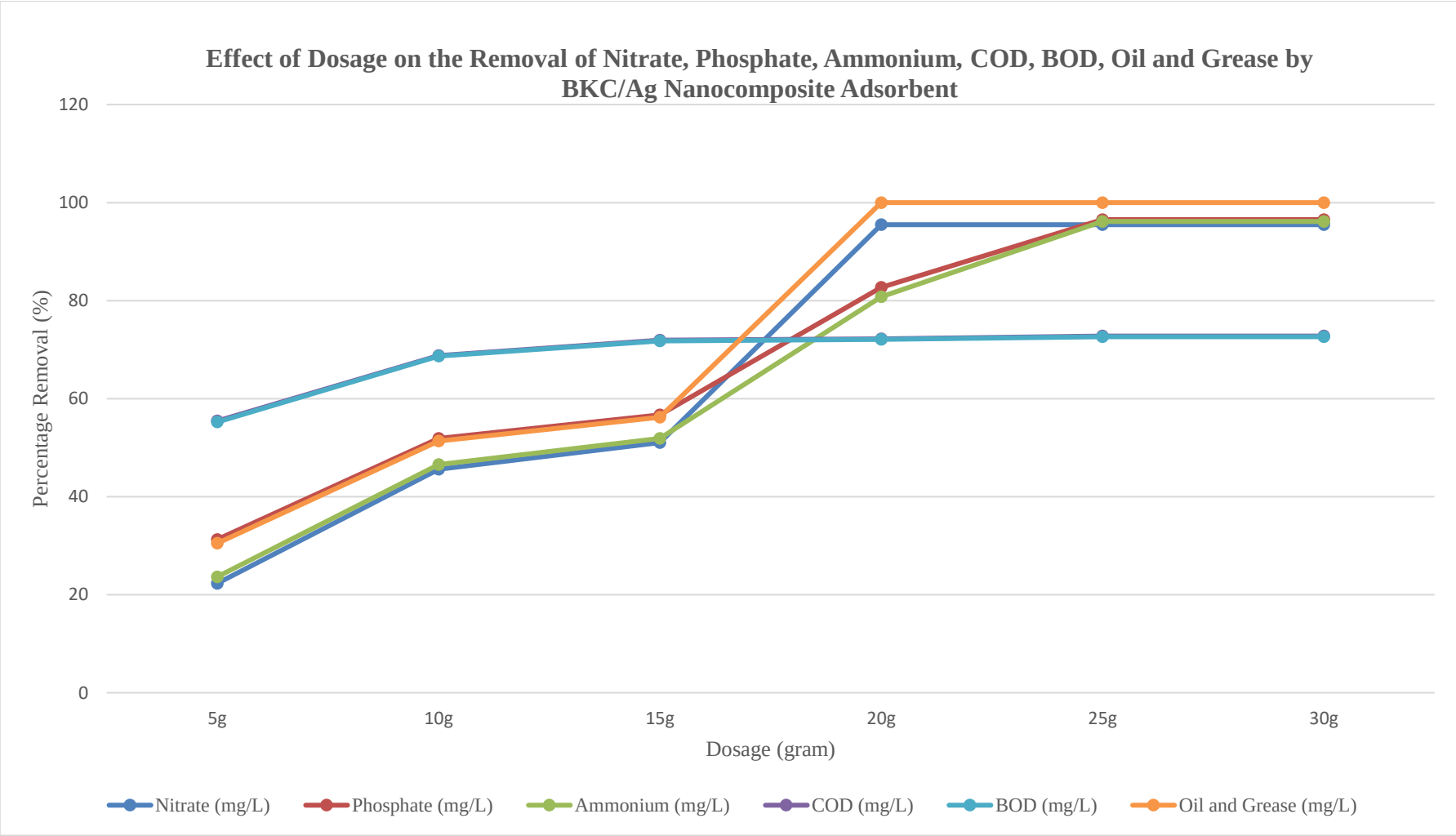

Figure 4.17 (c): Effect of Dosage on the Removal of Nitrate, Phosphate, Ammonium, COD, BOD, Oil and Grease by BKC/Ag Nanocomposite Adsorbent

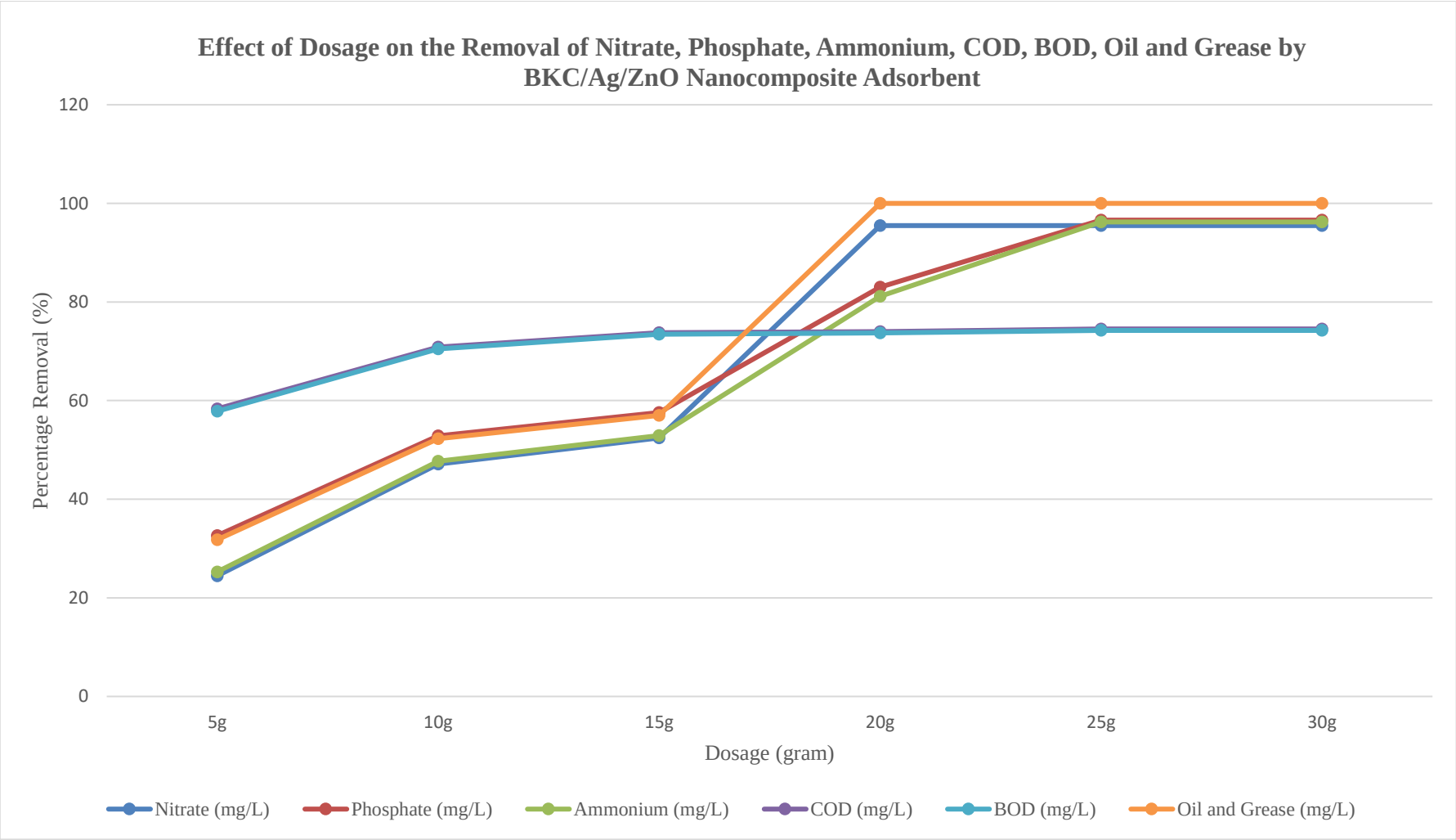

Figure 4.17 (d): Effect of Dosage on the Removal of Nitrate, Phosphate, Ammonium, COD, BOD, Oil and Grease by BKC/Ag/ZnO Nanocomposite Adsorbent

4.11.3 Effect of dosage on physical parameters

Figure 4.18 (a – e) describes the effect of dosage on the removal of turbidity, suspended solids, colour, EC, improvement of pH and dissolved oxygen using BKC Adsorbent, BKC/Ag, BKC/ZnO and BKC/Ag/ZnO nanocomposite adsorbents.

Effects of BKC adsorbent, BKC/ZnO, BKC/Ag and BKC/Ag/ZnO adsorbent dosages on the removal of turbidity, suspended solid, colour, EC and improvement of pH and dissolved oxygen of the domestic wastewater during treatment was studied at adsorbent dosages of 5 – 30 g, constant pH 6.9, temperature of 29.4 °C and contact time of 30 minutes.

Percentage removal efficiencies of turbidity, suspended solids, colour, EC and improvement of pH and dissolved oxygen by the BKC adsorbent, BKC/ZnO, BKC/Ag and BKC/Ag/ZnO nanocomposite adsorbents are presented in Figures 4.18 (a – e). It was observed that the removal of the turbidity, suspended solids, colour and EC followed similar trends.

The observed trend in terms of turbidity, suspended solids, colour and EC removal was BKC/Ag/ZnO > BKC/Ag > BKC/ZnO > BKC. This behavioural pattern could be linked to the differences in the atomic weights and ionic radii of the concerned ions. The pH improved from 8.96 to 7.20 for BKC/Ag/ZnO, 7.29 for BKC/Ag, 7.38 for BKC/ZnO and 7.45 for BKC respectively after treatment as presented in Figure 4.18 (a). The dissolved oxygen improved from 1.00 mg/L in the wastewater to 4.82 mg/L in BKC/Ag/ZnO, BKC/Ag, BKC and 4.81 mg/L in BKC/ZnO respectively after treatment. The dissolved oxygen improved due to the removal of the pollutants such as nutrients depleting oxygen in the wastewater.

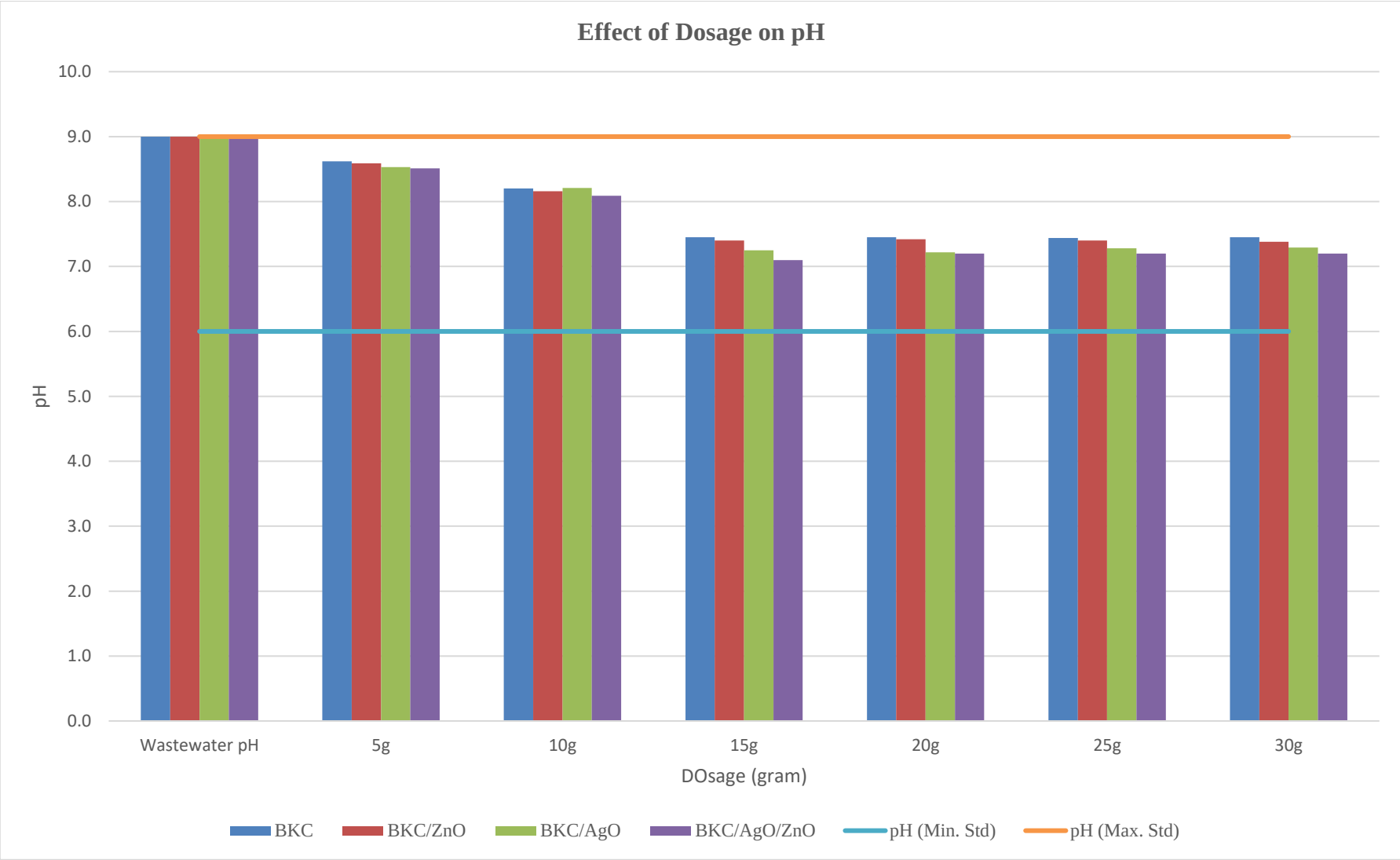

Figure 4.18 (a): Effect of Dosage on pH

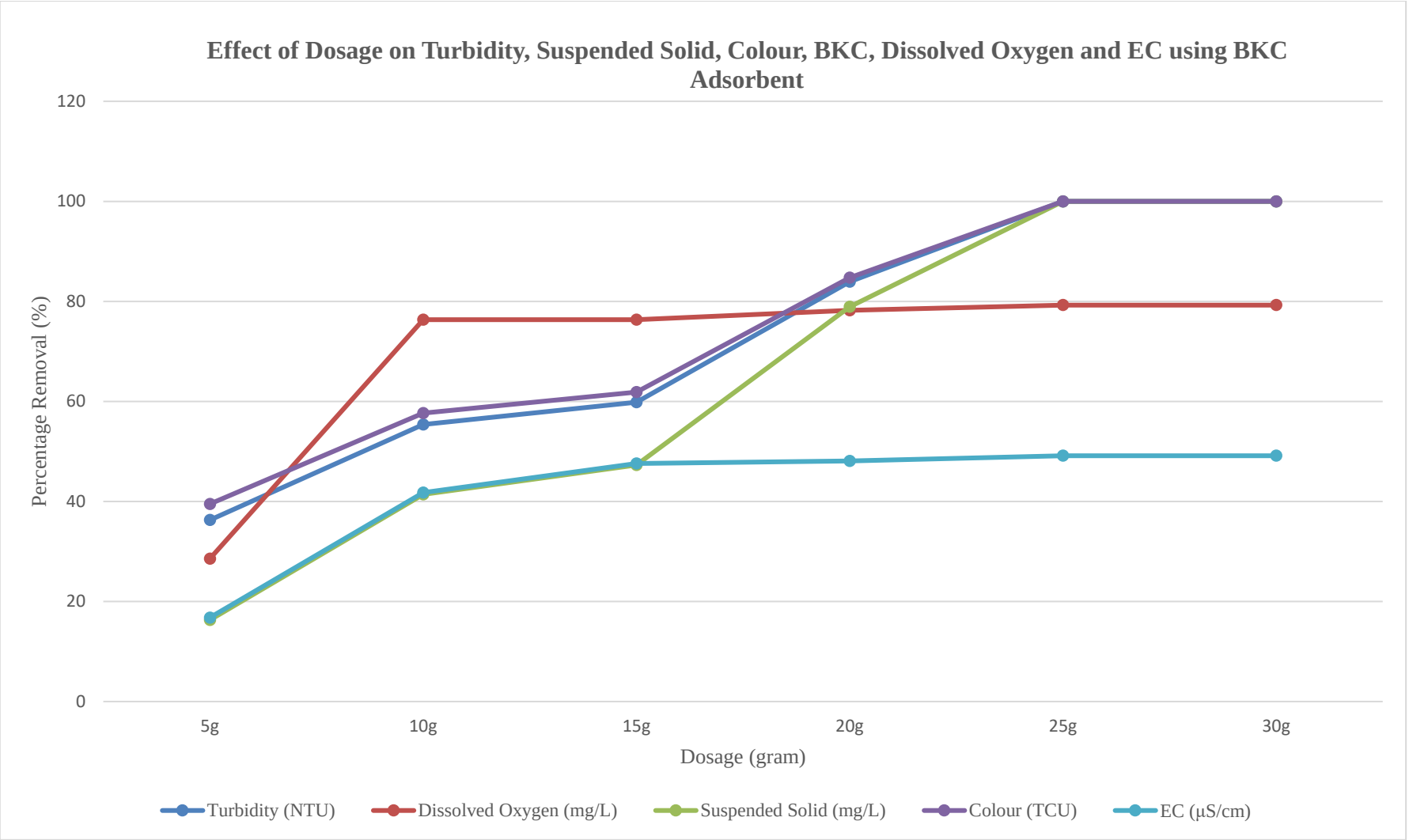

Figure 4.18 (b): Effect of Dosage on Turbidity, Suspended Solid, Colour, BKC, Dissolved Oxygen and EC using BKC Adsorbent

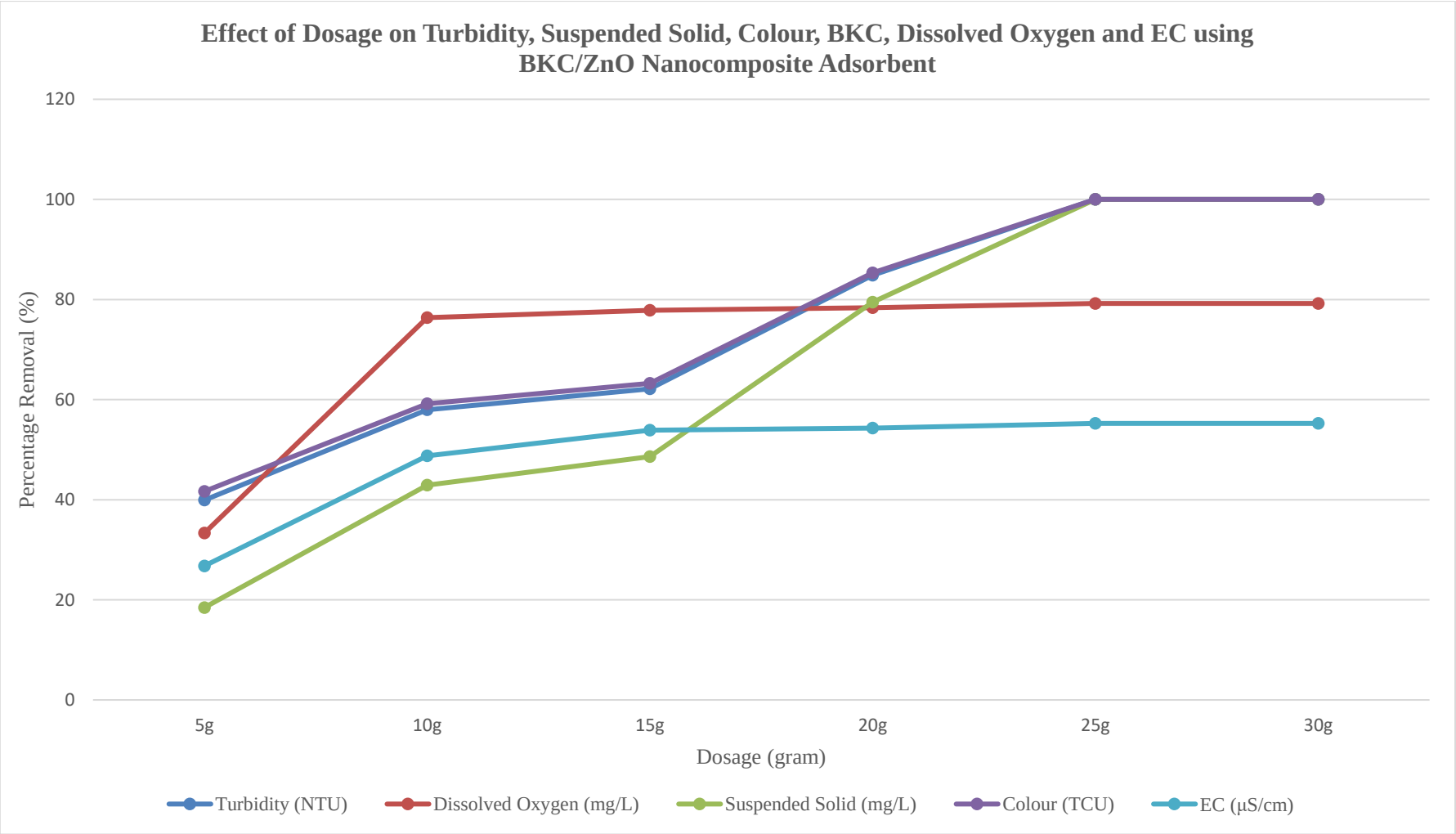

Figure 4.18 (c): Effect of Dosage on Turbidity, Suspended Solid, Colour, BKC, Dissolved Oxygen and EC using BKC/ZnO Nanocomposite Adsorbent

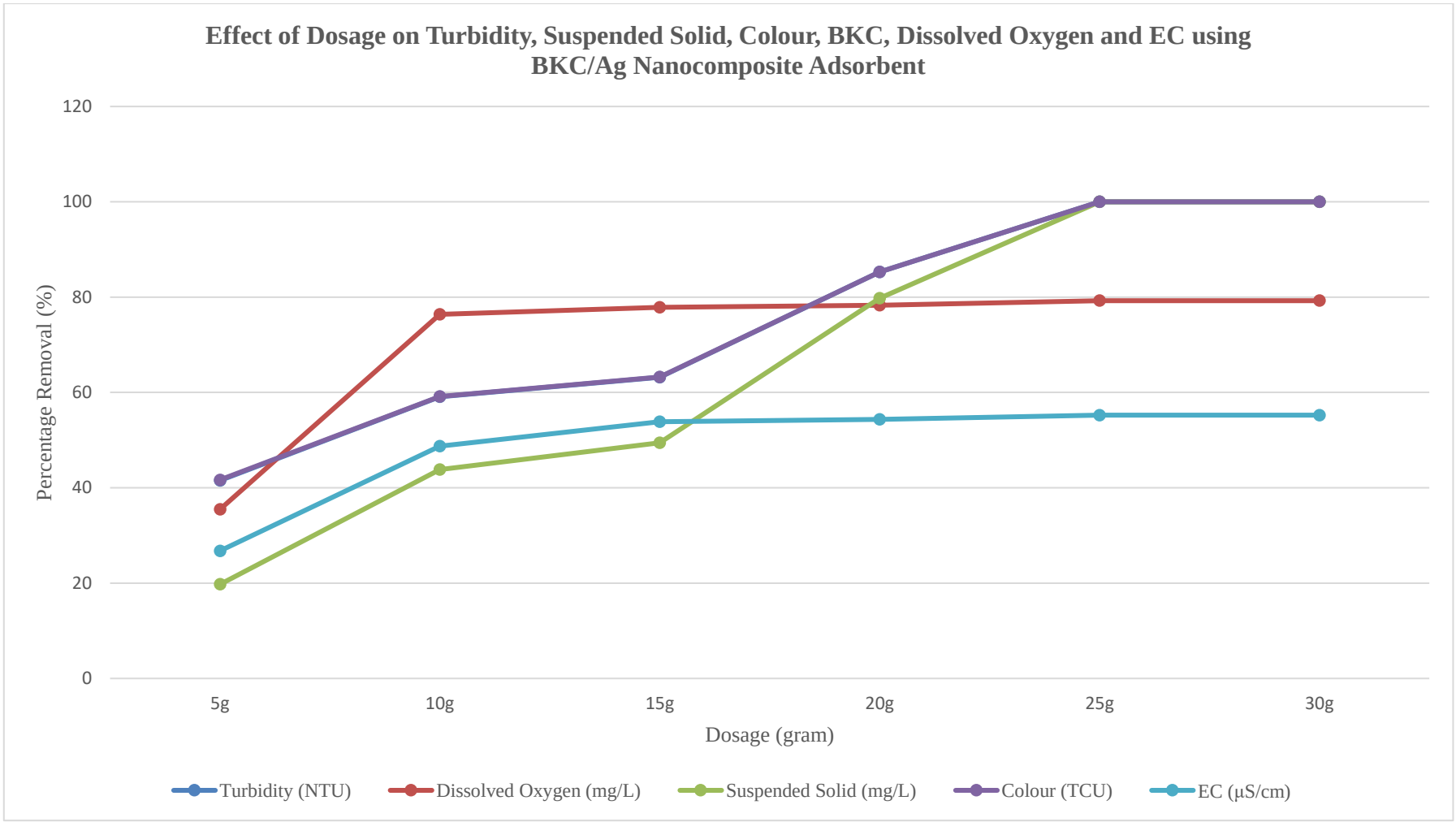

Figure 4.18 (d): Effect of Dosage on Turbidity, Suspended Solid, Colour, BKC, Dissolved Oxygen and EC using BKC/Ag Nanocomposite Adsorbent

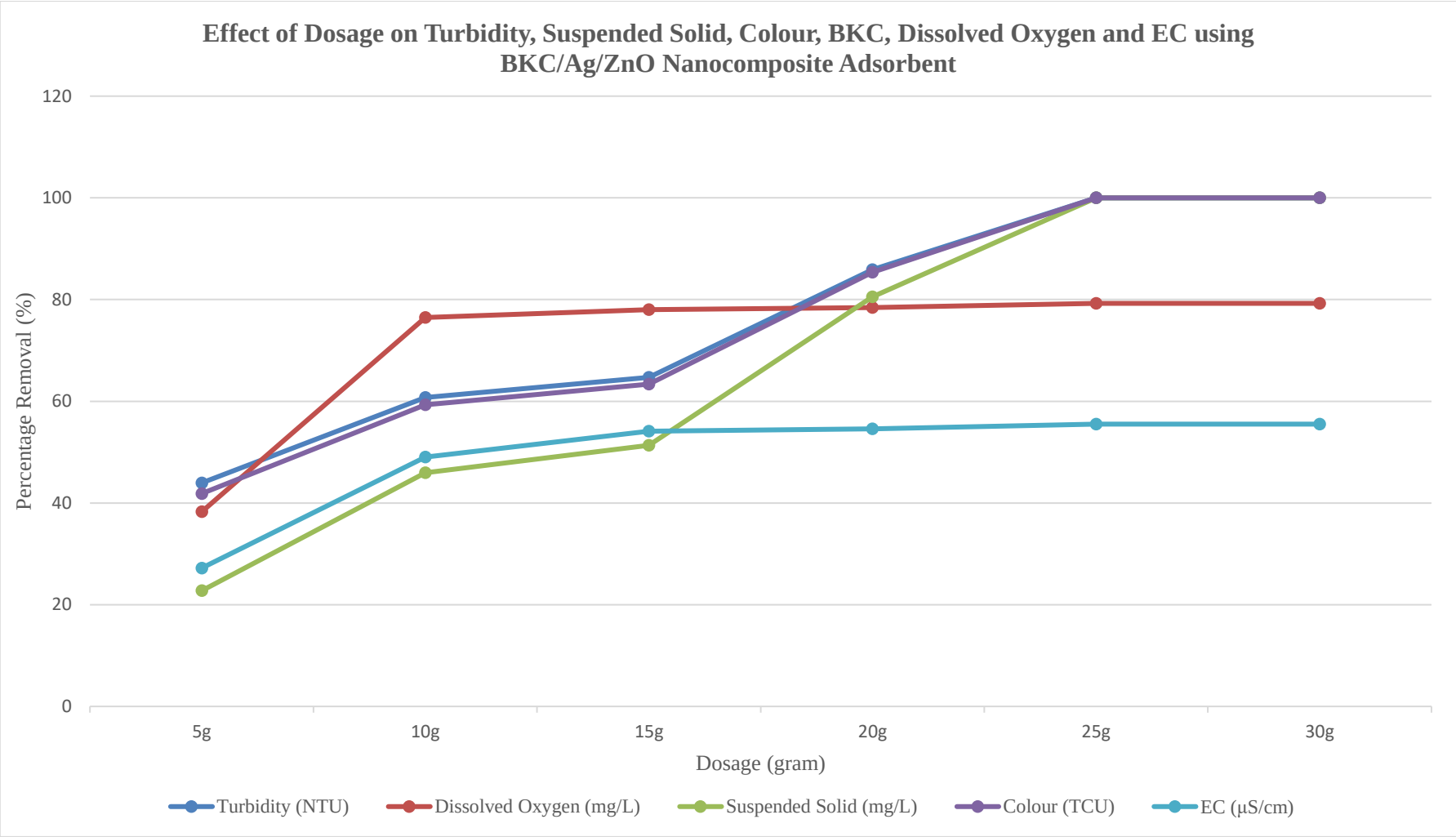

Figure 4.18 (e): Effect of Dosage on Turbidity, Suspended Solid, Colour, BKC, Dissolved Oxygen and EC using BKC/Ag/ZnO Nanocomposite Adsorbent

4.11.4 Effect of dosage on microbial removal

Figure 4.19 (a – d) describes the effect of dosage on the removal of total coliforms, faecal coliforms, *Clostridium perfringens* and *E. coli* onto BKC Adsorbent, BKC/Ag, BKC/ZnO and BKC/Ag/ZnO nanocomposite adsorbents.

The effects of BKC, BKC/ZnO, BKC/Ag and BKC/Ag/ZnO nanocomposites adsorbent dosages on the removal of total coliforms, faecal coliforms, C*lostridium perfringens* and *E. coli* in the domestic wastewater was studied at adsorbent dosages of 5 – 30 g, constant of pH 6.9, temperature of 29.4 °C and contact time of 30 minutes.

Rapid percentage removal was obtained between the adsorbent dosage of 5 – 10 g for BKC adsorbent and BKC/ZnO nanocomposite adsorbent and continuous removal of microbes was noticed when BKC adsorbent and BKC/ZnO nanocomposite adsorbent was used to treat wastewater. The slight increase in percentage removal of total coliforms, faecal coliforms, *Clostridium perfringens* and *E. coli* for BKC and BKC/ZnO nanocomposite adsorbents with further increase in dosages was due to low antimicrobial activity of the two adsorbents.

The complete removal of total coliforms, faecal coliforms, *Clostridium perfringens* and *E. coli* at 15 g dosage for BKC/Ag and BKC/Ag/ZnO nanocomposite adsorbents was mainly due to the antibacterial activity of silver and zinc nanoparticles as shown in Figure (c - d).

The detailed results of dosage on the removal of contaminants by BKC, BKC/ZnO, BKC/Ag and BKC/Ag/ZnO nanocomposite adsorbents are presented in Appendix D.

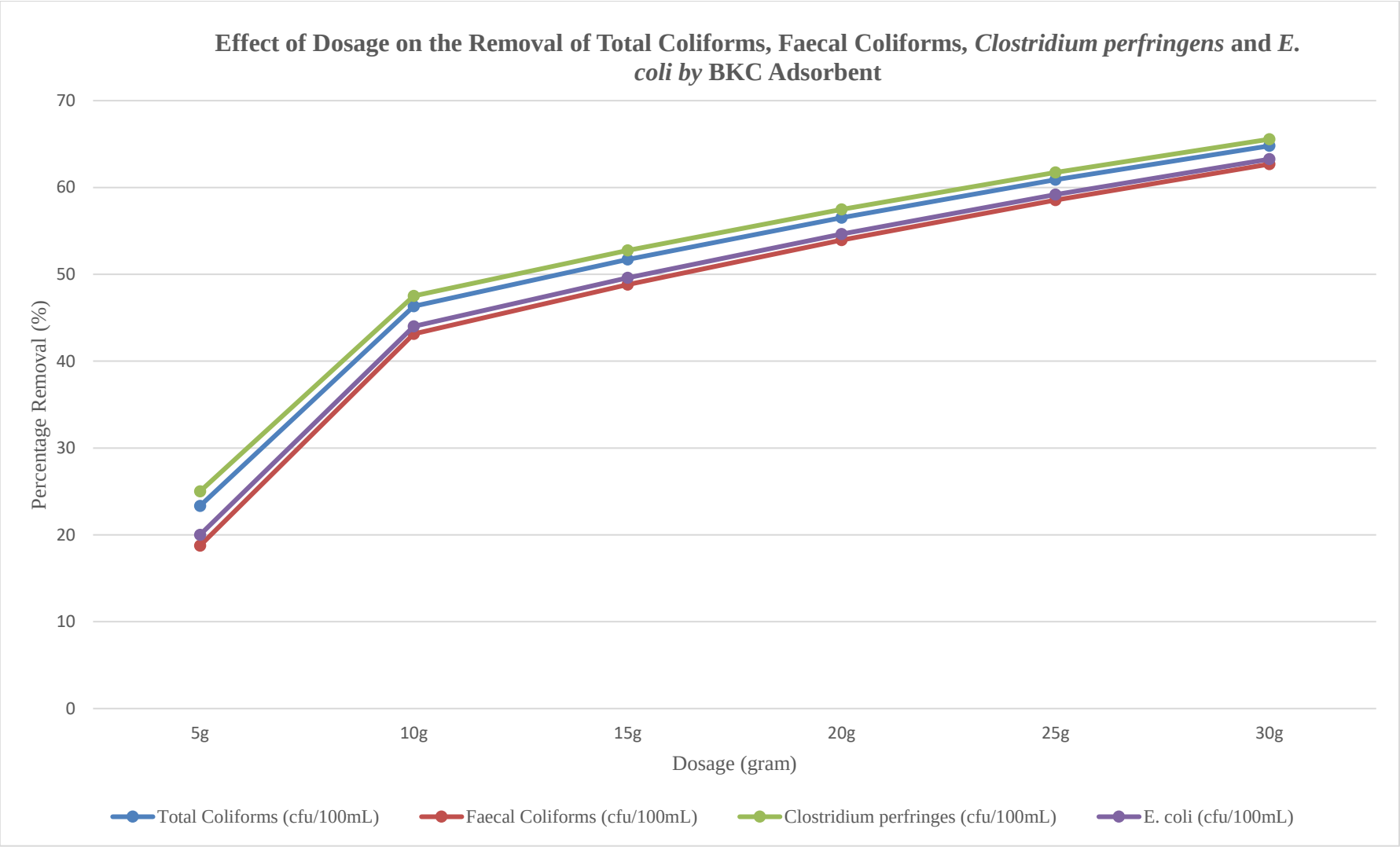

Figure 4.19 (a): Effect of Dosage on the Removal of Total Coliforms, Faecal Coliforms, *Clostridium perfringens* and *E. coli by* BKC Adsorbent

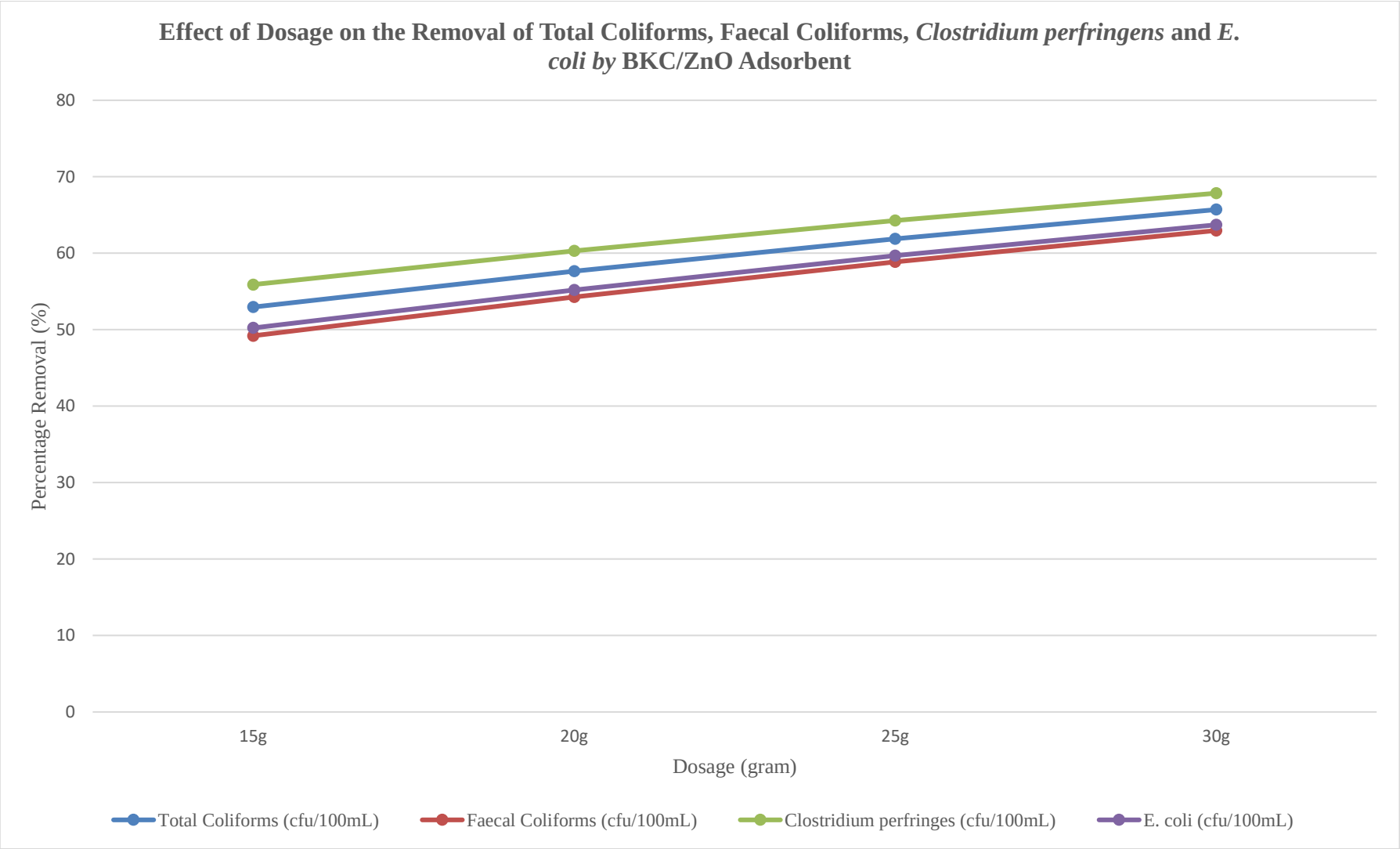

Figure 4.19 (b): Effect of Dosage on the Removal of Total Coliforms, Faecal Coliforms, *Clostridium perfringens* and *E. coli by* BKC/ZnO Adsorbent

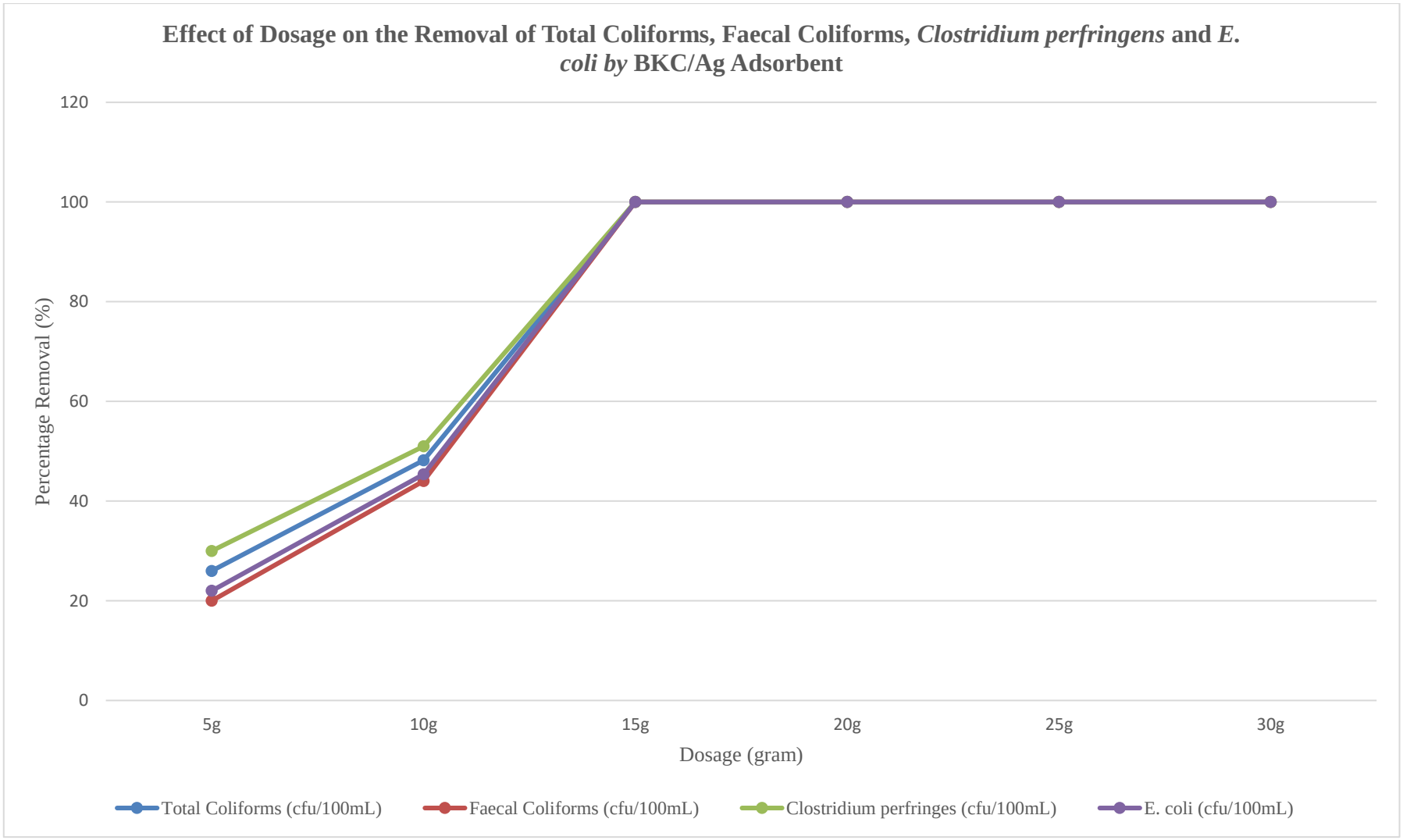

Figure 4.19 (c): Effect of Dosage on the Removal of Total Coliforms, Faecal Coliforms, *Clostridium perfringens* and *E. coli by* BKC/Ag Adsorbent

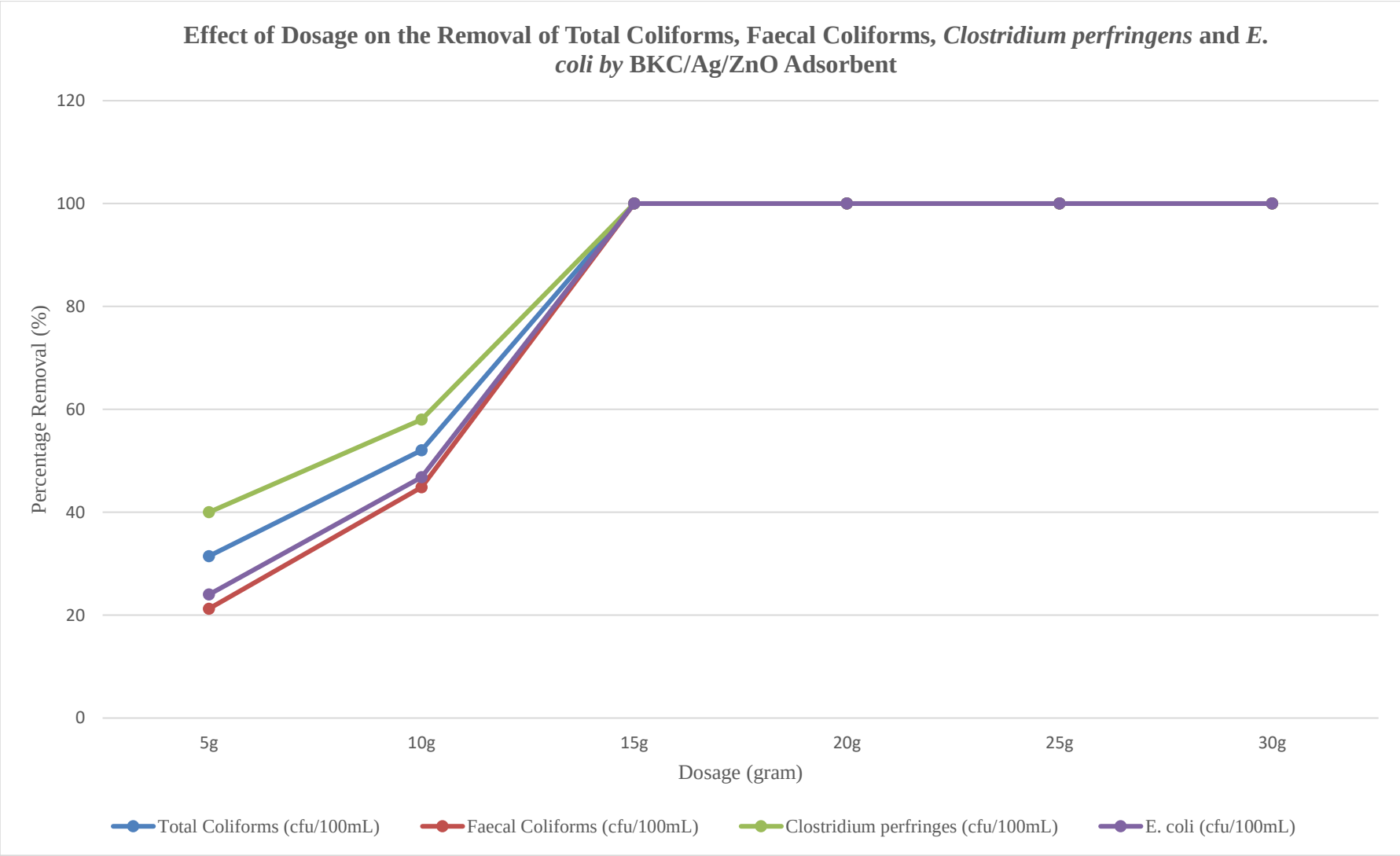

Figure 4.19 (d): Effect of Dosage on the Removal of Total Coliforms, Faecal Coliforms, *Clostridium perfringens* and *E. coli by* BKC/Ag/ZnO Adsorbent

4.12 Effect of Temperature

4.12.1 Effect of temperatures on heavy metals removal

The effect of temperatures on the adsorption of iron, lead, copper, manganese, arsenic, mercury silver and zinc onto BKC, BKC/ZnO, BKC/Ag and BKC/Ag/ZnO nanocomposites was studied at temperatures of 30, 40, 50, 60, 70 and 80 °C using an adsorbent dosage of 25 g/100 mL of wastewater at a temperature of 29.5 °C and pH of 6.9. The effect of temperature on the removal of iron, lead, copper, manganese, arsenic, mercury silver and zinc is presented in Figure 4.20 (a – d).

The observation revealed that an increase in the fraction of the heavy metals adsorbed occurred with a corresponding increase in the temperature. The temperatures increased the removal efficiency rate for all the metals.

The increase in temperature from 30 – 80 °C for BKC adsorbent gradually increased heavy metal adsorption. The rate of adsorption equals the rate of desorption at an equilibrium temperature of between 70 – 80 °C for BKC/ZnO, BKC/Ag and BKC/Ag/ZnO nanocomposite adsorbents as presented in Figure 20 (b – c); therefore, slow uptake of pollutants was observed from 70 °C to 80 °C. The slow uptake and the slight or no increase in percentage removal with a further increase in temperature might be due to saturation of the surface area of the adsorbent with heavy metal pollutants.

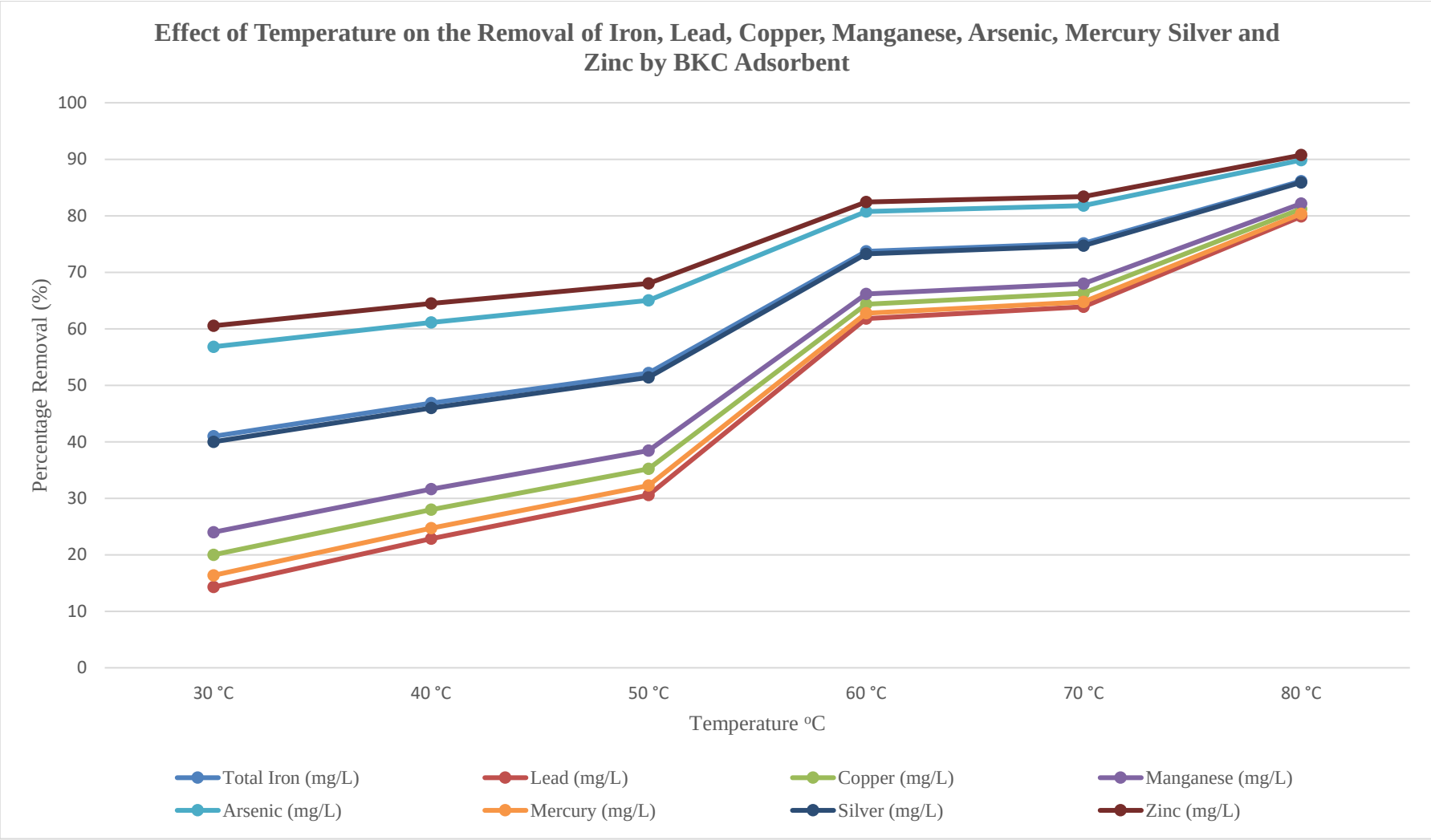

Figure 4.20 (a): Effect of Temperature on the Removal of Iron, Lead, Copper, Manganese, Arsenic, Mercury Silver and Zinc by BKC Adsorbent

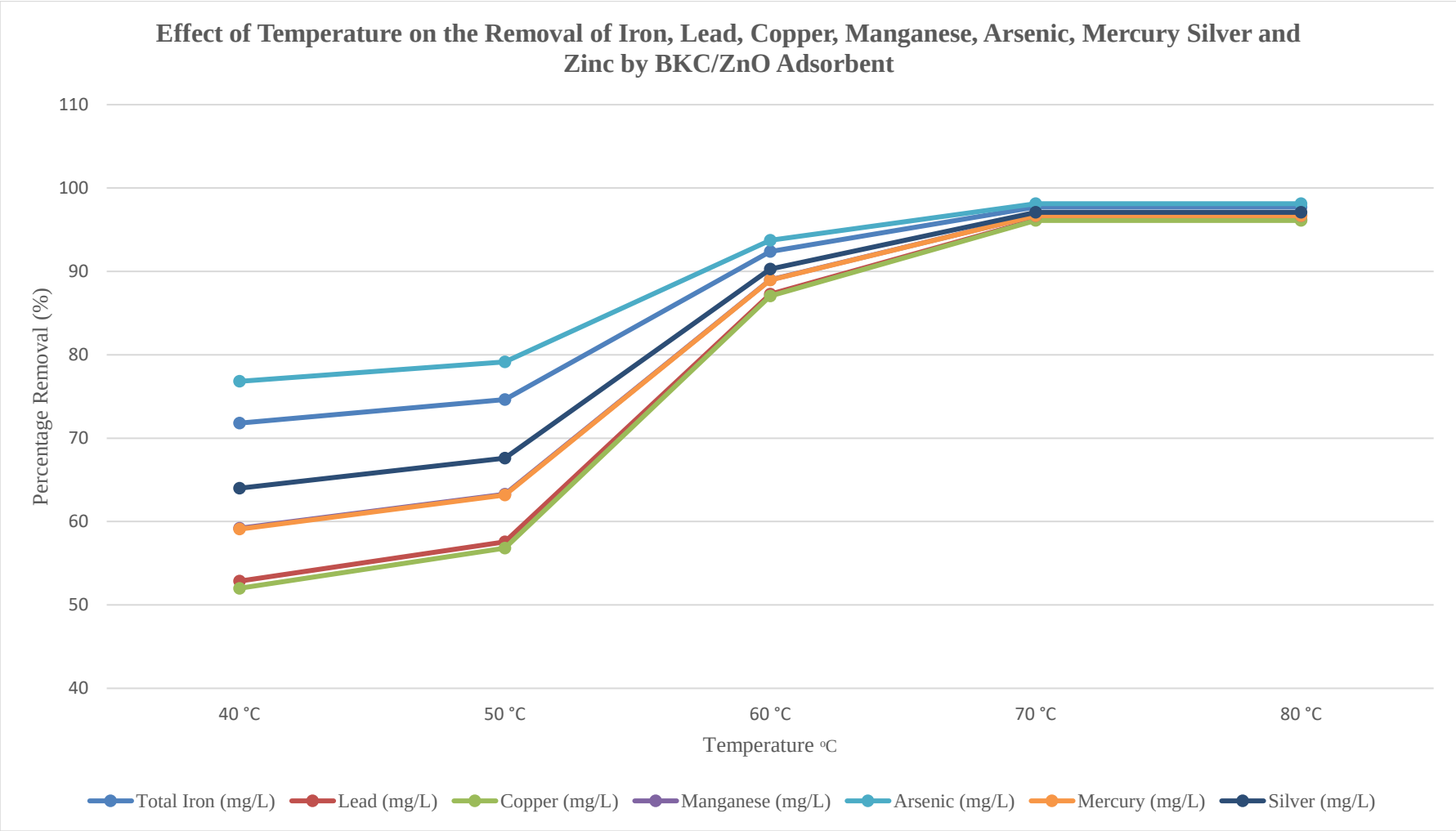

Figure 4.20 (b): Effect of Temperature on the Removal of Iron, Lead, Copper, Manganese, Arsenic, Mercury Silver and Zinc by BKC/ZnO Adsorbent

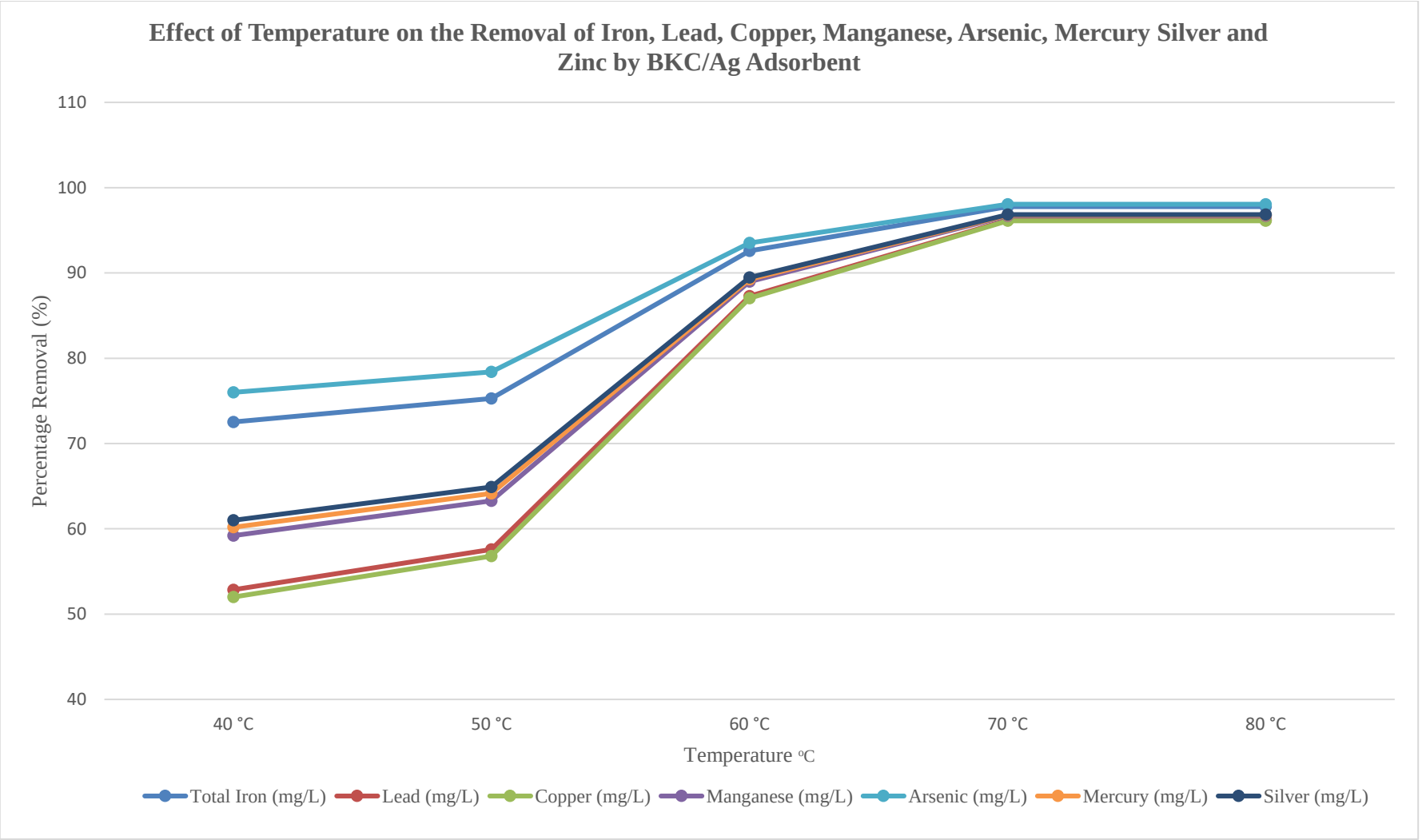

Figure 4.20 (c): Effect of Temperature on the Removal of Iron, Lead, Copper, Manganese, Arsenic, Mercury Silver and Zinc by BKC/Ag Adsorbent

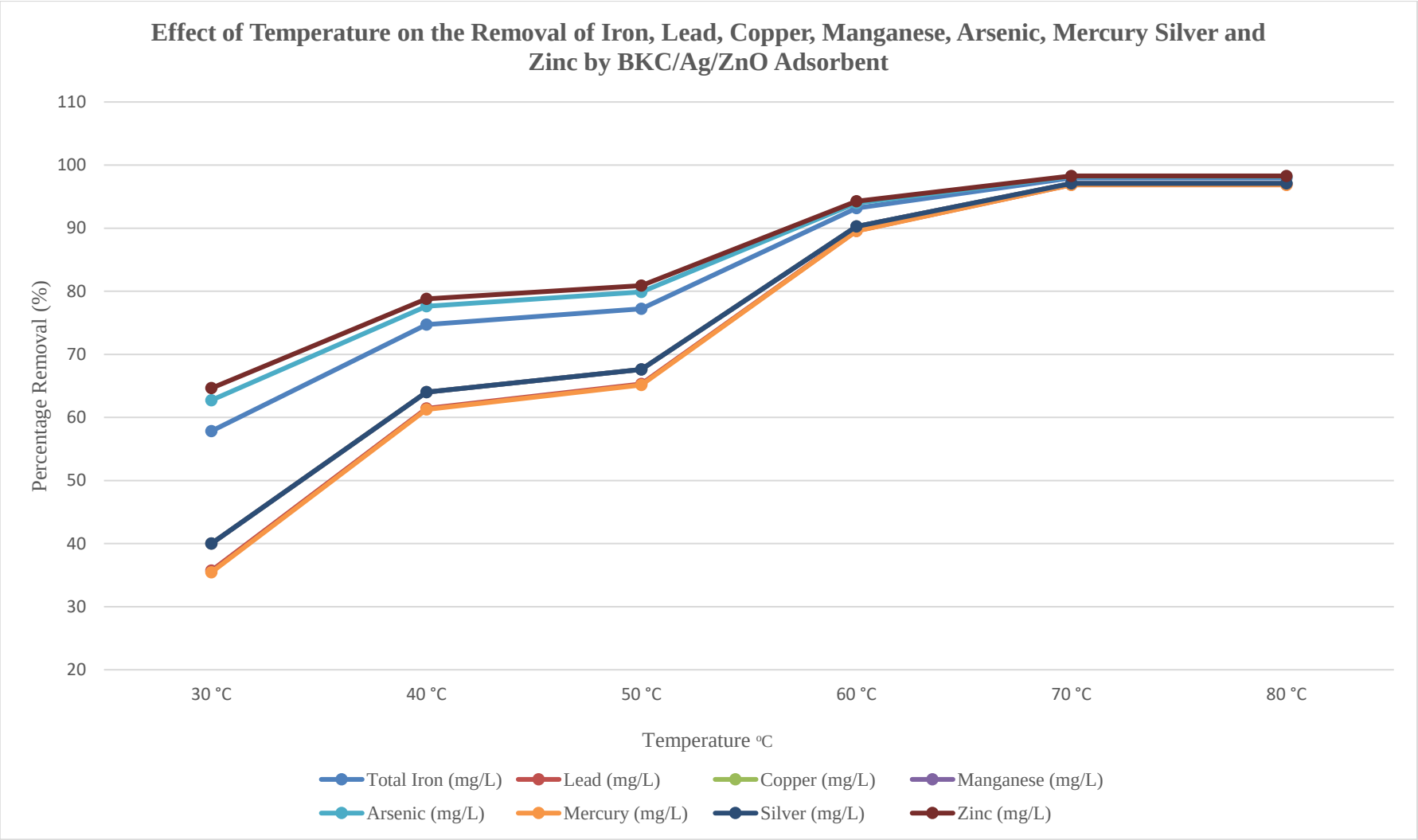

Figure 4.20 (d): Effect of Temperature on the Removal of Iron, Lead, Copper, Manganese, Arsenic, Mercury Silver and Zinc by BKC/Ag/ZnO Adsorbent

4.12.2 Effect of temperatures on nitrate, phosphate, ammonium, COD, BOD, oil and grease removal

The effect of temperatures on the adsorption of nitrate, phosphate, ammonium, COD, BOD and oil and grease onto BKC, BKC/ZnO, BKC/Ag and BKC/Ag/ZnO nanocomposites was studied at temperature of 30, 40, 50, 60, 70 and 80 °C using an adsorbent dosage of 25 g/100 mL and pH of 6.9.

The effect of temperature on the removal of nitrate, phosphate, ammonium, COD, BOD and oil and grease is presented in Figure 4.21 (a – d). The observation revealed that an increase in the fraction of the nitrate, phosphate, ammonium, COD, BOD and oil and grease occurred with a corresponding increase in the temperature.

The increase in temperature from 30 °C to 40 °C gradually increased nitrate, phosphate, ammonium, COD, BOD and oil and grease for BKC adsorbent, BKC/ZnO, BKC/Ag and BKC/Ag/ZnO nanocomposite adsorbents. The rate of adsorption equals the rate of desorption at equilibrium; therefore, slow uptake of pollutants was observed from 40 °C to 80 °C for BKC adsorbent, BKC/ZnO, BKC/Ag and BKC/Ag/ZnO nanocomposite adsorbents.

The slow uptake and the slight or no increase in percentage removal with further increase in temperature might be due to saturation of the surface area of the adsorbent with nitrate, phosphate, ammonium, COD, BOD and oil and grease pollutants.

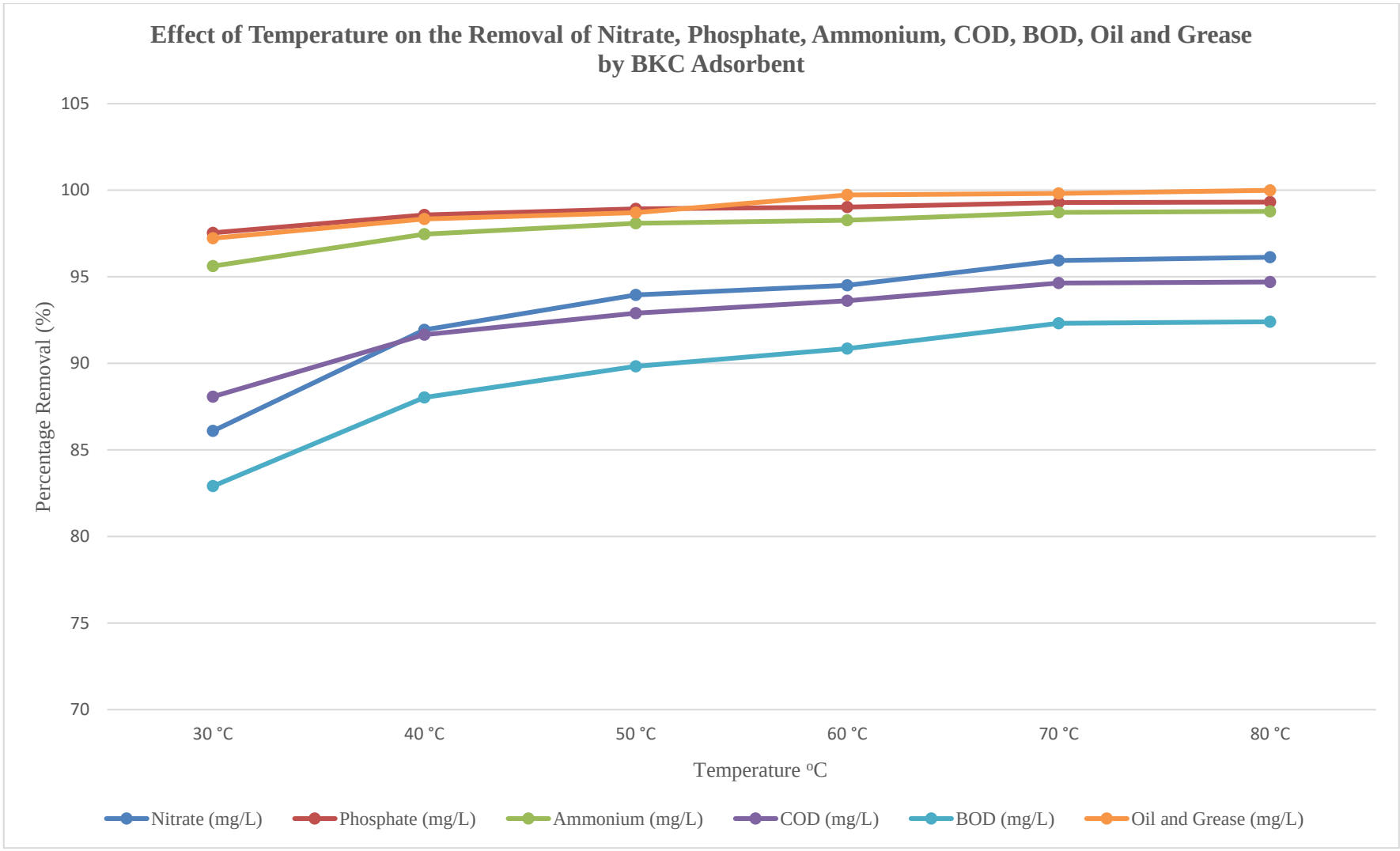

Figure 4.21 (a): Effect of Temperature on the Removal of Nitrate, Phosphate, Ammonium, COD, BOD, Oil and Grease by BKC Adsorbent

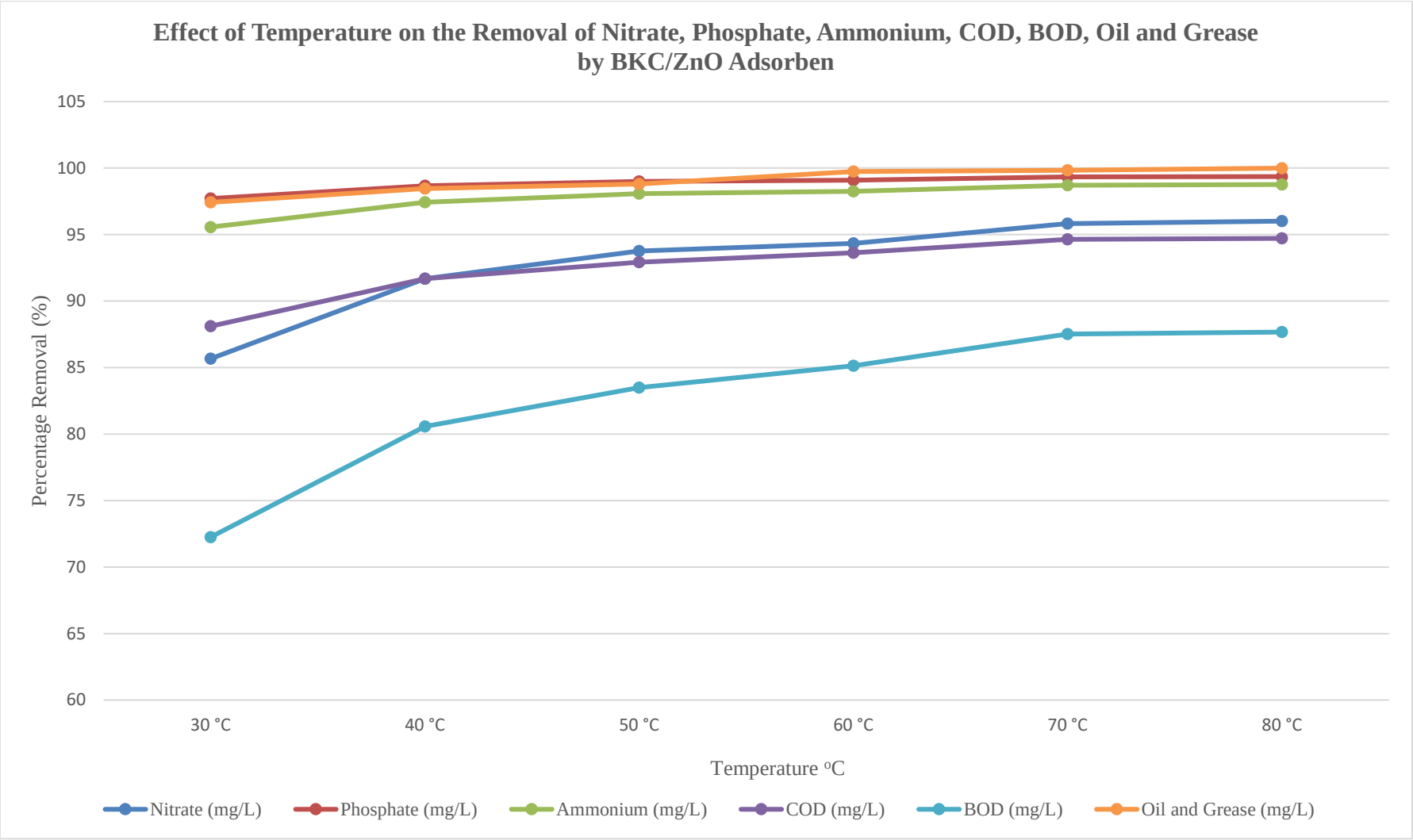

Figure 4.21 (b): Effect of Temperature on the Removal of Nitrate, Phosphate, Ammonium, COD, BOD, Oil and Grease by BKC/ZnO Adsorbent

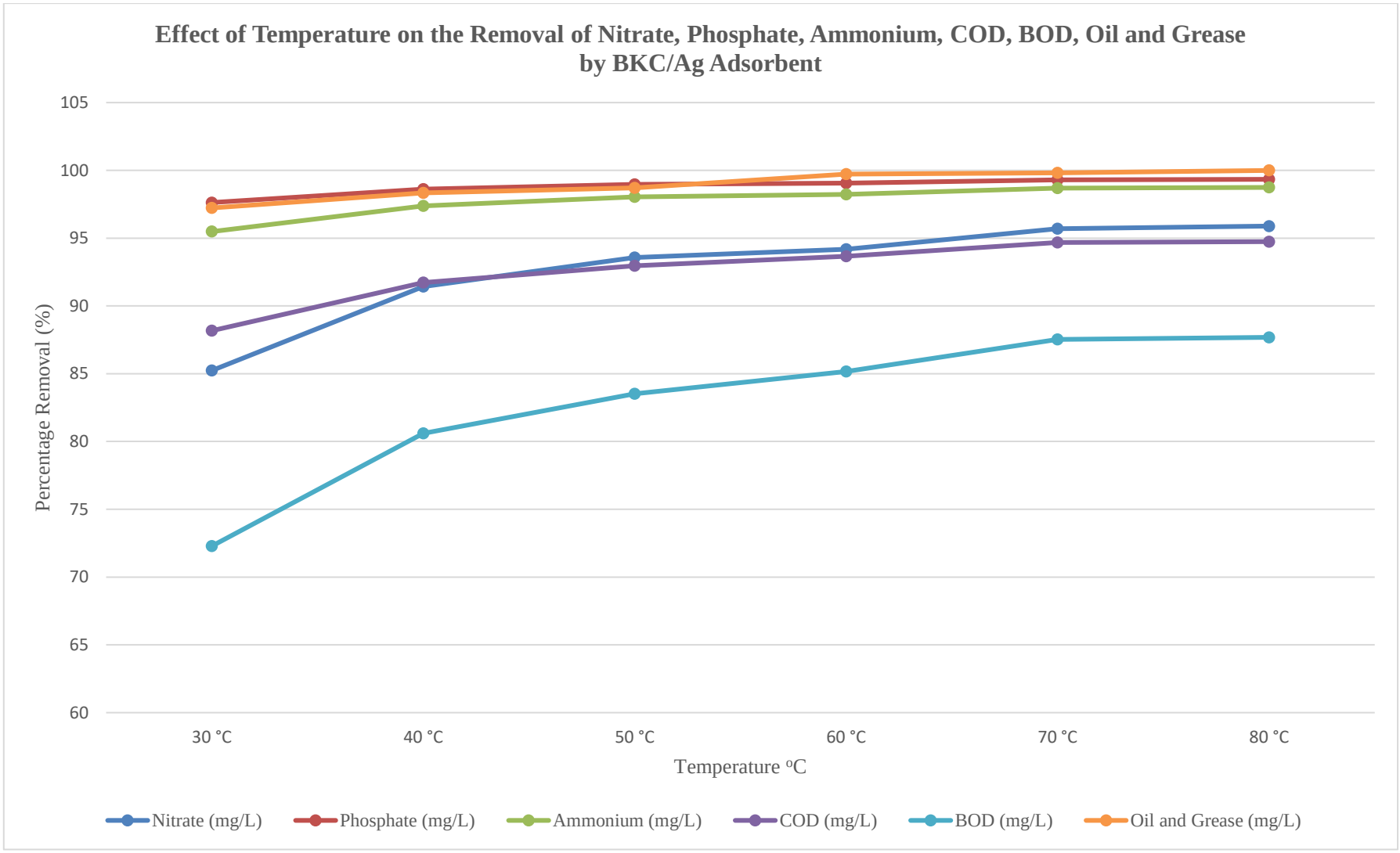

Figure 4.21 (c): Effect of Temperature on the Removal of Nitrate, Phosphate, Ammonium, COD, BOD, Oil and Grease by BKC/Ag Adsorbent

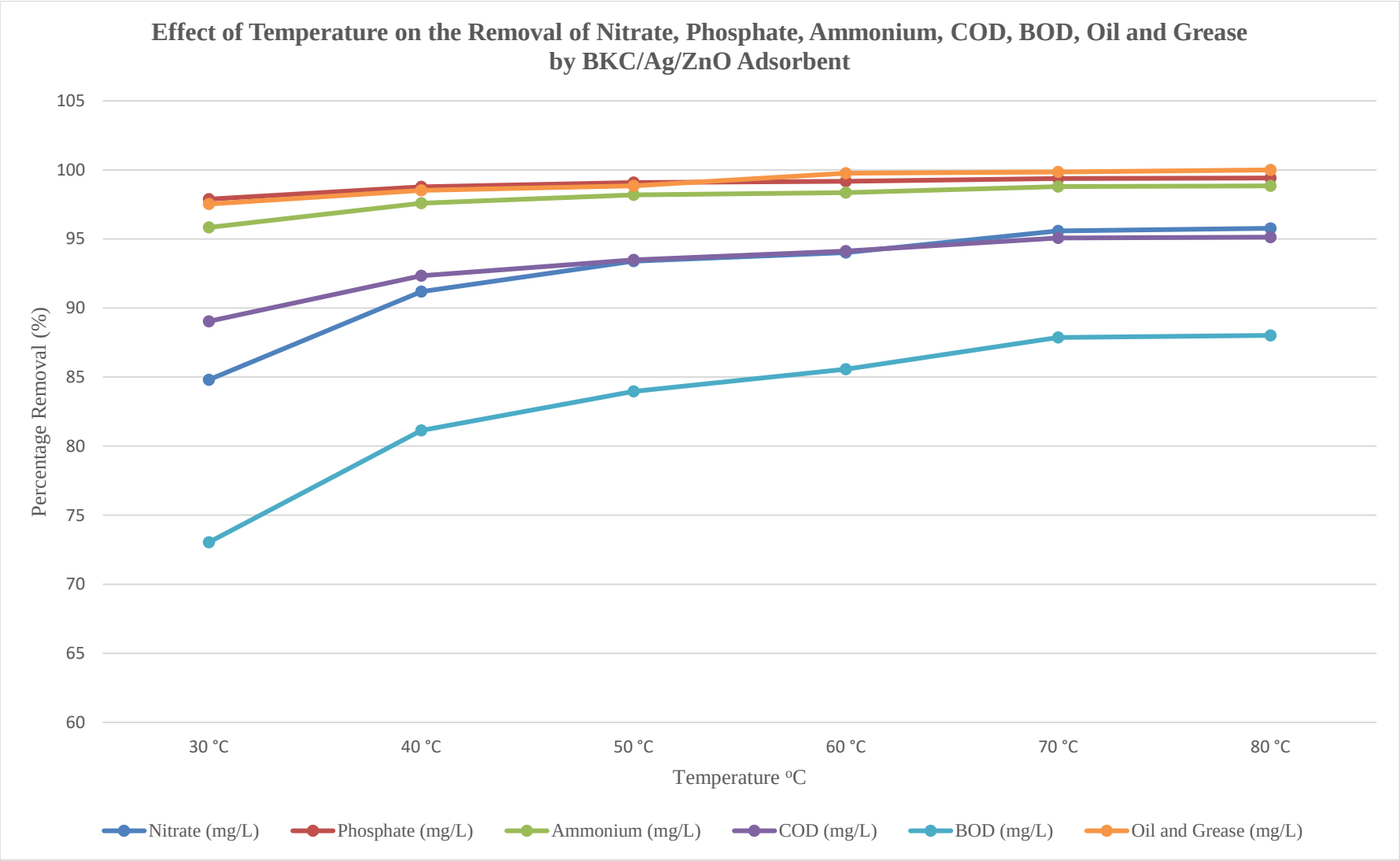

Figure 4.21 (d): Effect of Temperature on the Removal of Nitrate, Phosphate, Ammonium, COD, BOD, Oil and Grease by BKC/Ag/ZnO Adsorbent

4.12.3 Effect of temperature on physical parameters

The effects of temperatures on the removal of turbidity, suspended solids, colour, EC and improvement of pH and dissolved oxygen of the domestic wastewater during treatment was studied at temperature of 30, 40, 50, 60, 70 and 80 °C using an adsorbent dosage of 25 g/100 ml of wastewater and pH of 6.9. The concentrations and percentage removal efficiencies for turbidity, suspended solids, colour, EC and improvement of pH and dissolved oxygen by the BKC, BKC/ZnO, BKC/Ag and BKC/Ag/ZnO nanocomposites adsorbents at different temperatures are presented in Figure 4.22 (a – e).

It was observed that the increase in temperature increased the removal of turbidity, suspended solids, colour and EC from the wastewater. This observed trend in terms of removal efficiencies was BKC/Ag/ZnO > BKC/Ag > BKC/ZnO > BKC and the behaviour pattern could be linked to the fact that temperature increases the rate of chemical reaction.

It was discovered that pH concentration was directly related to an increase in the water temperature as shown in Figure 4.22 (a). The pH increased from 7.55, 7.81, 6.77, and 6.97 at 40 ^{o}C to 8.42, 8.68, 7.64, and 7.84 at 80 °C for BKC adsorbent, BKC/ZnO, BKC/Ag and BKC/Ag/ZnO nanocomposite adsorbent respectively as presented in Figure 4.22 (a). The experiment showed that the concentration of dissolved oxygen was inversely related to an increase in water temperature. The dissolved oxygen reduced from 4.05, 4.11, 4.02, and 4.18 mg/L at 30 °C to 3.48, 3.53, 3.46 and 3.59 mg/L at 80 °C for BKC adsorbent, BKC/ZnO, BKC/Ag and BKC/ZnO/Ag nanocomposite adsorbents respectively as could be seen in the downward trends of the percentage removal presented in Figure 4.22 (b – e). The solubility of oxygen decreases as temperature increases.

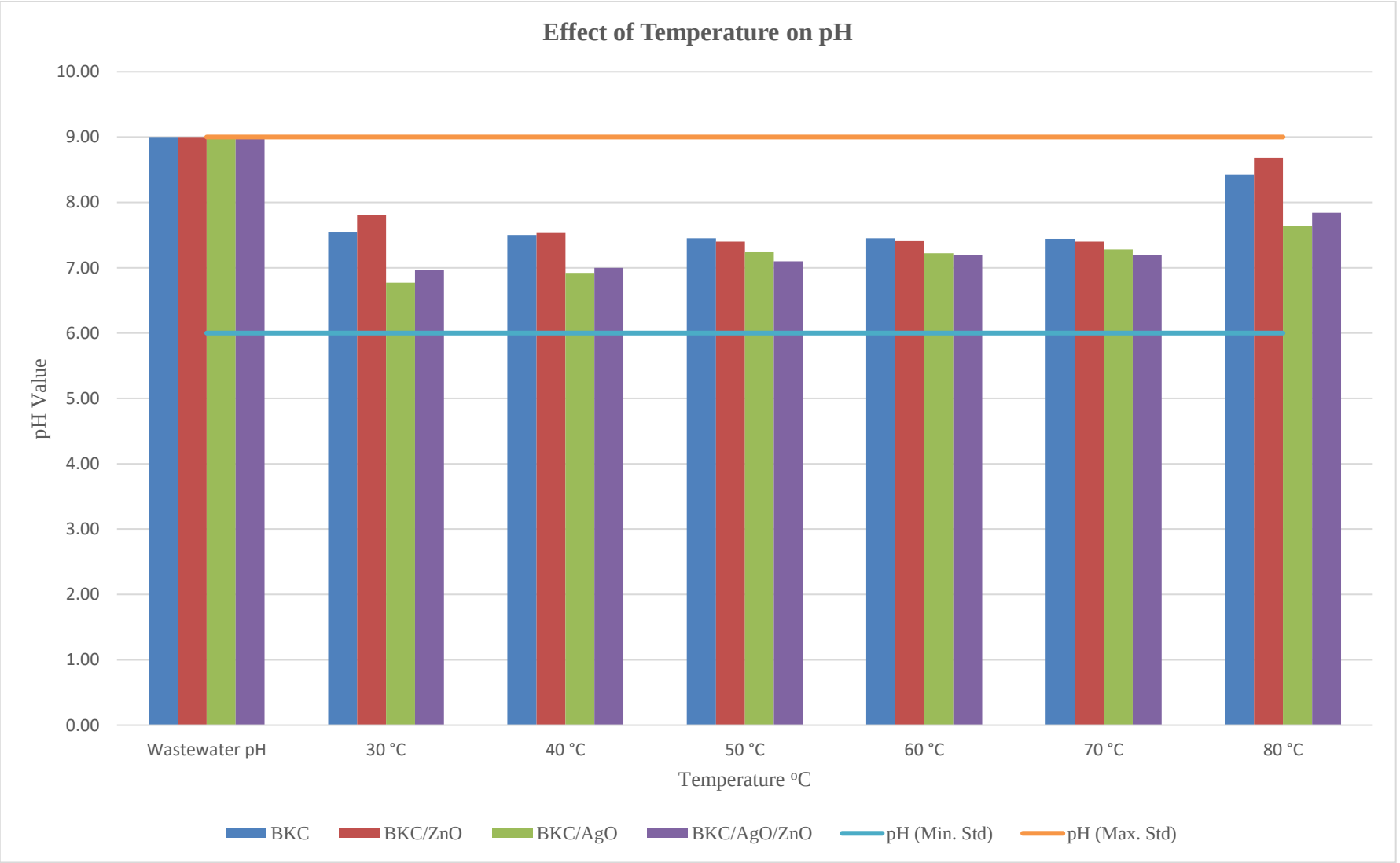

Figure 4.22 (a): Effect of Temperature on pH

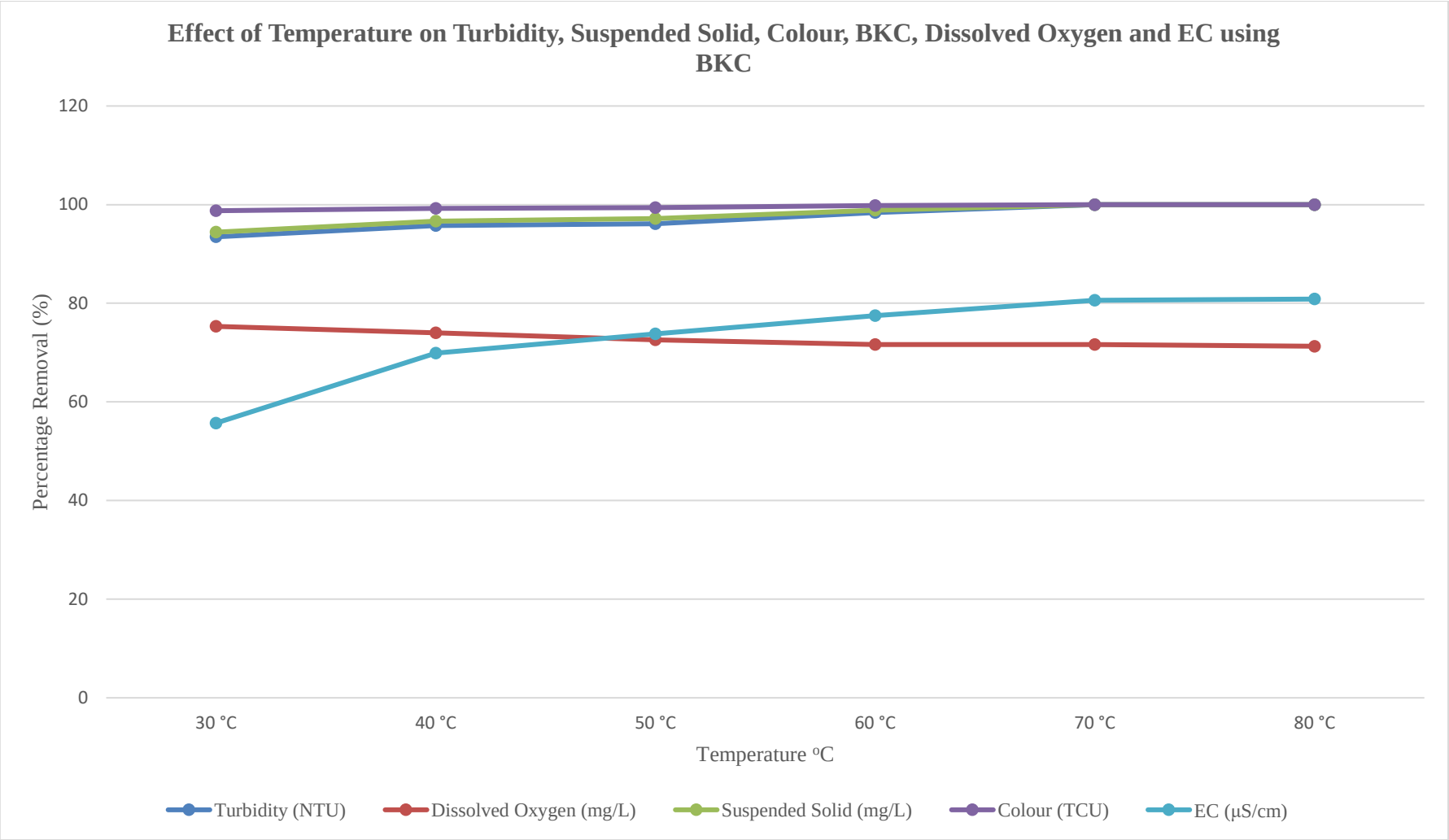

Figure 4.22 (b): Effect of Temperature on Turbidity, Suspended Solid, Colour, BKC, Dissolved Oxygen and EC using BKC Adsorbent

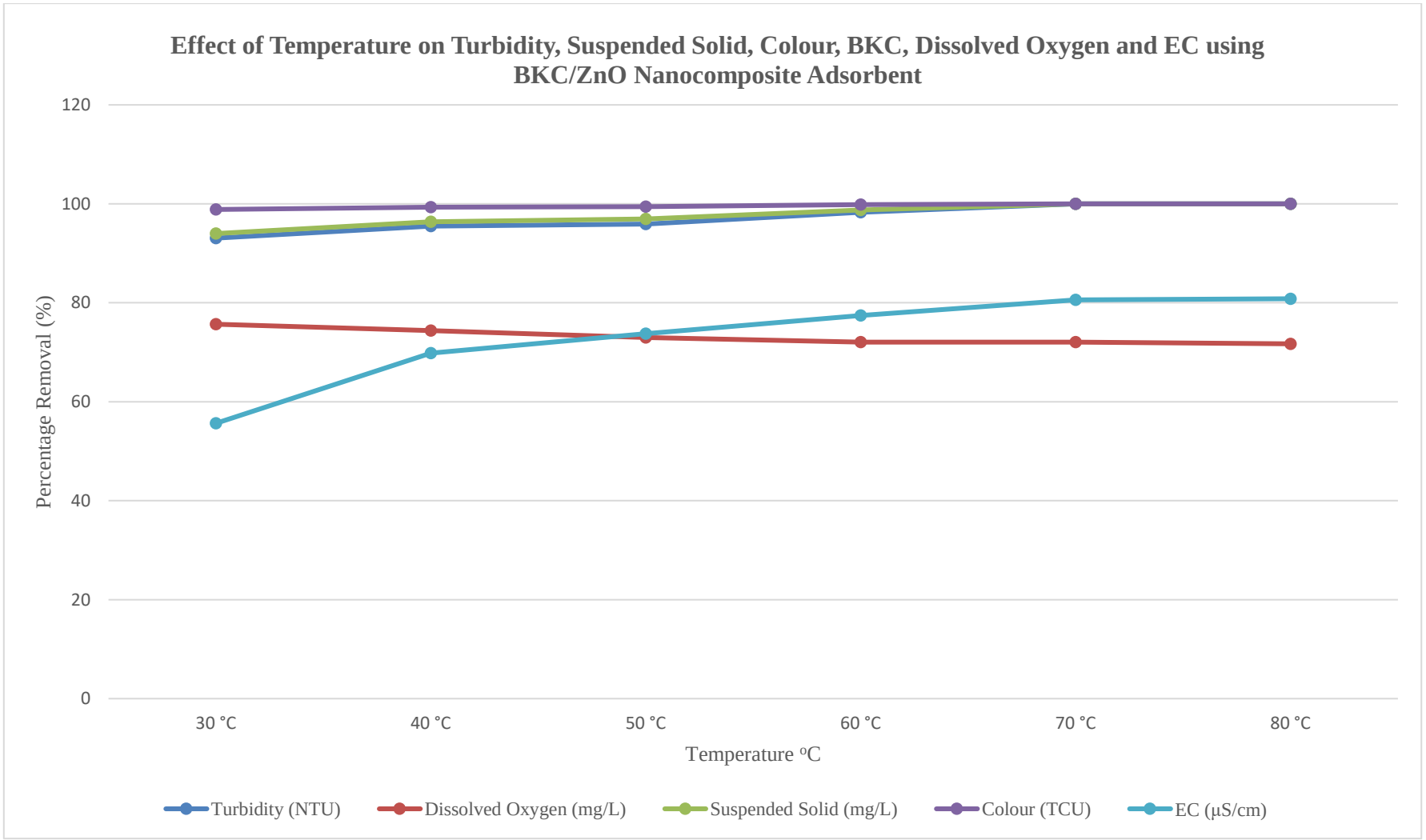

Figure 4.22 (c): Effect of Temperature on Turbidity, Suspended Solid, Colour, BKC, Dissolved Oxygen and EC using BKC/ZnO Nanocomposite Adsorbent

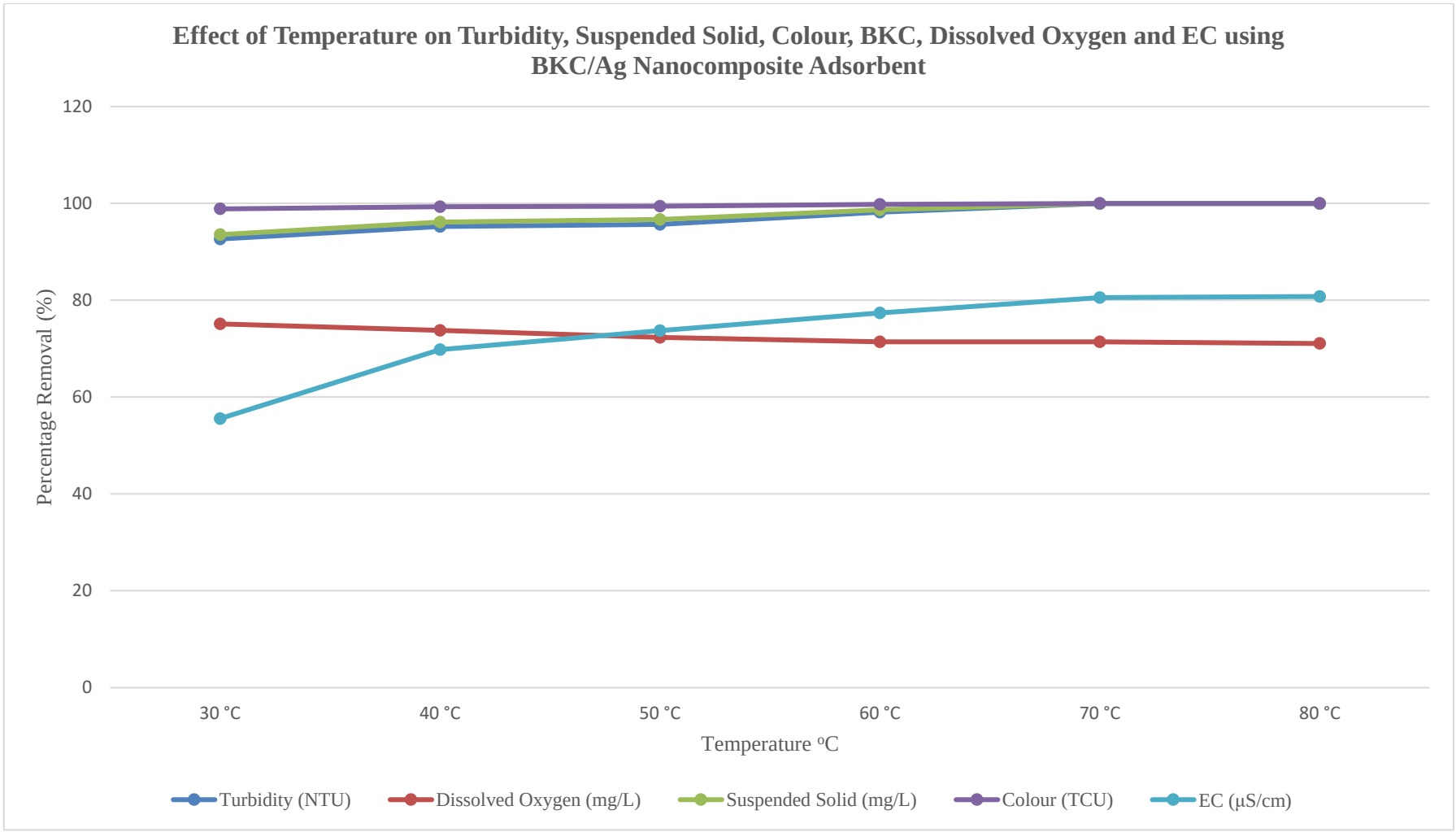

Figure 4.22 (d): Effect of Temperature on Turbidity, Suspended Solid, Colour, BKC, Dissolved Oxygen and EC using BKC/Ag Nanocomposite Adsorbent

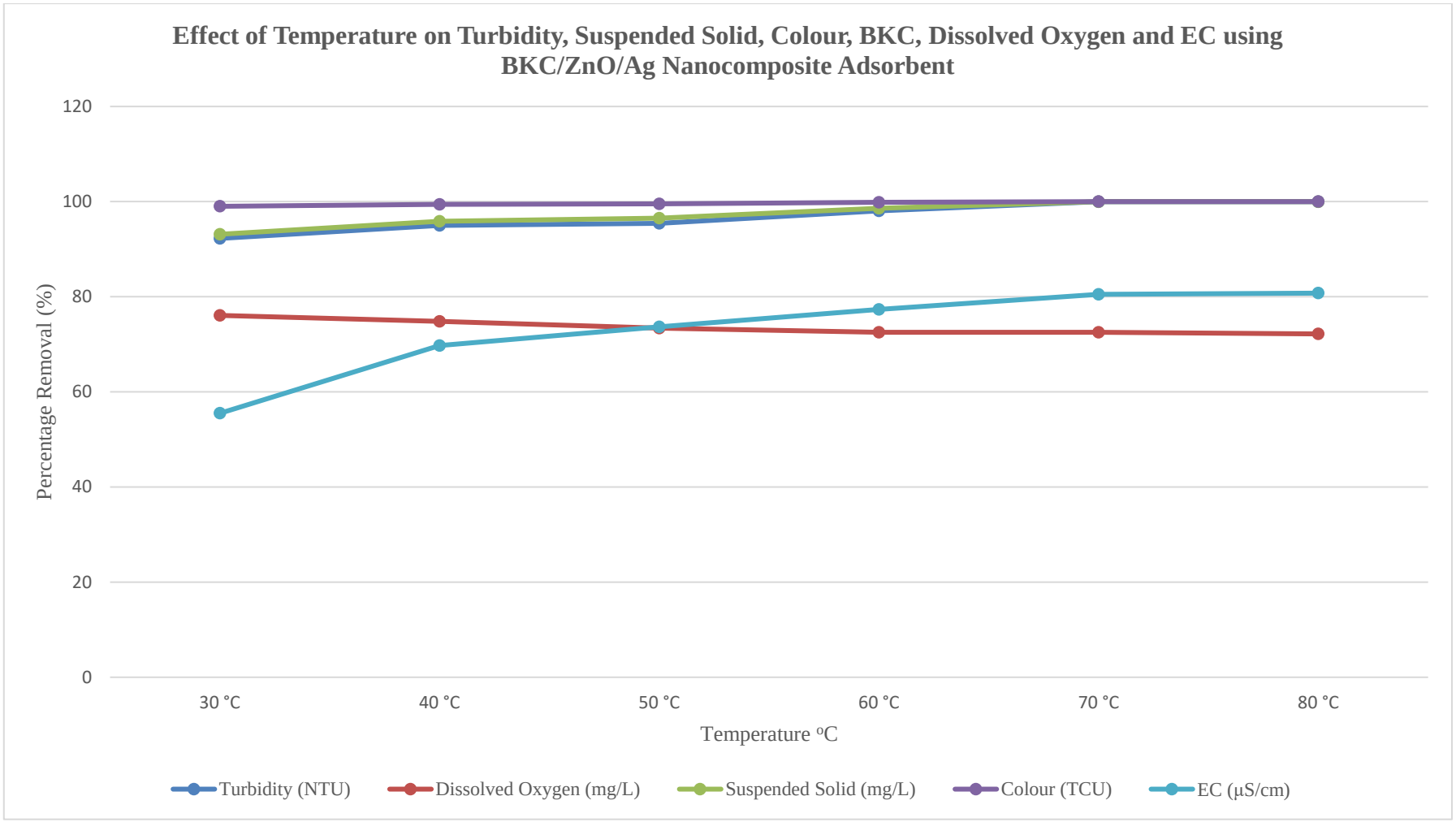

Figure 4.22 (e): Effect of Temperature on Turbidity, Suspended Solid, Colour, BKC, Dissolved Oxygen and EC using BKC/ZnO/Ag Nanocomposite Adsorbent

4.12.4 Effect of temperature on the removal of total coliforms, faecal coliforms, *Clostridium perfringens* and *E. coli*

The effects of temperatures on the removal of total coliforms, faecal coliforms, C*lostridium perfringens* and *E. coli* of the domestic wastewater was studied at a temperature of 30, 40, 50, 60, 70 and 80 °C using an adsorbent dosage of 25 g/100 mL of wastewater at a temperature of 29.5 °C and pH of 6.9. The effect of temperature on the percentage removal efficiencies of total coliforms, faecal coliforms, *Clostridium perfringens* and *E. coli* by the BKC, BKC/ZnO, BKC/Ag and BKC/Ag/ZnO nanocomposites adsorbents are presented in Figure 4.23 (a – d).

The observation revealed that an increase in the temperature to 50 °C upward resulted in the complete removal of total coliforms, faecal coliforms, *Clostridium perfringens* and *E. coli* for BKC, BKC/ZnO, BKC/Ag and BKC/Ag/ZnO nanocomposite adsorbents. For BKC/Ag and BKC/Ag/ZnO, the temperature increment to 40 °C resulted in the removal of all the microbial contaminants in the wastewater.

The complete removal of total coliforms, faecal coliforms, *Clostridium perfringens* and *E. coli* at 40 ^{o}C for BKC/Ag and BKC/Ag/ZnO nanocomposite adsorbents was strongly due to the antibacterial activity of silver nanoparticles as shown in Figure 23 (a - d), while the complete removal of total coliforms, faecal coliforms, *Clostridium perfringens* and *E. Coli* at 80 °C for BKC and BKC/ZnO nanocomposite was mainly due to increase in temperature.

The detailed results of temperature on the removal of contaminants by BKC, BKC/ZnO, BKC/Ag and BKC/Ag/ZnO nanocomposite adsorbents are presented in Appendix E.

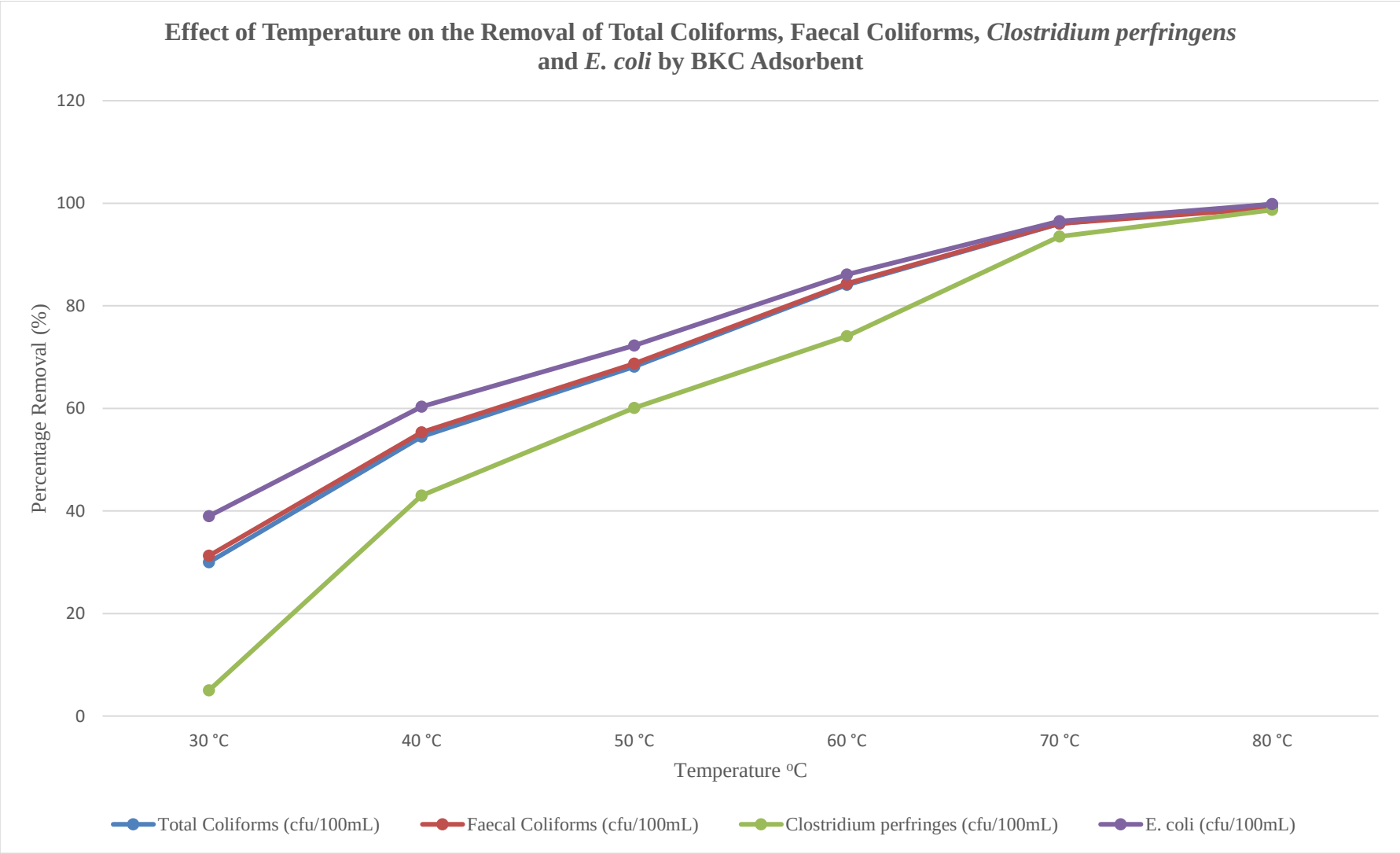

Figure 4.23 (a): Effect of Temperature on the Removal of Total Coliforms, Faecal Coliforms, *Clostridium perfringens* and *E. coli* by BKC Adsorbent

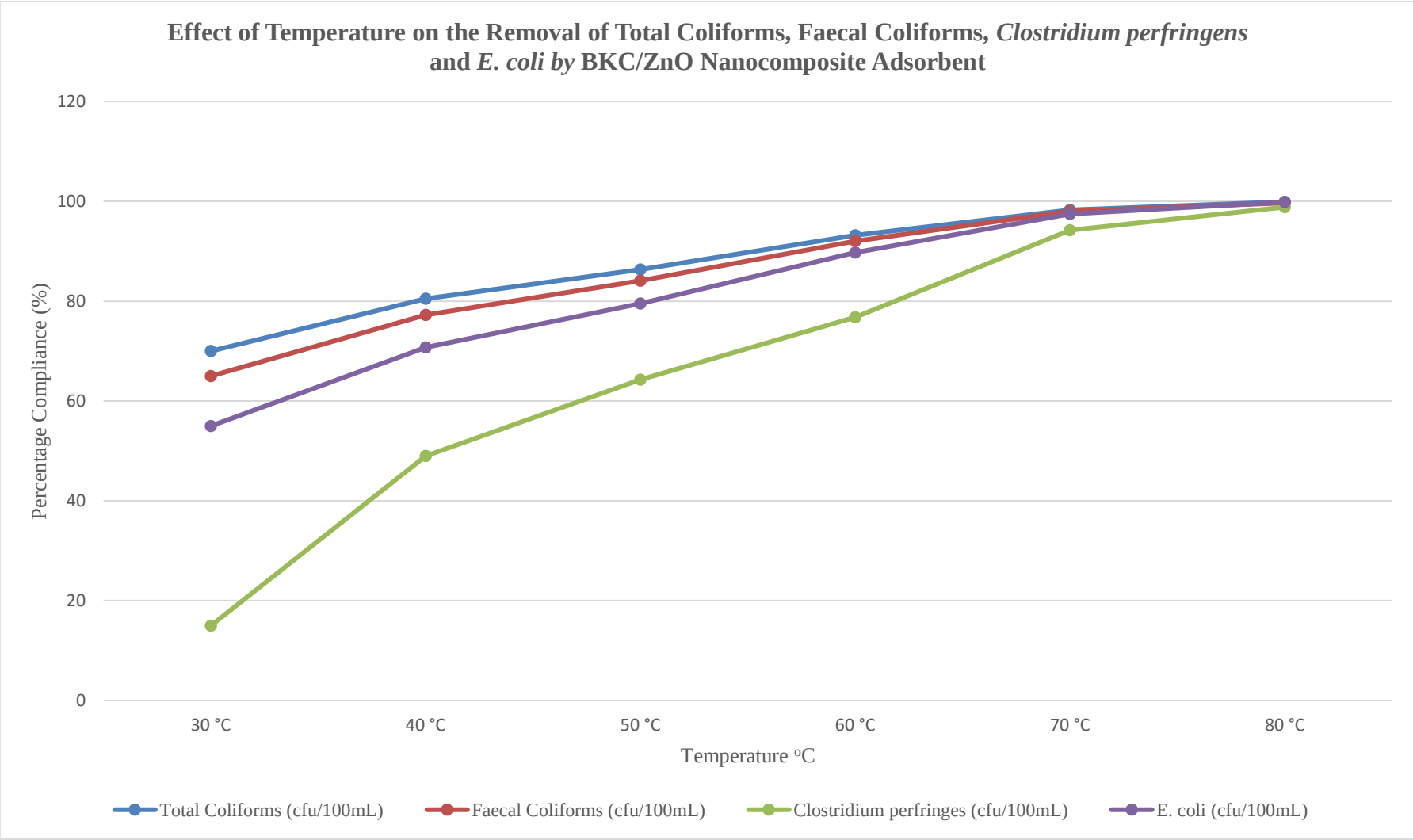

Figure 4.23 (b): Effect of Temperature on the Removal of Total Coliforms, Faecal Coliforms, *Clostridium perfringens* and *E. coli* by BKC/ZnO Nanocomposite Adsorbent

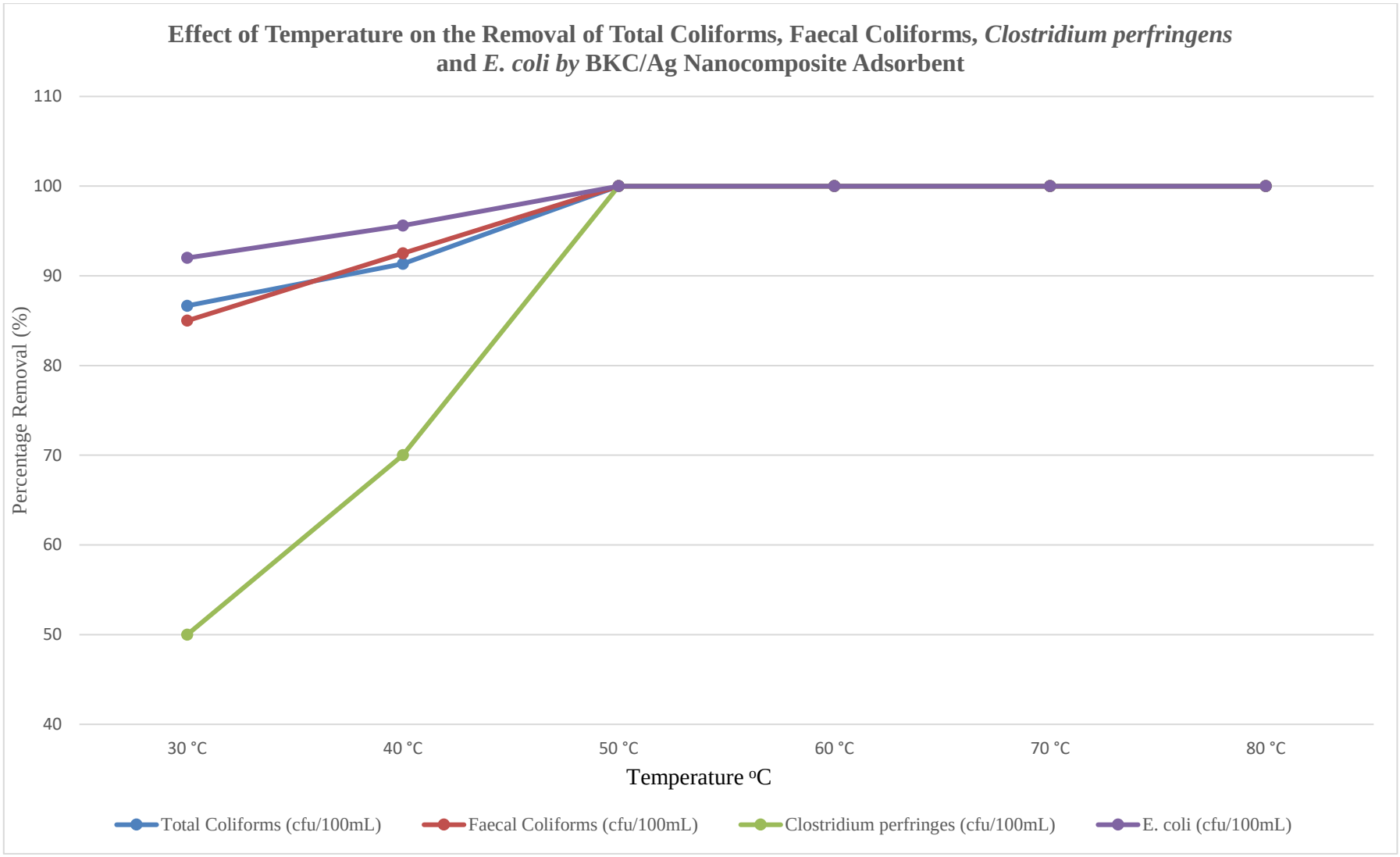

Figure 4.23 (c): Effect of Temperature on the Removal of Total Coliforms, Faecal Coliforms, *Clostridium perfringens* and *E. coli by* BKC/Ag Nanocomposite Adsorbent

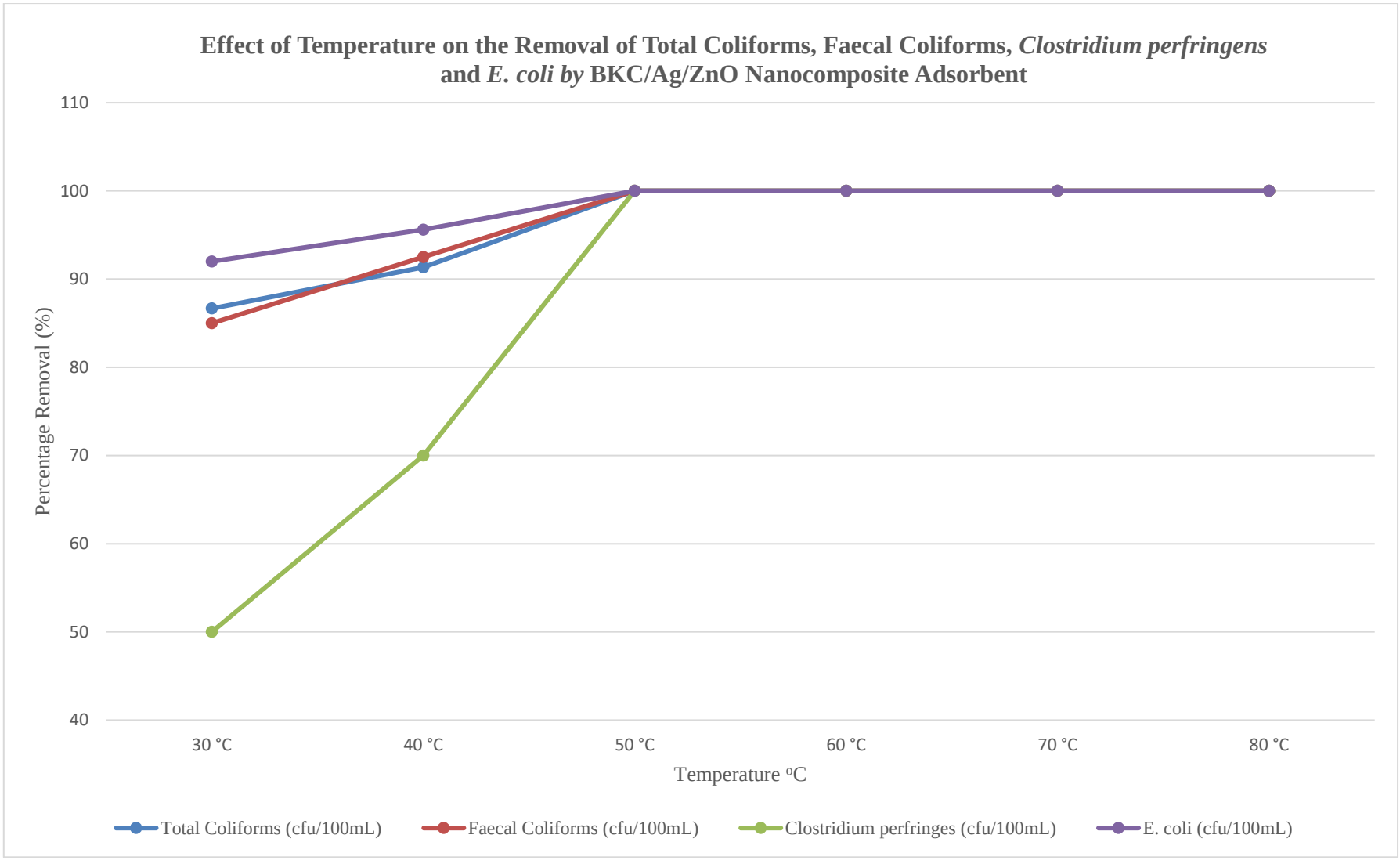

Figure 4.23 (d): Effect of Temperature on the Removal of Total Coliforms, Faecal Coliforms, *Clostridium perfringens* and *E. coli* by BKC/Ag/ZnO Nanocomposite Adsorbent

4.13 Average Percentage Reduction

In furtherance to the effect of time, dosage and temperature on the contaminants removal in the wastewater using the BKC, BKC/ZnO, BKC/Ag, and BKC/Ag/ZnO nanocomposite adsorbents as discussed above, the average percentage reduction level of total iron, lead, copper, manganese, arsenic, mercury silver, zinc, nitrate, phosphate, ammonium, COD, BOD, oil, and grease in the domestic wastewater after treatment with the produced nanocomposite adsorbents, is tabulated in Table 4.33.

Table 4.33: Average Percentage Reduction Level of the Nanocomposite Adsorbents

FILTER POT	EFFECT OF TIME	EFFECT OF DOSAGE	EFFECT OF TEMPERATURE	AVERAGE % REDUCTION
BKC	76.5	57.0	67.9	67.1
BKC/ZnO	76.7	59.1	74.0	69.9
BKC/Ag	76.7	60.4	73.9	70.3
BKC/Ag/ZnO	78.2	62.6	75.3	72.0

The results showed that kaolin clay, mixed with silver oxide nanoparticles, zinc oxide nanoparticles, (BKC/Ag/ZnO), and rice husks as burnout material, produces the best nanocomposite adsorbents. The results established that the BKC/Ag/ZnO nanocomposite adsorbents earlier produced can reduce the contaminant concentrations of total iron, lead, copper, manganese, arsenic, mercury silver, zinc, nitrate, phosphate, ammonium, COD, BOD, oil and grease in the domestic wastewater by an average of 72 % reduction level as shown in Table 4.33.

The produced BKC/Ag/ZnO nanocomposite adsorbent removed 100 % of the total coliforms, faecal coliforms, *Clostridium perfringens, E. coli*, turbidity, suspended solids, and colour in domestic wastewater between 30 – 60 minutes contact time, 15 – 30 g dosage, and 50 – 80 °C temperature.

The BKC/Ag/ZnO nanocomposite adsorbent possessed the adsorption pore size of 16.9233 nm that fell in the mesopore width and was classified as type IV isotherm when compared with the IUPAC pore size classification. Therefore, the produced BKC/Ag/ZnO nanocomposite adsorbent is best for filter pot production that will be suitable for domestic wastewater treatment.

4.14 Adsorption Experiment

Adsorption experiment for the removal of iron, lead, copper, manganese, arsenic, mercury silver, zinc nitrate, phosphate, ammonium, COD and BOD in wastewater when treated with BKC adsorbent, BKC/ZnO, BKC/Ag, BKC/Ag/ZnO nanocomposite adsorbents was performed using both Langmuir and Freundlich isotherms models and the result is presented and discussed under this section.

4.14.1 Langmuir adsorption isotherm

Appendix F showed the Langmuir model isotherm for the determination of Q_o and b. From the slopes and intercepts of the plots of $\frac{Ce}{q_e}$ versus Ce for the removal of iron, lead, copper, manganese, arsenic, mercury silver, zinc nitrate, phosphate, ammonium, COD and BOD in wastewater, the model showed the multilayer adsorption patterns and the fitting to the heterosporous nature of BKC, BKC/ZnO, BKC/Ag and BKC/Ag/ZnO nanocomposite adsorbents.

It was evident that the linear correlation coefficients (R^2) for BKC, BKC/ZnO, BKC/Ag and BKC/Ag/ZnO nanocomposite adsorbents in the removal of total iron, lead, copper, manganese, arsenic, mercury silver, zinc nitrate, phosphate, ammonium, COD and BOD were all greater than 0.90 (Appendix F). This showed that the experimental data moderately fit Langmuir adsorption isotherm.

The calculated R_L values for total iron, lead, copper, manganese, arsenic, mercury silver, zinc nitrate, phosphate, ammonium, COD and BOD indicated the favourability of the adsorption process and type of the isotherm which is $R_L < 1$ as shown in Appendix F.

The Langmuir isotherms display a linear relationship between Ce and $\frac{Ce}{q_e}$ for all the tested parameters when treated with BKC adsorbent, BKC/ZnO, BKC/Ag and BKC/Ag/ZnO nanocomposite adsorbents. The slopes and R^2 are present in Appendix F. The plot exhibits linearity and a good correlation coefficient. The values of R^2 were very close to the unit, showing a strong agreement with the Langmuir isotherm. The results displayed that the correlation coefficients, which were obtained by the Langmuir Equation arranged as follows: BKC/Ag/ZnO > BKC/Ag >BKC/ZnO > BKC. The value of the Langmuir constant for adsorbent BKC/Ag/ZnO was found to be considerably higher than those obtained by adsorbents BKC/ZnO, BKC/Ag and BKC. The results show that all adsorbents agreed with the Langmuir model and that the best linear relationship obtained was for the adsorbent BKC/Ag/ZnO.

4.14.2 Freundlich adsorption isotherm

Appendix G showed the Freundlich model isotherm values of K_f and n obtained from the intercept and slope of a plot of adsorption capacity (q_e) against equilibrium concentration (C_e). Both parameters K_f and n affect the adsorption isotherm. The larger the K_f and n values, the higher the adsorption capacity. From the plot of adsorption capacity (q_e) against equilibrium concentration (C_e) for the removal of iron, lead, copper, manganese, arsenic, mercury silver, zinc nitrate, phosphate, ammonium, COD and BOD in wastewater, the model showed the multilayer adsorption patterns and the fitting to the heterosporous nature of BKC, BKC/ZnO, BKC/Ag and BKC/Ag/ZnO nanocomposite adsorbents. It was evident that the linear correlation coefficients (R^2) for BKC,

BKC/ZnO, BKC/Ag and BKC/Ag/ZnO nanocomposite adsorbents in the removal of total iron, lead, copper, manganese, arsenic, mercury silver, zinc nitrate, phosphate, ammonium, COD and BOD were all greater than 0.90. This showed that the experimental data moderately fit Freundlich adsorption isotherm.

The larger the K_f and n values, the higher the adsorption capacity. Furthermore, the magnitude of the exponent n indicated the favourability of the adsorption process. When the value of n is greater than unity (1< n < 10), the adsorption process is favourable. The calculated n values for total iron, lead, copper, manganese, arsenic, mercury silver, zinc nitrate, phosphate, ammonium, COD and BOD gave an indication of the favourability of the adsorption process as shown in Appendix G.

The slopes and R^2 are present in Appendix G. The plot exhibits linearity and a good correlation coefficient. The values of R^2 were very close to the unit, showing a strong agreement with the Freundlich isotherm. The results displayed that the correlation coefficients, which were obtained by the Freundlich Equation arranged as follows: BKC/Ag/ZnO > BKC/Ag > BKC/ZnO > BKC. The value of the Freundlich constant for adsorbent BKC/Ag/ZnO was found to be considerably higher than those obtained by adsorbents BKC/ZnO, BKC/Ag and BKC. The results show that all adsorbents corresponded to the Freundlich model and that the best linear relationship obtained was for the adsorbent BKC/Ag/ZnO. In summary, the results show that the adsorption of metal follows Langmuir and Freundlich isotherm models.

4.15 **Thermodynamic studies**

The determination of the basic thermodynamic parameters: enthalpy of adsorption (ΔH), Gibb's free energy of adsorption (ΔG) and entropy of adsorption (ΔS) were done to assess

the spontaneity of the system and to ascertain the exothermic or endothermic nature of the treatment process and the results are presented and discussed under this section.

4.15.1 Enthalpy (ΔH), Gibb's free energy and entropy of adsorption

The values of enthalpy change (ΔH^o) and entropy change (ΔS^o) for the removal of iron, lead, copper, manganese, arsenic, mercury silver, zinc nitrate, phosphate, ammonium, COD and BOD in wastewater when treated with BKC adsorbent, BKC/ZnO, BKC/Ag, BKC/Ag/ZnO nanocomposite adsorbents as presented in Appendix H were obtained from the slope and intercept of $\ln K_d$ versus 1/T plots. The values of ΔH° and ΔS° were found to be positive. The positive values of ΔH° showed that the adsorption processes of BKC, BKC/ZnO, BKC/Ag and BKC/Ag/ZnO nanocomposite adsorbents were endothermic. The negative values of ΔG^o indicated the adsorption of the tested parameters is spontaneous and exothermic over the study range of temperatures (Abbas *et al.,* 2020).

The results of enthalpy of adsorption (ΔH), Gibb's free energy of adsorption (ΔG) and entropy of adsorption (ΔS) were done to assess the spontaneity of the system and to ascertain the exothermic or endothermic nature of the treatment process were presented in Appendix H.

The Gibbs free energy is reduced with an increase in temperature, which indicates a driving force that leads to higher adsorption capacity. At elevated temperatures, the adsorption process increased because of the increase in randomness and non-spontaneity of the process. The thermodynamic study on the removal of total iron, cadmium, lead, copper, manganese, arsenic, mercury silver, zinc nitrate, phosphate, ammonium, COD and BOD pollutants suggested chemical adsorption due to strong interface where the sorbates adhered on the surfaces of the adsorbents through strong forces forming chemical bonds.

4.16 Antimicrobial Activities of Nanocomposite Adsorbents

Antimicrobial prowess of BKC adsorbent, BKC/ZnO, BKC/Ag, BKC/Ag/ZnO nanocomposite adsorbents for the removal of Total Coliforms, Faecal Coliforms, *Clostridium perfringens* and *E. coli* in wastewater were studied and the results discussed in this section.

4.16.1 Antimicrobial activities of BKC adsorbents BKC/Ag, BKC/ZnO and BKC/Ag/ZnO nanocomposite adsorbents

The microbial loads of the domestic wastewater are presented in Table 4.34.

Table 4.34: Microbial Analyses of Wastewater Before Treatment

Parameters	**Units**	**Wastewater**	**NESREA (2011)**
Total Coliforms (TC)	cfu/mL	6.45×10^3	5×10^3
E. coli	cfu/mL	400	Absent
Faecal Coliforms	cfu/mL	640	Absent
Clostridium Perfringens	cfu/mL	48	Absent

The microbial load in the domestic wastewater samples collected were far above the permissible limits set by the NESREA (2011). The total coliforms, faecal coliforms, *Clostridium perfringens* and *E. coli* were present in large quantity as presented in Table 4.34.

The antibacterial activities of BKC, BKC/ZnO, BKC/Ag and BKC/Ag/ZnO nanocomposite adsorbents against the total coliforms, faecal coliforms, *Clostridium perfringens* and *E. coli* in the domestic wastewater were observed at a contact time of 10, 20, 30, 40, 50 and 60 minutes using an adsorbent dosage of 25 g/100 mL of wastewater at a temperature of 29.5 °C and pH of 6.9. It was observed that bacteria inactivation increased at the constant adsorbent dosage of 25 g with an increase in contact time. Plate XVII (a – b) presented the laboratory results of the domestic wastewater on Petri dishes.

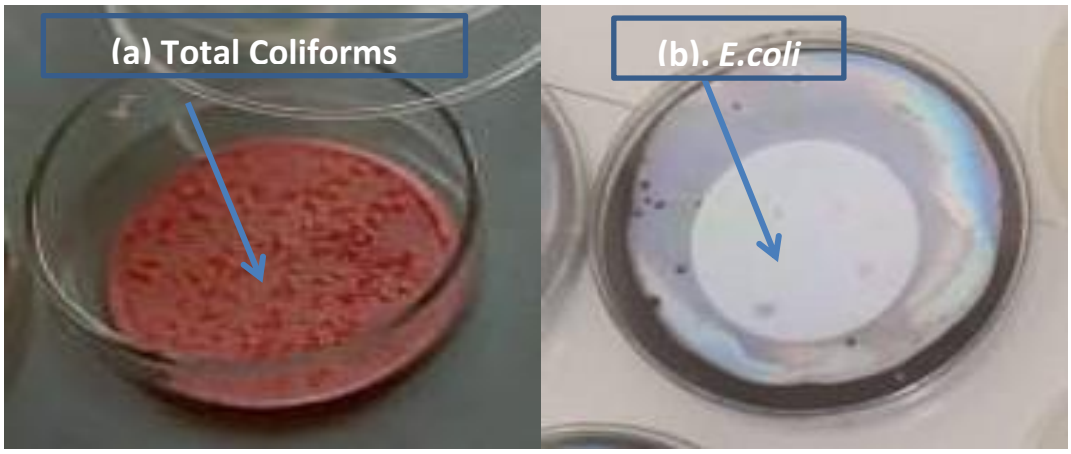

Plate XVII: Microbial Loads of the Domestic Wastewater

There was a complete removal of total coliforms, faecal coliforms, *Clostridium perfringens* and *E. coli* between 30 – 60 minutes contact time for BKC/Ag and BKC/Ag/ZnO nanocomposite adsorbents as presented in Table 4.35 and Plate XVIII (a – b). Anti-bactericidal effect of these two adsorbents could be attributed to the mechanical and chemical properties of the nanoparticles in addition to the large surface area of kaolin. Therefore, the BKC/Ag and BKC/Ag/ZnO nanocomposite adsorbents produced in this study were efficient in the treatment of wastewater against the test organisms.

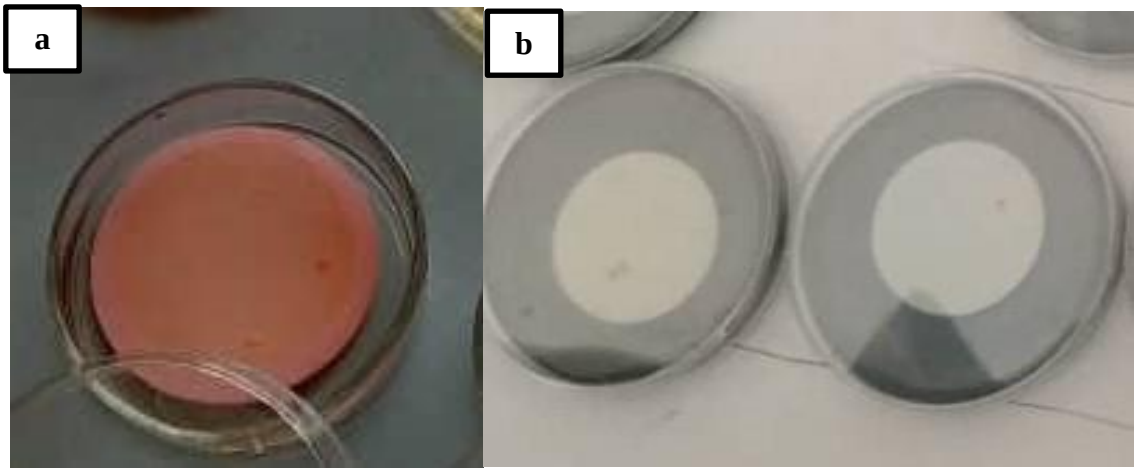

Plate XVIII: Anti-bactericidal of BKC/Ag and BKC/Ag/ZnO Nanocomposite Adsorbents

Table 4.35: Antimicrobial Study of BKC, BKC/ZnO, BKC/Ag and BKC/Ag/ZnO Nanocomposites Adsorbent

Microbial Parameters	Adsorbents	Wastewater Load	Anti-microbial Effects at Various Contact time						Percentage Removal (%) at various contact times					
			10 min	20 min	30 min	40 min	50 min	60 min	10 min	20 min	30 min	40 min	50 min	60 min
Total Coliforms (cfu/100ml)	BKC	6000	4200	2940	2646	2381	2143	1929	30.0	51.0	55.9	60.3	64.3	67.9
	BKC/ZnO	6000	1800	1260	1134	1021	919	827	70.0	79.0	81.1	83.0	84.7	86.2
	BKC/Ag	6000	800	560	0	0	0	0	86.7	90.7	100.0	100.0	100.0	100.0
	BKC/Ag/ZnO	6450	680	476	0	0	0	0	89.5	92.6	100.0	100.0	100.0	100.0
Faecal Coliforms (cfu/100ml)	BKC	640	440	308	277	249	225	202	31.3	51.9	56.7	61.0	64.9	68.4
	BKC/ZnO	640	224	157	141	127	114	103	65.0	75.5	78.0	80.2	82.1	83.9
	BKC/Ag	640	96	67	0	0	0	0	85.0	89.5	100.0	100.0	100.0	100.0
	BKC/Ag/ZnO	640	80	56	0	0	0	0	87.5	91.3	100.0	100.0	100.0	100.0
Clostridium Perfringens (cfu/100ml)	BKC	40	38	27	24	22	19	17	5.0	33.5	40.2	46.1	51.5	56.4
	BKC/ZnO	40	34	24	21	19	17	16	15.0	40.5	46.5	51.8	56.6	61.0
	BKC/Ag	40	20	14	0	0	0	0	50.0	65.0	100.0	100.0	100.0	100.0
	BKC/Ag/ZnO	40	16	11	0	0	0	0	60.0	72.0	100.0	100.0	100.0	100.0
***E. coli* (cfu/100ml)**	BKC	400	244	171	154	138	125	112	39.0	57.3	61.6	65.4	68.9	72.0
	BKC/ZnO	400	180	126	113	102	92	83	55.0	68.5	71.7	74.5	77.0	79.3
	BKC/Ag	400	32	22	0	0	0	0	92.0	94.4	100.0	100.0	100.0	100.0
	BKC/Ag/ZnO	400	24	17	0	0	0	0	94.0	95.8	100.0	100.0	100.0	100.0

4.17 Batch Treatment Comparative Analyses Studies

The filtrates obtained when the domestic wastewater was treated with the BKC, BKC/ZnO, BKC/Ag and BKC/Ag/ZnO nanocomposite adsorbents were subjected to comprehensive water quality testing and results of the analyses are presented in Appendix I.

The BKC, BKC/ZnO, BKC/Ag and BKC/Ag/ZnO nanocomposite adsorbents reduced the wastewater contaminants to the level it could no longer be harmful to the receiving water body when the water quality result was compared with the NESREA, 2011 effluent discharges, irrigation and reuse standard. BKC/Ag and BKC/Ag/ZnO removed 100 % of the microbial contaminants at 30 minutes of contact time.

The receiving waterbody for the domestic wastewater used in this study is River Kaduna. A water sample was collected from Shiroro Hydropower Dam on River Kaduna to serve as a control to confirm the effectiveness of the produced BKC, BKC/ZnO, BKC/Ag and BKC/Ag/ZnO nanocomposite adsorbents as water treatment methods to improve freshwater quality.

The microbial results of the domestic wastewater treated with BKC/Ag and BKC/Ag/ZnO nanocomposite adsorbents were better than that of dam water quality. These results presented a strong indication that treating the domestic wastewater with the produced BKC/Ag and BKC/Ag/ZnO nanocomposite adsorbents improved freshwater quality as well as fauna and flora of the ecosystem.

The batch adsorption study of this research produced an encouraging result in domestic wastewater treatment with the following order: BKC/Ag/ZnO > BKC/Ag > BKC/ZnO > BKC.

4.18 Production of Filter Pots

4.18.1 Pre-filter Bucket

The coarse materials that could quickly block the filter pots and affect the life span were removed with a 5-micron pore size screener placed in the 2-litre capacity pre-filter bucket. The pre-filter bucket also served as a water screener, reservoir and aid for the removal of contaminants in the domestic wastewater by gravity.

4.18.2 Clay filter housing design

The clay filter housing is necessary to collect the filtrate from the clay filter pots. It is important to protect the produced filter pot from breakage and the filtrate from recontamination.

4.18.3 Moulding of clay filter pot

The clay filter pots (FP) produced were labelled – BKC-FP 1, BKC-FP 2, BKC/ZnO-FP 1, and BKC/ZnO-FP 2. BKC/Ag-FP1, BKC/Ag-2, BKC/Ag/ZnO-FP 1, BKC/Ag/ZnO-FP 2. The rice husks, BKC, Ag and ZnO nanoparticles were mixed in the right proportion as described previously in the methodology. The mixture was moulded into shapes by round metal clamps (Plate XIX) to produce the trial filter ceramics as shown in Plate XX. The moulding of trial clay filter ceramics was important to get the right firing temperature.

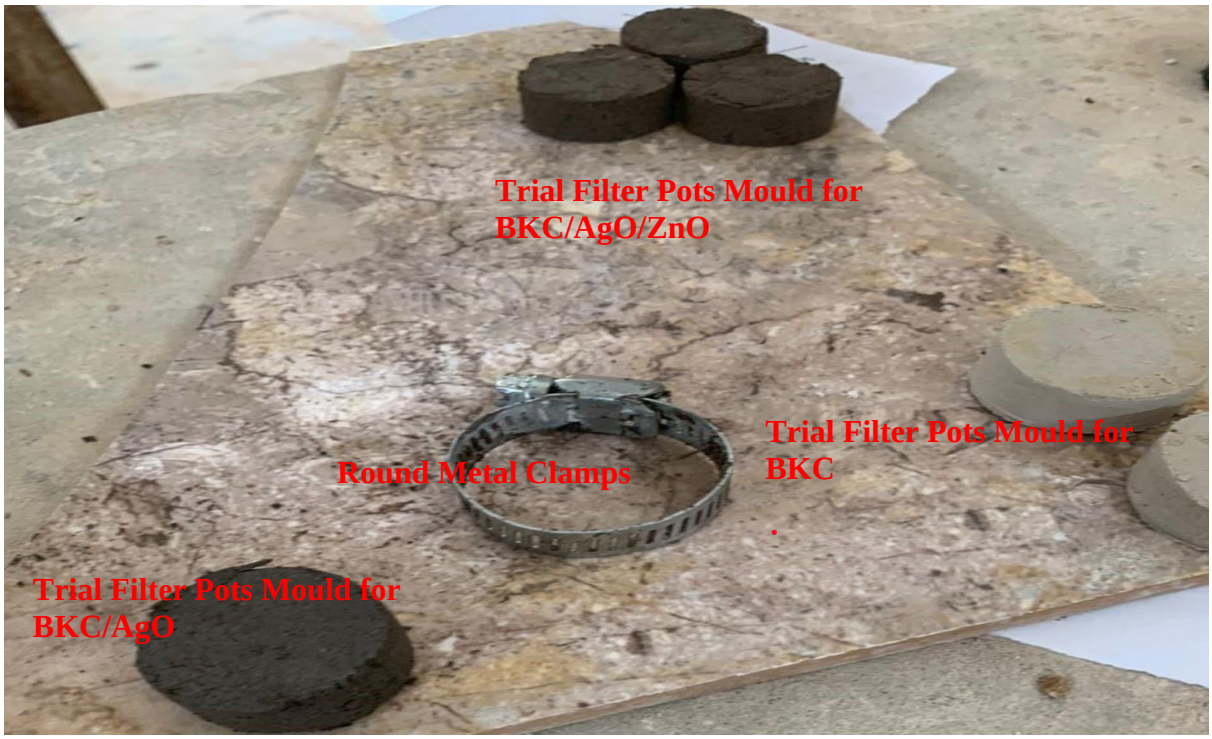

Plate XIX: Trial Clay Filter Ceramics Moulds

The produced trial filter ceramics are presented in Plate XIX.

Plate XX: Trial Filter Ceramics

The water absorption, porosity and shrinkage were performed on the produced trial clay filter before the production of the clay pots commenced. This was done to minimise errors and breaking of the clay pots.

After the fabrication of the trial filter ceramics, the clay pots were moulded and fired in a gas and electric kiln at 900 °C. The produced clay filter pots at different proportions of kaolin clay to rice husks blended with Ag and ZnO-NPs are presented in Plate XXI. Plate XXI (a) is the BKC/Ag/ZnO filter pot, Plate XXI (b) is the BKC/Ag filter pot, Plate XXI (c) is the BKC/ZnO filter pot while Plate XXI (d) is the BKC filter pot.

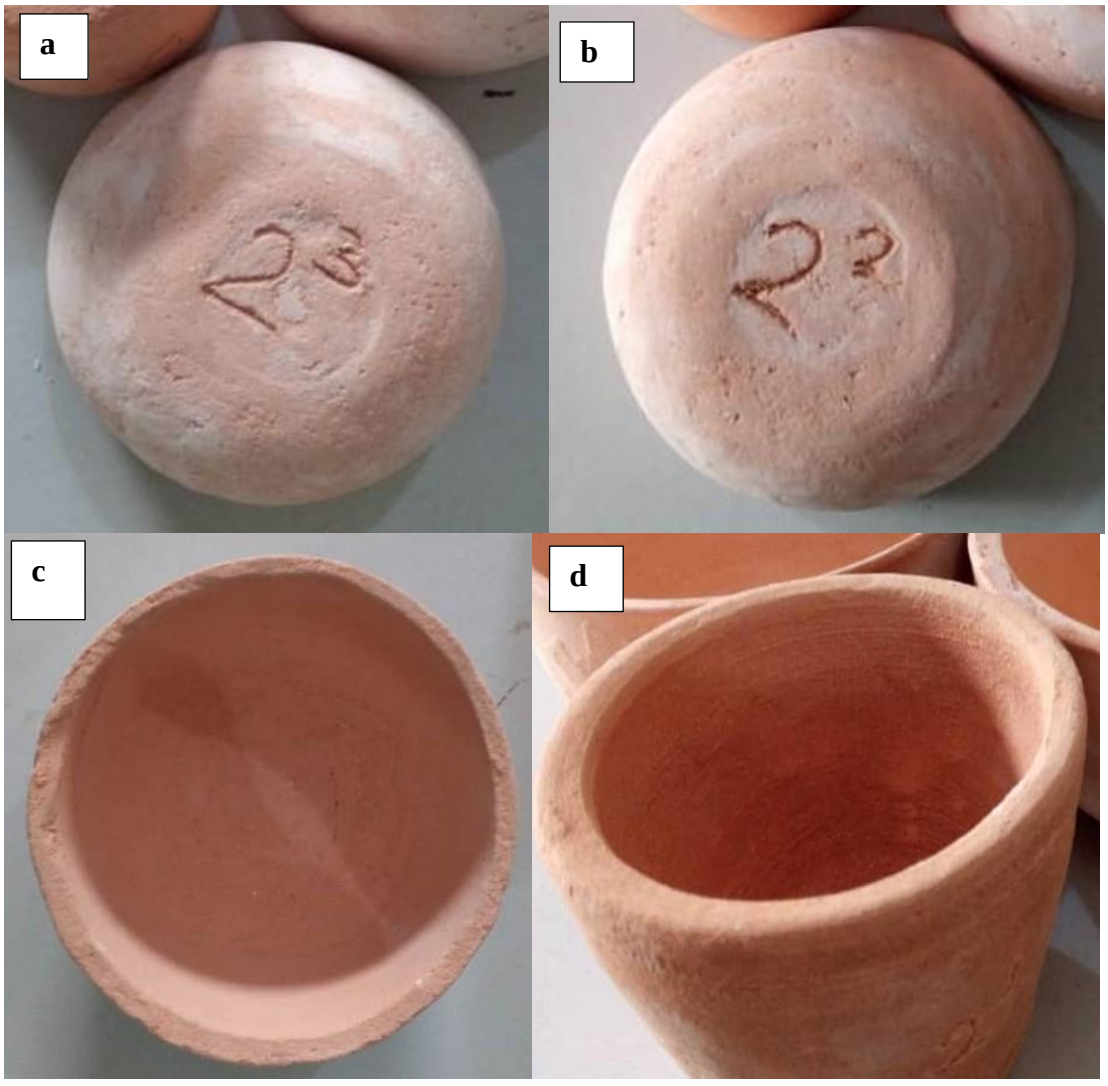

Plate XXI: (a). BKC/Ag/ZnO Filter Pot, (b). BKC/Ag Filter Pot, (c). BKC/ZnO Filter Pot and (d). BKC Filter Pot

4.18.4 Water absorption, porosity and shrinkage tests

The water absorption, porosity, shrinkage and flow rate tests were done on the clay pots. The results of the water absorption, porosity and shrinkage are presented in Table 4.36. Temperature and the ratios of beneficiated kaolin clay to rice husks are the principal factors governing the percentage porosity of the filter pots.

Table 4.36: Water Absorption, Porosity and Shrinkage Test

Sample	Shrinkage (%) Wet-dry (Length)	Shrinkage (%) wet-dry (Weight)	Shrinkage (%) dry-fired (Length)	Shrinkage (%) dry-fired (Weight)	Porosity (%)	Water absorption (%)
BKC-FP 1	12.0	26.4	1.00	20.0	27.8	19.5
BKC-FP 2	11.9	26.5	1.10	19.9	28.0	20.5
BKC/ZnO-FP 1	12.0	32.4	0.50	26.0	27.3	16.1
BKC/ZnO-FP 2	12.2	32.5	0.70	26.2	28.0	16.7
BKC/Ag-FP 1	12.0	31.0	4.50	26.0	6.96	3.95
BKC/Ag-FP 2	12.1	31.2	4.50	26.2	7.20	4.10
BKC/Ag/ZnO-FP1	12.0	34.3	1.00	23.4	9.00	5.00
BKC/Ag/ZnO-FP 2	12.0	34.3	1.00	23.4	9.40	5.20

The shrinkage after firing decreased and the porosity increased with an increase in the ratios of rice husk to beneficiated kaolin clay. At a higher ratio of beneficiated kaolin clay to rice husk, low porosity and shrinkage were observed. This was an indication that the application of temperature above 900 °C would compress the clay filter pots.

The low shrinkage implied that a high level of burn-out (rice husk) was present in the filter pots. The decrease in the shrinkage when the rice husk weight was reduced could be attributed to the closure of pores created by the burn-out. It was established in this study, that porosity is directly related to shrinkage.

The higher the weight of the burn-out in the formulation of the clay pots, the more the porosity of the clay body. The interstitial spaces in the clay filter pots after kilning were a result of the burning off of the carbonaceous materials at high temperatures.

The LOI of the filter pots produced at the refractoriness of 900 °C is 5.01 %. The 5.01 % LOI was attributed to the dihydroxylation reaction in the beneficiated kaolin mineral. The results obtained indicated that the clay filter pot did not rupture at 900 °C.

4.18.5 Chemical resistance behaviour of the filter pots

The resistance to acid-base corrosion performed on the clay filter pot showed significant weight loss on soaking in an acidic solution.

The clay filter pots exhibited slight weight loss in a weakly acidic solution. The poor acid corrosion resistance of the clay filter pots was a result of the dissolution of some elements from kaolin in an acidic medium. However, the clay filter pots produced did not give any significant weight loss in NaOH. This is because of the strong interaction between hydroxide ions and the clay.

4.18.6 Flow rates of the filter pots

The flow rate of the produced filter pots (FP) is presented in Table 4.37. The flow rate varied with an increase in the proportion of rice husks. The flow rate increased as the rice husk weight increased for all the produced filter pots. The rate of water discharge increased with the increase in the fraction of rice husks used as burn-out material in making the filter pots. However, the higher the time of filtration, the lower the volume of the filtrate from the clay pots. The low filtrate at a higher time of treatment was attributed to the blockage of the pores in the filter pots.

Table 4.37: Flow Rates of the produced Filter Pots

Clay Pots	Time (T1), Hour	Time (T2), Hour	Volume (V1), mL	Volume (V2), mL	Flow Rates (Q1), mL/hr	Flow Rates (Q2), mL/hr
BKC-FP 1	1.00	2.00	16.2	25.7	16.2	12.9
BKC-FF 2	1.00	2.00	21.5	35.4	21.5	17.7
BKC/ZnO-FP 1	1.00	2.00	14.6	24.0	14.6	12.0
BKC/ZnO-FP 2	1.00	2.00	20.9	33.8	20.9	16.9
BKC/Ag-FP 1	1.00	2.00	15.2	23.5	15.2	11.8
BKC/Ag-FP 2	1.00	2.00	20.4	32.6	20.4	16.3
BKC/Ag/ZnO-FP 1	1.00	2.00	15.4	24.2	15.4	12.1
BKC/Ag/ZnO -CP 2	1.00	2.00	20.5	32.9	20.5	16.5

At certain intervals of time, pores got clogged due to fine colloidal particles and decreased the efficiency of the filter bed. This was a major performance reduction and a great challenge associated with clay filter pot technology. However, this challenge of performance reduction was resolved by adopting a dirt removal system for the produced filter pots. The flow rate experiment is presented in Plate XXII.

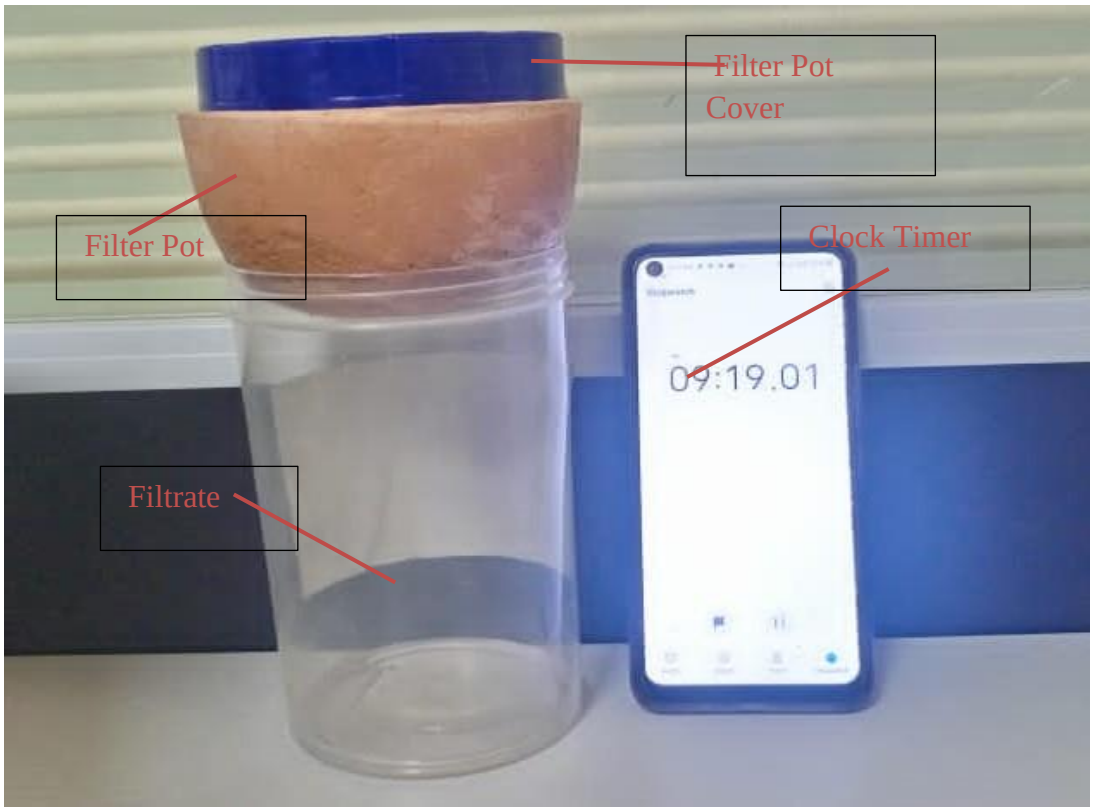

Plate XXII: Flow Rate Determination

4.18.7 Antibacterial activities of the produced kaolin clay filter pot

Antibacterial activities of the clay filter pots produced were tested for the removal of total coliforms, faecal coliforms, *Clostridium perfringens* and *E. coli* in the domestic wastewater. There was a complete removal of total coliforms, faecal coliforms, clostridium perfringens and *E. coli* by BKC/Ag and BKC/Ag/ZnO filter pots as presented in Table 4.38.

Table 4.38: Antimicrobial Activities of the Clay Filter Pots

Filter Pots	Total Coliforms (cfu/mL)	*E. coli*, cfu/mL	Faecal Coliforms, cfu/mL	*Clostridium perfringens*, cfu/mL
Wastewater	6.45×10^3	400	640	144
BKC-FP 1	800	10	36	6
BKC-FF 2	820	14	40	7
BKC/ZnO-FP 1	16	3	10	0
BKC/ZnO-FP 2	20	4	12	0
BKC/Ag-FP 1	0	0	0	0
BKC/Ag-FP 2	2	0	0	0
BKC/Ag/ZnO-FP 1	0	0	0	0
BKC/Ag/ZnO -FP 2	0	0	0	0

Anti-bactericidal effect of the produced filter pots could be attributed to the chemical properties of the nanoparticles in addition to the large surface area of kaolin. The antimicrobial effect of the Ag nanoparticles was more effective than ZnO nanoparticles. The order of potency in the antimicrobial activities of the produced filter pots is BKC/Ag/ZnO-FP > BKC/Ag-FP > BKC/ZnO-FP > BKC-FP. Anti-bactericidal effect of these produced filter pots could be attributed to the mechanical and chemical properties of the nanoparticles in addition to the large surface area of kaolin clay.

4.18.8 Adsorption study of the produced kaolin clay filter

The physico-chemical and bacteriological results obtained when the domestic wastewater was treated with the produced nanocomposite clay filter pots are presented in Table 4.39.

The reduction in the concentrations of each tested parameter was significant for all the produced filter pots.

Complete elimination of odour and turbidity were observed after treatment. The pH of the prepared filter pots was between 6.99 – 7.86. A great reduction in the conductivity, total dissolved solids, and total suspended solids was obtained. All the produced filter pots were effective in the treatment of nitrate, phosphates and ammonium. A reduction in the heavy metal contaminants was observed.

All the filtrates obtained BKC-FP 1, BKC-FP 2, BKC/ZnO-FP 1, BKC/ZnO-FP 2. BKC/Ag-FP1, BKC/Ag-2, BKC/Ag/ZnO-FP 1 and BKC/Ag/ZnO-FP 2 filter pots were analysed. The results were compared with the maximum permissible limits established for effluent discharge by NESREA, 2011. The lower the rice husks in the clay pots, the better the treatment and the slower the flow rates, across the filter pots produced.

The results in Table 4.39 have shown that kaolin clay, mixed with silver oxide nanoparticles, zinc oxide nanoparticles, (BKC/Ag/ZnO), and rice husks as burnout material, produces the best nanocomposite filter pot. The results established that the BKC/Ag/ZnO filter pot produced at a crystallize size of 26.934 nm from beneficiated kaolin clay of 75 % mixed with silver oxide of 0.5 %, zinc oxide nanoparticles of 1.0 % and rice husks of 23.5 % is the best nanocomposite filter pot. The produced BKC/Ag/ZnO filter pot possessed the adsorption pore size of 16.9233 nm that fell in the mesopore width and was classified as type IV isotherm when compared with the IUPAC pore size classification. Therefore, the produced filter pot is suitable for domestic wastewater treatment.

Table 4.39: Adsorption Study of the Kaolin Clay Filter Pots

Parameters	**Units**	**BKC-FP - 1**	**BKC-FP- 2**	**BKC/ ZnO – FP 1**	**BKC/ ZnO – FP 2**	**BKC/Ag – FP 1**	**BKC/Ag – FP 2**	**BKC/ Ag/ ZnO-FP 1**	**BKC/Ag/ ZnO-FP 2**	**Dam Water**	**NESREA, 2011**	Remarks
pH	8.96	7.20	7.25	7.05	7.10	6.98	6.98	7.15	6.99	7.86	6.5 -8.5	Good
Turbidity, NTU	248	0.00	0.00	0.00	0.00	0.00	0.00	0.00	0.00	15.0		Good
EC, µS/cm	1382	340	350	350	352	340	345	335	245	55.0		Good
TSS, mg/L	233	0.00	0.00	0.00	0.00	0.00	0.00	0.00	0.00	35.0		Good
TDS, mg/L	926	230	235	234	236	230	231	224	164	36.9		Good
Colour, NTU	1620	BDL	BDL	BDL	BDL	BDL	BDL	BDL	BDL	168		Good
Nitrate, mg/L	230	1.24	1.25	1.18	1.20	1.97	1.98	1.11	0.98	21.4	40	Good
Phosphates, mg/L	11.8	0.145	0.150	0.120	0.121	0.110	0.120	0.101	0.084	0.22	3.5	Good
Ammonium	37.2	0.472	0.470	0.360	0.360	0.350	0.358	0.375	0.150	20.2	2	Good
Chloride	133	6.84	6.88	6.44	6.50	6.46	6.49	6.48	4.66	4.61	350	Good
COD, mg/L	312	5.15	5.20	5.13	5.15	5.10	5.10	3.97	3.22	12.0	30	Good
BOD_5, mg/L	30.6	0.49	0.50	0.40	0.42	0.40	0.41	0.40	0.20	0.60	6	Good
Oil and Grease	10.1	0.00	0.00	0.00	0.00	0.00	0.00	0.00	0.00	0.00	0.1	Good
Total Iron, mg/L	0.83	0.05	0.05	0.03	0.04	0.04	0.05	0.03	0.02	0.10	0.5	Good
Lead, mg/L	0.14	0.003	0.003	0.02	0.02	0.02	0.02	0.002	0.000	BDL	0.1	Good
Copper, mg/L	0.05	0.004	0.004	0.003	0.003	0.0034	0.0035	0.003	0.000	BDL		Good
Manganese, mg/L	0.25	0.004	0.005	0.004	0.004	0.003	0.003	0.002	0.001	BDL		Good
Arsenic, mg/L	0.22	0.007	0.007	0.0072	0.0075	0.0069	0.0070	0.0042	0.0045	0.04	0.05	Good
Mercury, mg/L	0.11	0.009	0.009	0.0082	0.0085	0.0087	0.0088	0.0069	0.0065	0.09		Good
Silver, mg/L	0.02	0.000	0.000	0.000	0.000	0.000	0.000	0.000	0.000	BDL		Good
Zinc, mg/L	2.46	0.078	0.078	0.074	0.079	0.080	0.081	0.050	0.0445	BDL	0.2	Good

CHAPTER FIVE

5.0 CONCLUSION AND RECOMMENDATION

In this research, the kaolin clay, silver and zinc oxide nanocomposite filter were successfully developed for the treatment of domestic wastewater. This research established that the filter pot produced reduced the contaminant concentrations of total iron, lead, copper, manganese, arsenic, mercury silver, zinc, nitrate, phosphate, ammonium, COD, BOD, oil and grease in the domestic wastewater by an average of 72 % reduction level. The kaolin clay, silver and zinc oxide nanocomposite filter pot also removed 100 % of the total coliforms, faecal coliforms, *Clostridium perfringens, E. Coli*, turbidity, suspended solids, and colour in domestic wastewater at 30 – 60 minutes contact time, 15 – 30 g dosage, and 50 – 80 ^{o}C temperature.

5.1 Conclusion

Kaolin clay from a clay deposit in Kutigi, Niger State was beneficiated and characterised for its crystal structure and morphology using X-Ray Diffractometer (XRD), Dispersive X–Ray Fluorescence (XRF) Machine, High-Resolution Transmission Electron Microscope (HRTEM) and Brunauer – Emmett – Teller (BET) Nitrogen Absorption Analyser. Silver and zinc oxide nanoparticles were produced in a single-step green synthesis process using *Mangifera indica* plant extract. Similarly, the Beneficiated Kaolin Clay (BKC), BKC/Ag, BKC/ZnO and BKC/Ag/ZnO nanocomposite adsorbents were produced via wet impregnation and characterised for their surface areas, chemical composition and crystal structure. The nanocomposite filter pots were successfully produced to treat domestic wastewater. The produced filter pots were labelled – BKC – 1, BKC – 2, BKC/Ag – 1, BKC/Ag – 2, BKC/ZnO – 1, BKC/ZnO – 2, BKC/Ag/ZnO – 1, BKC/Ag/ZnO – 2. The research showed that BKC/Ag/ZnO filter pot produced at a

crystallize size of 26.934 nm from the beneficiated kaolin clay of 75 % mixed with silver oxide of 0.5 %, zinc oxide nanoparticles of 1.0 % and rice husks of 23.5 % produces the best nanocomposite filter pot. The removal efficiency of the produced nanocomposite adsorbents (BKC, BKC/Ag, BKC/ZnO and BKC/Ag/ZnO) and the filter pots (BKC – 1, BKC – 2, BKC/Ag – 1, BKC/Ag – 2, BKC/ZnO – 1, BKC/ZnO – 2, BKC/Ag/ZnO – 1, BKC/Ag/ZnO – 2) were performed. The research established that the BKC/Ag/ZnO filter pot produced at a crystallize size of 26.934 nm from beneficiated kaolin clay of 75 % mixed with silver oxide of 0.5 %, zinc oxide nanoparticles of 1.0 % and rice husks of 23.5 % reduced the contaminant concentrations of total iron, lead, copper, manganese, arsenic, mercury silver, zinc, nitrate, phosphate, ammonium, COD, BOD, oil and grease in the domestic wastewater by an average of 72 % reduction level, and removed 100 % of the total coliforms, faecal coliforms, *Clostridium perfringens*, *E. coli*, turbidity, suspended solids, and colour in domestic wastewater at 30 – 60 minutes contact time, 15 – 30 g dosage, and 50 – 80 ^{o}C temperature.

5.2 Recommendations

Based on the summarised conclusions, below are the recommendations:

i. Leaching of Ag/ZnO nanoparticles and regeneration of nanocomposite adsorbents be investigated in further study.

ii. The produced nanocomposite filter pots are effective against the removal of the selected contaminants from domestic wastewater, however, the need to carry out further investigation on its use for industrial wastewater treatment is necessary.

iii. The mechanical properties such as strength, tension, ductility, hardness, and stiffness of the produced filter pots be carried out in further research.

5.3 Contribution to Knowledge

The research has shown that kaolin clay, mixed with silver oxide nanoparticles, zinc oxide nanoparticles and rice husks as burnout material is capable of producing the best nanocomposite filter pot. The research established that the filter pot produced at a crystallize size of 26.934 nm from beneficiated kaolin clay of 75 % mixed with silver oxide of 0.5 %, zinc oxide nanoparticles of 1.0 % and rice husks of 23.5 % has the capacity to reduce the contaminant concentrations by average of 72 % reduction level of total iron, lead, copper, manganese, arsenic, mercury silver, zinc, nitrate, phosphate, ammonium, COD, BOD, oil and grease in the domestic wastewater. The filter pot also has the ability to remove 100 % of the total coliforms, faecal coliforms, *Clostridium perfringens, E. coli*, turbidity, suspended solids, and colour in domestic wastewater at 30 – 60 minutes contact time, 15 – 30 g dosage, and 50 – 80 ^{o}C temperature. The produced nanocomposite filter pot possessed the adsorption pore size of 16.9233 nm that fell in the mesopore width and was classified as type IV isotherm when compared with the IUPAC pore size classification. Therefore, the produced filter pot is suitable for domestic wastewater treatment.

REFERENCES

Abbas, M., Harrache, Z., & Trari, M. (2020). Mass-transfer processes in the adsorption of crystal violet by activated carbon derived from pomegranate peels: Kinetics and thermodynamic studies. *Journal of Engineered Fibers and Fabrics*, 15, 1-11, doi:10.1177 /1558925020919847.

Abdulah, O. (2005). Sedimentation Characteristics of Kaolin and Bentonite in Concentrated Solutions. *Acta Montanistica Slovaca*, 10(1), 145-150.

Abdullah, A. A., Mansor, B. A., Naif, M. A., Halimah, M. K., Hussein, M. Z., & Nor, A. I. (2017). Preparation of Zeolite/Zinc Oxide Nanocomposites for toxic metals removal from water. *Elsevier Results in Physics*, 7, 723–731, http://dx.doi.org/10.1016/j.rinp.2017.01.036.

Abdullahi, T., Harun, Z., & Othman, M. H. D. (2017). A review on sustainable synthesis of zeolite from kaolinite resources via hydrothermal process. *Advanced Powder Technology*, 28(8), 1827–1840, doi: 10.1016/j.apt.2017.04.028.

Abukhadra, M. R., & Mohamed, A. S. (2019). Adsorption removal of safranin dye contaminants from water using various types of natural zeolite. *Silicon*, 11(3), 1635-1647, https://doi.org/10.1007/s12633-018-9980-3.

Adewole, T. A. (2006). Changing the face of my local community through waste to wealth programme in Lagos State, Nigeria. Strength Based Strategies, Close 12 House 10 Satellite Town, Lagos, Retrieved from https://api.semantic scholar.org/CorpusID:199530344, 15th April, 2020.

Agbo, S. C., Ekpunobi, E. U., Onu, C. C., & Akpomie, K. G. (2019). Development of Ceramic Filter Candle from NSU (Kaolinite Clay) for Household Water Treatment, *International Journal of Multidisciplinary Sciences and Engineering*, 6(10), 2045-7057.

Aguilar, F., Charrondiere, U. R., Dusemund, B., Galtier, P., Gilbert, J., Gott, D. M., Grilli S., Guertler, R., Kass, G. E. N., Koenig, J., Lambré, C., Larsen, J. C., Leblanc, J. C., Mortensen, A., Parent, M. I. Pratt, I. M. C. M., Rietjens, I., Stankovic, P., Tobback, T., Verguieva, R. A., & Woutersen, D. (2009). Copper (II) oxide as a source of copper added for nutritional purposes to food supplements. *The European Food Safety Authority Journal*, 7(6), 1-15, doi: 10.2903/ j. efsa.2009.1089.

Alansari, A., Salim, A. M. A., Janjuhah, H. T., Bin, A., Rahman, A. H., & Fello, N. M. (2019). Quantification of Clay Mineral Microporosity and its Application to Water Saturation and Effective Porosity Estimation: A case Study from Upper Ordovician Sandstone reservoir, *Libya. Journal of Natural Gas Geoscience*, 4, 139-150, doi: 10.1016/j.jnggs.2019.04.005.

Ali, I. (2012). New generation adsorbents for water treatment, *Chemical Review*, 112(10), 5073 – 5091, doi: 10.1021/cr300133d.

Al-Kadhi, N. S. (2019). The kinetic and thermodynamic study of the adsorption Lissamine Green B dye by micro-particle of wild plants from aqueous solutions.

The Egyptian Journal of Aquatic Research, 45, 231-238, doi: 10.1016/j.ejar.2019.05.004.

Al-Rekabi, W. S., Qiang, H., & Wei, W. Q. (2007). Improvements in Wastewater Treatment Technology. *Pakistan Journal of Nutrition*, 6(2), 1680-5194.

Amandeep, K., & Sangeeta, S. (2017). Removal of Heavy Metals from Wastewater by using various adsorbents - A Review. *Indian Journal of Science and Technology*, 10(34), 1-14, doi: 10.17485/ijst/2017/v10i34/117269.

America Public Health Association (APHA) (2017). *Standard methods for Examination of Water and Wastewater*. APHA, AWWA, WEF. 23rd Edition, Published by E and FN SPON, Washington D.C.

America Society for Testing and Materials (ASTM) (2001). *Standard Practices for Evaluating the Resistance of Plastics to Chemical Reagents*, D543**.** Retrieved from https://img42. chem17.com/5/2008/ 633675497864149872.pdf, 25th September, 2022.

Amit, K. M., Yusuf, C., & Uttam, C. B. (2013). Synthesis of metallic nanoparticles using plant extracts, *Journal of Biotechnology Advances*, 31(2), 346-356.

Anijiofor, S. C., Azreen, M. J., Jabbar, S., Saad, S., & Chandima, G. (2017). Aerobic and Anaerobic Sewage Biodegradable Processes: The Gap Analysis. *International Journal of Research in Environmental Science*, 3(3), 9-19, doi: http://dx.doi.org/10.20431/2454-9444.0303002.

Anis, S. F., Hashaikeh, R., & Hilal, N. (2019). Reverse osmosis pretreatment technologies and future trends: A comprehensive review. *Desalination*, 452, 159 - 195, doi: 10.1016/j. desal. 2018.11.006.

Aroke, U. O., & Onatola, M. S. (2016). Comparative Sorption of Diatomic Oxyanions onto HDTMA-Br Modified Kaolinite Clay. *International Journal of Engineering and Science*, 6(7), 1-9.

Auta, M., & Hameed, B. H. (2013). Acid modified local clay beads as effective low-cost adsorbent for dynamic adsorption of methylene blue. *Elsevier Journal of Industrial and Engineering Chemistry*, 19(4), 1153-1161, http://dx.doi.org/ 10.1016/j.jiec.2012.12.012.

Ayalew, A. A. (2020). Development of Kaolin Clay as a Cost-Effective Technology for Defluorination of Groundwater. *International Journal of Chemical Engineering*, 1-10, doi:10.1155/2020/8820727.

Azizi, S., Mahdavi, S. M., & Mohamad, R. (2017). Green Synthesis of Zinc Oxide Nanoparticles for Enhanced Adsorption of Lead Ions from Aqueous Solutions: Equilibrium, Kinetic and Thermodynamic Studies. *Molecules*, 22(6), 1-15, doi:10.3390/molecules22060831.

Bachiri, E. M., Akichouh E., Miz, H., Salhi, S., & Tahani, A. (2014). Adsorptions desorption and kinetics studies of Methylene Blue Dye on Na-bentonite from Aqueous Solution. *Journal of Applied Chemistry*, 7(7), 60-78.

Baker, R. W. (2012). *Membrane Technology and Applications*, John Wiley and Sons, Chichester, 3, 253-324.

Ballah, M., Bhoyroo, V., & Neetoo, H. (2019). Assessment of the physico-chemical quality and extent of algal proliferation in water from an impounding reservoir prone to eutrophication. *Journal of Ecology and Environment*, 43(1), 1-9, doi:10.1186/s41610-018-0094-z.

Bashir, A. D., Abdo, T., Abubakkar, W. & Mazahar, F. (2013). Isotherms and thermodynamic studies on adsorption of copper on powder of shed pods of *Acacia nilotica. Journal of Environmental Chemistry and Ecotoxicology*, 5(2), 17-20, doi: 10.5897 /JECE12.013.

Benakashani, F., Allafchian, A. R., & Jalali. S. A. H. (2016). Biosynthesis of silver nanoparticles using *Capparis spinosa* L. leaf extract and their antibacterial activity. *International Journal of Karbala International Journal of Modern Science*, 2(4), 251-258, http://dx.doi.org/ 10.1016/j.kijoms.2016.08.004.

Berekaa, M. M. (2016). Nanotechnology in Wastewater treatment: influence of Nanomaterials on Microbial Systems. *International Journal of Current Microbiology and Applied Sciences*, 5(1), 713 – 726, doi:10.20546/ ijcmas.2016.501.072.

Bingjun, P., Bingcai, P., Weiming, Z., Lu, L., Quanxing, Z. & Shourong, Z. (2009). Development of polymeric and polymer-based hybrid adsorbents for pollutants removal from waters, *Elsevier Chemical Engineering Journal*, 151(1-3), 19-29, doi: 10.1016/j.cej.2009.02.036.

Bora, T., & Dutta, J. (2014). Applications of nanotechnology in wastewater treatment: a review. *Journal of Nanoscience and Nanotechnology*, 14(1), 613-626, doi:10.1166/jnn.2014.8898.

Brain, R., Lynch, J., & Kopp, K. (2015). Grey water systems. Retrieved from http://extension.usu.edu/files/publications/publication/Sustainability_2015 01pr.pdf, 17th July, 2020.

Briffa, J., Sinagra, E., & Blundell, R. (2020). Heavy metal pollution in the environment and their toxicological effects on humans. *Heliyon*, 6(9), 1-26, doi: 10.1016/j.heliyon. 2020.e04691.

Campbell, E. (2005). Study on life span of ceramic filter colloidal silver pot shaped model. Retrieved from http://potterswithoutborders.com/wp-content/uploads /2011/06/filter-longevity-study.pdf, 12th January, 2023.

Cerato, A. B., & Lutenegger, A. J. (2006). Shrinkage of Clays. Unsaturated Soils, 189(89), 1-12, doi:10.1061/40802(189)89.

Chan, Y. J., Chong, M. F., Law, C. L., & Hassell, D. G. (2009). A review on anaerobic–aerobic treatment of industrial and municipal wastewater. *Elsevier Chemical Engineering Journal*, 155(1-2), 1-18, doi: 10.1016/j.cej.2009.06.041.

Chandrasekhar, S., & Ramaswamy, S. (2002). Influence of mineral impurities on the properties of kaolin and its thermally treated products**.** *Applied Clay Science*, 21(3), 133–142, doi:10.1016/s0169-1317(01)00083-7.

Cheng, Q, Li, H, Xu, Y, Chen, S, Liao, Y, & Deng, F. (2017). Study on the adsorption of nitrogen and phosphorus from biogas slurry by NaCl- modified zeolite. *Plos One*, 12(5), 1-12, https://doi.org/10.1371/journal.pone.0176109.

Chun, H. Z., & John, K. (2013). Fundamental and applied research on clay minerals: From climate and environment to nanotechnology. *Applied Clay Science*, 74(9), 3-9, http://dx.doi.org /10.1016/ j. clay.2013.02.013.

Cigdem, Y. G. (2010). High-rate anaerobic treatment of domestic wastewater at ambient operating temperatures: A review on benefits and drawbacks, *Journal of Environmental Science and Health*, 45(10), 1169-1184, doi: 10.1080/ 10934529.2010.493774.

Crespo, J. (2010). Development in membrane science for downstream processing. In: Drioli, E., Giorno, L. (Eds.), *Membrane Operations*. Wiley-VCH, Weinheim.

Cushnie, T. P. T., & Lamb, A. J. (2005). Antimicrobial activity of flavonoids. International Journal of Antimicrobial Agents, 26(5), 343–356, doi: 10.1016/j.ijantimicag.2005.09.002.

Daizy, P. (2010). Mangifera Indica leaf-assisted biosynthesis of well-dispersed silver nanoparticles. *Elsevier*,78(1), 327-331, https://doi.org/10.1016/j.saa.2010.10.015.

Dar, A. (1999). Water Quality Laboratory and Monitoring Network Study Report. Federal Ministry of Water Resources, Abuja, Nigeria.

Dhaval, P., & Painter, Z. Z. (2017). Batch and Column Study for Treatment of Sugar Industry Effluent by using low-cost Adsorbent. *International Journal of Advance Research and Innovative Ideas in Education,* 3(3), 2395-4396.

Dina, D., Etoh M. A., Ngomo, H. M., & Ketcha, J. M. (2015). Adsorption of Pb^{2+} ions on two clays: Smectite and Kaolin the role of their textural and some physicochemical properties. *International Journal of Applied Research*, 1(13), 793-803.

Echevarría, C., Valderrama, C., Cortina, J. L., Martín, I., Arnaldos, M., Bernat, X., Boleda, M. R., Vega, A., Teuler, A., & Castellví, E. (2020). Hybrid sorption and pressure-driven membrane technologies for organic micropollutants removal in advanced water reclamation: A techno-economic assessment. *Journal of Cleaner Production*, 273,108-123, doi: 10.1016/j.jclepro.2020.123108.

Edema, N. (2012). Effects of Crude Oil Contaminated Water on the Environment. Crude Oil Emulsions- Composition Stability and Characterization, *Erratum*, 1-12.

Edwin, G., Rahul K. G., & Pronoy, K. S. (2017). Adsorption Studies on Removal of Chromium from Synthetic Wastewater using Activated Carbon prepared from

Rice Husk and Sugarcane Bagasse. *International Journal of Engineering Development and Research*, 5(2), 1856-1870.

Efeovbokhan, V. E., Olurotimi, O. O., Yusuf, E. O., Abatan, O. G., & Alagbe, E.E. (2019). Production of Clay Filters for Wastewater Treatment. *Journal of Physics: Conference Series, 1378, 032028*, 1-10, doi:10.1088/1742-6596/1378/3/032028.

Environmental Protection Agency (EPA) (2020). Water Treatment Manuals – Filtrations. United State Environmental Protection Agency, Johnstown Castle, Co. Wexford. Retrieved from https://www.epa.ie/ publications/compliance--enforcement/ drinking-water/advice--guidance/ EPA-Water-Filtration-Manual, pdf, 18th December, 2022.

Enyew, A.Z., & Tegene, D. (2019). Preparation and characterization of sintered clay ceramic membranes water filters, *Open Material Science Journal*, 5(1), 24–33, https://doi.org/ 10.1515/oms-2019-0005.

Erhan, G. (2017). The Adsorption of Basic Dye (Astrazon Blue FGRL) from Aqueous Solutions onto Two Different Clays: Talc and Chrysotile, 7(2), 438-448, https://www.acarindex. com/pdfler/acarindex-a59c2b3f-bf99.pdf.

Erhuanga, E., Bolaji, K. I., & Lawrence, A. T. (2014) Development of Ceramic Filters for Household Water Treatment in Nigeria. *Scientific Research*, 2(1), 6-10, doi: 10.4236/ adr.2014.21002.

Fondriest (2014). Turbidity, Total Suspended Solids and Water Clarity. Fundamentals of Environmental Measurements. Retrieved from https://www.fondriest.com /environmental-measurements/parameters/waterquality/turbidity-total-suspended - solids-water-clarity/, 20th August, 2022.

Fu, F., & Wang, Q. (2011). Removal of heavy metal ions from wastewaters: A review. *Journal of Environmental Management*, 92(3), 407-418, doi: 10.1016/ j. jenvman.2010.11.011.

Gadzama, L. D. M., Ameh, A. O., & Olakunle, S. M. (2020). Development of Ceramic Candle Filter from Alkaleri Kaolin, Bauchi State, Nigeria. *Advances in Engineering Design Technology*, 2(4), 42-50, https://doi.org/10.37933 /nipes. a/2.2020.4.

Galadima, A. & Garba, Z. N. (2012). Heavy metals pollution in Nigeria, causes and consequences. *Elixir Pollution*, 45(1), 7917-7922.

Getie, S., Belay, A., Chandra, R. A. & Belay, Z. (2017). Synthesis and Characterization of Zinc Oxide Nanoparticles by Solution Combustion Method: DC Conductivity Studies. *Indian Journal of Advances in Chemical Science*, 5(3), 137-141, doi: 10.22607/IJACS. 2017. 503004.

Google Map (2020). Google map of Kutigi Town. Retrieved from https://www.google.com/ maps/place/913102, +Kutigi, +Niger/, 12th January, 2020.

Gregorio, C., & Eric, L. (2019). Advantages and disadvantages of techniques used for wastewater treatment. Environmental Chemistry Letters. *Springer Verlag*, 17(1),145-155.

Grema, A. S., Idriss, I. M., Alkali, A. N., Ahmed, M. M., & Iyodo, H. M. (2021). Production of Clay-based Ceramic Filter for Water Purification. *European Journal of Engineering and Technology Research,* 6(7), 140-143, doi: http://dx.doi.org/10.24018/ejers.2021.6.7.2623.

Guo, D., Xiao, Y., Li, T., Zhou, Q., Shen, L., Li, R., Xu, Y., & Lin, H. (2019), Fabrication of high performance composite nanofiltration membranes for dye wastewater treatment: mussel-inspired layer-by-layer**.** *Elsevier Journal of Colloid and Interface Science*, 560(1), 273-283, doi: 10.1016/j.jcis. 2019.10.078.

Gushit, J. S., Olotu, P. N., Maikudi, S., & Gyang, J. D. (2010). Overview of the Availability and Utilization of Kaolin as a Potential Raw Material in Chemicals and Drugs Formulation in Nigeria. *Continental Journal Sustainable Development*, 1(1), 17 – 22.

Haijiao, L., Jingkang, W., Marco, S., Ting, W., Ying, B., & Hongxun, H. (2016). An Overview of Nanomaterials for Water and Wastewater Treatment. *Advances in Materials Science and Engineering,* 2016(1), 1-10, http://dx.doi.org /10.1155/ 2016/4964828.

Haritha, M., Meena, V., Seema, C. C., & Srinivasa, R. B. (2011). Synthesis and Characterization of Zinc Oxide Nanoparticles and Its Antimicrobial Activity against Bacillus Subtilis and Escherichia Coli. *Rasayan Journal of Chemistry*, 4(1), 217-222, https://rasayan journal.c.in/vol-4/issue-1/33.pdf.

Hocaoglu, M. S., Insel, G., Ubay, C. E., Baban, A., & Orhon, D. (2010) COD fractionation and biodegradation kinetics of segregated domestic wastewater: black and grey water fractions. *Journal of Chemical Technology and Biotechnology*, 85(9), 1241– 1249, https://doi.org/ 10.1002 /jctb.2423.

Hossam, H. (2017). Nanotechnology and Sensors - Introduction to nanotechnology. Technion Institute of Technology. Retrieved from https://www.scribd.com/doc/253557701/ Nanotechnology-and-Nanosensors-by-Prof-Hossam-Haick, 19th November, 2018.

Hube, S., Eskafi, M., Hrafnkelsdóttir, K. F., Bjarnadóttir, B., Bjarnadóttir, M. A., Axelsdóttir, S., & Wu, B. (2020). Direct membrane filtration for wastewater treatment and resource recovery: A review. *Science of the Total Environment*, 710(1), 136-375.

Hussaini, A. A., Nuhu, A., & Kabiru, M. S. (2015). Design of a filtration system for a small-scale water treatment plant for a rural community around Maiduguri Area in Borno State, Nigeria. *International Journal of Engineering Science Invention*, 4(8), 39-43.

Idris-Nda, A., Aliyu, H. K., & Dalil, M. (2013), The challenges of domestic wastewater management in Nigeria: A case study of Minna, central Nigeria", *International Journal of Development and Sustainability*, 2(2), 1169-1182.

Ikhazuangbe, P. M. O., Kamen, F. L., Opebiyi, S. O., Nwakaudu, M. S., & Onyelucheya, O. E. (2017). Equilibrium Isotherm, Kinetic and Thermodynamic Studies of the Adsorption of Erythrosine Dye onto Activated Carbon from Coconut Fibre. *International Journal of Advanced Engineering Research and Science*, 4(5), 48-54, https://dx.doi.org/10.22161/ ijaers.4.5.9.

International Standard Organisation (ISO) (2015). Determination of loss on ignition by Gravimetric Method, 11536:2015(E). 11536, Geneva, Switzerland.

Joseph, M. B. (2007). Effectiveness of Ceramic Filtration for Drinking Water Treatment in Cambodia. A dissertation submitted to the faculty of the University of North Carolina at Chapel Hill, Department of Environmental Sciences and Engineering. Retrieved from https://core.ac.uk/download/pdf/210596717.pdf, 15-20, 15th January, 2023.

Jovanovic, M., & Mujkanovic, A. (2013, September 10-11). Characterisation, Beneficiation and Utilization of the Clay from Central Bosnia, BandH. *Proceedings of 17th International Research / Expert Conference "Trends in the Development of Machinery and Associated Technology*", TMT, Istanbul, Turkey, https://www.tmt.unze.ba/zbornik/TMT2013/046-TMT13-149.pdf.

Kaczmarek, B. (2020). Tannic Acid with Antiviral and Antibacterial Activity as A Promising Component of Biomaterials: A Minireview. *Materials,* 3224, 13(14), 1-13, doi:10.3390/ ma13143224.

Karishma, K. C., & Mehali, J. M. (2015). Application of Nanotechnology in Wastewater Treatment. *International Journal of Innovative and Engineering Research in Engineering*, 2(1), 21 – 25.

Karl, T., Ralph, B. P., & Gholamreza, M. (1996). *Soil Mechanics in Engineering Practice*. Third edition published by John Wiley and Sons Inc., New York, USA.

Khushbu, G. P., Rakshith, R. S. & Nirendra, M. M. (2017). Recent advance in silica production technologies from agricultural waste stream: Review. *Journal of Advanced Agricultural Technologies*, 4(3), 274-279, doi: 10.18178/joaat.4.3.274-279.

Kimberly, L. F. (2015). Considerations for implementing source separation and treatment of urine, greywater, and blackwater. Colorado State University Fort Collins, Colorado. Retrieved from https://api.mountainscholar.org/server/api/core/ bitstreams/4bab44cb-73c0-42e3-8a0 8-53a028fc6e75/content, 13th January, 2022.

Kovo, A. S., & Edoga, M. O. (2005). Production and Characterization of Zeolite from Ahako Clay in Kogi State, Nigeria. *Leonardo Electronic Journal of Practices and Technologies.* Retrieved from https://www.researchgate.net/publication /26446260_Production_ and_ Characterisation_of_Zeolite_from_Ahako_Clay_ in_Kogi_State_Nigeria, 12th February, 2022.

Krishan, K. S., Vikas, S., & Manjit, K. S. (2013). Green synthesis of silver nanoparticles using leaf extract of *Mangifera indica* and evaluation of their antimicrobial activity. *Journal of Microbiology and Biotechnology Research,* 3(5), 2231 –3168.

Kujawa, R. K., & Zeeman, G. (2006**)**. Anaerobic treatment in decentralized and source separation-based sanitation concepts. *Springer Journal of Review in Environmental Science and Biotechnology, 5*(1), 115–139, doi:10.1007/s11157-005-5789-9.

Kuranga, I. A., Alafara, A. B., Halimah, F., Fausat, A. M., Mercy, O. B., & Tripathy, B. C. (2018). Production and Characterization of Water Treatment Coagulant from locally sourced Kaolin Clays. *Journal of Applied Science and Environment*, 22(1), 103-109, doi: https://dx.doi.org /10.4314/ jasem. v22i1.19.

Lantagne, D. (2001a). Investigation of the potters for peace colloidal silver impregnated ceramic filter – report 1: intrinsic effectiveness. Alethia Environmental. Allston, MA. Retrieved from http://potterswithoutborders.com/wp-content/uploads /2011/06/alethia-report-1.pdf, 25th August, 2022.

Lantagne, D. (2001b). Investigation of the potters for peace colloidal silver impregnated ceramic filter – report 2: field investigations. Alethia Environmental. Allston, MA. Retrieved from http://potterswithoutborders.com/wp-content/ uploads/ 2011/06/ alethia-report-2.pdf, 25th August, 2022.

Levard, C., Hotze, E. M., Lowry, G. V., & Brown, G. E. (2012). Environmental transformations of silver nanoparticles: impact on stability and toxicity. *Environmental Science Technology*, 46, 6900−6914, dx.doi.org/10.1021 /es203740.

Lo, Y., Dooyema, C. A., Neri, A., Durant, J., Jefferies, T., Medina, M. A., Ravello, L., Thoroughman, D., Davis, L., Dankoli, R. S., Samson, M. Y., L. M. Ibrahim, O. Okechukwu, U., Tsafe, N. T., Dama, A. H., & Brown, M. J. (2010). Childhood lead poisoning associated with gold ore processing: a village-level investigation: Zamfara State, Nigeria, *Environmental Health Perspectives*, 120(1), 1450-1455, doi:10.1289/ ehp.1104793.

Ludwig, A. (2012). Create an oasis with grey water: Choosing, building and using grey water systems. 0-9643433-9-8. Retrieved from https://www.rainharvest.com /create-an-oasis-with-greywater-by-art-ludwig.asp, 15th September, 2021.

Maity, J., Sukanta, P., Sourav, M., & Ratul, M. (2018). Synthesis and characterization of ZnO nanoparticles using moringa oleifera leaf extract: investigation of photocatalytic and antibacterial activity. *International Journal of Nanoscience and Nanotechnology*, 14(2), 111-119.

Manokari, M., & Mahipal, S. S. (2016). Zinc oxide nanoparticles synthesis from *Moringa oleifera* Lam - Extracts and their characterization. *World Scientific News*, 55(1), 252-262.

Marthe, S., Graaff, D., Hardy, T., Grietje Z., & Cee, J. N. B. (2010) Anaerobic treatment of concentrated black water in a up flow anaerobic sludge blanket (UASB) reactor at a short hydraulic retention time, *Water*, 2(1), 101-119.

Micrometrics. (2009). TriStar II 3020 operator's manual V1.03. Micromeritics Instrument Corporation, 2008-2009. 4356 Communications Drive, Norcross, GA 30093-187.

Miklasińska, M.M., Kępa, M., Wojtyczka, R., Idzik, D., & Wąsik, T. (2018). Phenolic compounds diminish antibiotic resistance of staphylococcus aureus clinical strains. *International Journal of Environmental Research and Public Health*, 15(10), 1-18, doi:10.3390/ ijerph15102321.

Ming, H., Shujuan, Z., Bingcai, P., Weiming, Z., Lu, L., & Quanxing Z. (2012). Heavy metal removal from water/wastewater by nanosized metal oxides: a review. *Elsevier Journal of Hazardous Materials*, 211(1), 317– 331, doi: 10.1016/j.jhazmat.2011.10.016.

Mohan, A. C., & Renjanadevi, B. (2016). Preparation of Zinc Oxide Nanoparticles and its Characterization Using Scanning Electron Microscopy (SEM) and X-Ray Diffraction (XRD). *Procedia Technology*, 24(1), 761-766, https://doi.org /10.1016/j.protcy.2016.05. 07824.

Mohd, S. Y., Mohamad, A. K., Hamidi, A. A, & Christopher, A. O. (2013). Recent developments of textile wastewater treatment by adsorption process: a review. *International Journal of Scientific Research in Knowledge*, 1(4), 60-73.

Muhammad, S., Ashiru, I. Ibrahim, D., Salawu, K., Muhammad, D. T. N., & Muhammad, A. (2014). Determination of some heavy metals in wastewater and sediment of artisanal gold local mining site of Abare Area in Nigeria. *Journal of Environmental Treatment Technology,* 2(1), 1-9.

Muharrem, I., & Kaplan, O. I. (2017). An overview of adsorption technique for heavy metal removal from water/wastewater: a critical review. *International Journal of Pure and Applied Science* 3(2), 10-19.

Murray, H. H. (2000). Traditional and new applications for kaolin, smectite, and palygorskite: a general overview. *Applied Clay Science* 17(1), 207–221, https://doi.org/10.1016/S0169-1317(00)00016-8.

Nadia, M. A. P., & Yousef, N. S. (2015). Synthesis and characterization of zinc oxide nanoparticles for the removal of Cr (VI). 2229-5518, *International Journal of Scientific and Engineering Research*, 6(7), 1-9.

National Bureau of Statistics (NBS) (2017). State disaggregated mining and quarrying data. Retrieved from https://www.nigerianstat.gov.ng/pdfuploads/ State-Disaggregated-Mining-and-Quarrying-Data-2017.pdf, 10th October, 2019.

National Environmental Standards Regulations and Enforcement Agency (NESREA) (2011). National environmental (surface and groundwater control) regulations, 2011. Federal Government Printer, Lagos, Nigeria. FGP71/72011/400 (OL,46).

National Water Quality Reference Laboratories (NWQRL) (2020). Atlas of rivers and open waterbodies monitoring activities of 2020. Department of Water Quality Control and Sanitation, Federal Ministry of Water Resources, Abuja.

National Water Quality Reference Laboratories (NWQRL) (2021). Rivers and open waterbodies monitoring activities report of 2021, Water Quality Control and Sanitation Departments, Federal Ministry of Water Resources, Abuja.

Ng, L.Y., Mohammad, A. W., Rohani, R., & Hairom, N. H. H. (2015). Development of a nanofiltration membrane for humic acid removal through the formation of polyelectrolyte multilayers that contain nanoparticles. *Desalination and Water Treatment*, 57(17), 7627–7636, *doi*:10.1080/19443994.2015.1029009.

Nigeria Standard or Drinking Water Quality (NSDWQ) (2015). Nigeria Industrial Standard, Standard Organisation of Nigeria. ICS 13.060.20. Retrieved from https://africacheck.org/sites/default/files/Nigerian-Standard-for-Drinking-Water-Quality-NIS-554-2015.pdf, 25th March, 2023.

Njagi, E. C., Hui, H., Lisa, S., Homer, G., Hugo, M. G., John, B. C., George, E. H., & Steven, L. S. (2010). Biosynthesis of Iron and Silver Nanoparticles at Room Temperature Using Aqueous Sorghum Bran Extracts. *Langmuir article*, 27(1), 264–271, doi: 10.1021 /la103190n Langmuir 2011.

Nnaji, C., Afangideh, B., & Ezeh, C. (2016). Performance evaluation of clay-sawdust composite filter for point of use water treatment. *Nigerian Journal of Technology,* 35(4*)*, 949, doi:10.4314/njt. v35i4.33 10.4314/njt. v35i4.33.

Odenigbo, C. O., & Musa, A. J. (2018). Production of ceramic candle water filters using saw dust, rice husk as burnt-out materials**.** *International Journal of Civil Engineering, Construction and Estate Management*, 6(1), 17-21.

Odigie, J. O. (2014). Harmful effects of wastewater disposal into water bodies: a case review of the Ikpoba River, Benin City, Nigeria**,** *Tropical Freshwater Biology*, 23(1), 87-101, doi: http://dx.doi.org/10.4314/tfb.v23i1.5.

Ojo, G. P., Igbokwe, U. G., Egbuachor, C. J., & Nwozor, K. K. (2017). Geotechnical properties and geochemical composition of kaolin deposits in parts of Ifon, Southwestern Nigeria. *American Journal of Engineering Research,* 6(3), 15-24.

Okereke, J. N., Ogidi, O. I., & Obasi, K. O. (2016). Environmental and health impact of industrial wastewater effluents in Nigeria - A Review, *International Journal of Advanced Research in Biology Science*, 3(6), 55-67, http://s-o-i.org/1.15/ijarbs-2016-3-6-8.

OriginPro (2021). Student Trial Version of OriginPro Data and Analysis Software, OriginLab Corporation, Northampton, MA, USA.

Parthibana, C., & Sundaramurthy, N. (2015). Biosynthesis, characterization of ZnO nanoparticles by using *Pyrus pyrifolia* – leaf extract and their photocatalytic activity. *International Journal of Innovative Research in Science, Engineering and Technology*, 4(10), 9710-9718, doi:10.15680/IJIRSET.2015.0410031.

Pathak, R. K., & Dikshit, A. K. (2011). Atrazine and human health. *International Journal of Ecosystem.*1(1), 14-23, doi: 10. 5923/j.ije.20110101.03.

Pradeep, T. (2009). Noble metal nanoparticles for water purification: a critical review. *Elsevier Thin Solid Film*, 517(24), 6441-6478, doi: 10.1016/j.tsf.2009.03.195.

Rajasulochana, P., & Preethy, V. (2016). Comparison on efficiency of various techniques in treatment of waste and sewage water: a comprehensive review. *Resource Efficient Technologies*, 2(4), 175–184, http://dx.doi.org/10.1016/ j. reffit.2016.09.004.

Ralf, K. I., Andreas, V., Brian, S., Steffen, Z., Harald, H., Michael, B., & Hansruedi, S. (2011). Behaviour of metallic silver nanoparticles in a pilot wastewater treatment plant, *Environmental Science Technology,* 45(1), 3902–3908, dx.doi.org/ 10.1021/es1041892.

Ramesh, R, P, & Arumugam, A. (2014). Synthesis of Zinc Oxide Nanoparticle from Fruit of Citrus Aurantifolia by Chemical and green Method. *Asian Journal of Phytomedicine and Clinical Research*, 2(4), 189-195.

Rathore, S. S., Chandravanshi, P., Chandravanshi, A., & Jaiswal, K. (2016). Eutrophication: impacts of excess nutrient inputs on aquatic ecosystem. *Journal of Agriculture and Veterinary Science,* 9(10), 89-96.

Roadmap (2022). Nigerian Road Map for Water Quality Management. Federal Ministry of Water Resources, Abuja.

Robina, A., Saira, R., Muhammad, K., & Shahzad, N. (2013). Synthesis and characterization of ZnO nanoparticles. Centre of Excellence in Solid State Physics, University of the Punjab, Pakistan, GC University, Lahore, Pakistan.

Rui M., Clément L., Jonathan, D. J., Jason, M. U., Mark D., Ben, M., Bruce, J., & Gregory, V.L. (2013). Fate of zinc oxide and silver nanoparticles in a pilot wastewater treatment plant and in processed biosolids. *Environmental Science Technology,* 48(1), 104-112, doi: 10.1021 /es403646x.

Sachin, K., Achyut, K. P., & Singh, R. K. (2013). Preparation and Characterization of Acids and Alkali Treated Kaolin Clay. *Bulletin of Chemical Reaction Engineering and Catalysis*, 8(1), 61 – 69.

Saikia, N. J., Bharali, D. J., Sengupta, P., Bordoloi, D., Goswamee, R. L., Saikia, P. C., & Borthakur, P. C. (2003). Characterization, beneficiation and utilization of a kaolinite clay from Assam, India. *Applied Clay Science*, 24(1), 93– 103, doi:10.1016/S0169-1317(03)00151-0.

Samanta, H. S., Das, R., & Bhattachajee, C. (2016). Influence of nanoparticles for wastewater treatment- a short review. *Austin Chemical Engineering*, 3(3), 1036.

Sanjeeva, M. N. (2013). Scattering techniques for structural analysis of biomaterials. *Characterization of Biomaterials*, 34–72, doi:10.1533/9780857093684.34.

Shimadzu (2008). Instruction Manual Operation Guide for Ultraviolet 1800 Shimadzu spectrophotometer. Analytical and Measuring Instruments Division, Shimadzu Corporation, Kyoto Japan.

Shittu, K. O., & Ikebana, O. (2017). Purification of simulated wastewater using green synthesized silver nanoparticles of *Piliostigma thonningii* aqueous leave extract. *Advance in Natural Science.: Nanoscience. Nanotechnology*, 8(4), 1-10, https://doi.org/10.1088/2043-6254/ aa8536.

Shuying, W., Jinyang, F., Cong, Z., & Junsheng, Y. (2021). Slurry treatment for shield tunnelling and waste slurry recycling: Chapter 10. *Elsevier*, 10(2), 491-521.

Sierra, M. J., Adriana, Herrera, P., & Karina, A. O. (2018). Synthesis of zinc oxide nanoparticles from mango and soursop leaf extracts. *Contemporary Engineering Sciences*, 11(8), 395 – 403, https://doi.org/10.12988/ces.2018.8228.

Stoyanova, A. H., Hitkova, A., Bachvarova-Nedelcheva, R., Iordanova, N. I., & Sredkova, M. (2013). *Journal of Chemical Technology and Metallurgy*, 48(2), 154-161.

Sukdeb, P., Yu, K. T., & Joon, M. S. (2007). Does the antibacterial activity of silver nanoparticles depend on the shape of the nanoparticle? A study of the gram-negative bacterium *Escherichia coli*. *Applied and Environmental Microbiology*, 73(6), 1712–1720, doi:10. 1128/AEM.02218-06.

Sulekha, M. S. (2016). Nanotechnology for Wastewater Treatment. *International Journal of Chemical Studies*, 4(2), 22 – 24.

Surya, P. G. (2012). Synthesis and Characterization of zinc oxide nanoparticles by sol-gel process. National Institute of Technology, Rourkela Rourkela-769008, Orissa, India. Retrieved from https://core.ac.uk/download/pdf/53188276.pdf, 28th May, 2022.

Susan, A., Mahnaz, M. S., & Rosfarizan, M. (2017). Green synthesis of zinc oxide nanoparticles for enhanced adsorption of lead ions from aqueous solutions: equilibrium, kinetic and thermodynamic studies. *Molecules*, 22(1), 831, doi:10.3390/molecules22060831, www. mdpi .com /journal/molecules.

Syafiqa, A., Norzila, O., Wahid, A. H. A, Faisal, S. K, Norshila, A. B, Muhammad, T., & Eddy, S. S. (2021). A Review on adsorption of heavy metals from wood-industrial wastewater by oil palm waste. *Journal of Ecological Engineering*, 22(3), 249–265, https://doi.org/ 10.12911/22998993/ 132854, 2299-8993.

Syamala, D., Bai1, V., Ramesh, K., & Suvarna, R. P. (2017). Synthesis and characterization of zinc oxide nanoparticles by solution combustion method: DC conductivity studies. *Indian Journal of Advances in Chemical Science*, 5(3), 137-141.

Sylla, A. M, Rihani, J., Amine O., Assobhei, S., & Etahiri, B. (2018). Anaerobic Treatment of Black Water and the Effect of Nitrate on Bioreactor Performance. *Journal of Natural Sciences Research*, 8(7), 1-8.

Tait, D. R., Erler, D. V., Dakers, A., Davison, L., & Eyre, B. D. (2013). Nutrient processing in a novel on-site wastewater treatment system designed for permeable

carbonate sand environments. *Elsevier Ecological Engineering.* 57, 413–421, doi: 10.1016/j.ecoleng .2013.04.027.

Thabet, M. Tolaymat, A. M., El, B., Ash, G., Kirk, G., Scheckel, T. P., & Luxton, M. S. (2010). An evidence-based environmental perspective of manufactured silver nanoparticle in syntheses and applications: A systematic review and critical appraisal of peer-reviewed scientific papers. *Elsevier*, 408(5), 999–1006, doi: 10.1016/j.scitotenv.2009.11.003 Science of the Total Environment 408.

Thair, A., & Olli, S. (2008). Clay and Clay Mineralogy Physical – Chemical Properties and Industrial Uses. Geological Survey of Finland, Report M19/3232/2008/41. Retrieved from https://www.researchgate.net/publication/292706105_Clay_and _clay mineralogy, 22nd June, 2021.

Thirunavukkarasu, R., Archana, S., Sharmila, B., & Janarthanan, J. C. (2016). preparation and characterization of ZnO nanoparticles using *Moringa oleifera* extract by green synthesis method. *Asian Journal of Phytomedicine and Clinical Research*, 4(3), 121-132.

Thyagaraju, N. (2016). Water Pollution and its Impact on Environment of Society. *International Research Journal of Management, Information Technology and Social Sciences*, 3(5), 1-7.

Timothy, O. F., Adinife, P. A., & Williams, K. J. (2021). The Effect of Burnt Clay Brick Production Process on the Compressive Strength and Water Absorption Properties. *SNRU Journal of Science and Technology*, 3(2), 63-70.

Tommy, K. K., Ngai, R. R., Shrestha, B. D., Makhan, M., & Susan, E. M. (2007). Design for sustainable development: household drinking water filter for arsenic and pathogen treatment in Nepal, *Journal of Environmental Science and Health*, Part A: Toxic/Hazardous Substances and Environmental Engineering, 42(12), 1879 - 1888, doi: 10.1080/1093452070 1567148.

United Nation-Water (UN-Water) (2018). Sustainable development goal 6 synthesis report on water and sanitation draft. United Nations New York, New Yo*rk* 10017, United States of America. Retrieved from www.un.org/publications, 18th December, 2022.

University of South Africa (UNISA) (2022a). *XRD* Analyser Instruction Manual for Determination of Mineral Phases and Compounds in Materials. Emma 0141 X-Ray Machine, University of South Africa, Johannesburg, South Africa.

University of South Africa (UNISA) (2022b). Chemical Analyses of Materials Instruction Manual. TECNAI G2 F20 twin model Transmission Electron Microscope Machine, University of South Africa, Johannesburg, South Africa.

University of South Africa (UNISA) (2022c). Surface Area and Pore Size Measurements and Analysis of Materials Instruction Manual. TriStar II 3020 Brunauer–Emmett–Teller Nitrogen Absorption Analysis Machine, University of South Africa, Johannesburg, South Africa

University of South Africa (UNISA) (2022d). Chemical Analyses of Materials Instruction Manual. EDXRF-3600B machine, University of South Africa, Johannesburg, South Africa.

Van der, B. B. (2009). Fundamentals of membrane solvent separation and pervaporation. In: Drioli, E., Giorno, L. (Eds.), *Membrane Operations*. Wiley-VCH, Weinheim.

Van, H. D., Vander, L. H., Soppe, A. I. A., & Heijman, S. G. J. (2017). High flow ceramic pot filters. *Water Research,* 124(1), 398–406, doi: 10.1016/j.watres.2017.07.045.

Vikas, S., Krishan, K. S., & Manjit, K. S. (2013). Green synthesis of silver nanoparticles using leaf extract of Mangifera indica and evaluation of their antimicrobial activity. *Journal of. Microbiology Biotechnology Research*. 3(5), 27-32.

Water Research Commission (WRC) (2015). Wastewater Treatment Technologies: Basic guide. Retrieved from https://www.wrc.org.za/wp-content/uploads/mdocs/TT% 20651%20-%201 5.pdf, 20th November, 2022.

Water, Sanitation and Hygiene National Outcome Routine Mapping (WASHNORM) (2019). Water, Sanitation and Hygiene Outcome Routine Mapping: A report of findings. Retrieved from https://www.unicef.org/nigeria/media/3576/file/WASH %20NORM%20Report%202019.pdf, 27th June, 2022.

Westerhoff, P., Pedro, A., Qilin, L., Jorge, G., & Julie, Z. (2016). Overcoming implementation barriers for nanotechnology in drinking water treatment, *Environmental Science Nanotechnology*, 3(6), 1225 – 1522, doi: 10.1039/c6en00183a.

Wilson, A. M. (2017). Crystallization of NBA-ZSM-5 from kaolin. Department of Civil, Environmental and Natural Resources Engineering Division of Chemical Engineering, Luleå University of Technology. Retrieved from https://www.diva-portal.org/smash/ get/diva2: 1091512/fulltext01.pdf, 18th December, 2022.

Worch, E. (2012). *Adsorption Technology in Water Treatment Fundamentals, Processes, and Modeling*. Walter de Gruyter GmbH and Co. KG, Berlin.

World Water Development Report on Wastewater (WWDR) (2017). The untapped resource. United Nations Educational, Scientific and Cultural Organization, 7, Place de Fontenoy, 75352 Paris 07 SP, France.

Xu, L., Zhang, J., Ding, J., Liu, T., Shi, G., Li, X., & Guo, R. (2020). Pore structure and fractal characteristics of different shale lithofacies in the Dalong formation in the Western Area of the Lower Yangtze Platform. *Minerals*, 10(1), 1-25.

Yahaya, S., Suzi, S. J., Nur, A. B., & Ajiya, D. A. (2017). Chemical Composition and Particle Size Analysis of Kaolin, *Path of Science*, 3(10), 1001-1004, doi: 10.22178/pos.27-1.

Yang, Z., Yongsheng, C., Paul, W., Kiril, H., & John, C. C. (2008). Stability of commercial metal oxide nanoparticles in water, 42(1), 2204 – 2212, doi: 10.1016/j.watres.2007.11.036.

Ying, C., Hao, D., & Sijia, S. (2017). Preparation and Characterization of ZnO Nanoparticles Supported on Amorphous SiO_2. *Journal of Nanomaterials* 7(1), 217, doi:10.3390/ nano7080217 www. mdpi .com/journal/nanomaterials.

Zahra, M. K., Amirali, Y., & Nima, N. (2015). Optical Properties of Zinc Oxide Nanoparticles Prepared by a One-Step Mechanochemical Synthesis Method. *Journal of Physical Science*, 26(2), 41–51.

Zhou, C. H., & Keeling, J. (2013). Fundamental and applied research on clay minerals: From climate and environment to nanotechnology. *Applied Clay Science*, 74(1), 3-9, http://dx.doi.org/10.1016/j.clay.2013.02.013.

APPENDIX A

DETAILED LIST OF EQUIPMENT

S/N	Test Equipment	Model No.	Manufacturer	Uses	Location
1	X-ray diffractometer (XRD)	Emma 0141	GCB SCIENTIFIC EQUIPMENT	Determination of mineral phases and compounds in materials. Study of crystal structure of the mineral phases and compounds in materials	University of South Africa Johannesburg, South Africa
2	Dispersive X-ray fluorescence (XRF) machine	EDXRF-3600B	OXFORD INSTRUMENT	Chemical analyses of materials	University of South Africa Johannesburg, South Africa
3	High-Resolution Transmission Electron Microscope (HRTEM)	TECNAI G2	FEI Netherlands	Determination of Microstructure and particle size of materials	University of South Africa Johannesburg, South Africa
4	BET Nitrogen Absorption Analyser	TriStar II 3020	MICROMETRICS, USA	Surface area and pore size	University of South Africa Johannesburg, South Africa
5	UV – Spectrometer	UV – 1800	SHMADZU, Japan	Determination of purity and concentration of a solution	Centre for Genetic Engineering and Biotechnology, FUT Minna
6	Muffle furnace	7/99/1540	LENTON	Gravimetric Analysis	National Water Quality Reference Laboratory Minna
7	Hot Air Oven	SG 99/06/120	GALLENKAMP	Gravimetric Analysis	National Water Quality Reference Laboratory Minna
8	Sieve Shaker	2000/2/4801-99	EFL	Gravimetric Analysis	National Water Quality Reference Laboratory Minna
9	Grant water bath, 28 litre flat with 6 ring sets, temperature range 5-98^{o}c,	SUB 28	GRANT	Microbiological Analysis	National Water Quality Reference Laboratory Minna

10	Laboratory Thermometer		FISHER	Temperature Measurement	National Water Quality Reference Laboratory Minna
11	Weighing Balance	PR 2003	METLER TOLEDO	Weight Measurement	National Water Quality Reference Laboratory Minna
12	pH Meter	AZ86P3, RS232	WAGTECH	pH Analysis	National Water Quality Reference Laboratory Minna
13	Conductivity Meter	CMD 8000	LINTON CAMBRIDGE	Conductivity Measurement	National Water Quality Reference Laboratory Minna
14	Titration Apparatus	-	FISHER	Volumetric Analysis	National Water Quality Reference Laboratory Minna
15	Metalyser	HM 1000/ 5000	TRACE O2	Heavy Metals Analysis	National Water Quality Reference Laboratory Minna
16	Atomic Absorption Spectrometer	AAS	BULK SCIENTIFIC	Heavy Metal Analysis	National Water Quality Reference Laboratory Minna
17	Membrane Filtration Machine	D-79112	NEUBERGER	Microbiological Analysis	National Water Quality Reference Laboratory Minna
18	Thermometer K type thermocouple with penetrating probe.		FISHER	COD Analysis	National Water Quality Reference Laboratory Minna
19	Centrifuge centaur 2, max speed 4600 rev / min, max. vol. 4 x 200 ml,, Timer 0 – 30mins with integral digital speed indicator without rotor,	MSB020.CX 1.5	CENTUR 2 SANYOR	Used in the production of Nanoparticles	National Water Quality Reference Laboratory Minna
20	Hotplate 35 x 30 cm, Aluminium plate Ambient = 50 to 250 ^{o}C	HOT PLATE SH3D	STUART SCIENTIFIC	Gravimetric Analysis	National Water Quality Reference Laboratory Minna
21	EFL 2000/2 Sieve Shaker 220/240 V, 50Hz.	EPL 2000/2/4801	ENDECOLLS	For shaking of reaction medium at room temperature	National Water Quality Reference Laboratory Minna
22	Stirrer Heildolph RGL500, High viscosity with electro control speed 250 – 5000 Rev/Min. without paddle	RZR2101	HEIDOLPH	Homogenisation of the kaolin clay	National Water Quality Reference Laboratory Minna

23	Stirrer Magnetic with Hotplate, 1 place speed to 130 RPM, Max Temp. 400OC, Hotplate 139mm	MSH-1	CLIFTON	Homogenisation of the kaolin clay	National Water Quality Reference Laboratory Minna
24	FISTREEM Calypso Still 4 litre Tank HR220V, 50 Hz.	L9810120	SANYO GALLENKAMP	Storage of Deionized Distilled Water (DDW)	National Water Quality Reference Laboratory Minna
25	Refrigerator MPR-41F 422L, 230V, 50 Hz.	MPR-411FR	SANYO MEDICOOL	Preservation of the Water Samples	National Water Quality Reference Laboratory Minna
26	Transport Box, 7 Litre including 10x0.6 litre ice pack.	MRT 8V	ELECTROLUX	Water Sample Collection	National Water Quality Reference Laboratory Minna
27	Fume Hood fitted with LPG,	2-410 NLS	KOTTERMAN	Preparation of the Standard	National Water Quality Reference Laboratory Minna
28	Sturdy Industrial Autoclave (2no.) with diameter 40 cm each	8A-40 CAR, 8A- 400 AV	STURDY	Sterilization for Microbiological Analysis	National Water Quality Reference Laboratory Minna
29	Pselecta incubator with temperature set point fixed at 37 ^{o}C.	COD-2000207	P-SELECTA	Microbiological Analysis	National Water Quality Reference Laboratory Minna
30	Sanyo GallenKamp Water distiller with accessories	WCA004.MH1.4	SANYO GALLENKAMP	Production of Distilled Water	National Water Quality Reference Laboratory Minna

APPENDIX B

METHOD OF DOMESTIC WASTEWATER ANALYSIS

S/No	Parameter	Unit	Test Equipment	Model No.	Reagents Used	Method	SOPs
1	pH		PH METER	RS232	4,7,10 BUFFER	Electrometric	APHA 4500HB
2	Turbidity	NTU	Colorimeter	DR 890	Formazin Standards	Colorimetric	APHA 2130B
3	Conductivity	µs/Cm	Conductivity Meter	CMD 8000	KCl Standards	Electrometric	APHA 2510B
4	Dissolved Oxygen	mg/L	Titration		Manganese Solution, Alkali-Iodide, Sulphuric Acid and Starch Solution	Winkler	APHA 4500-O C
5	Suspended Solid	mg/L	Colorimeter	DR 890	Deionised Distilled Water	Colorimetric	APHA
6	Colour	Pt Co	Colorimeter	DR 890	Deionised Distilled Water	Colorimetric	APHA 2120 B
7	Nitrate	mg/L	Colorimeter	DR 890	Nitraver 5 Pillows	Cadmium Reduction	APHA 4500-NO_3E
8	Ammonium	mg/L	Colorimeter	DR 890	Nessler Reagent	Nesslerization	APHA
9	Chloride	mg/L	Titration		Dichromate and Silver Nitrate Solution	Argentometric	APHA 4500CL^- B
10	Nitrite	mg/L	Colorimeter	DR 890	Colour Reagent	Colorimetric	APHA 4500-NO_2^- B
11	Phosphates	mg/L	Colorimeter	DR 890	Phosphate Buffer And Stannous Chloride	Stannous Chloride	APHA 4500-P D
12	Ammonium	mg/L	Colorimeter	DR 890	Nessler Reagent	Nesslerization	APHA
13	COD	mg/L	Colorimeter	DR 890	Cod Digestion Vile	Colorimetric	APHA 5220 D
14	BOD_5	mg/L	Titration	Volumetric	Manganese Solution, Alkali-Iodide, Sulphuric Acid and Starch Solution	Winkler	APHA 5210B
15	Sodium	mg/L	Flame Photometer	410	Sodium Standard	Flame Photometry	APHA 3500 NA- D
16	Potassium	mg/L	Flame Photometer	410	Potassium Standard	Flame Photometry	APHA 3500 K-D
17	Cadmium	mg/L	Metalyser	HM 1000	Cadmium Standard and Buffer	Voltametric Stripping	APHA 3130 A
18	Iron	mg/L	Colorimeter	DR 890	Phenanthroline, Ammonium Acetate Buffer, HCl	Phenanthroline	APHA 3500-FE D
19	Lead	mg/L	Metalyser	HM 1000	Lead Standard and Buffer	Voltametric Stripping	APHA 3130 A
20	Copper	mg/L	Metalyser	HM 1000	Copper Standard, Buffer	Voltametric Stripping	APHA 3130 A

21	Manganese	mg/L	Metalyser	HM 1000	Manganese Standard, Buffers	Voltametric Stripping	APHA 3130 A
22	Arsenic	mg/L	Metalyser	HM 1000	Arsenic Standard, Buffers	Voltametric Stripping	APHA 3130 A
23	Chromium	mg/L	Colorimeter	HM 1000	Diphenyl Carbazide, Nitric Acid	Colorimetric	APHA 3500-CR B
24	Mercury	mg/L	Metalyser	HM 1000	Mercury Standard and Buffer	Voltametric Stripping	APHA 3130 A
25	Silver	mg/L	AAS	BULK	Silver Standard	AAS	APHA
26	TBC	cfu/ml	Membrane Filtration Machine	D-79112	Pads, Media and Filters	Membrane Filtration	APHA 9222B
27	E – Coli	cfu/ml		D-79112	Pads, Media and Filters	Membrane Filtration	APHA 9222B

APPENDIX C

EFFECT OF CONTACT TIME

Table 1: Effect of Contact Time on the Removal of Total Iron from Domestic Wastewater

Adsorbents	Mass (g)	Iron (mg/L)	Temp (°C)	Total Iron Concentration (mg/L) at various contact times						Adsorbents Percentage Removal (%) at various contact time					
				10 min	20 min	30 min	40 min	50 min	60 min	10 min	20 min	30 min	40 min	50 min	60 min
BKC	25.0	0.830	29.5	0.490	0.343	0.3087	0.123	0.139	0.139	41.0	58.7	62.8	85.1	83.3	83.3
BKC/ZnO	25.0	0.830	29.5	0.390	0.273	0.2457	0.098	0.034	0.034	53.0	67.1	70.4	88.2	95.9	95.9
BKC/Ag	25.0	0.830	29.5	0.380	0.266	0.2394	0.096	0.034	0.034	54.2	68.0	71.2	88.5	96.0	96.0
BKC/Ag/ZnO	25.0	0.830	29.5	0.350	0.245	0.2205	0.088	0.026	0.026	57.8	70.5	73.4	89.4	96.8	96.8

Table 2: Effect of Contact Time on the Removal of Lead from Domestic Wastewater

Adsorbents	Mass (g)	Lead (mg/L)	Temp (°C)	Lead Concentration (mg/L) at various contact time						Adsorbents Percentage Removal (%) at various contact time					
				10 min	20 min	30 min	40 min	50 min	60 min	10 min	20 min	30 min	40 min	50 min	60 min
BKC	25.0	0.140	29.5	0.120	0.084	0.076	0.030	0.009	0.009	14.3	40.0	46.0	78.4	93.5	93.5
BKC/ZnO	25.0	0.140	29.5	0.110	0.079	0.071	0.028	0.008	0.008	21.4	43.6	50.5	80.2	94.1	94.1
BKC/Ag	25.0	0.140	29.5	0.110	0.081	0.073	0.029	0.009	0.009	21.4	42.1	47.9	79.2	93.8	93.8
BKC/Ag/ZnO	25.0	0.140	29.5	0.090	0.063	0.057	0.023	0.007	0.007	35.7	55.0	59.5	83.8	95.1	95.1

Table 3: Effect of Contact Time on the Removal of Copper from Domestic Wastewater

Adsorbents	Mass (g)	Copper (mg/L)	Temp (°C)	Copper Concentration (mg/L) at various contact time						Adsorbents Percentage Removal (%) at various contact time					
				10 min	20 min	30 min	40 min	50 min	60 min	10 min	20 min	30 min	40 min	50 min	60 min
BKC	25.0	0.050	29.5	0.043	0.032	0.0259	0.010	0.008	0.008	20.0	36.0	48.2	79.8	84.9	84.9
BKC/ZnO	25.0	0.050	29.5	0.040	0.029	0.0257	0.010	0.002	0.002	21.0	42.0	48.6	79.4	95.9	95.9
BKC/Ag	25.0	0.050	29.5	0.041	0.028	0.0252	0.010	0.002	0.002	22.0	44.0	49.6	79.8	96.0	96.0
BKC/Ag/ZnO	25.0	0.050	29.5	0.030	0.021	0.0189	0.008	0.002	0.002	40.0	58.0	62.2	84.9	97.0	97.0

Table 4: Effect of Contact Time on the Removal of Manganese from Domestic Wastewater

Adsorbents	Mass (g)	Manganese (mg/L)	Temp (°C)	Manganese Concentration (mg/L) at various contact time						Adsorbents Percentage Removal (%) at various contact time					
				10 min	20 min	30 min	40 min	50 min	10 min	10 min	20 min	30 min	40 min	50 min	60 min
BKC	25.0	0.250	29.5	0.190	0.133	0.1197	0.048	0.010	0.010	24.0	46.8	52.1	80.8	96.2	96.2
BKC/ZnO	25.0	0.250	29.5	0.170	0.119	0.1071	0.043	0.009	0.009	32.0	52.4	57.2	82.9	96.6	96.6
BKC/Ag	25.0	0.250	29.5	0.170	0.119	0.1071	0.043	0.009	0.009	32.0	52.4	57.2	82.9	96.6	96.6
BKC/Ag/ZnO	25.0	0.250	29.5	0.150	0.105	0.0945	0.038	0.008	0.008	40.0	58.0	62.2	84.9	97.0	97.0

Table 5: Effect of Contact Time on the Removal of Arsenic from Domestic Wastewater

Adsorbents	Mass (g)	Arsenic (mg/L)	Temp (°C)	Arsenic Concentration (mg/L) at various contact time						Adsorbents Percentage Removal (%) at various contact time					
				10 min	20 min	30 min	40 min	50 min	10 min	10 min	20 min	30 min	40 min	50 min	60 min
BKC	25.0	0.220	29.5	0.095	0.0665	0.05985	0.024	0.020	0.020	56.8	69.8	72.8	89.1	90.8	90.8
BKC/ZnO	25.0	0.220	29.5	0.085	0.0595	0.05355	0.021	0.020	0.020	61.4	73.0	75.7	90.3	90.8	90.8
BKC/Ag	25.0	0.220	29.5	0.088	0.0616	0.05544	0.022	0.020	0.020	60.0	72.0	74.8	89.9	90.8	90.8
BKC/Ag/ZnO	25.0	0.220	29.5	0.082	0.0574	0.05166	0.021	0.020	0.020	62.7	73.9	76.5	90.6	90.8	90.8

Table 6: Effect of Contact Time on the Removal of Mercury from Domestic Wastewater

Adsorbents	Mass (g)	Mercury (mg/L)	Temp (°C)	Mercury Concentration (mg/L) at various contact time						Adsorbents Percentage Removal (%) at various contact time					
				10 min	20 min	30 min	40 min	50 min	10 min	10 min	20 min	30 min	40 min	50 min	60 min
BKC	25.0	0.110	29.5	0.092	0.0644	0.05796	0.023	0.018	0.018	16.4	41.5	47.3	78.9	84.0	84.0
BKC/ZnO	25.0	0.110	29.5	0.075	0.0525	0.04725	0.019	0.018	0.018	31.8	52.3	57.0	82.8	84.0	84.0
BKC/Ag	25.0	0.110	29.5	0.073	0.0511	0.04599	0.018	0.018	0.018	33.6	53.5	58.2	83.3	84.0	84.0
BKC/Ag/ZnO	25.0	0.110	29.5	0.071	0.0497	0.04473	0.018	0.018	0.018	35.5	54.8	59.3	83.7	84.0	84.0

Table 7: Effect of Contact Time on the Removal of Silver from Domestic Wastewater

Adsorbents	Mass (g)	Silver (mg/L)	Temp (°C)	Silver Concentration (mg/L) at various contact time						Adsorbents Percentage Removal (%) at various contact time					
				10 min	20 min	30 min	40 min	50 min	10 min	10 min	20 min	30 min	40 min	50 min	60 min
BKC	25.0	0.0200	29.5	0.012	0.0084	0.00756	0.003	0.003	0.003	40	58.0	62.2	84.9	87.4	87.4
BKC/ZnO	25.0	0.0200	29.5	0.012	0.0084	0.00756	0.003	0.003	0.003	40	58.0	62.2	84.9	87.4	87.4
BKC/Ag	25.0	0.0200	29.5	0.013	0.0091	0.00819	0.003	0.003	0.003	35	54.5	59.1	83.6	87.4	87.4
BKC/Ag/ZnO	25.0	0.0200	29.5	0.012	0.0084	0.00756	0.003	0.003	0.003	40	58.0	62.2	84.9	87.4	87.4

Table 8: Effect of Contact Time on the Removal of Zinc from Domestic Wastewater

Adsorbents	Mass (g)	Zinc (mg/L)	Temp (°C)	Zinc Concentration (mg/L) at various contact time						Adsorbents Percentage Removal (%) at various contact time					
				10 min	20 min	30 min	40 min	50 min	10 min	10 min	20 min	30 min	40 min	50 min	60 min
BKC	25.0	2.46	29.5	0.971	0.6797	0.61173	0.245	0.219	0.219	60.5	72.4	75.1	90.1	91.1	91.1
BKC/ZnO	25.0	2.46	29.5	0.994	0.6958	0.62622	0.250	0.219	0.219	59.6	71.7	74.5	89.8	91.1	91.1
BKC/Ag	25.0	2.46	29.5	0.959	0.6713	0.60417	0.242	0.219	0.219	61.0	72.7	75.4	90.2	91.1	91.1
BKC/Ag/ZnO	25.0	2.46	29.5	0.87	0.6090	0.5481	0.219	0.219	0.219	64.6	75.2	77.7	91.1	91.1	91.1

Table 9: Effect of Contact Time on the Removal of Nitrate from Domestic Wastewater

Adsorbents	Mass (g)	Nitrate (mg/L)	Temp (°C)	Nitrate Concentration (mg/L) at various contact time						Adsorbents Percentage Removal (%) at various contact time					
				10 min	20 min	30 min	40 min	50 min	10 min	10min	20 min	30 min	40 min	50 min	60 min
BKC	25.0	233	29.5	40.4	28.28	25.452	20.362	10.500	10.500	82.7	87.9	89.1	91.3	95.5	95.5
BKC/ZnO	25.0	233	29.5	35.7	24.99	22.491	17.993	10.500	10.500	84.7	89.3	90.3	92.3	95.5	95.5
BKC/Ag	25.0	233	29.5	34.8	24.36	21.924	17.539	10.500	10.500	85.1	89.5	90.6	92.5	95.5	95.5
BKC/Ag/ZnO	25.0	233	29.5	32.4	22.68	20.412	16.330	10.500	10.500	86.1	90.3	91.2	93.0	95.5	95.5

Table 10: Effect of Contact Time on the Removal of Phosphate from Domestic Wastewater

Adsorbents	Mass (g)	Phosphate (mg/L)	Temp (°C)	Phosphate Concentration (mg/L) at various contact time						Adsorbents Percentage Removal (%) at various contact time					
				10 min	20 min	30 min	40 min	50 min	10 min	10 min	20 min	30 min	40 min	50 min	60 min
BKC	25.0	11.8	29.5	0.29	0.203	0.1827	0.073	0.015	0.015	97.5	98.3	98.5	99.4	99.9	99.9
BKC/ZnO	25.0	11.8	29.5	0.27	0.189	0.1701	0.068	0.014	0.014	97.7	98.4	98.6	99.4	99.9	99.9
BKC/Ag	25.0	11.8	29.5	0.28	0.196	0.1764	0.071	0.014	0.014	97.6	98.3	98.5	99.4	99.9	99.9
BKC/Ag/ZnO	25.0	11.8	29.5	0.25	0.175	0.1575	0.063	0.013	0.013	97.9	98.5	98.7	99.5	99.9	99.9

Table 11: Effect of Contact Time on the Removal of Ammonium from Domestic Wastewater

Adsorbents	Mass (g)	Ammonium (mg/L)	Temp (°C)	Ammonium Concentration (mg/L) at various contact time						Adsorbents Percentage Removal (%) at various contact time					
				10 min	20 min	30 min	40 min	50 min	10 min	10 min	20 min	30 min	40 min	50 min	10 min
BKC	25.0	37.2	29.5	1.63	1.141	1.0269	0.411	0.082	0.082	95.6	96.9	97.2	98.9	99.8	99.8
BKC/ZnO	25.0	37.2	29.5	1.65	1.155	1.0395	0.416	0.083	0.083	95.6	96.9	97.2	98.9	99.8	99.8
BKC/Ag	25.0	37.2	29.5	1.68	1.176	1.0584	0.423	0.085	0.085	95.5	96.8	97.2	98.9	99.8	99.8
BKC/Ag/ZnO	25.0	37.2	29.5	1.55	1.085	0.9765	0.391	0.078	0.078	95.8	97.1	97.4	99.0	99.8	99.8

Table 12: Effect of Contact Time on the Removal of COD from Domestic Wastewater

Adsorbents	Mass (g)	COD (mg/L)	Temp (°C)	COD Concentration (mg/L) at various contact time						Adsorbents Percentage Removal (%) at various contact time					
				10 min	20 min	30 min	40 min	50 min	10 min	10 min	20 min	30 min	40 min	50 min	10 min
BKC	25.0	312	29.5	37.2	26.04	23.436	23.202	22.738	22.738	88.1	91.7	92.5	92.6	92.7	92.7
BKC/ZnO	25.0	312	29.5	37.1	25.97	23.373	23.139	22.676	22.676	88.1	91.7	92.5	92.6	92.7	92.7
BKC/Ag	25.0	312	29.5	36.9	25.83	23.247	23.015	22.554	22.554	88.2	91.7	92.5	92.6	92.8	92.8
BKC/Ag/ZnO	25.0	312	29.5	34.2	23.94	21.546	21.331	20.904	20.904	89.0	92.3	93.1	93.2	93.3	93.3

Table 13: Effect of Contact Time on the Removal of BOD from Domestic Wastewater

Adsorbents	Mass (g)	BOD (mg/L)	Temp (°C)	BOD Concentration (mg/L) at various contact time						Adsorbents Percentage Removal (%) at various contact time					
				10 min	20 min	30 min	40 min	50 min	10 min	10 min	20 min	30 min	40 min	50 min	10 min
BKC	25.0	30.6	29.5	5.23	3.661	3.2949	3.262	3.197	3.197	82.9	88.0	89.2	89.3	89.6	89.6
BKC/ZnO	25.0	30.6	29.5	8.49	5.943	5.3487	5.295	5.189	5.189	72.3	80.6	82.5	82.7	83.0	83.0
BKC/Ag	25.0	30.6	29.5	8.48	5.936	5.3424	5.289	5.183	5.183	72.3	80.6	82.5	82.7	83.1	83.1
BKC/Ag/ZnO	25.0	30.6	29.5	8.25	5.775	5.1975	5.146	5.043	5.043	73.0	81.1	83.0	83.2	83.5	83.5

Table 14: Effect of Contact Time on the Removal of Oil and Grease from Domestic Wastewater

Adsorbents	Mass (g)	Oil and Grease (mg/L)	Temp (°C)	Oil and Grease Concentration (mg/L) at various contact time						Adsorbents Percentage Removal (%) at various contact time					
				10 min	20 min	30 min	40 min	50 min	10 min	10 min	20 min	30 min	40 min	50 min	10 min
BKC	25.0	10.1	29.5	0.28	0.196	0.1764	0.000	0.000	0.000	97.2	98.1	98.3	100.0	100.0	100.0
BKC/ZnO	25.0	10.1	29.5	0.26	0.182	0.1638	0.000	0.000	0.000	97.4	98.2	98.4	100.0	100.0	100.0
BKC/Ag	25.0	10.1	29.5	0.28	0.196	0.1764	0.000	0.000	0.000	97.2	98.1	98.3	100.0	100.0	100.0
BKC/Ag/ZnO	25.0	10.1	29.5	0.25	0.175	0.1575	0.000	0.000	0.000	97.5	98.3	98.4	100.0	100.0	100.0

Table 15: Effect of Contact Time on the pH Improvement of the Domestic Wastewater

Adsorbents	Mass (g)	Initial pH	Temp (°C)	Adsorbents Treated pH at various contact time					
				10 min	20 min	30 min	40 min	50 min	10 min
BKC	25.0	8.96	29.5	7.55	7.50	7.45	7.45	7.44	7.45
BKC/ZnO	25.0	8.96	29.5	7.81	7.54	7.40	7.42	7.4	7.38
BKC/Ag	25.0	8.96	29.5	6.77	6.92	7.25	7.22	7.28	7.29
BKC/Ag/ZnO	25.0	8.96	29.5	6.97	7.00	7.10	7.200	7.200	7.20

Table 16: Effect of Contact Time on the Removal of Turbidity from Domestic Wastewater

Adsorbents	Mass (g)	Initial Turbidity (NTU)	Temp (°C)	Turbidity Values (NTU) at various contact time						Adsorbents Percentage Removal (%) at various contact time					
				10 min	20 min	30 min	40 min	50 min	10 min	10 min	20 min	30 min	40 min	50 min	10 min
BKC	25.0	248	29.5	16.20	11.34	10.21	4.08	0.02	0.02	93.47	95.43	95.88	98.35	99.99	99.99
BKC/ZnO	25.0	248	29.5	15.80	11.06	9.95	3.98	0.02	0.02	93.63	95.54	95.99	98.39	99.99	99.99
BKC/Ag	25.0	248	29.5	15.50	10.85	9.77	3.91	0.02	0.02	93.75	95.63	96.06	98.43	99.99	99.99
BKC/Ag/ZnO	25.0	248	29.5	15.00	10.50	9.45	3.78	0.02	0.02	93.95	95.77	96.19	98.48	99.99	99.99

Table 17: Effect of Contact Time on the Improvement of Dissolved Oxygen (DO) of Domestic Wastewater

Adsorbents	Mass (g)	DO (mg/L)	Temp (°C)	Concentration (mg/L) at various Dosages						Percentage Removal (%) at various Dosages					
				10 min	20 min	30 min	40 min	50 min	10 min	10 min	20 min	30 min	40 min	50 min	10 min
BKC	25.0	1.00	29.5	4.05	4.20	4.23	4.59	4.80	4.86	75.3	76.2	76.4	78.2	79.2	79.4
BKC/ZnO	25.0	1.00	29.5	4.11	4.40	4.6	4.62	4.81	4.85	75.7	77.3	78.3	78.4	79.2	79.4
BKC/Ag	25.0	1.00	29.5	4.02	4.24	4.65	4.68	4.82	4.87	75.1	76.4	78.5	78.6	79.3	79.5
BKC/Ag/ZnO	25.0	1.00	30.0	4.18	4.25	4.55	4.64	4.82	4.88	76.1	76.5	78.0	78.4	79.3	79.5

Table 18: Effect of Contact Time on the Removal of Suspended Solids (SS) from Domestic Wastewater

Adsorbents	Mass (g)	SS (mg/L)	Temp (°C)	Suspended Solid Concentration (NTU) at various contact time						Adsorbents Percentage Removal (%) at various contact time					
				10 min	20 min	30 min	40 min	50 min	10 min	10 min	20 min	30 min	40 min	50 min	10 min
BKC	25.0	233	29.5	13.0	9.1	8.19	3.276	0.020	0.020	94.4	96.1	96.5	98.6	100	100
BKC/ZnO	25.0	233	29.5	14.0	9.8	8.82	3.528	0.020	0.020	94.0	95.8	96.2	98.5	100	100
BKC/Ag	25.0	233	29.5	15.0	10.5	9.45	3.780	0.020	0.020	93.6	95.5	95.9	98.4	100	100
BKC/Ag/ZnO	25.0	233	29.5	16.0	11.2	10.08	4.032	0.020	0.020	93.1	95.2	95.7	98.3	100	100

Table 19: Effect of Contact Time on the Removal of Colour from Domestic Wastewater

Adsorbents	Mass (g)	Colour (TCU)	Temp (°C)	Colour (TCU) at various Contact Time						Adsorbents Percentage Removal (%) at various contact time					
				10 min	20 min	30 min	40 min	50 min	10 min	10 min	20 min	30 min	40 min	50 min	10 min
BKC	25.0	1620	29.5	20.0	14.00	12.6	5.040	0.000	0.000	98.8	99.1	99.2	99.7	100	100
BKC/ZnO	25.0	1620	29.5	18.5	12.95	11.655	4.662	0.000	0.000	98.9	99.2	99.3	99.7	100	100
BKC/Ag	25.0	1620	29.5	18.2	12.74	11.466	4.586	0.000	0.000	98.9	99.2	99.3	99.7	100	100
BKC/Ag/ZnO	25.0	1620	29.5	16.0	11.20	10.08	4.032	0.000	0.000	99.0	99.3	99.4	99.8	100	100

Table 20: Effect of Contact Time on the Reduction of Electrical Conductivity (EC) of the Domestic Wastewater

Adsorbents	Mass (g)	EC ((µS/cm)	Temp (°C)	Adsorbents Treated EC (NTU) at various contact time						Adsorbents Percentage Removal (%) at various contact time					
				10 min	20 min	30 min	40 min	50 min	10 min	10 min	20 min	30 min	40 min	50 min	10 min
BKC	25.0	1382	29.5	612	428	386	382	374	374	55.7	69.0	72.1	72.4	73.0	73.0
BKC/ZnO	25.0	1382	29.5	613	429	386	382	375	375	55.6	69.0	72.1	72.3	73.0	73.0
BKC/Ag	25.0	1382	29.5	614	430	387	383	375	375	55.6	68.9	72.0	72.3	73.0	73.0
BKC/Ag/ZnO	25.0	1382	29.5	615	431	387	384	376	376	55.5	68.8	72.0	72.2	73.0	73.0

Table 21: Effect of Contact Time on the Removal of Total Coliforms (TC) of the Domestic Wastewater

Adsorbents	Mass (g)	TC (cfu/100mL)	Temp (°C)	Total Coliforms loads (cfu/ml) at various contact time						Adsorbents Percentage Removal (%) at various contact time					
				10 min	20 min	30 min	40 min	50 min	10 min	10 min	20 min	30 min	40 min	50 min	10 min
BKC	25.0	6000	29.5	4200	2940	2646	2381	2143	1929	30.0	51.0	55.9	60.3	64.3	67.9
BKC/ZnO	25.0	6000	29.5	1800	1260	1134	1021	919	827	70.0	79.0	81.1	83.0	84.7	86.2
BKC/Ag	25.0	6000	29.5	800	560	0	0	0	0	86.7	90.7	100	100	100	100
BKC/Ag/ZnO	25.0	6450	29.5	680	476	0	0	0	0	89.5	92.6	100	100	100	100

Table 22: Effect of Contact Time on the Removal of Faecal Coliforms of the Domestic Wastewater

Adsorbents	Mass (g)	FC (cfu/mL)	Temp (°C)	Adsorbents Treated Values of FC (cfu/ml) at various contact time						Adsorbents Percentage Removal (%) at various contact time					
				10 min	20 min	30 min	40 min	50 min	10 min	10 min	20 min	30 min	40 min	50 min	10 min
BKC	25.0	640	29.5	440	308	277	249	225	202	31.3	51.9	56.7	61.0	64.9	68.4
BKC/ZnO	25.0	640	29.5	224	157	141	127	114	103	65.0	75.5	78.0	80.2	82.1	83.9
BKC/Ag	25.0	640	29.5	96	67	0	0	0	0	85.0	89.5	100	100	100	100
BKC/Ag/ZnO	25.0	640	29.5	80	56	0	0	0	0	87.5	91.3	100	100	100	100

Table 23: Effect of Contact Time on the Removal of *Clostridium Perfringens* of the Domestic Wastewater

Adsorbents	Mass (g)	*Clostridium perfringens* (cfu/mL)	Temp (°C)	*Clostridium perfringens* loads (cfu/ml) at various contact time						Adsorbents Percentage Removal (%) at various contact time					
				10 min	20 min	30 min	40 min	50 min	10 min	10 min	20 min	30 min	40 min	50 min	10 min
BKC	25.0	40	29.5	38	27	24	22	19	17	5.0	33.5	40.2	46.1	51.5	56.4
BKC/ZnO	25.0	40	29.5	34	24	21	19	17	16	15.0	40.5	46.5	51.8	56.6	61.0
BKC/Ag	25.0	40	29.5	20	14	0	0	0	0	50.0	65.0	100	100	100	100
BKC/Ag/ZnO	25.0	40	29.5	16	11	0	0	0	0	60.0	72.0	100	100	100	100

Table 24: Effect of Contact Time on the Removal of *E. coli* of the Domestic Wastewater

Adsorbents	**Mass (g)**	***E. coli* (cfu/mL)**	**Temp (°C)**	**Adsorbents Treated Values of *E. coli* (cfu/ml) at various contact time**					**Adsorbents Percentage Removal (%) at various contact time**					
				10 min	**20 min**	**30 min**	**40 min**	**50 min**	**10 min**	**10 min**	**20 min**	**30 min**	**40 min**	**50 min**	**10 min**
BKC	25.0	400	29.5	244	171	154	138	125	112	39.0	57.3	61.6	65.4	68.9	72.0
BKC/ZnO	25.0	400	29.5	180	126	113	102	92	83	55.0	68.5	71.7	74.5	77.0	79.3
BKC/Ag	25.0	400	29.5	32	22	0	0	0	0	92.0	94.4	100.0	100.0	100.0	100.0
BKC/Ag/ZnO	25.0	400	29.5	24	17	0	0	0	0	94.0	95.8	100.0	100.0	100.0	100.0

APPENDIX D

EFFECT OF DOSAGE

Table 1: Effect of Dosage on the Removal of Total Iron from Domestic Wastewater

Adsorbents	Contact Time (Min)	Total Iron (mg/L)	Temp (°C)	Total Iron Concentration (mg/L) at various Dosages						Adsorbents Percentage Removal (%) at various Dosages					
				5 g	10 g	15 g	20 g	25 g	30 g	5 g	10 g	15 g	20 g	25 g	30 g
BKC	30.0	0.830	29.5	0.730	0.511	0.4599	0.184	0.139	0.139	12.0	38.4	44.6	77.8	83.3	83.3
BKC/ZnO	30.0	0.830	29.5	0.710	0.497	0.4473	0.179	0.063	0.063	14.5	40.1	46.1	78.4	92.5	92.5
BKC/Ag	30.0	0.830	29.5	0.713	0.4991	0.44919	0.180	0.063	0.063	14.1	39.9	45.9	78.4	92.4	92.4
BKC/Ag/ZnO	30.0	0.830	29.5	0.690	0.483	0.4347	0.174	0.052	0.052	16.9	41.8	47.6	79.1	93.7	93.7

Table 2: Effect of Dosage on the Removal of Lead from Domestic Wastewater

Adsorbents	Contact Time (Min)	Lead (mg/L)	Temp (°C)	Concentration (mg/L) at various Dosages						Percentage Removal (%) at various Dosages					
				5 g	10 g	15 g	20 g	25 g	30 g	5 g	10 g	15 g	20 g	25 g	30 g
BKC	30.0	0.140	29.5	0.125	0.088	0.079	0.032	0.009	0.009	10.7	37.5	43.8	77.5	93.3	93.3
BKC/ZnO	30.0	0.140	29.5	0.122	0.085	0.077	0.031	0.009	0.009	12.9	39.0	45.1	78.0	93.4	93.4
BKC/Ag	30.0	0.140	29.5	0.123	0.086	0.077	0.031	0.009	0.009	12.1	38.5	44.7	77.9	93.4	93.4
BKC/Ag/ZnO	30.0	0.140	29.5	0.111	0.078	0.070	0.028	0.008	0.008	20.7	44.5	50.1	80.0	94.0	94.0

Table 3: Effect of Dosage on the Removal of Copper from Domestic Wastewater

Adsorbents	Contact Time (Min)	Copper (mg/L)	Temp (°C)	Concentration (mg/L) at various Dosages						Percentage Removal (%) at various Dosages					
				5 g	10 g	15 g	20 g	25 g	30 g	5 g	10 g	15 g	20 g	25 g	30 g
BKC	30.0	0.050	29.5	0.048	0.0336	0.03024	0.012	0.008	0.008	4.0	32.8	39.5	75.8	84.9	84.9
BKC/ZnO	30.0	0.050	29.5	0.047	0.0329	0.02961	0.012	0.002	0.002	6.0	34.2	40.8	76.3	95.3	95.3
BKC/Ag	30.0	0.050	29.5	0.047	0.0329	0.02961	0.012	0.002	0.002	6.0	34.2	40.8	76.3	95.3	95.3
BKC/Ag/ZnO	30.0	0.050	29.5	0.045	0.0315	0.02835	0.011	0.002	0.002	10.0	37.0	43.3	77.3	95.5	95.5

Table 4: Effect of Dosage on the Removal of Manganese from Domestic Wastewater

Adsorbents	Contact Time (Min)	Manganese (mg/L)	Temp (°C)	Concentration (mg/L) at various Dosages						Percentage Removal (%) at various Dosages					
				5 g	10 g	15 g	20 g	25 g	30 g	5 g	10 g	15 g	20 g	25 g	30 g
BKC	30.0	0.250	29.5	0.238	0.1666	0.14994	0.060	0.012	0.012	4.8	33.4	40.0	76.0	95.2	95.2
BKC/ZnO	30.0	0.250	29.5	0.230	0.161	0.1449	0.058	0.012	0.012	8.0	35.6	42.0	76.8	95.4	95.4
BKC/Ag	30.0	0.250	29.5	0.228	0.1596	0.14364	0.057	0.011	0.011	8.8	36.2	42.5	77.0	95.4	95.4
BKC/Ag/ZnO	30.0	0.250	29.5	0.225	0.1575	0.14175	0.057	0.011	0.011	10.0	37.0	43.3	77.3	95.5	95.5

Table 5: Effect of Dosage on the Removal of Arsenic from Domestic Wastewater

Adsorbents	Contact Time (Min)	Arsenic (mg/L)	Temp (°C)	Concentration (mg/L) at various Dosages						Percentage Removal (%) at various Dosages					
				5 g	10 g	15 g	20 g	25 g	30 g	5 g	10 g	15 g	20 g	25 g	30 g
BKC	30.0	0.220	29.5	0.215	0.1505	0.13545	0.054	0.020	0.020	2.3	31.6	38.4	75.4	90.8	90.8
BKC/ZnO	30.0	0.220	29.5	0.2	0.14	0.126	0.050	0.020	0.020	9.1	36.4	42.7	77.1	90.8	90.8
BKC/Ag	30.0	0.220	29.5	0.199	0.1393	0.12537	0.050	0.020	0.020	9.5	36.7	43.0	77.2	90.8	90.8
BKC/Ag/ZnO	30.0	0.220	29.5	0.17	0.119	0.1071	0.043	0.020	0.020	22.7	45.9	51.3	80.5	90.8	90.8

Table 6: Effect of Dosage on the Removal of Mercury from Domestic Wastewater

Adsorbents	Contact Time (Min)	Mercury (mg/L)	Temp (°C)	Concentration (mg/L) at various Dosages						Percentage Removal (%) at various Dosages					
				5 g	10 g	15 g	20 g	25 g	30 g	5 g	10 g	15 g	20 g	25 g	30 g
BKC	30.0	0.110	29.5	0.101	0.0707	0.06363	0.025	0.018	0.018	8.2	35.7	42.2	76.9	84.0	84.0
BKC/ZnO	30.0	0.110	29.5	0.1	0.07	0.063	0.025	0.018	0.018	9.1	36.4	42.7	77.1	84.0	84.0
BKC/Ag	30.0	0.110	29.5	0.1	0.07	0.063	0.025	0.018	0.018	9.1	36.4	42.7	77.1	84.0	84.0
BKC/Ag/ZnO	30.0	0.110	29.5	0.099	0.0693	0.06237	0.025	0.018	0.018	10.0	37.0	43.3	77.3	84.0	84.0

Table 7: Effect of Dosage on the Removal of Silver from Domestic Wastewater

Adsorbents	Contact Time (Min)	Silver (mg/L)	Temp (°C)	Concentration (mg/L) at various Dosages						Percentage Removal (%) at various Dosages					
				5 g	10 g	15 g	20 g	25 g	30 g	5 g	10 g	15 g	20 g	25 g	30 g
BKC	30.0	0.02	29.5	0.02	0.014	0.0126	0.005	0.003	0.003	0	30.0	37.0	74.8	87.4	87.4
BKC/ZnO	30.0	0.02	29.5	0.017	0.0119	0.01071	0.004	0.003	0.003	15	40.5	46.5	78.6	87.4	87.4
BKC/Ag	30.0	0.02	29.5	0.017	0.0116	0.0104	0.004	0.003	0.003	18	42.3	48.0	79.2	87.4	87.4
BKC/Ag/ZnO	30.0	0.02	29.5	0.016	0.0112	0.01008	0.004	0.003	0.003	20	44.0	49.6	79.8	87.4	87.4

Table 8: Effect of Dosage on the Removal of Zinc from Domestic Wastewater

Adsorbents	Contact Time (Min)	Zinc (mg/L)	Temp (°C)	Concentration (mg/L) at various Dosages						Percentage Removal (%) at various Dosages					
				5 g	10 g	15 g	20 g	25 g	30 g	5 g	10 g	15 g	20 g	25 g	30 g
BKC	30.0	2.46	29.5	2.05	1.435	1.2915	0.517	0.219	0.219	16.7	41.7	47.5	79.0	91.1	91.1
BKC/ZnO	30.0	2.46	29.5	1.96	1.372	1.2348	0.494	0.219	0.219	20.3	44.2	49.8	79.9	91.1	91.1
BKC/Ag	30.0	2.46	29.5	1.94	1.358	1.2222	0.489	0.219	0.219	21.1	44.8	50.3	80.1	91.1	91.1
BKC/Ag/ZnO	30.0	2.46	29.5	1.87	1.309	1.1781	0.471	0.219	0.219	24.0	46.8	52.1	80.8	91.1	91.1

Table 9: Effect of Dosage on the Removal of Nitrate from Domestic Wastewater

Adsorbents	Contact Time (Min)	Nitrate (mg/L)	Temp (°C)	Concentration (mg/L) at various Dosages						Percentage Removal (%) at various Dosages					
				5 g	10 g	15 g	20 g	25 g	30 g	5 g	10 g	15 g	20 g	25 g	30 g
BKC	30.0	233	29.5	187	130.9	117.81	10.5	10.7	10.5	19.7	43.8	49.4	95.5	95.5	95.2
BKC/ZnO	30.0	233	29.5	180	126	113.4	10.5	10.4	10.5	22.7	45.9	51.3	95.5	95.5	95.5
BKC/Ag	30.0	233	29.5	181	126.7	114.03	10.5	10.5	10.6	22.3	45.6	51.1	95.5	95.5	95.5
BKC/Ag/ZnO	30.0	233	29.5	176	123.2	110.88	10.5	10.1	10.1	24.5	47.1	52.4	95.5	95.5	95.5

Table 10: Effect of Dosage on the Removal of Phosphate from Domestic Wastewater

Adsorbents	Contact Time (Min)	Phosphate (mg/L)	Temp (°C)	Concentration (mg/L) at various Dosages						Percentage Removal (%) at various Dosages					
				5 g	10 g	15 g	20 g	25 g	30 g	5 g	10 g	15 g	20 g	25 g	30 g
BKC	30.0	11.8	29.5	8.45	5.915	5.3235	2.129	0.426	0.426	28.4	49.9	54.9	82.0	96.4	96.4
BKC/ZnO	30.0	11.8	29.5	8.1	5.67	5.103	2.041	0.408	0.408	31.4	51.9	56.8	82.7	96.5	96.5
BKC/Ag	30.0	11.8	29.5	8.11	5.677	5.1093	2.044	0.409	0.409	31.3	51.9	56.7	82.7	96.5	96.5
BKC/Ag/ZnO	30.0	11.8	29.5	7.95	5.565	5.0085	2.003	0.401	0.401	32.6	52.8	57.6	83.0	96.6	96.6

Table 11: Effect of Dosage on the Removal of Ammonium from Domestic Wastewater

Adsorbents	Contact Time (Min)	Ammonium (mg/L)	Temp (°C)	Concentration (mg/L) at various Dosages						Percentage Removal (%) at various Dosages					
				5 g	10 g	15 g	20 g	25 g	30 g	5 g	10 g	15 g	20 g	25 g	30 g
BKC	30.0	37.2	29.5	29.2	20.44	18.396	7.358	1.472	1.472	21.5	45.1	50.5	80.2	96.0	96.0
BKC/ZnO	30.0	37.2	29.5	28.9	20.23	18.207	7.283	1.457	1.457	22.3	45.6	51.1	80.4	96.1	96.1
BKC/Ag	30.0	37.2	29.5	28.4	19.88	17.892	7.157	1.431	1.431	23.7	46.6	51.9	80.8	96.2	96.2
BKC/Ag/ZnO	30.0	37.2	29.5	27.8	19.46	17.514	7.006	1.401	1.401	25.3	47.7	52.9	81.2	96.2	96.2

Table 12: Effect of Dosage on the Removal of COD from Domestic Wastewater

Adsorbents	Contact Time (Min)	COD (mg/L)	Temp (°C)	Concentration (mg/L) at various Dosages						Percentage Removal (%) at various Dosages					
				5 g	10 g	15 g	20 g	25 g	30 g	5 g	10 g	15 g	20 g	25 g	30 g
BKC	30.0	312	29.5	144	101	90.7	89.8	88.0	88.0	53.8	67.7	70.9	71.2	71.8	71.8
BKC/ZnO	30.0	312	29.5	138	96.6	86.9	86.1	84.3	84.3	55.8	69.0	72.1	72.4	73.0	73.0
BKC/Ag	30.0	312	29.5	139	97.3	87.6	86.7	85.0	85.0	55.4	68.8	71.9	72.2	72.8	72.8
BKC/Ag/ZnO	30.0	312	29.5	130	91.0	81.9	81.1	79.5	79.5	58.3	70.8	73.8	74.0	74.5	74.5

Table 13: Effect of Dosage on the Removal of BOD from Domestic Wastewater

Adsorbents	Contact Time (Min)	BOD (mg/L)	Temp (°C)	Concentration (mg/L) at various Dosages						Percentage Removal (%) at various Dosages					
				5 g	10 g	15 g	20 g	25 g	30 g	5 g	10 g	15 g	20 g	25 g	30 g
BKC	30.0	30.6	29.5	15.2	10.64	9.576	9.480	9.291	9.291	50.3	65.2	68.7	69.0	69.6	69.6
BKC/ZnO	30.0	30.6	29.5	14.3	10.01	9.009	8.919	8.741	8.741	53.3	67.3	70.6	70.9	71.4	71.4
BKC/Ag	30.0	30.6	29.5	13.7	9.59	8.631	8.545	8.374	8.374	55.2	68.7	71.8	72.1	72.6	72.6
BKC/Ag/ZnO	30.0	30.6	29.5	12.9	9.03	8.127	8.046	7.885	7.885	57.8	70.5	73.4	73.7	74.2	74.2

Table 14: Effect of Dosage on the Removal of Oil and Grease from Domestic Wastewater

Adsorbents	Contact Time (Min)	Oil and Grease (mg/L)	Temp (°C)	Concentration (mg/L) at various Dosages						Percentage Removal (%) at various Dosages					
				5 g	10 g	15 g	20 g	25 g	30 g	5 g	10 g	15 g	20 g	25 g	30 g
BKC	30.0	10.1	29.5	7.22	5.054	4.5486	0.000	0.000	0.000	28.5	50.0	55.0	100	100	100
BKC/ZnO	30.0	10.1	29.5	7.21	5.047	4.5423	0.000	0.000	0.000	28.6	50.0	55.0	100	100	100
BKC/Ag	30.0	10.1	29.5	7.02	4.914	4.4226	0.000	0.000	0.000	30.5	51.3	56.2	100	100	100
BKC/Ag/ZnO	30.0	10.1	29.5	6.89	4.823	4.3407	0.000	0.000	0.000	31.8	52.2	57.0	100	100	100

Table 15: Effect of Dosage on the Improvement of pH of Domestic Wastewater

Adsorbents	Contact Time (Min)	Wastewater pH Value	Temp (°C)	Concentration (mg/L) at various Dosages					
				5g	10g	15g	20g	25g	30g
BKC	30.0	8.96	29.5	8.62	8.20	7.45	7.45	7.45	7.45
BKC/ZnO	30.0	8.96	29.5	8.59	8.16	7.40	7.42	7.40	7.38
BKC/Ag	30.0	8.96	29.5	8.53	8.21	7.25	7.22	7.28	7.29
BKC/Ag/ZnO	30.0	8.96	29.5	8.51	8.09	7.10	7.20	7.20	7.20

Table 16: Effect of Dosage on the Removal of Turbidity from Domestic Wastewater

Adsorbents	Contact Time (Min)	Turbidity (NTU)	Temp (°C)	Concentration (mg/L) at various Dosages						Percentage Removal (%) at various Dosages					
				5 g	10 g	15 g	20 g	25 g	30 g	5 g	10 g	15 g	20 g	25 g	30 g
BKC	30.0	248	29.5	158.0	110.60	99.54	39.82	0.02	0.02	36.29	55.40	59.86	83.9	100	100
BKC/ZnO	30.0	248	29.5	149.0	104.30	93.87	37.55	0.02	0.02	39.92	57.94	62.15	84.9	100	100
BKC/Ag	30.0	248	29.5	145.0	101.50	91.35	36.54	0.02	0.02	41.53	59.07	63.17	85.3	100	100
BKC/Ag/ZnO	30.0	248	29.5	139.0	97.30	87.57	35.03	0.02	0.02	43.95	60.77	64.69	85.9	100	100

Table 17: Effect of Dosage on the Improvement of Dissolved Oxygen of Domestic Wastewater

Adsorbents	Contact Time (Min)	Dissolved Oxygen (mg/L)	Temp (°C)	Concentration (mg/L) at various Dosages						Percentage Removal (%) at various Dosages					
				5 g	10 g	15 g	20 g	25 g	30 g	5 g	10 g	15 g	20 g	25 g	30 g
BKC	30.0	1.00	29.5	1.40	4.23	4.23	4.59	4.82	4.82	28.6	76.4	76.4	78.2	79.3	79.3
BKC/ZnO	30.0	1.00	29.5	1.50	4.23	4.51	4.62	4.81	4.81	33.3	76.4	77.8	78.4	79.2	79.2
BKC/Ag	30.0	1.00	29.5	1.55	4.24	4.52	4.61	4.82	4.82	35.5	76.4	77.9	78.3	79.3	79.3
BKC/Ag/ZnO	30.0	1.00	29.5	1.62	4.25	4.55	4.64	4.82	4.82	38.3	76.5	78.0	78.4	79.3	79.3

Table 18: Effect of Dosage on the Removal of Suspended Solid from Domestic Wastewater

Adsorbents	Contact Time (Min)	Suspended Solid (mg/L)	Temp (°C)	Concentration (mg/L) at various Dosages						Percentage Removal (%) at various Dosages					
				5 g	10 g	15 g	20 g	25 g	30 g	5 g	10 g	15 g	20 g	25 g	30 g
BKC	30.0	233	29.5	195.0	136.5	122.85	49.140	0.020	0.020	16.3	41.4	47.3	78.9	100	100
BKC/ZnO	30.0	233	29.5	190.0	133	119.7	47.880	0.020	0.020	18.5	42.9	48.6	79.5	100	100
BKC/Ag	30.0	233	29.5	187.0	130.9	117.81	47.124	0.020	0.020	19.7	43.8	49.4	79.8	100	100
BKC/Ag/ZnO	30.0	233	29.5	180.0	126	113.4	45.360	0.020	0.020	22.7	45.9	51.3	80.5	100	100

Table 19: Effect of Dosage on the Removal of Colour from Domestic Wastewater

Adsorbents	Contact Time (Min)	Colour (TCU)	Temp (°C)	Concentration (mg/L) at various Dosages						Percentage Removal (%) at various Dosages					
				5 g	10 g	15 g	20 g	25 g	30 g	5 g	10 g	15 g	20 g	25 g	30 g
Adsorbents				5g	10g	15g	20g	25g	30g	5g	10g	15g	20g	25g	30g
BKC	30.0	1620	29.5	980.0	686	617.4	246.96	0.000	0.000	39.5	57.7	61.9	84.8	100	100
BKC/ZnO	30.0	1620	29.5	950.0	665	598.5	239.40	0.000	0.000	41.4	59.0	63.1	85.2	100	100
BKC/Ag	30.0	1620	29.5	945.0	661.5	595.35	238.14	0.000	0.000	41.7	59.2	63.3	85.3	100	100
BKC/Ag/ZnO	30.0	1620	29.5	942.0	659.4	593.46	237.38	0.000	0.000	41.9	59.3	63.4	85.3	100	100

Table 20: Effect of Dosage on the Removal of EC from Domestic Wastewater

Adsorbents	Contact Time (Min)	EC (µS/cm)	Temp (°C)	Concentration (mg/L) at various Dosages						Percentage Removal (%) at various Dosages					
				5 g	10 g	15 g	20 g	25 g	30 g	5 g	10 g	15 g	20 g	25 g	30 g
BKC	30.0	1382	29.5	1150	805	724.5	717.3	702.9	702.9	16.8	41.8	47.6	48.1	49	49
BKC/ZnO	30.0	1382	29.5	1021	714.7	643.23	636.8	624.1	624.1	26.1	48.3	53.5	53.9	55	55
BKC/Ag	30.0	1382	29.5	1012	708.4	637.56	631.2	618.6	618.6	26.8	48.7	53.9	54.3	55	55
BKC/Ag/ZnO	30.0	1382	29.5	1006	704.2	633.78	627.4	614.9	614.9	27.2	49.0	54.1	54.6	56	56

Table 21: Effect of Dosage on the Removal of Total Coliforms (TC) from Domestic Wastewater

Adsorbents	Contact Time (Min)	TC Load (cfu/mL)	Temp (°C)	Concentration (cfu//ml) at various Dosages						Percentage Removal (%) at various Dosages					
				5 g	10 g	15 g	20 g	25 g	30 g	5 g	10 g	15 g	20 g	25 g	30 g
BKC	30.0	6000	29.5	4600	3220	2898	2608	2347	2113	23.3	46.3	51.7	56.5	60.9	64.8
BKC/ZnO	30.0	6000	29.5	4480	3136	2822	2540	2286	2058	25.3	47.7	53.0	57.7	61.9	65.7
BKC/Ag	30.0	6000	29.5	4440	3108	0	0	0	0	26.0	48.2	100.0	100	100	100
BKC/Ag/ZnO	30.0	6450	29.5	4420	3094	0	0	0	0	31.5	52.0	100.0	100	100	100

Table 22: Effect of Dosage on the Removal of Faecal Coliforms (FC) from Domestic Wastewater

Adsorbents	Contact Time (Min)	FC Load (cfu/mL)	Temp (°C)	Concentration (cfu/ml) at various Dosages						Percentage Removal (%) at various Dosages					
				5 g	10 g	15 g	20 g	25 g	30 g	5 g	10 g	15 g	20 g	25 g	30 g
BKC	30.0	640	29.5	520	364	328	295	265	239	18.8	43.1	48.8	53.9	58.5	62.7
BKC/ZnO	30.0	640	29.5	516	361	325	293	263	237	19.4	43.6	49.2	54.3	58.9	63.0
BKC/Ag	30.0	640	29.5	512	358	0	0	0	0	20.0	44.0	100	100	100	100
BKC/Ag/ZnO	30.0	640	29.5	504	353	0	0	0	0	21.3	44.9	100	100	100	100

Table 23: Effect of Dosage on the Removal of *Clostridium perfringens* from Domestic Wastewater

Adsorbents	Contact Time (Min)	*Clostridium perfringens* (cfu/100mL)	Temp (°C)	Concentration (cfu/ml) at various Dosages						Percentage Removal (%) at various Dosages					
				5 g	10 g	15 g	20 g	25 g	30 g	5 g	10 g	15 g	20 g	25 g	30 g
BKC	30.0	40	29.5	30	21	19	17	15	14	25.0	47.5	52.8	57.5	61.7	65.6
BKC/ZnO	30.0	40	29.5	28	20	18	16	14	13	30.0	51.0	55.9	60.3	64.3	67.9
BKC/Ag	30.0	40	29.5	28	20	0	0	0	0	30.0	51.0	100	100	100	100
BKC/Ag/ZnO	30.0	40	29.5	24	17	0	0	0	0	40.0	58.0	100	100	100	100

Table 24: Effect of Dosage on the Removal of *E. coli from* Domestic Wastewater

Adsorbents	Contact Time (Min)	*E. coli* Load (cfu/100mL)	Temp (°C)	Concentration (mg/L) at various Dosages						Percentage Removal (%) at various Dosages					
				5 g	10 g	15 g	20 g	25 g	30 g	5 g	10 g	15 g	20 g	25 g	30 g
BKC	30.0	400	29.5	320	224	202	181	163	147	20.0	44.0	49.6	54.6	59.2	63.3
BKC/ZnO	30.0	400	29.5	316	221	199	179	161	145	21.0	44.7	50.2	55.2	59.7	63.7
BKC/Ag	30.0	400	29.5	312	218	0	0	0	0	22.0	45.4	100	100	100	100
BKC/Ag/ZnO	30.0	400	29.5	304	213	0	0	0	0	24.0	46.8	100	100	100	100

APPENDIX E

EFFECT OF TEMPERATURE

Table 1: Effect of Temperature on the Removal of Total Iron from Domestic Wastewater

Adsorbents	Iron (mg/L)	Contact Time (Minutes)	Dosage (g)	Concentration (mg/L) at various Temperature						Percentage Removal (%) at various Temperature					
				30 °C	40 °C	50 °C	60 °C	70 °C	80 °C	30 °C	40 °C	50 °C	60 °C	70 °C	80 °C
BKC	0.830	30.0	25.0	0.490	0.441	0.3969	0.218	0.206	0.115	41.0	46.9	52.2	73.7	75.1	86.1
BKC/ZnO	0.830	30.0	25.0	0.390	0.234	0.2106	0.063	0.019	0.019	53.0	71.8	74.6	92.4	97.7	97.7
BKC/Ag	0.830	30.0	25.0	0.380	0.228	0.2052	0.062	0.018	0.018	54.2	72.5	75.3	92.6	97.8	97.8
BKC/Ag/ZnO	0.830	30.0	25.0	0.350	0.210	0.189	0.057	0.017	0.017	57.8	74.7	77.2	93.2	98.0	98.0

Table 2: Effect of Temperature on the Removal of Lead from Domestic Wastewater

Adsorbents	Lead (mg/L)	Contact Time (Minutes)	Dosage (g)	Concentration (mg/L) at various Temperature						Percentage Removal (%) at various Temperature					
				30 °C	40 °C	50 °C	60 °C	70 °C	80 °C	30 °C	40 °C	50 °C	60 °C	70 °C	80 °C
BKC	0.140	30.0	25.0	0.120	0.108	0.0972	0.053	0.051	0.028	14.3	22.9	30.6	61.8	63.9	79.9
BKC/ZnO	0.140	30.0	25.0	0.110	0.066	0.0594	0.018	0.005	0.005	21.4	52.9	57.6	87.3	96.2	96.2
BKC/Ag	0.140	30.0	25.0	0.110	0.066	0.0594	0.018	0.005	0.005	21.4	52.9	57.6	87.3	96.2	96.2
BKC/Ag/ZnO	0.140	30.0	25.0	0.090	0.054	0.0486	0.015	0.004	0.004	35.7	61.4	65.3	89.6	96.9	96.9

Table 3: Effect of Temperature on the Removal of Copper from Domestic Wastewater

Adsorbents	Copper (mg/L)	Contact Time (Min)	Dosage (g)	Concentration (mg/L) at various Temperature						Percentage Removal (%) at various Temperature					
				30 °C	40 °C	50 °C	60 °C	70 °C	80 °C	30 °C	40 °C	50 °C	60 °C	70 °C	80 °C
BKC	0.050	30.0	25.0	0.040	0.036	0.0324	0.018	0.017	0.009	20.0	28.0	35.2	64.4	66.3	81.2
BKC/ZnO	0.050	30.0	25.0	0.040	0.024	0.0216	0.006	0.002	0.002	20.0	52.0	56.8	87.0	96.1	96.1
BKC/Ag	0.050	30.0	25.0	0.040	0.024	0.0216	0.006	0.002	0.002	20.0	52.0	56.8	87.0	96.1	96.1
BKC/Ag/ZnO	0.050	30.0	25.0	0.030	0.018	0.0162	0.005	0.001	0.001	40.0	64.0	67.6	90.3	97.1	97.1

Table 4: Effect of Temperature on the Removal of Manganese from Domestic Wastewater

Adsorbents	Manganese (mg/L)	Contact Time (Min)	Dosage (g)	Concentration (mg/L) at various Temperature						Percentage Removal (%) at various Temperature					
				30 °C	40 °C	50 °C	60 °C	70 °C	80 °C	30 °C	40 °C	50 °C	60 °C	70 °C	80 °C
BKC	0.250	30.0	25.0	0.190	0.171	0.1539	0.085	0.080	0.045	24.0	31.6	38.4	66.1	68.0	82.1
BKC/ZnO	0.250	30.0	25.0	0.170	0.102	0.0918	0.028	0.008	0.008	32.0	59.2	63.3	89.0	96.7	96.7
BKC/Ag	0.250	30.0	25.0	0.170	0.102	0.0918	0.028	0.008	0.008	32.0	59.2	63.3	89.0	96.7	96.7
BKC/Ag/ZnO	0.250	30.0	25.0	0.150	0.090	0.081	0.024	0.007	0.007	40.0	64.0	67.6	90.3	97.1	97.1

Table 5: Effect of Temperature on the Removal of Arsenic from Domestic Wastewater

Adsorbents	Arsenic (mg/L)	Contact Time (Minutes)	Dosage (g)	Concentration (mg/L) at various Temperature						Percentage Removal (%) at various Temperature					
				30 °C	40 °C	50 °C	60 °C	70 °C	80 °C	30 °C	40 °C	50 °C	60 °C	70 °C	80 °C
BKC	0.220	30.0	25.0	0.095	0.0855	0.077	0.042	0.040	0.022	56.8	61.1	65.0	80.8	81.8	89.9
BKC/ZnO	0.220	30.0	25.0	0.085	0.051	0.0459	0.014	0.004	0.004	61.4	76.8	79.1	93.7	98.1	98.1
BKC/Ag	0.220	30.0	25.0	0.088	0.0528	0.0475	0.014	0.004	0.004	60.0	76.0	78.4	93.5	98.1	98.1
BKC/Ag/ZnO	0.220	30.0	25.0	0.082	0.049	0.0443	0.013	0.004	0.004	62.7	77.6	79.9	94.0	98.2	98.2

Table 6: Effect of Temperature on the Removal of Mercury from Domestic Wastewater

Adsorbents	Mercury (mg/L)	Contact Time (Min)	Dosage (g)	Concentration (mg/L) at various Temperature						Percentage Removal (%) at various Temperature					
				30 °C	40 °C	50 °C	60 °C	70 °C	80 °C	30 °C	40 °C	50 °C	60 °C	70 °C	80 °C
BKC	0.110	30.0	25.0	0.092	0.0828	0.0745	0.041	0.039	0.022	16.4	24.7	32.3	62.7	64.8	80.4
BKC/ZnO	0.110	30.0	25.0	0.075	0.045	0.0405	0.012	0.004	0.004	31.8	59.1	63.2	89.0	96.7	96.7
BKC/Ag	0.110	30.0	25.0	0.073	0.0438	0.0394	0.012	0.004	0.004	33.6	60.2	64.2	89.2	96.8	96.8
BKC/Ag/ZnO	0.110	30.0	25.0	0.071	0.043	0.0383	0.012	0.003	0.003	35.5	61.3	65.1	89.5	96.9	96.9

Table 7: Effect of Temperature on the Removal of Silver from Domestic Wastewater

Adsorbents	Silver (mg/L)	Contact Time (Min)	Dosage (g)	Concentration (mg/L) at various Temperature						Percentage Removal (%) at various Temperature					
				30 °C	40 °C	50 °C	60 °C	70 °C	80 °C	30 °C	40 °C	50 °C	60 °C	70 °C	80 °C
BKC	0.02	30.0	25.0	0.012	0.0108	0.0097	0.005	0.005	0.003	40	46.0	51.4	73.3	74.7	85.9
BKC/ZnO	0.02	30.0	25.0	0.012	0.0072	0.0065	0.002	0.001	0.001	40	64.0	67.6	90.3	97.1	97.1
BKC/Ag	0.02	30.0	25.0	0.013	0.0078	0.007	0.002	0.001	0.001	35	61.0	64.9	89.5	96.8	96.8
BKC/Ag/ZnO	0.02	30.0	25.0	0.012	0.007	0.0065	0.002	0.001	0.001	40	64.0	67.6	90.3	97.1	97.1

Table 8: Effect of Temperature on the Removal of Zinc from Domestic Wastewater

Adsorbents	Zinc (mg/L)	Contact Time (Min)	Dosage (g)	Concentration (mg/L) at various Temperature						Percentage Removal (%) at various Temperature					
				30 °C	40 °C	50 °C	60 °C	70 °C	80 °C	30 °C	40 °C	50 °C	60 °C	70 °C	80 °C
BKC	2.46	30.0	25.0	0.971	0.8739	0.7865	0.433	0.409	0.228	60.5	64.5	68.0	82.4	83.4	90.7
BKC/ZnO	2.46	30.0	25.0	0.994	0.5964	0.5368	0.161	0.048	0.048	59.6	75.8	78.2	93.5	98.0	98.0
BKC/Ag	2.46	30.0	25.0	0.959	0.5754	0.5179	0.155	0.047	0.047	61.0	76.6	78.9	93.7	98.1	98.1
BKC/Ag/ZnO	2.46	30.0	25.0	0.87	0.522	0.4698	0.141	0.042	0.042	64.6	78.8	80.9	94.3	98.3	98.3

Table 9: Effect of Temperature on the Removal of Nitrate from Domestic Wastewater

Adsorbents	Nitrate (mg/L)	Contact Time (Min)	Dosage (g)	Concentration (mg/L) at various Temperature						Percentage Removal (%) at various Temperature					
				30 °C	40 °C	50 °C	60 °C	70 °C	80 °C	30 °C	40 °C	50 °C	60 °C	70 °C	80 °C
BKC	233	30.0	25.0	32.4	18.792	14.094	12.8	9.4	9.020	86.1	91.9	94.0	94.5	95.9	96.1
BKC/ZnO	233	30.0	25.0	33.4	19.372	14.529	13.2	9.7	9.299	85.7	91.7	93.8	94.3	95.8	96.0
BKC/Ag	233	30.0	25.0	34.4	19.952	14.964	13.6	10.0	9.577	85.2	91.4	93.6	94.2	95.7	95.9
BKC/Ag/ZnO	233	30.0	25.0	35.4	20.532	15.399	14.0	10.3	9.855	84.8	91.2	93.4	94.0	95.6	95.8

Table 10: Effect of Temperature on the Removal of Phosphate from Domestic Wastewater

Adsorbents	Phosphate (mg/L)	Contact Time (Min)	Dosage (g)	Concentration (mg/L) at various Temperature						Percentage Removal (%) at various Temperature					
				30 °C	40 °C	50 °C	60 °C	70 °C	80 °C	30 °C	40 °C	50 °C	60 °C	70 °C	80 °C
BKC	11.8	30.0	25.0	0.29	0.1682	0.1262	0.114	0.085	0.081	97.5	98.6	98.9	99.0	99.3	99.3
BKC/ZnO	11.8	30.0	25.0	0.27	0.1566	0.1175	0.106	0.079	0.075	97.7	98.7	99.0	99.1	99.3	99.4
BKC/Ag	11.8	30.0	25.0	0.28	0.1624	0.1218	0.110	0.082	0.078	97.6	98.6	99.0	99.1	99.3	99.3
BKC/Ag/ZnO	11.8	30.0	25.0	0.25	0.145	0.1088	0.099	0.073	0.070	97.9	98.8	99.1	99.2	99.4	99.4

Table 11: Effect of Temperature on the Removal of Ammonium from Domestic Wastewater

Adsorbents	Ammonium (mg/L)	Contact Time (Min)	Dosage (g)	Concentration (mg/L) at various Temperature						Percentage Removal (%) at various Temperature					
				30 °C	40 °C	50 °C	60 °C	70 °C	80 °C	30 °C	40 °C	50 °C	60 °C	70 °C	80 °C
BKC	37.2	30.0	25.0	1.63	0.9454	0.7091	0.643	0.475	0.454	95.6	97.5	98.1	98.3	98.7	98.8
BKC/ZnO	37.2	30.0	25.0	1.65	0.957	0.7178	0.651	0.481	0.459	95.6	97.4	98.1	98.3	98.7	98.8
BKC/Ag	37.2	30.0	25.0	1.68	0.9744	0.7308	0.663	0.490	0.468	95.5	97.4	98.0	98.2	98.7	98.7
BKC/Ag/ZnO	37.2	30.0	25.0	1.55	0.899	0.6743	0.611	0.452	0.432	95.8	97.6	98.2	98.4	98.8	98.8

Table 12: Effect of Temperature on the Removal of COD from Domestic Wastewater

Adsorbents	COD (mg/L)	Contact Time (Min)	Dosage (g)	Concentration (mg/L) at various Temperature						Percentage Removal (%) at various Temperature					
				30 °C	40 °C	50 °C	60 °C	70 °C	80 °C	30 °C	40 °C	50 °C	60 °C	70 °C	80 °C
BKC	312	30.0	25.0	37.2	26.0	22.1	19.9	16.7	16.5	88.1	91.7	92.9	93.6	94.6	94.7
BKC/ZnO	312	30.0	25.0	37.1	26.0	22.1	19.9	16.7	16.5	88.1	91.7	92.9	93.6	94.7	94.7
BKC/Ag	312	30.0	25.0	36.9	25.8	22.0	19.8	16.6	16.4	88.2	91.7	93.0	93.7	94.7	94.7
BKC/Ag/ZnO	312	30.0	25.0	34.2	23.9	20.3	18.3	15.4	15.2	89.0	92.3	93.5	94.1	95.1	95.1

Table 13: Effect of Temperature on the Removal of BOD from Domestic Wastewater

Adsorbents	BOD (mg/L)	Contact Time (Min)	Dosage (g)	Concentration (mg/L) at various Temperature						Percentage Removal (%) at various Temperature					
				30 °C	40 °C	50 °C	60 °C	70 °C	80 °C	30 °C	40 °C	50 °C	60 °C	70 °C	80 °C
BKC	30.6	30.0	25.0	5.23	3.661	3.1119	2.801	2.353	2.325	82.9	88.0	89.8	90.8	92.3	92.4
BKC/ZnO	30.6	30.0	25.0	8.49	5.943	5.0516	4.546	3.819	3.774	72.3	80.6	83.5	85.1	87.5	87.7
BKC/Ag	30.6	30.0	25.0	8.48	5.936	5.0456	4.541	3.814	3.769	72.3	80.6	83.5	85.2	87.5	87.7
BKC/Ag/ZnO	30.6	30.0	25.0	8.25	5.775	4.9088	4.418	3.711	3.667	73.0	81.1	84.0	85.6	87.9	88.0

Table 14: Effect of Temperature on the Removal of Oil and Grease from Domestic Wastewater

Adsorbents	Oil and Grease (mg/L)	Contact Time (Min)	Dosage (g)	Concentration (mg/L) at various Temperature						Percentage Removal (%) at various Temperature					
				30 °C	40 °C	50 °C	60 °C	70 °C	80 °C	30 °C	40 °C	50 °C	60 °C	70 °C	80 °C
BKC	10.1	30.0	25.0	0.28	0.168	0.131	0.028	0.018	0.001	97.2	98.3	98.7	99.7	99.8	100
BKC/ZnO	10.1	30.0	25.0	0.26	0.156	0.1217	0.026	0.017	0.001	97.4	98.5	98.8	99.7	99.8	100
BKC/Ag	10.1	30.0	25.0	0.28	0.168	0.131	0.028	0.018	0.001	97.2	98.3	98.7	99.7	99.8	100
BKC/Ag/ZnO	10.1	30.0	25.0	0.25	0.15	0.117	0.025	0.016	0.000	97.5	98.5	98.8	99.8	99.8	100

Table 15: Effect of Temperature on the pH

Adsorbents	Initial pH (mg/L)	Contact Time (Minutes)	Dosage (g)	Concentration (mg/L) at various Temperature					
				30 °C	40 °C	50 °C	60 °C	70 °C	80 °C
BKC	8.96	30.0	25.0	7.55	7.75	8.05	8.27	8.37	8.42
BKC/ZnO	8.96	30.0	25.0	7.81	8.01	8.31	8.53	8.63	8.68
BKC/Ag	8.96	30.0	25.0	6.77	6.97	7.27	7.49	7.59	7.64
BKC/Ag/ZnO	8.96	30.0	25.0	6.97	7.17	7.47	7.69	7.79	7.84

Table 16: Effect of Temperature on the Removal of Turbidity from Domestic Wastewater

Adsorbents	Turbidity (mg/L)	Contact Time (Min)	Dosage (g)	Concentration (mg/L) at various Temperature						Percentage Removal (%) at various Temperature					
				30 °C	40 °C	50 °C	60 °C	70 °C	80 °C	30 °C	40 °C	50 °C	60 °C	70 °C	80 °C
BKC	248	30.0	25.0	16.20	10.53	9.58	4.02	0.023	0.023	93.5	95.8	96.1	98.4	100	100
BKC/ZnO	248	30.0	25.0	17.20	11.18	10.17	4.27	0.023	0.023	93.1	95.5	95.9	98.3	100	100
BKC/Ag	248	30.0	25.0	18.20	11.83	10.77	4.52	0.023	0.023	92.7	95.2	95.7	98.2	100	100
BKC/Ag/ZnO	248	30.0	25.0	19.20	12.48	11.36	4.77	0.023	0.023	92.3	95.0	95.4	98.1	100	100

Table 17: Effect of Temperature on Dissolved Oxygen

Adsorbents	Dissolved Oxygen (mg/L)	Contact Time (Min)	Dosage (g)	Concentration (mg/L) at various Temperature						Percentage Removal (%) at various Temperature					
				30 °C	40 °C	50 °C	60 °C	70 °C	80 °C	30 °C	40 °C	50 °C	60 °C	70 °C	80 °C
BKC	1.00	30.0	25.0	4.05	3.85	3.65	3.52	3.52	3.48	75.3	74.0	72.6	71.6	71.6	71.3
BKC/ZnO	1.00	30.0	25.0	4.11	3.90	3.70	3.58	3.58	3.53	75.7	74.4	73.0	72.0	72.0	71.7
BKC/Ag	1.00	30.0	25.0	4.02	3.82	3.62	3.50	3.50	3.46	75.1	73.8	72.4	71.4	71.4	71.1
BKC/Ag/ZnO	1.00	30.0	25.0	4.18	3.97	3.76	3.637	3.64	3.59	76.1	74.8	73.4	72.5	72.5	72.2

Table 18: Effect of Temperature on the Removal of Suspended Solid from Domestic Wastewater

Adsorbents	Suspended Solid (mg/L)	Contact Time (Min)	Dosage (g)	Concentration (mg/L) at various Temperature						Percentage Removal (%) at various Temperature					
				30 °C	40 °C	50 °C	60 °C	70 °C	80 °C	30 °C	40 °C	50 °C	60 °C	70 °C	80 °C
BKC	233	30.0	25.0	13.0	7.8	6.63	2.652	0.020	0.020	94.4	96.7	97.2	98.9	100	100
BKC/ZnO	233	30.0	25.0	14.0	8.4	7.14	2.856	0.020	0.020	94.0	96.4	96.9	98.8	100	100
BKC/Ag	233	30.0	25.0	15.0	9	7.65	3.060	0.020	0.020	93.6	96.1	96.7	98.7	100	100
BKC/Ag/ZnO	233	30.0	25.0	16.0	9.6	8.16	3.264	0.020	0.020	93.1	95.9	96.5	98.6	100	100

Table 19: Effect of Temperature on the Removal of Colour from Domestic Wastewater

Adsorbents	Colour (mg/L)	Contact Time (Min)	Dosage (g)	Concentration (mg/L) at various Temperature						Percentage Removal (%) at various Temperature					
				30 °C	40 °C	50 °C	60 °C	70 °C	80 °C	30 °C	40 °C	50 °C	60 °C	70 °C	80 °C
BKC	1620	30.0	25.0	20.0	12	9.6	2.880	0.000	0.000	98.8	99.3	99.4	99.8	100	100
BKC/ZnO	1620	30.0	25.0	18.5	11.1	8.88	2.664	0.000	0.000	98.9	99.3	99.5	99.8	100	100
BKC/Ag	1620	30.0	25.0	18.2	10.92	8.736	2.621	0.000	0.000	98.9	99.3	99.5	99.8	100	100
BKC/Ag/ZnO	1620	30.0	25.0	16.0	9.6	7.68	2.304	0.000	0.000	99.0	99.4	99.5	99.9	100	100

Table 20: Effect of Temperature on Electrical Conductivity (EC) of Domestic Wastewater

Adsorbents	EC (µS/cm)	Contact Time (Min)	Dosage (g)	Concentration (mg/L) at various Temperature						Percentage Removal (%) at various Temperature					
				30 °C	40 °C	50 °C	60 °C	70 °C	80 °C	30 °C	40 °C	50 °C	60 °C	70 °C	80 °C
BKC	1382	30.0	25.0	612	416	362	311	268	265	55.7	69.9	73.8	77.5	80.6	80.8
BKC/ZnO	1382	30.0	25.0	613	417	363	312	268	265	55.6	69.8	73.8	77.4	80.6	80.8
BKC/Ag	1382	30.0	25.0	614	418	363	312	269	266	55.6	69.8	73.7	77.4	80.6	80.8
BKC/Ag/ZnO	1382	30.0	25.0	615	418	364	313	269	266	55.5	69.7	73.7	77.4	80.5	80.8

Table 21: Effect of Temperature on the Removal of Total Coliforms (TC)from Domestic Wastewater

Adsorbents	TC Load (cfu/100mL)	Contact Time (Min)	Dosage (g)	Concentration (mg/L) at various Temperature						Percentage Removal (%) at various Temperature					
				30 °C	40 °C	50 °C	60 °C	70 °C	80 °C	30 °C	40 °C	50 °C	60 °C	70 °C	80 °C
BKC	6000	30.0	25.0	4200	2730	1911	956	239	12	30	55	68	84	96	99.8
BKC/ZnO	6000	30.0	25.0	1800	1170	819	410	102	5	70	81	86	93	98	99.9
BKC/Ag	6000	30.0	25.0	800	520	0	0	0	0	87	91	100	100	100	100
BKC/Ag/ZnO	6450	30.0	25.0	680	440	0	0	0	0	89	93	100	100	100	100

Table 22: Effect of Temperature on the Removal of Faecal Coliforms (FC) from Domestic Wastewater

Adsorbents	FC (cfu/mL)	Contact Time (Min)	Dosage (g)	Concentration (cfu/ml) at various Temperature						Percentage Removal (%) at various Temperature					
				30 °C	40 °C	50 °C	60 °C	70 °C	80 °C	30 °C	40 °C	50 °C	60 °C	70 °C	80 °C
BKC	640	30.0	25.0	440	286	200	100	25	6	31.3	55.3	68.7	84.4	96.1	99.1
BKC/ZnO	640	30.0	25.0	224	146	102	51	13	2	65.0	77.3	84.1	92.0	98.0	99.7
BKC/Ag	640	30.0	25.0	96	48	0	0	0	0	85.0	92.5	100.0	100	100	100
BKC/Ag/ZnO	640	30.0	25.0	80	40	0	0	0	0	87.5	93.8	100.0	100	100	100

Table 23: Effect of Temperature on the Removal of *Clostridium Perfringens* from Domestic Wastewater

Adsorbents	*Clostridium Perfringens* (cfu/100mL)	Contact Time (Min)	Dosage (g)	Concentration (cfu/ml) at various Temperature						Percentage Removal (%) at various Temperature					
				30 °C	40 °C	50 °C	60 °C	70 °C	80 °C	30 °C	40 °C	50 °C	60 °C	70 °C	80 °C
BKC	40	30.0	25.0	38	23	16	10	3	1	5.0	43.0	60.1	74.1	93.5	98.7
BKC/ZnO	40	30.0	25.0	34	20	14	9	2	0	15.0	49.0	64.3	76.8	94.2	98.8
BKC/Ag	40	30.0	25.0	20	12	0	0	0	0	50.0	70.0	100.0	100	100	100
BKC/Ag/ZnO	40	30.0	25.0	16	10	0	0	0	0	60.0	76.0	100.0	100	100	100

Table 24: Effect of Temperature on the Removal of *E. coli* from Domestic Wastewater

Adsorbents	*E. coli* Load (cfu/100mL)	Contact Time (Min)	Dosage (g)	Concentration (cfu/ml) at various Temperature						Percentage Removal (%) at various Temperature					
				30 °C	40 °C	50 °C	60 °C	70 °C	80 °C	30 °C	40 °C	50 °C	60 °C	70 °C	80 °C
BKC	400	30.0	25.0	244	159	111	56	14	1	39.0	60.4	72.2	86.1	96.5	99.8
BKC/ZnO	400	30.0	25.0	180	117	82	41	10	1	55.0	70.8	79.5	89.8	97.4	99.9
BKC/Ag	400	30.0	25.0	32	18	0	0	0	0	92.0	95.6	100.0	100	100	100
BKC/Ag/ZnO	400	30.0	25.0	24	13	0	0	0	0	94.0	96.8	100.0	100	100	100

APPENDIX F

LANGMUIR ADSORPTION ISOTHERM CONSTANTS FOR BKC, BKC/Ag, BKC/ZnO AND BKC/Ag/ZnO

Parameters	Sample	Intercept = 1/Qob	Slope =1/Qo	Qo	B	R_L	R^2
Total Iron	BKC	0.0122	0.2754	3.631082	22.57377	0.050668	0.9934
	BKC/Ag	0.005	0.1702	5.875441	34.04	0.034184	0.9882
	BKC/ZnO	0.0089	0.0521	19.19386	5.853933	0.170684	0.9672
	BKC/Ag/ZnO	0.0042	0.1479	6.761325	35.21429	0.033082	0.9965
Lead	BKC	0.0071	1.1212	0.891902	157.9155	0.043275	0.9787
	BKC/Ag	0.0073	0.9596	1.042101	131.4521	0.051538	0.9822
	BKC/ZnO	0.0071	0.9635	1.037883	135.7042	0.050004	0.9631
	BKC/Ag/ZnO	0.0067	0.9205	1.086366	137.3881	0.049421	0.9952
Copper	BKC	0.016	2.0667	0.483863	129.1688	0.134076	0.9369
	BKC/Ag	0.0106	79.47	0.012583	7497.17	0.002661	0.9941
	BKC/ZnO	0.0119	1.2395	0.806777	104.1597	0.161083	0.9767
	BKC/Ag/ZnO	0.0086	1.7186	0.581869	199.8372	0.090976	0.991
Manganese	BKC	0.004	0.6663	1.500825	166.575	0.023450	0.9815
	BKC/Ag	0.0042	0.5856	1.70765	139.4286	0.027888	0.9804
	BKC/ZnO	0.0045	0.5536	1.806358	123.0222	0.031491	0.9691
	BKC/Ag/ZnO	0.004	0.5564	1.797268	139.1	0.027952	0.9809
Arsenic	BKC	0.202	3.3463	0.298838	16.56584	0.215309	0.9311
	BKC/Ag	0.1976	1.6134	0.619809	8.16498	0.357616	0.9501
	BKC/ZnO	0.1807	1.7948	0.557165	9.932485	0.313957	0.9719
	BKC/Ag/ZnO	0.0977	1.7992	0.555803	18.41556	0.197964	0.9638
Mercury	BKC	0.1395	3.2893	0.304016	23.57921	0.278264	0.9453
	BKC/Ag	0.1175	3.8017	0.26304	32.35489	0.219345	0.9828
	BKC/ZnO	0.1084	4.0524	0.246767	37.38376	0.19561	0.9748
	BKC/Ag/ZnO	0.0724	4.7933	0.208625	66.2058	0.120734	0.9841
Silver	BKC	0.3093	18.319	0.054588	59.22729	0.457761	0.9453
	BKC/Ag	0.2787	21.549	0.046406	77.3197	0.392712	0.9616
	BKC/ZnO	0.2712	21.99	0.045475	81.08407	0.381435	0.9683
	BKC/Ag/ZnO	0.2619	22.469	0.044506	85.79229	0.368209	0.9697
Zinc	BKC	0.2320	0.2493	4.011231	1.074569	0.274466	0.9912
	BKC/Ag	0.1888	0.2956	3.38295	1.565678	0.206119	0.9816
	BKC/ZnO	0.2037	0.3023	3.307972	1.484045	0.215019	0.9765
	BKC/Ag/ZnO	0.1632	0.3255	3.072197	1.994485	0.169307	0.9843
Nitrate	BKC	0.1275	0.0013	769.2308	0.010196	0.296236	0.9613
	BKC/Ag	0.1248	0.0013	769.2308	0.010417	0.291793	0.9933
	BKC/ZnO	0.117	0.0014	714.2857	0.011966	0.263989	0.9944
	BKC/Ag/ZnO	0.1172	0.0014	714.2857	0.011945	0.264321	0.9959
Phosphate	BKC	0.0646	0.0405	24.69136	0.626935	0.119078	0.9899
	BKC/Ag	0.0683	0.0372	26.88172	0.544656	0.134645	0.9971
	BKC/ZnO	0.071	0.0364	27.47253	0.512676	0.141852	0.9924

	BKC/Ag/ZnO	0.0641	0.0368	27.17391	0.574103	0.128627	0.9936
Ammonium	BKC	0.0772	0.0103	97.08738	0.13342	0.167695	0.9444
	BKC/Ag	0.077	0.0103	97.08738	0.133766	0.167333	0.9773
	BKC/ZnO	0.0752	0.0105	95.2381	0.139628	0.161443	0.9891
	BKC/Ag/ZnO	0.0741	0.0105	95.2381	0.1417	0.159458	0.9941
COD	BKC	0.1441	0.0014	714.2857	0.009715	0.248063	0.9842
	BKC/Ag	0.1437	0.0013	769.2308	0.009047	0.261606	0.9951
	BKC/ZnO	0.1511	0.0013	769.2308	0.008604	0.271421	0.9904
	BKC/Ag/ZnO	0.1423	0.0013	769.2308	0.009136	0.259719	0.9917
BOD	BKC	0.1020	0.0085	117.6471	0.083333	0.28169	0.9524
	BKC/Ag	0.1007	0.0075	133.3333	0.074479	0.304967	0.9735
	BKC/ZnO	0.0914	0.0078	128.2051	0.085339	0.276903	0.9782
	BKC/Ag/ZnO	0.0661	0.0087	114.9425	0.131619	0.198905	0.9784
Oil and Grease	BKC	0.0284	0.0249	40.161	0.876761	0.035934	0.9770
	BKC/Ag	0.0317	0.0257	38.911	0.810726	0.038747	0.9790
	BKC/ZnO	0.0346	0.0242	41.322	0.699422	0.044638	0.9600
	BKC/Ag/ZnO	0.0182	0.029	34.483	1.593407	0.020097	0.9811

APPENDIX G

FREUNDLICH ADSORPTION ISOTHERM CONSTANTS FOR BKC, BKC/Ag, BKC/ZnO AND BKC/Ag/ZnO

Parameter	Sample	Intercept = log K	Slope = 1/n	N	K	R^2
Total Iron	BKC	0.7723	0.3789	2.639219	5.919704	0.9924
	BKC/Ag	1.3575	0.5808	1.721763	22.77718	0.9985
	BKC/ZnO	1.7951	0.8777	1.139341	62.38785	0.9986
	BKC/Ag/ZnO	1.5296	0.6394	1.563966	33.85322	0.995
Lead	BKC	1.0632	0.6455	1.549187	11.56645	0.9703
	BKC/Ag	1.2293	0.7055	1.417434	16.95509	0.9787
	BKC/ZnO	1.2498	0.7106	1.407261	17.77461	0.9678
	BKC/Ag/ZnO	1.2695	0.7083	1.411831	18.59945	0.9942
Copper	BKC	1.0592	0.7682	1.301744	11.46041	0.9962
	BKC/Ag	2.0419	1.0654	0.938615	110.1286	0.9936
	BKC/ZnO	1.4556	0.8586	1.164687	28.5496	0.9999
	BKC/Ag/ZnO	1.3846	0.8015	1.247661	24.24376	0.9995
Manganese	BKC	1.0796	0.5500	1.818182	12.01158	0.9989
	BKC/Ag	1.2264	0.6057	1.650982	16.84225	0.9982
	BKC/ZnO	1.2689	0.6273	1.594134	18.57377	0.9969
	BKC/Ag/ZnO	1.2983	0.6265	1.596169	19.87467	0.9999
Arsenic	BKC	-0.2105	0.5283	1.892864	0.615886	0.8866
	BKC/Ag	0.1336	0.6904	1.448436	1.360191	0.9658
	BKC/ZnO	0.0862	0.6459	1.548227	1.219551	0.9692
	BKC/Ag/ZnO	0.0236	0.5672	1.763047	1.055845	0.9929
Mercury	BKC	0.0269	0.6217	1.608493	1.063898	0.9397
	BKC/Ag	0.0758	0.5485	1.823154	1.190694	0.9568
	BKC/ZnO	0.1099	0.5245	1.906578	1.287953	0.9199
	BKC/Ag/ZnO	0.3071	0.3792	2.637131	2.02815	0.9727
Silver	BKC	-0.2209	0.7376	1.355748	0.601312	0.9821
	BKC/Ag	-0.3401	0.6796	1.471454	0.456983	0.982
	BKC/ZnO	-0.3438	0.676	1.47929	0.453106	0.9788
	BKC/Ag/ZnO	-0.4022	0.6461	1.547748	0.396096	0.987
Zinc	BKC	0.3006	0.5611	1.782214	1.998021	0.9725
	BKC/Ag	0.2973	0.491	2.03666	1.982896	0.9404
	BKC/ZnO	0.2781	0.5	2.00000	1.897143	0.9396
Nitrate	BKC	1.3139	0.6354	1.573812	20.60155	0.9879
	BKC/Ag	1.2978	0.6506	1.537043	19.8518	0.9883
	BKC/ZnO	1.3494	0.622	1.607717	22.3563	0.9829
	BKC/Ag/ZnO	1.3458	0.6246	1.601025	22.17175	0.9834
Phosphate	BKC	0.978	0.4235	2.361275	9.506048	0.9015
	BKC/Ag	0.978	0.4552	2.196837	9.506048	0.9535
	BKC/ZnO	0.9766	0.4562	2.192021	9.475453	0.9668
	BKC/Ag/ZnO	0.9929	0.4526	2.209456	9.837846	0.9312

Ammonium	BKC	1.2494	0.4707	2.124495	17.75824	0.9890
	BKC/Ag	1.2374	0.4823	2.073398	17.27428	0.9966
	BKC/ZnO	1.2411	0.4778	2.092926	17.42208	0.998
	BKC/Ag/ZnO	1.2405	0.4826	2.072109	17.39803	0.9961
COD	BKC	1.3812	0.5729	1.745505	24.0547	0.9588
	BKC/Ag	1.3598	0.5929	1.686625	22.89813	0.9775
	BKC/ZnO	1.3367	0.5978	1.6728	21.71201	0.9741
	BKC/Ag/ZnO	1.3495	0.6015	1.66251	22.36145	0.9723
BOD	BKC	1.0437	0.68	1.470588	11.0586	0.9718
	BKC/Ag	1.0508	0.7013	1.425923	11.24087	0.9866
	BKC/ZnO	1.0915	0.6762	1.478852	12.34525	0.9879
	BKC/Ag/ZnO	1.197	0.6249	1.600256	15.73983	0.968
Oil and Grease	BKC	1.2280	0.6354	1.573811772	16.90441	0.9358
	BKC/Ag	1.1926	0.6506	1.53704273	15.58117	0.9363
	BKC/ZnO	1.1865	0.622	1.607717042	15.36385	0.9306
	BKC/Ag/ZnO	1.2697	0.6246	1.601024656	18.60801	0.9694

APPENDIX H

THERMODYNAMIC PARAMETERS OF TOTAL IRON, CADMIUM, LEAD, COPPER, MANGANESE, ARSENIC, MERCURY SILVER, ZINC NITRATE, PHOSPHATE, AMMONIUM, COD AND BOD USING BKC, BKC/Ag, BKC/ZnO AND BKC/Ag/ZnO

Parameters	Adsorbents	Intercept = $\Delta S^o/R$	Slope = $-\Delta H^o/R$	R^2	R ($Jmol^{-1} K^{-1}$)	ΔS^o	ΔH^o	ΔG^o					
								303	313	323	333	343	353
Total Iron	BKC	16.465	-4738	0.9366	8.3145	137	39394	-2086	-3455	-4824	-6193	-7562	-8931
	BKC/ZnO	29.58	-8560	0.9396	8.3145	246	71172	-3349	-5808	-8267	-10727	-13186	-15646
	BKC/Ag	29.476	-8515	0.939	8.3145	245	70798	-3461	-5912	-8362	-10813	-13264	-15715
	BKC/Ag/ZnO	29.185	-8386	0.9373	8.3145	243	69725	-3800	-6227	-8653	-11080	-13507	-15933
Lead	BKC	22.167	-6873.9	0.9643	8.3145	184	57153	1308	-535	-2378	-4221	-6064	-7908
	BKC/ZnO	34.078	-10285	0.9545	8.3145	283	85515	-338	-3171	-6005	-8838	-11672	-14505
	BKC/Ag	34.074	-10285	0.9545	8.3145	283	85515	-328	-3161	-5994	-8827	-11660	-14493
	BKC/Ag/ZnO	31.502	-9331	0.9482	8.3145	262	77583	-1780	-4399	-7019	-9638	-12257	-14876
Copper	BKC	20.284	-6192.9	0.9571	8.3145	169	51491	390	-1297	-2984	-4670	-6357	-8043
	BKC/ZnO	34.426	-10410	0.9549	8.3145	286	86554	-175	-3038	-5900	-8762	-11625	-14487
	BKC/Ag	34.426	-10410	0.9549	8.3145	286	86554	-175	-3038	-5900	-8762	-11625	-14487
	BKC/Ag/ZnO	30.938	-9113.5	0.9461	8.3145	257	75774	-2168	-4740	-7312	-9885	-12457	-15029
Manganese	BKC	19.275	-5821	0.9524	8.3145	160	48399	-161	-1763	-3366	-4969	-6571	-8174
	BKC/ZnO	32.054	-9540.7	0.9501	8.3145	267	79326	-1427	-4092	-6758	-9423	-12088	-14753
	BKC/Ag	32.054	-9540.7	0.9501	8.3145	267	79326	-1427	-4092	-6758	-9423	-12088	-14753
	BKC/Ag/ZnO	30.938	-9113	0.9461	8.3145	257	75770	-2172	-4744	-7317	-9889	-12461	-15034
Arsenic	BKC	14.985	-4095.8	0.9256	8.3145	125	34055	-3697	-4943	-6189	-7435	-8681	-9927
	BKC/ZnO	28.928	-8267	0.9357	8.3145	241	68736	-4142	-6547	-8953	-11358	-13763	-16168
	BKC/Ag	29.024	-8312.3	0.9363	8.3145	241	69113	-4007	-6421	-8834	-11247	-13660	-16073
	BKC/Ag/ZnO	28.836	-8222.6	0.9351	8.3145	240	68367	-4280	-6677	-9075	-11472	-13870	-16267
Mercury	BKC	21.406	-6600.2	0.9616	8.3145	178	54877	949	-830	-2610	-4390	-6170	-7950
	BKC/ZnO	32.082	-9551.5	0.9502	8.3145	267	79416	-1408	-4075	-6743	-9410	-12078	-14745
	BKC/Ag	31.803	-9446.1	0.9493	8.3145	264	78540	-1581	-4226	-6870	-9514	-12159	-14803
	BKC/Ag/ZnO	31.539	-9345.6	0.9484	8.3145	262	77704	-1752	-4374	-6997	-9619	-12241	-14864

Silver	BKC	16.582	-4785.9	0.9374	8.3145	138	39792	-1983	-3361	-4740	-6119	-7497	-8876
	BKC/ZnO	30.938	-9113	0.9461	8.3145	257	75770	-2172	-4744	-7317	-9889	-12461	-15034
	BKC/Ag	31.603	-9370.3	0.9486	8.3145	263	77909	-1708	-4336	-6963	-9591	-12218	-14846
	BKC/Ag/ZnO	30.938	-9113.5	0.9461	8.3145	257	75774	-2168	-4740	-7312	-9885	-12457	-15029
Zinc	BKC	14.74	-3974.6	0.9233	8.3145	123	33047	-4088	-5313	-6539	-7764	-8990	-10215
	BKC/ZnO	29.054	-8326	0.9365	8.3145	242	69227	-3969	-6385	-8800	-11216	-13632	-16048
	BKC/Ag	28.952	-8278.4	0.9359	8.3145	241	68831	-4108	-6515	-8922	-11329	-13737	-16144
	BKC/Ag/ZnO	28.713	-8161.9	0.9342	8.3145	239	67862	-4474	-6862	-9249	-11636	-14024	-16411
Nitrate	BKC	12.823	-2856.7	0.9306	8.3145	107	23752	-8553	-9619	-10685	-11751	-12818	-13884
	BKC/ZnO	12.813	-2864	0.9304	8.3145	107	23813	-8467	-9532	-10598	-11663	-12728	-13794
	BKC/Ag	12.803	-2871.2	0.9301	8.3145	106	23873	-8382	-9446	-10511	-11575	-12640	-13704
	BKC/Ag/ZnO	12.794	-2878.5	0.9299	8.3145	106	23933	-8299	-9362	-10426	-11490	-12554	-13617
Phosphate	BKC	14.071	-2678.2	0.9363	8.3145	117	22268	-13181	-14351	-15521	-16691	-17861	-19031
	BKC/ZnO	14.135	-2675.7	0.9364	8.3145	118	22247	-13363	-14538	-15714	-16889	-18064	-19239
	BKC/Ag	14.102	-2676.9	0.9364	8.3145	117	22257	-13270	-14443	-15615	-16788	-17960	-19133
	BKC/Ag/ZnO	14.206	-2673.3	0.9365	8.3145	118	22227	-13562	-14743	-15924	-17105	-18287	-19468
Ammonium	BKC	13.569	-2706.4	0.9354	8.3145	113	22502	-11682	-12810	-13938	-15067	-16195	-17323
	BKC/ZnO	13.559	-2707.2	0.9354	8.3145	113	22509	-11650	-12777	-13905	-15032	-16160	-17287
	BKC/Ag	13.544	-2708.4	0.9354	8.3145	113	22519	-11602	-12728	-13855	-14981	-16107	-17233
	BKC/Ag/ZnO	13.61	-2703.2	0.9355	8.3145	113	22476	-11812	-12943	-14075	-15207	-16338	-17470
COD	BKC	9.5828	-1841.2	0.9307	8.3145	79.7	15309	-8833	-9630	-10427	-11224	-12020	-12817
	BKC/ZnO	9.5844	-1840.8	0.9308	8.3145	79.7	15305	-8841	-9637	-10434	-11231	-12028	-12825
	BKC/Ag	9.5877	-1839.9	0.9308	8.3145	79.7	15298	-8856	-9654	-10451	-11248	-12045	-12842
	BKC/Ag/ZnO	9.6347	-1828.5	0.9312	8.3145	80	15203	-9070	-9871	-10672	-11473	-12274	-13075
BOD	BKC	9.4053	-1912.6	0.9284	8.3145	78.2	15902	-7792	-8574	-9356	-10138	-10920	-11702
	BKC/ZnO	9.3551	-2080.3	0.9226	8.3145	77.8	17297	-6272	-7049	-7827	-8605	-9383	-10161
	BKC/Ag	9.3548	-2079.7	0.9226	8.3145	77.8	17292	-6276	-7054	-7831	-8609	-9387	-10165
	BKC/Ag/ZnO	9.3488	-2066.8	0.9231	8.3145	78	17184	-6368	-7145	-7923	-8700	-9477	-10254
	BKC	43.568	-11906	0.8193	8.3145	362	98992	-10768	-14391	-18013	-21636	-25258	-28880

Oil and Grease	BKC/ZnO	43.535	-11908	0.8194	8.3145	362	99009	-10668	-14288	-17908	-21528	-25147	-28767
	BKC/Ag	43.473	-11912	0.8195	8.3145	361	99042	-10479	-14093	-17708	-21323	-24937	-28552
	BKC/Ag/ZnO	43.475	-11915	0.8196	8.3145	361	99067	-10459	-14074	-17688	-21303	-24918	-28533

APPENDIX I

BATCH TREATMENT COMPARATIVE ANALYSIS STUDY

Parameters	Units	Waste water	Nanocomposite Adsorbents				Control	Standards
			BKC	BKC/ZnO	BKC/Ag	BKC/Ag/ZnO	Dam Water	NESREA, 2011
Odour	-	Smelling	OK	OK	OK	OK	OK	
pH	-	8.96	7.45	7.40	7.28	7.20	7.86	6.5 -8.5
Turbidity	NTU	248	0.00	0.00	0.00	0.00	15.0	
EC	µS/cm	1382	703	624	619	615	55.0	
Dissolved Oxygen	mg/L	1.00	4.82	4.81	4.82	4.83	6.30	4 (Min)
TSS	mg/L	233	0.00	0.00	0.00	0.00	35.0	
TDS	mg/L	926	471	418	415	412	36.9	
Colour	TCU	1620	BDL	BDL	BDL	BDL	168	
Nitrate	mg/L	230	10.5	10.4	10.5	10.1	21.4	40
Phosphates	mg/L	11.8	0.426	0.408	0.409	0.401	0.22	3.5
Ammonium	mg/L	37.2	1.472	1.457	1.431	1.401	20.2	2
Chloride	mg/L	133	26.5	26.1	26.8	25.2	4.61	350
COD	mg/L	312	28.9	27.6	26.5	27.9	12.0	30
BOD_5	mg/L	30.6	2.55	2.79	2.82	2.88	0.60	6
Oil and Grease	mg/L	10.1	BDL	BDL	BDL	BDL	BDL	0.1
Sodium	mg/L	29.0	13.5	13.8	13.9	13.5	8.00	120
Potassium	mg/L	23.0	4.30	4.42	4.22	4.00	3.90	50
Total Iron	mg/L	0.83	0.139	0.063	0.061	0.052	0.10	0.5
Lead	mg/L	0.14	0.009	0.008	0.009	0.008	BDL	0.1
Copper	mg/L	0.05	0.008	0.005	0.004	0.002	BDL	
Manganese	mg/L	0.25	0.012	0.012	0.011	0.011	BDL	
Arsenic	mg/L	0.22	0.021	0.022	0.023	0.022	0.04	0.05
Mercury	mg/L	0.11	0.018	0.017	0.018	0.016	0.09	

Silver	mg/L	0.02	BDL	BDL	0.002	0.002	BDL	
Zinc	mg/L	2.46	0.197	0.195	0.196	0.195	BDL	0.2
Total Coliforms	cfu/mL	6.45×10^3	2348	2286	0	0	44	5×10^3
E. coli	cfu/mL	400	162	140	0	0	12	Absent
Faecal Coliforms	cfu/mL	640	260	200	0	0	4	Absent
Clostridium Perfringens	cfu/mL	48	15	10	0	0	0	Absent